

# **Biofabrication and Applications of Metal Nanoparticles from Indigenous Fungi**



By

**Shama Zainab**

**Department of Microbiology  
Faculty of Biological Sciences  
Quaid-i-Azam University  
Islamabad  
2022**

# **Biofabrication and Applications of Metal Nanoparticles from Indigenous Fungi**

A thesis submitted in partial fulfillment of the requirements for the

Degree of

**Doctor of Philosophy**

In

**Microbiology**



By

**Shama Zainab**

**Department of Microbiology**

**Faculty of Biological Sciences**

**Quaid-i-Azam University**

**Islamabad**

**2022**

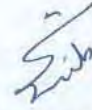
*Dedicated to*  
*Empathy and Comradeship*

DRSML OAU

**Author's Declaration**

I **Ms. Shama Zainab** hereby state that my Ph.D. thesis titled "**Biofabrication and Applications of Metal Nanoparticles from Indigenous Fungi**" is my own work and has not been submitted previously by me for taking any degree from Quaid-i-Azam University, Islamabad, Pakistan.

At any time if my statement is found to be incorrect even after I Graduate, the University has the right to withdraw my Ph.D. degree.



**Ms. Shama Zainab**

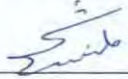
**Date: 03-11-2022**

**Plagiarism Undertaking**

“**Biofabrication and Applications of Metal Nanoparticles from Indigenous Fungi**” is solely my research work with no significant contribution from any other person. Small contribution / help wherever taken has been duly acknowledged and that complete thesis has been written by me.

I understand the zero tolerance policy of the HEC and Quaid-i-Azam University towards plagiarism. Therefore I as an Author of the above titled thesis declare that no portion of my thesis has been plagiarized and any material used as reference is properly referred/cited.

I undertake that if I am found guilty of any formal plagiarism in the above titled thesis even after award of Ph.D degree and that HEC and the University has the right to publish my name on the HEC/University Website on which names of students are placed who submitted plagiarized thesis.

Student / Author Signature:  \_\_\_\_\_  
Name: Ms. Shama Zainab

### Certificate of Approval

This is to certify that the research work presented in this thesis, entitled titled "Biosynthesis and Applications of Metal Nanoparticles from Indigenous Fungi" was conducted by Ms. Shama Zainab under the supervision of Prof. Dr. Naeem Ali. No part of this thesis has been submitted anywhere else for any other degree. This thesis is submitted to the Department of Microbiology, Quaid-i-Azam University, Islamabad in partial fulfillment of the requirements for the degree of Doctor of Philosophy in field of Microbiology.

Student Name: Ms. Shama Zainab

Signature: 

#### Examination Committee:

a) External Examiner 1:

Signature: 

Prof. Dr. Arshid Pervez  
Department of Environmental Sciences  
COMSATS University Abbottabad Campus  
Abbottabad

b) External Examiner 2:


Signature: 

Dr. Allah Nawaz  
(Ex-Principal Biochemist)  
House No 667, Street No. 18,  
Sector I-8/2, Islamabad

Supervisor Name: Prof. Dr. Naeem Ali

Signature: 

Name of HOD: Prof. Dr. Aamer Ali Shah

Signature: 

# Contents

List of Figures.....	viii
List of Tables .....	xii
List of abbreviations .....	xiii
Acknowledgments .....	xiv
Abstract.....	xv
Chapter 1: Introduction .....	1
Chapter 2: Review of Literature.....	5
Chapter 3: Isolation, screening and selection of fungi for silver nanoparticles' synthesis.....	24
Chapter 4: Green synthesis of Ag NP <sub>myc</sub> and their stabilization by <i>Thermomyces lanuginosus</i> .....	43
Chapter 5: Identification of the role of nitrate reductase involvement in nano-silver mycogenesis using <i>Aspergillus</i> sp. ....	63
Chapter 6: Fluconazole and Biogenic Silver Nanoparticles-based Nano-fungicidal System for Highly Efficient Elimination of Multi-drug Resistant <i>Candida</i> Biofilms.....	87
Chapter 7: Mycosynthesis of nanosilver particles using extracellular secretions of silver tolerant oleaginous fungus <i>Mucor circinelloides</i> SZ3 .....	113
Conclusions.....	128
Future Prospects .....	130
References.....	131
Publication .....	149

# List of Figures

## Chapter 2

Figure 2.1. Diagram showing the mechanisms of resistance and adaptation to metal ions by microorganisms.....	7
Figure 2.2. Proposed mechanism for silver nanoparticle synthesis by bacteria. a: uptake of ionic silver and silver reduction, b: electron shuttle system activation, c, d: intra or extracellular synthesis of nanoparticles, e: interaction of ionic silver with cell wall, f: extracellular reduction of ionic silver. ....	9
Figure 2.3. Various fungal enzymes for metal nanoparticle synthesis .....	12
Figure 2.4. Proposed antibacterial effects caused by nanomaterials: inhibition of biofilm formation, generation of free radicals, disruption of cell signaling, damaging cell proteins, release of metal ions from nanomaterial. ....	17
Figure 2.5. Antifungal drug resistance and drug target mechanisms by metal nanoparticles..	18
Figure 2.6. Diagram showing classes of nanoparticles, properties affecting nanoparticle toxicity and methods for assessing nanoparticle based toxicity.....	22

## Chapter 3

Figure 3.1. Concentration of metal ions (ppm) in samples from different soils. ....	30
Figure 3. 2. Silver tolerance index for NS isolates .....	31
Figure 3.3. Silver tolerance index for MS isolates.....	32
Figure 3.4. Silver tolerance index for KS isolates .....	32
Figure 3.5. Silver tolerance index for selected fungal isolates .....	33
Figure 3.6. Silver tolerance plate assay against selected fungal isolates. The fungus being shown in the figure is <i>Aspergillus flavus</i> .....	33
Figure 3.7. Growth of selected fungal isolates on solid and liquid media (a) <i>Mucor circinelloides</i> (b) <i>Aspergillus oryzae</i> (c) <i>Aspergillus flavus</i> (d) <i>Thermomyces lanuginosus</i> ...	34
Figure 3. 8. pH optimization for fungal growth.....	34
Figure 3.9. Temperature optimization for fungal growth .....	35
Figure 3.10. Extracellular silver reduction test by selected fungal isolates: (a) <i>Mucor circinelloides</i> (b) <i>Aspergillus oryzae</i> (c) <i>Aspergillus flavus</i> (d) <i>Thermomyces lanuginosus</i> ...	36
Figure 3.11. UV-Vis spectra for scanning silver reduction between 400-500 nm wavelengths .....	36
Figure 3.12. Phylogenetic analysis of <i>Aspergillus oryzae</i> SZ1 by using Mega 6.1 neighborhood joining method.....	38
Figure 3. 13. Phylogenetic analysis of <i>Aspergillus flavus</i> SZ2 by using Mega 6.1 neighborhood joining method .....	39
Figure 3. 14. Phylogenetic analysis of <i>Mucor circinelloides</i> SZ3 by using Mega 6.1 neighborhood joining method .....	39

## Chapter 4

Figure 4.1. Schematic illustration of Ag NP <sub>myc</sub> synthesis procedure.....	47
Figure 4.2. The Pareto chart, indicating the influence (by their t value) of important factors on Ag NP <sub>myc</sub> synthesis .....	53
Figure 4.3. A: UV-Vis spectrum of reaction vessel for Ag NP <sub>myc</sub> synthesis showing absorbance near 410 nm. Change in color as indication of Ag NP <sub>myc</sub> synthesis as compared to control and reaction vessels, is also shown. B: UV-Vis spectrum for control vessel with silver and nitrate ions.....	54



Figure 4.4. A: Representative TEM micrograph of Ag NP <sub>myc</sub> and B: particle size distribution of Ag NP <sub>myc</sub> C: XRD pattern for the mycogenic silver nanoparticles. Note: The bars in 4.4. B represent the values of number of nanoparticles at different size scale. ....	56
Figure 4.5. FTIR spectrum of mycogenic silver nanoparticles. Note: The lines represent the percent transmittance of each sample. ....	57
Figure 4.6. A: SDS-PAGE results depicting the size of capping protein glucoamylase on Ag NP <sub>myc</sub> ; B and C: MS/MS data for identification of the capping protein's peptide sequences. ....	58
Figure 4.7. Dose-response plot showing viability (%) and LC <sub>50</sub> of <i>A. salina</i> at different concentrations of Ag NP <sub>myc</sub> (blue line) and Ag NO <sub>3</sub> (red line) after 24 hours. Note: The lines represent the mean values of percentage of alive brine shrimps. The error bars represent standard error being calculated after taking average of three replicates of each sample and calculating standard deviation.....	59
Figure 4.8. Glucoamylase capped silver nanoparticles production mechanism .....	61
<b>Chapter 5</b>	
Figure 5.1. UV–Visible spectrum for the (a) silver nitrate solution and (b) mycogenic silver nanoparticles .....	72
Figure 5.2. Representative (a, b) TEM micrographs and (c) XRD pattern for Ag NP <sub>myc</sub> . ....	72
Figure 5.3. Standard curves of (a) Nitrite for NR assay and (b) Bovine serum albumin for protein quantification .....	73
Figure 5.4. The in-vitro effect of various inhibitors on activity of nitrate reductase from <i>Aspergillus flavus</i> SZ2. Note: The bars represent the mean values, while the error bars represent standard error of triplicate samples after calculating standard deviation. ....	74
Figure 5.5. Using gel-filtration chromatography, partially purified fractions with protein activity and specific activity of nitrate reductase enzyme in total extracellular protein content from filtrate of <i>Aspergillus flavus</i> SZ2 .....	75
Figure 5.6. Positive correlation (R = 0.855) indicating the involvement of nitrate reductase in the mycosynthesis of AgNPs by reducing silver nitrate. ....	75
Figure 5.7. Effect of temperature on production of nitrate reductase from <i>A. flavus</i> SZ2. Note: The bars represent the mean values, while the error bars represent standard error of triplicate samples after calculating standard deviation. ....	76
Figure 5.8. Effect of different pH on production of nitrate reductase from <i>A. flavus</i> SZ2 .....	76
Figure 5.9. Effect of NaCl on NR production by <i>A. flavus</i> SZ2 .....	77
Figure 5. 10. Effect of carbon sources on NR production by <i>A. flavus</i> SZ2.....	77
Figure 5. 11. Effect of nitrogen sources on NR production by <i>A. flavus</i> SZ2 .....	78
Figure 5. 12. Optimized value of NR produced by <i>A. flavus</i> SZ2 .....	78
Figure 5. 13. Ammonium Sulfate precipitation of crude nitrate reductase from <i>A. flavus</i> SZ2 showing comparison of specific activities of pellets and supernatants at different concentrations of ammonium sulfate (10-80%).....	79
Figure 5.14. The elution profile of fungus <i>A. flavus</i> SZ2 nitrate reductase on Sephadex G-100 chromatography. ....	79
Figure 5.15. Effect of temperature on specific activity of nitrate reductase from <i>A. flavus</i> SZ2 .....	80
Figure 5.16. Effect of pH on specific activity of nitrate reductase from <i>A. flavus</i> SZ2 .....	81
Figure 5.17. Temperature stability of nitrate reductase from <i>A. flavus</i> SZ2 .....	81
Figure 5.18. pH stability profile of nitrate reductase from <i>A. flavus</i> SZ2.....	82
Figure 5.19. Effect of metals on activity of nitrate reductase from <i>A. flavus</i> SZ2.....	82

Figure 5.20. Effect of surfactant and detergents on activity of nitrate reductase from <i>A. flavus</i> SZ2.....	83
Figure 5.21. Effect of organics solvent on activity of nitrate reductase from <i>A. flavus</i> SZ2 ...	83
Figure 5. 22. Kinetics analysis (Lineweaver Burk plot) of nitrate reductase from <i>A. flavus</i> SZ2 .....	84
Figure 5. 23. (a) PCR results for identification of nitrate reductase gene of <i>A. flavus</i> SZ2 (b) SDS-PAGE of nitrate reductase of <i>A. flavus</i> SZ2 showing two bands of 70 and 45 kDa. ....	84
<b>Chapter 6</b>	
Figure 6.1. Phylogenetic tree of <i>Aspergillus oryzae</i> SZ1 .....	98
Figure 6.2. Schematic illustration of Ag NP <sub>myc</sub> synthesis procedure.....	99
Figure 6.3. UV–Vis spectrum for the mycogenic silver nanoparticles.....	100
Figure 6.4. XRD pattern and data for the mycogenic silver nanoparticles .....	101
Figure 6.5. Representative TEM micrographs of mycogenic silver nanoparticles produced from <i>A. oryzae</i> SZ1 .....	101
Figure 6. 6. FTIR spectrum of mycogenic silver nanoparticles produced from <i>A. oryzae</i> SZ1 .....	102
Figure 6.7. In vitro acute toxicity analysis - brine shrimp mortality assay .....	104
Figure 6.8. Combined effect of Ag NP <sub>myc</sub> and FLC alone or in combination on planktonic cells of <i>Candida sp.</i> for time-kill curve analysis (CFU) at 0, 2, 6, 12, 24 hours at 37°C. $1 \times 10^6$ . CFU values are represented with mean $\pm$ SE of three independent experiments. ....	106
Figure 6.9. Combined effect of different concentrations of fluconazole (FLC) alone and in combination with Ag NP <sub>myc</sub> (15 ppm) (Figure a) and Ag NP <sub>myc</sub> (25 ppm) (Figure b) on percentage inhibition in biofilm metabolic activity (XTT) of six <i>Candida</i> species.....	107
Figure 6.10. Effect of FLC alone and in combination with Ag NP <sub>myc</sub> (15 ppm) and Ag NP <sub>myc</sub> (25 ppm) on percentage inhibition in EPS of planktonic (a, b) and biofilm (c, d) forms of six <i>Candida</i> species .....	109
Figure 6.11. Effect of FLC alone and in combination with Ag NP <sub>myc</sub> (15 ppm) and Ag NP <sub>myc</sub> (25 ppm) on percentage inhibition in SAP of planktonic (a, b) and biofilm (c, d) forms of six <i>Candida</i> species after 24 hours .....	110
<b>Chapter 7</b>	
Figure 7.1. UV–Vis spectrum for the Ag NP <sub>myc</sub> synthesized by fungus <i>M. circinelloides</i> SZ3 .....	119
Figure 7.2. Representative TEM micrograph (a) and size distribution (b) for Ag NP <sub>myc</sub> synthesized by fungus <i>M. circinelloides</i> SZ3. ....	119
Figure 7.3. XRD pattern (a) and data (b) for Ag NP <sub>myc</sub> synthesized by fungus <i>M. circinelloides</i> SZ3 .....	120
Figure 7.4. FTIR spectrum of Ag NP <sub>myc</sub> synthesized by fungus <i>M. circinelloides</i> SZ3 .....	121
Figure 7.5. Proposed mechanism of synthesis of Ag NP <sub>myc</sub> by fungus <i>M. circinelloides</i> SZ3 .....	121
Figure 7.6. UV-Vis absorbance spectrum of different concentrations of Ag NP <sub>myc</sub> to observe DPPH scavenging. (b) Anti-oxidant effect (%) of different concentrations of Ag NP <sub>myc</sub> . Note: The bars in 7.6 (b) represent the mean values with the error bars representing standard error being calculated after taking average of three replicates of each sample and calculating standard deviation. ....	122
Figure 7. 7. Anti-oxidant effect of Ag NP <sub>myc</sub> as compared with ascorbic acid (b) Kinetic curve of DPPH inhibition by Ag NP <sub>myc</sub> for 30 min with ascorbic acid as positive control. Note: The bars and lines represent the mean values with the error bars representing standard error being	

calculated after taking average of three replicates of each sample and calculating standard deviation..... 123

Figure 7.8. Effect of different capping agents on surface plasmon resonance of Ag NP<sub>myc</sub> (a) fungal extract (b) 2 hours (c) 24 hours (d) 48 hours with capping agents. .... 124

Figure 7.9. Effect of different capping agents on antibacterial activity of Ag NP<sub>myc</sub>. Note: The bars represent the mean values with the error bars representing standard error being calculated after taking average of three replicates of each sample and calculating standard deviation. . 125

DRSML QAU

# List of Tables

## Chapter 3

Table 3.1. Location of site showing the name of isolates .....	31
Table 3.2. Growth of selected fungal isolates.....	37
Table 3.3. 18S rRNA sequence based molecular homology, closest related species, gene bank accession number, growth conditions (pH and temperature) and silver ion reduction potential of metal resistant fungal isolates.....	38

## Chapter 4

Table 4.1. Statically designed experimental model (Plackett–Burman) for Ag NP <sub>myc</sub> synthesis .....	52
Table 4.2. ANOVA and <i>F</i> -test) of Plackett–Burman experimental model.....	53
Table 4.3. XRD data for the mycogenic silver nanoparticles .....	55

## Chapter 5

Table 5.1. Set of primer designed for NR gene of <i>A. flavus</i> .....	71
Table 5.2. Purification steps of nitrate reductase from <i>A. flavus</i> SZ2.....	79

## Chapter 6

Table 6.1. Other examples of mycogenic silver nanoparticles from literature. ....	99
Table 6.2. Cytotoxicity (% mortality and LD50) of Ag NP <sub>myc</sub> in brine shrimps .....	103
Table 6.3. Antifungal effect of Ag NP <sub>myc</sub> alone/or in combination with fluconazole (FLC) against <i>Candida sp.</i> .....	105

## Chapter 7

Table 7.1. SPR peaks of Ag NP <sub>myc</sub> using different capping agents at 2, 24 and 48hr.....	124
--	-----

## List of abbreviations

Ag NP <sub>myc</sub>	Mycogenic Silver Nanoparticles
AgNP	Silver Nanoparticles
SPR	Surface Plasmon Resonance
KS	Khewra Soil
MS	Metal polluted Soil
NS	Neelam Valley Soil
XRD	X-Ray Diffraction
UV-Vis	Ultraviolet Visible
TEM	Transmission Electron Microscopy
FTIR	Fourier transform infrared spectroscopy
NR	Nitrate Reductase
SAP	Secreted Aspartyl Proteinase
EPS	Exopolymeric Substances
XTT	2,3-bis[2- Methoxy-4-nitro-5-sulphophenyl]-2H-tetrazolium-5-carboxanilide inner salt
Tween 80	Polyoxyethylene (20) sorbitan monooleate
CTAB	Cetyl trimethyl ammonium bromide
PVP	Polyvinylpyrrolidone
CMC	Carboxy methyl cellulose
FLC	Fluconazole
kDa	Kilo Daltons
FICI	Fractional Inhibitory Concentration Index
MGYP	Malt Glucose Yeast Peptone
h	Hour/s
g/l	Gram per litre
DPPH	2,2-diphenyl-1-picrylhydrazyl

# Acknowledgments

I am extremely grateful to my research supervisor, Prof. Dr. Naeem Ali, Department of Microbiology, Quaid-i-Azam University, Islamabad, Pakistan. His guidance, encouragement, necessary criticism, moral support, patience and knowledge helped me a lot for research and completion of this thesis.

I am grateful to the entire faculty of Department of Microbiology especially Dr. Abdul Hameed (late), Dr. Safia Ahmed, Dr. Rani Faryal, Dr. Fariha Hassan, Dr. Malik Badshah, Dr. Sami ullah Khan, Dr. Aamer Ali Shah, Dr. Imran, Dr. Ishtiaq Ali and rest of faculty for supporting during research.

I feel thankful to the technical and non-teaching staff, Shehzad bhai, Shahid bhai, Tanveer bhai, Shabbir sahib, Sharjeel sahib at Department of Microbiology, QAU, Islamabad, for their kind assistance.

I am grateful to Higher Education Commission (HEC) for providing me opportunity of 'International Research Support Initiative Program (IRSIP)' and to Dr. Claudio F. Gonzalez at Department of Microbiology and Cell Science, University of Florida for allowing me to work in his lab during my PhD research work.

I do not find enough words to express my heartfelt gratitude for Sabahat Hamid, Dr. Akif Khan, Zawar Hussain, Nusrat Hussain, Dr. Shafaq Sahar, Zeeshan Ahmed, Akram Awan and those anonymous reviewers who helped in publication of my research article.

I extend my great depth of loving thanks to all my friends Neelam Farid, Dr. Nida Nosheen, Shafaq Shafiq, Dr. Aiman Ali, Dr. Sadia Latif, Sadaf Malik, Amber, Abdul Rehman, Dr. Fauzia, Zaufishan, Maqsoom, Huma, Usman, Dr. Irum Bibi, Angela, Yishui and many more.

I am thankful to my lab mates (seniors and juniors) especially Dr. Zeeshan Haider, Dr. Sadaf Shabbir, Dr. Shomaila Sikandar, Dr. Noshaba Hassan, Maliha Ahmed, Anum Munir, Dr. Iqra Sharafat, Dania Khalid, Dr. Mohsin Gulzar, Dr. Aftab, Hafsa Iqbal, Gul Parween, Dr. Aiman, Dr. Mahwish Ali, Uzma, Dr. Pervaiz Ali (late), Dr. Abdul Haleem, Dr. Wasim Sajjad, Dr. Ihsan Ali, Dr. Muhammad Irfan, Dr. Tawaf, Dr. Rafiq, Dr. Anum Khan, Dr. Jafar Ali, Dr. Muzna, Dr. Anila, Dr. Nazia, Dr. Muneer Qazi, Dr. Leena, Dr. Sadia Satti, Dr. Maria, Dr. Ramla, Dr. Saima, Dr. Zara, Dr. Hira, Dr. Muneeba Jadoon, Dr. Nigaht, Dr. Amber, Kamran, Dr. Hassan, Dr. Zarghona and many more.

A non-payable debt to my loving family members Abbu ji (late), Ammi ji, Aadil, Ameer, Baba Ali Ahmed Kurd, Aunty Nasira, Sazain, Itrat, for bearing all the ups and downs of my life during my PhD research, motivating me, sharing my burden and making sure that I sailed through smoothly. Completion of this work would not have been possible without the unconditional support and encouragement of my loving family members and friends. Finally, I express my gratitude and apology to all those who provided me the opportunity to achieve my endeavors but I missed to mention them personally.

**Shama Zainab**

## Abstract

**Hypothesis:** The innovative field of nanoscience, has remarkable ability to influence various fields of humans' lives. The fusion of microbiology, biotechnology and nanoscience has given birth to the field of bionanoscience which has enabled scientists to explore the potential of microbial processes and systems to fabricate novel nanostructures of biological importance. Use of biological procedures, eliminate the use of expensive chemicals, intensive energy use and are eco-friendly in nature as compared to the chemical and physical approaches. Nanotechnology today offers new approaches by altering the physical and chemical properties of various types of materials to create effective antimicrobial products. Applications of metal nanoparticles especially silver nanoparticles are wide in range from bioremediation, biosensing to biomedicine. Fungi belong to versatile group of microorganisms which can withstand adverse life circumstances. Among different biological routes, fungus-mediated green approach of synthesis of nanomaterials includes advantages of fast growth, high amounts of extracellular biomolecules, easy processing, economic viability and easy biomass handling.

**Experiments:** This study involves the use of indigenous fungi for synthesis of mycogenic silver nanoparticles (Ag NP<sub>myc</sub>) and to explore the mechanisms of this synthesis (reducing and capping agents). For this purpose, in the **first part**, fungi were isolated from different soils, their silver tolerance and extracellular silver reduction potential was determined. In **second part**, thermophilic fungus *Thermomyces lanuginosus* STm was used to synthesize Ag NP<sub>myc</sub>. The size and shape of Ag NP<sub>myc</sub> were characterized using ultraviolet-visible spectroscopy, transmission electron microscopy (TEM) and X-ray diffraction techniques. The most significant process variables affecting mycosynthesis of Ag NP<sub>myc</sub> were screened using statistical experimental design of Plackett Berman model. The mechanism of mycosynthesis and capping on mycogenic nanoparticles was explored using sodium dodecyl sulphate-polyacrylamide gel electrophoresis (SDS-PAGE) and Liquid chromatography–mass spectrometry (LC-MS/MS). In **third part**, Ag NP<sub>myc</sub> were synthesized using *Aspergillus flavus* SZ2 extracellularly and role of nitrate reductase (NR) in synthesis of mycogenic silver nanoparticles was determined. Nitrate reductase was purified and characterized. In **fourth part**, Ag NP<sub>myc</sub> were synthesized using *Aspergillus oryzae* SZ1, the organismic level acute-cytotoxicity effect of Ag NP<sub>myc</sub> was determined against brine shrimps. The potent synergistic effect of Ag NP<sub>myc</sub> along with antifungal fluconazole on planktonic growth and biofilm formation on six fluconazole resistant clinical isolates of *Candida* species (*C. albicans*, *C. galabrata*, *C. parapsilosis*, *C. krusei*, *C. tropicalis*, *C. albicans* ATCC 24433) was investigated. The combined effect of fluconazole and Ag NP<sub>myc</sub> on exopolymeric substance (EPS) and secretion of secreted aspartyl proteinases (SAP) of planktonic and biofilm matrix composition of six *Candida* sp. was investigated. In **fifth part**, Ag NP<sub>myc</sub> were synthesized using silver tolerant oleaginous fungus *Mucor circinelloides* SZ3, biocompatibility of Ag NP<sub>myc</sub> was studied through determination of antioxidant potential and the effect of different capping agents on stability and antibacterial potential of Ag NP<sub>myc</sub> was observed.

**Findings:** In the **first part**, four indigenous fungi were selected based upon their ability to tolerate high concentration of silver ions. These fungi included *Aspergillus oryzae* SZ1, *Aspergillus flavus* SZ2, *Mucor circinelloides* SZ3, and thermophilic fungus *Thermomyces lanuginosus* STm. The minimum inhibitory concentration in case of silver tolerance was found to be 2000 mg/l in case of *A. oryzae* SZ1, *A. flavus* SZ2 and *T. lanuginosus* whereas in case of *M. circinelloides* SZ3 wasn't able to grow beyond 1000mg/l. The characteristic spectra of surface plasmon resonance (SPR) for silver reduction was observed as 405 nm for *M. circinelloides*, 430 nm for *A. oryzae*, 450 nm for *A. flavus* and 410 nm in case of *T. lanuginosus*. The optimum growth conditions: *M. circinelloides* pH 5, for *A. oryzae* pH 7, for *A. flavus* pH 7 and for *T. lanuginosus* pH 5. In case of temperature, the optimum values were found to be 20 °C for *M. circinelloides*, 30 °C for *A. oryzae* and *A. flavus* and 50 °C for *T.*

*lanuginosus*. After 18S sequencing, the fungi were given accession numbers from NCBI: *A. oryzae* SZ1 (MH664050), *A. flavus* SZ2 (MH664051) and *M. circinelloides* SZ3 (MH664052). In **second part**, glucoamylase protein (67 kDa) secreted extracellularly by *T. lanuginosus* STm was discovered to be the capping protein surrounding Ag NP<sub>myc</sub>. Ag NP<sub>myc</sub> against brine shrimps, were found to be less toxic as compared to ionic form of silver. In **third part**, the size and morphology Ag NP<sub>myc</sub> synthesized using *Aspergillus flavus* SZ2 as determined by TEM, was found to be spherical shaped with particle size range of 1 to 70 nm. Inhibition in NR activity along with silver reduction by sodium azide suggested the involvement of NR in Ag NP<sub>myc</sub> production. Positive correlation ( $R = 0.855$ ) between specific activity of NR (U/mg) and Ag NP<sub>myc</sub> optical density at 450 nm, indicating the involvement of NR in the mycosynthesis of Ag NP<sub>myc</sub> by reducing silver nitrate. Specific activity of NR was improved from 15.54 to 17.77 U/mg after Sephadex-100 gel filtration. The  $K_m$  and  $V_{max}$  of NR were calculated as 13.18 mg/ml and 0.07 U/ml ( $\mu\text{mol/ml/min}$ ). The size of the NR gene was found to be 2604 kb and two protein bands of 70 and 45 kDa showed its dimer nature. In **fourth part**, Ag NP<sub>myc</sub> synthesized using *Aspergillus oryzae* SZ1 were found to be non-cytotoxic to brine shrimps. The results showed that combinational use of Ag NP<sub>myc</sub> with FLC exhibited strong in vitro antifungal synergy (FICI values ranged from 0.2812 to 0.375) against the majority of the *Candida* strains tested with gradual decrease in CFU till 12 hours. In case of percentage inhibition in biofilm metabolic activity (XTT) of six *Candida* species, >60% reduction of metabolic activity was observed in different *Candida* sp. at 16  $\mu\text{g/ml}$  FLC in combination with Ag NP<sub>myc</sub>. The EPS inhibition (%) in planktonic cells ranged from 2 to 73, 3–82 and 1–19 by 15 ppm Ag NP<sub>myc</sub>/FLC, 25 ppm Ag NP<sub>myc</sub>/FLC and FLC alone, respectively. Whereas in case of biofilm forms, EPS inhibition (%) ranged from 1 to 84, 1–93 and 1–32 by 15 ppm Ag NP<sub>myc</sub>/FLC, 25 ppm Ag NP<sub>myc</sub>/FLC and FLC alone, respectively. The results obtained, showed that combinations of 15 ppm and 25 ppm Ag NP<sub>myc</sub> with FLC effectively inhibited the SAP in *Candida* spp. with an inhibition range of 1–82% and 1–79%, respectively in case of planktonic cells. Whereas 1–78% and 2–92% in case of biofilm cells as compared to less inhibition (<20%) seen in case of FLC treated *Candida* spp. planktonic and biofilm cells. In **fifth part**, Ag NP<sub>myc</sub> synthesized using oleaginous fungus *Mucor circinelloides* SZ3 were found to be spherical and triangular shaped with particle size range of 10 to 50 nm. The FTIR spectra revealed the peaks for amide I, amide II, lipids, chitin/chitosan, and polyphosphate. The antioxidant activity of silver nanoparticles at different concentrations time intervals was studied and found that 100  $\mu\text{l}$  sample of 5 ppm concentration showed a very good free radical (DPPH) scavenging activity with time. Tween 80 and CTAB gave highest stability as determined by high intensity peaks of surface plasmon resonance and highest antibacterial activity.

**Conclusions:** The study concludes that biological methods involving fungi give an economical and simple step approach towards synthesizing silver nanoparticles. It is interesting to note that in case of Ag NP<sub>myc</sub> synthesized by extracellular titre of thermophilic fungus, the adsorbed thermostable protein glucoamylase can possibly help in resuming activity of Ag NP<sub>myc</sub> at high industrial temperatures. Current study revealed a new antifungal potential of mycogenic silver nanoparticles (Ag NP<sub>myc</sub>) via synergistic combination for anti-virulence against multi drug resistant pathogens. Synergistic combined drug therapy along with multi-target strategy, potentially reduce the usage dose of drug thus lowering its toxicity and resistance against it thus increasing the drug-efficacy.

**Key words:** Ag NP<sub>myc</sub>, *Thermomyces lanuginosus*, *Aspergillus oryzae*, oleaginous fungus *Mucor circinelloides*, glucoamylase, nitrate reductase, aspartyl proteinase enzyme (SAP)



## Chapter 1: Introduction

Nanoscience deals with natural and synthetic objects whose main components have at least one dimension between 1 and 100 nanometer (1, 2). In current years, advanced research in area of nanoscience has resulted in emergence of possible technologies due to remarkably different chemical, physical and biological properties of nanoparticles in contrast to relative bulk counterparts (3, 4). Due to these specific properties, the applications of nanoparticles (NPs) are popular in consumer goods, energy (5), environment (6, 7), engineering and particularly areas of material science and biomedicine (8).

The innovative field of nanoscience, has remarkable ability to influence various fields of humans' lives (9). Nanomaterials can be inorganic or organic in nature. Among inorganic nanomaterials, examples include semi-conductor nanoparticles (e.g. cadmium sulfide, zinc oxide etc.), noble metal nanoparticles (e.g. platinum, silver, gold etc.) and magnetic nanoparticles etc. whereas organic nanomaterials consist of carbon nanocomposites. The production of inorganic nanomaterials, has attracted great interest in recent years because of their increasing uses in the form of biosensors (10), optical devices (11), semiconductors (12), catalysts (13), encapsulating material on drugs (14) etc. Among inorganic nanomaterials, increase in research is observed in the synthesis of noble metal nanoparticles that provide functionally flexible good quality properties. Among noble metal nanoparticles, there are various applications of silver and gold nanoparticles in interdisciplinary research area of nanobiotechnology (15) and biomedical (pharmacy and medicine) science (16, 17).

Toxic heavy metals are found abundantly on earth and being exposed to microorganisms since beginning of life for billions of years ago, which led to evolution of resistance systems in microorganisms. Most bacteria have toxic metal ion resistances genes for  $Pb^{2+}$ ,  $Co^{2+}$ ,  $Ag^+$ ,  $Zn^{2+}$ ,  $CrO_4^{2-}$ ,  $Cd^{2+}$ ,  $Hg^{2+}$ ,  $Cu^{2+}$ , and  $Ni^{2+}$ . These resistance systems include energy-dependent efflux pumps (e.g. chemiosmotic ion/proton exchangers ATPases), metal-binding proteins (e.g. SilE-silver binding protein, CopZ-chaperone, SmtA-metallothionein), enzyme-based transformations (e.g. oxidation, methylation, reduction, demethylation) (18).

The metals-microbes interactions in marine as well as terrestrial ecosystems, are utilized in different applications in the areas of biomineralization (precipitation) (19), bioremediation (20), bioleaching (21), geochemical cycles of elements (22), biocorrosion (23) etc. Nanoparticle fabrication has been carried out from prokaryotic bacterial species to complicated eukaryotic systems (24). Microbial biogenic fabrication of metal nanoparticles can be considered as role of mechanisms involved in heavy metal tolerance. These mechanisms are present in various forms such as microbial structural proteins, efflux protein systems (which pump metal ions, through ATP hydrolysis, proton motive force or chemiosmotic gradients etc.) and redox enzymes that transform ionic forms of metals to inert forms (18). Metal nanoparticles are usually formed after reduction of their respective metal ions (by microbial cells or reductants released by them) and nucleation and finally surface growth of particles. After synthesis, nascent nanoparticles can be confined or entrapped by the surface protective agents to enhance functionality and stability (25, 26).

Use of biological procedures, eliminate the use of expensive chemicals, intensive energy use and are eco-friendly in nature as compared to the chemical and physical approaches. The biological procedures involve the use of bacteria, fungi, actinomycetes, plants and algae with a result of good biocompatibility of bionanoparticles (27). Among different biological routes, fungus-mediated green approach towards the NPs synthesis includes advantages such as fast growth, high amounts of extracellular biomolecules, easy processing, economic viability, easy biomass handling. The fungal biomass has resulted in synthesis of metal NPs either extra or intracellularly e.g. extracellular NPs production by *Aspergillus fumigatus* (AgNPs), *Fusarium oxysporum* (AgNPs), *Colletotrichum spp.* (Au NPs), *Verticillium spp.* (magnetite NPs), intracellular NPs production by *Schizosaccharomyces pombe* (CdS NPs), *Verticillium spp.* (AgNPs), *Pichia jadinii* (Au NPs) (28). In fungal mediated synthesis of metal nanoparticles, different types of functional groups have been reported with high affinity towards metal ions; examples include amino, cysteine, metallothionein hydroxyl, thiol, carboxyl and glutathione etc. (29).

Despite presence of high potency antimicrobial agents, bacterial and fungal infections are still causing high rates of mortality and morbidity. Biofilm associated infections and rising multidrug resistance has speeded up the research in the area of developing new bactericidal agents significantly. Antimicrobial agents being used today display many drawbacks like minimum antibiotic potential and thus increased risk of developments of resistance (30). Therefore, long-term and effective antimicrobial and anti-biofilm material are needed immediately. Treating mature biofilms using conventional antimicrobials is not useful in many cases due to lower penetration in extracellular polysaccharide sheath which as well as demand of higher than usual drug doses.

Nanotechnology today offers new approaches by altering the physical and chemical properties of various types of materials to create effective antimicrobial products (31). Nano sized particles may provide high activity due to higher surface area leading to use in small doses. As a result, nanosized material can be used as alternative source as antimicrobials to combat microbial infections caused by biofilm formers and multidrug-resistant mutants (32). The nanomaterials used with antimicrobial properties include variable chemical compositions e.g. metallic, metallic oxides and organic nanoparticles etc.(33).

Silver nanoparticles (AgNPs), due to their antimicrobial potential (34, 35), are employed widely in cosmetic products (36), food storage items (37), pharmaceuticals (38), water purification (39), medical devices (40), clothing items (41) etc. According to an analysis by Nanotechnology Consumer Product Inventory (CPI), more than 1,800 nano-sized commercial products are there in the market (42). Among which, nano-products of silver are the most frequently employed nanomaterials, and 435 products (24%) are impregnated with nano-sized silver (42).

### **Hypothesis:**

The mechanisms of nanoparticle synthesis by fungi and the anti-fungal actions of these nanoparticles can be identified and quantified.

**Research questions:**

- 1- Extracellular fungal metabolites (reducing agents) might be the biotransforming agents of metal ions into nanoparticles.
- 2- Enzymes of industrial importance might be the natural capping agents on surface of nanoparticles.
- 3- Combinational therapy including anti-microbial drug and nanoparticles might be more effective in mitigation of infectious agent compared to application of single drugs.

**Aim of study:**

To biofabricate, characterize mycogenic silver nanoparticles (Ag NP<sub>myc</sub>) and to find the molecular mechanism involved in the synthesis and applications of these nanoparticles from indigenous fungi. For this purpose, the objectives are given below:

**Objectives:**

- 1- To isolate and optimize the growth conditions for the strains of fungi, which will be efficient in silver metal tolerance, identification of these fungi based on phylogenetic analysis.
- 2- To screen isolated fungi for fabricating mycogenic silver nanoparticles (Ag NP<sub>myc</sub>), characterization of Ag NP<sub>myc</sub> using Ultraviolet-Visible spectroscopy, Fourier transform infrared spectroscopy (FTIR), X-ray diffraction (XRD) and transmission electron microscopy (TEM) etc.
- 3- To optimize conditions for synthesis of Ag NP<sub>myc</sub> using statistical models.
- 4- To study the cytotoxicity properties of Ag NP<sub>myc</sub>.
- 5- To explore the mechanism of synthesis (reducing and capping agents) of Ag NP<sub>myc</sub>.
- 6- To determine the efficacy and mechanism of these Ag NP<sub>myc</sub> as antifungal biofilm agents against drug resistant species of *Candida*.

## Chapter 2: Review of Literature

### 2.1 Background

Nanoscience deals with the fabrication and application of materials by exploiting and reshaping matter at nano-scale, and it is a day by day, growing area of research in science and technology. Microbiology when merges with nanoscience, helps in understanding metal-microbe interaction (18). The fusion of microbiology, biotechnology and nanoscience has given birth to the field of bionanoscience or nanobioscience. It has enable scientists to explore the potential of microbial processes and systems to fabricate novel nanostructures of biological importance (43).

The usage of nanostructures and nanomaterials in commercial products has generally increased. In 2013, the nano-products had worldwide market valued at 22.9 billion US\$ (44). It was expected to reach 64.2 billion US\$, with growth rate of 19.8% between 2014 and 2019 annually. On commercial scale, nearly 1800 nanoproducts have been identified according to Nanotechnology Consumer Products Inventory of the Woodrow Wilson International Center for Scholars (45).

Applications of nanoparticles are wide in range from optoelectronic, electronic, catalysis, data storage, magnetic, energy, bioimaging and nanomedicine etc. (46) (47) During the past decade, research on synthesis of conventional along with biogenic metallic nanoparticles has been increased remarkably to fight against antimicrobial resistance (48). Silver nanoparticles exhibit notable antimicrobial activity against different microorganisms (49).

This chapter highlights various aspects of metal nanomaterials, their synthesis and their biomedical application specifically antimicrobial mode of actions along with safety and sustainable usage.

### 2.2 Nanoparticle manufacturing processes

#### 2.2.1 Physical routes

The physical routes to synthesize nanomaterials involve melting, thermal energy or electrical energy, high-energy radiations, mechanical pressure, evaporation or condensation or material abrasion (47). These routes involve top-down strategy of

material synthesis and the advantages include, no solvent contamination and production of monodispersed nanoparticles. But disadvantages include the less economical production due to abundant waste generation.

Examples of physical methods of nanoparticle fabrication include, physical vapour deposition (50), high energy ball milling (51), flash spray and laser pyrolysis (52), electrospraying (53), laser ablation (54), inert gas condensation (55) etc.

### 2.2.2 Chemical routes

Chemical methods are based on liquid phase synthesis by solution precipitation which involves precipitation of nanoparticles in a fluid solvent system (56). These methods involve mostly bottom up strategy and advantages include less instrumentation, large production, self-assembly, variety of patterns (doping, colloids and thin films) (57). The disadvantages of chemical routes nanosized product formation, include very costly reactions, and application dangerous and poisonous chemicals (58).

Examples of chemical methods for nanoparticle fabrication include, microemulsion technique, sol-gel method, polyol synthesis, hydrothermal synthesis, plasma enhanced vapour deposition and chemical vapour synthesis (47).

### 2.2.3 Biological routes

#### 2.2.3.1 Bacteria:

Microbes come across many types of metals and metalloids in nature and acquire several biochemical as well as genetic metal resistance mechanisms, for their survival (59). These mechanisms include extracellular binding and complexation, extracellular precipitation, intracellular deposition, lack of a specific metal transport system, solubility and toxicity alteration, by bringing variation in the metal ions' redox state, and cellular efflux pumping system (60). Majority of the metals having established this resistance and homeostasis, involve one of the mechanisms or their combinations (Figure 2.1) (61). Examples of silver ion resistance showing microorganisms include *Enterobacter cloacae* (62), *E. coli* (63), *P. stutzeri* (64) and *Acinetobacter baumannii* (59). Silver-resistant mutants of *E. coli* show an active efflux of silver ions (63) whereas *P. stutzeri* AG259 accumulates silver ions intracellularly in the form of nanoparticles (65). By using cellular machinery, metal ions may be reduced to elemental metal. Although the mechanistic pathway of nanoparticle synthesis is yet to be fully understood, different hypotheses try to explain nanoparticle synthesis by

bacterial genes or proteins e.g. by attaching to cell surface (energy-independent) and then intracellular accumulation (66). In case of *A. baumannii*, plasmid-mediated silver resistance enables to accumulate silver and bind to metalloprotein (66). Three main gene homologues of silver resistance machinery, namely silP, silE and silS are known to play an important role in silver nanoparticle synthesis (67).

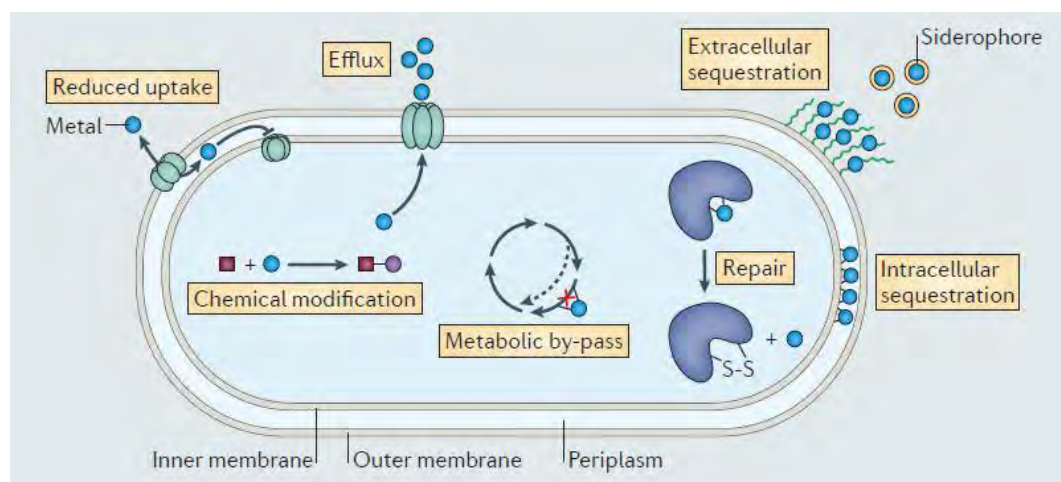


Figure 2.1. Diagram showing the mechanisms of resistance and adaptation to metal ions by microorganisms.

The bacterial cell wall components and enzymes play a key role in nanoparticle biogenesis (Figure 2.2) (68). In the primary phase of nanoparticle synthesis, nucleation of the silver ions clusters brings about an electrostatic contact between negatively charged carboxylate groups (cell wall) and silver ions (69). Redox proteins and cellular reductases, reduce silver ions trapped on bacterial cell surface to silver nanoparticles (70). Bacterial S (surface) layer can also help in interaction of metal surface and bacteria (71). Transmembrane proton gradient across bacterial cell wall can be another potential electrokinetic mechanism which along with silver ions from the surroundings is capable of driving active symport of sodium indirectly. For silver nanoparticle synthesis, silver ions are attracted readily by silver-binding proteins attached to membrane lipids employed by ATP binding on external bacterial surfaces (71).

Enzymatic electron shuttle silver reduction is caused by silver reduction machinery. Reducing cellular environment (due to hydrogen atoms) is created by NADH being produced during energy generating reactions of glycolysis and electron transport chain making it suitable for nanoparticle synthesis (72). Enzymes, especially NADH-nitrate reductase, play vital role in silver nanoparticle synthesis (73). Nitrate reductase is induced by nitrate ions of  $\text{AgNO}_3$  salt. NADH gives electrons to the enzyme and

undergoes oxidation to make  $\text{NAD}^+$ , thus enzyme get oxidized to nanosilver by reducing the silver ions. Nitrate ions ( $\text{NO}_3^-$ ) are reduced to nitrogen dioxide ( $\text{NO}_2$ ) then nitrogen oxide ( $\text{NO}$ ), nitrous oxide ( $\text{N}_2\text{O}$ ) and finally to nitrogen gas ( $\text{N}_2$ ) (74). On the other hand, *Acinetobacter* was found to exhibit nitrate reductase independent synthesis of silver nanoparticles (75). In cyanobacteria, hydrogenase and nitrogenase can cause reduction of ionic silver to silver nanoparticles (76). NfsA, present in Enterobacteriaceae, is an oxygen-insensitive nitroreductase, is known to reduce  $\text{AgNO}_3$  to silver nanoparticles as well (77). The key factor in bacterial mediated silver nanoparticle synthesis is higher pH (78). In the presence of high pH, closed rings of monosaccharide are catalyzed to the open-chain aldehydes which get oxidized to carboxylic acid in the presence of silver and reduce these ions to nanoparticles (79). High pH also brings about activation of the reductases of oxidoreductase enzymes (78). In addition, glutathione and thioredoxin systems are important for maintaining the reducing conditions indirectly and regulation of the activity of enzymes (72). Biosynthesis of silver nanoparticles can be stimulated by various reducing cofactors produced during activity of spore-associated enzymes such as catalase, alkaline phosphatase, glucose oxidase and laccase (80). In case of *Gluconacetobacter xylinum*, while overcoming metal stress, chloride ions are secreted from cytoplasm and reductases are generated to reduce silver ions resulting in formation of nanoparticles of  $\text{Ag}/\text{AgCl}$  as by-product (81). Silver-binding peptides have attracted much attention for fabrication and stabilizing of silver nanoparticles (82). Peptides generate reducing environment around preformed nanoclusters of silver, reduce silver ions polydispersed nanoparticle forms. Peptides containing glutamic acid, lysine, cysteine, methionine, aspartic acid, arginine etc. can recognize and reduce ionic silver to nanoparticles (83). The metal-peptide interactions are influenced by the physiological conditions of solution e.g. under alkaline conditions, tyrosine undergoes ionization on phenol group and converts to semiquinone structure which causes reduction of silver ions (84). High pH converts tryptophan into transient tryptophyl radical which helps in reduction of ionic silver by donating electrons (85).



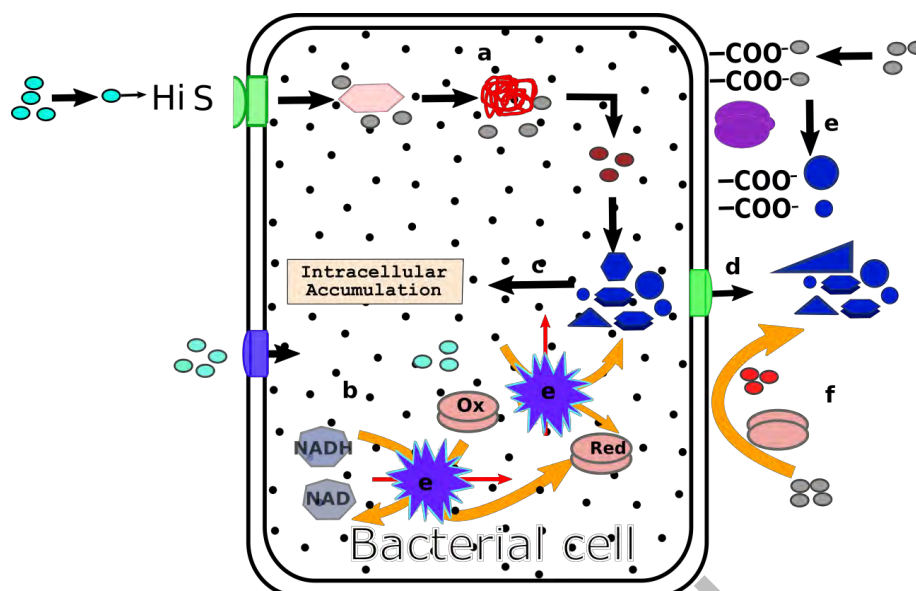


Figure 2.2. Proposed mechanism for silver nanoparticle synthesis by bacteria. a: uptake of ionic silver and silver reduction, b: electron shuttle system activation, c, d: intra or extracellular synthesis of nanoparticles, e: interaction of ionic silver with cell wall, f: extracellular reduction of ionic silver.

### 2.2.3.2 Fungi:

Fungi are studied as extensively for nanoparticle synthesis, as synthesis processes by bacteria. Fungi have some advantages over bacterial systems in terms of ease in developing and handling their biomasses, optimization according to application, economically viable growth, larger surface area of mycelia, production of diverse range of enzymes in higher quantities, can help in large scale synthesis of nanoparticles, easy and simple down streaming (86). Fungal species from different genera have found to be capable of producing variety of metal nanoparticles. These genera include *Fusarium*, *Aspergillus*, *Trichoderma*, *Verticillum*, and endophytic fungi (87-91). Studies have shown that certain reductase enzymes secreted by fungal cells reduced toxic metals e.g. nitrate-dependent reductases,  $\alpha$ -NADPH dependent reductases etc. (92).

Microorganisms try to get rid of the unnecessary elements from its environment. For such processes, fungi are preferred at large scale. Fungi secrete variety of peptides, proteins and enzymes as reducing agents e.g. nitrate reductase, anthraquinones naphthoquinones etc. which can reduce metal ions to nanoparticle forms (87).

Mycogenic nanoparticles can be formed intra or extra-cellular ways. Extra-cellular type of synthesis takes place when enzymes are secreted into surrounding reaction media on exposure of metal salts creating stressful conditions for organisms (86). These enzymes reduce the metal ions to nanoparticle form. In case of intracellular

type of synthesis, fungal cell wall (negatively charged) interrelates with metal ions (positively charged) with the help of cell wall membrane enzymes (93).

### **2.2.3.3 Plants:**

Presently, plants are also used in biosynthesis of metal nanoparticles. Usage of plants (living or inactivated plant tissue and plant extracts) in the biological synthesis of metal (in particular, silver and gold) nanoparticles, has gained more attention as an appropriate alternative to physical and chemical methods. Fabrication of metal nanoparticles with plant extracts, as a valuable economic alternative, is best for the large-scale production of metal nanoparticles. Plants extracts in nanoparticle synthesis, may serve both as capping and reducing agent (94). By using various combinations of biomolecules found in plant extracts (*e.g.* vitamins, enzymes, polysaccharides, proteins, amino acids, and organic acids like citrates) the process of bioynthesis of metal nanoparticles is eco-friendly, yet chemically intricate (95).

### **2.2.3.4 Viruses:**

Over the past decade, a range of viruses have turned out to be potential candidates in the metal nanoparticle synthesis. Some viruses gained much interest in the research of synthesis of virus-templated metal nanoparticle, having the merits of high yields, unique dimensions and structures, high chemical stability, and well-spaced functionalities. Uniform and accurately spaced binding sites for metal ions can be attained by using different strategies for handy modification of the capsids of viruses. Examples of viruses for the nanoparticle synthesis include filamentous (*e.g.* M13) (96), tubular (*e.g.* Tobacco Mosaic Virus (TMV) (97), icosahedral (*e.g.* Cowpea Mosaic Virus (CPMV) (98), elongated icosahedral viruses (*e.g.* T4 bacteriophages (99) and fd bacteriophages (100). Genetically and chemically modified and wild type viruses are also found to be able to synthesize nanoparticles.

Different strategies have been devised for wild type viruses pretreatment for metallization potential improvement for the synthesis of metal nanoparticles. One of the proposed strategies for enhanced nucleation is activation of the viral surfaces. For example, the metallization of TMV plant viruses inside the TMV channels, through a facile Ni deposition, mediated by Pd(II) (101). Contrarily, the high affinity of silver ions to the external amino acid of TMV followed by reduction with formaldehyde,

exclusively form AgNPs on TMV's external surface. The binding of metal precursors onto viruses is strengthened with the help of charge and genetic modifications (25).

#### **2.2.3.5 Extremophiles:**

Extremophilic microorganisms can be considered to beat the demerits in NP production e.g. the potential toxicity, low productivity and costly mass production. Extremophilic microorganisms have ability to grow in harsh physical or geochemical conditions, i.e. high temperature, extreme pH, and ion concentrations. For biosynthesis of nanoparticles, distinctive characteristics of extremophilic microorganisms make them one of the most ideal biocatalysts. Effectiveness of extremophilic enzymes, in industrial biotechnology, is undoubtedly high, owing to their ability to function in rough conditions resulting in substrate transformation, otherwise hard to achieve with normal enzymes (18).

#### **2.2.4 Mechanisms of Mycogenesis of metal NPs**

A large number of studies have been carried out on nanoparticle synthesis by microorganisms where they can be utilized in environment-friendly approach with much lower cost. Fungi are easy to grow at mass level and for nanoparticle synthesis they exhibit easy downstream processing (Figure 2.3) (86).

Biological studies have revealed that the design, as well as synthesis of these particles, is based upon natural mechanisms (e.g. bioaccumulation, biosorption, precipitation, and biomineralization) in microorganisms (29). Nanobiosynthesis is the simple detoxification mechanism in microorganisms which is solely responsible for nanoparticle synthesis (86).

##### **2.2.4.1 Mechanism of Synthesis**

Different types of microorganisms demonstrate various techniques, but the fundamental principle is reduction reaction which governs mechanisms of all types. Due to cellular polysaccharides and peptides, both intra and extracellular syntheses take place leading to enzymatic oxido-reduction, chelation, and sorption. Inter-membranous transport, nucleation and then growth of nanoparticles causes synthesis of nanoparticles extracellularly (86). The role of NADPH-dependent nitrate reductase was explained in case of *F. oxysporum*, how silver ions were reduced by an electron transfer involving NADP (co-factor). Moreover, quinine derivatives of naphthoquinones and anthraquinones are known to reduce silver nanoparticles (102).

*Verticillium* sp. were studied to explain the extracellular process of silver nanoparticle synthesis, where the silver ions are trapped on the cell wall and reductase enzyme reduce them to silver nuclei, these silver ions, ultimately, are accumulated on the generated nuclei (103). An oxidoreductase mechanism is observed, in the case of yeast. In *Saccharomyces cerevisiae*  $Cd^{+}$  were reduced by phytochelation synthase, and protein ligands were used to produce cadmium telluride (quantum dots) extracellularly (104). In case of yeast *Yarrowia lipolytica*, secreted melanin helped in extracellular fabrication of nanosilver and nanogold (105). During intracellular way of synthesis, trapping of ions, their reduction, and finally capping of the nuclei takes place. It also involve some ion transportation and electrostatic interaction between metal ions and microbial cells which leads to nanoparticle formation, while in case of extracellular biosynthesis, enzyme secretion, reduction and particle capping takes place. For most of cases in silver nanoparticle synthesis, nitrate reductase is the enzyme most commonly isolated so far (106). Extracellular synthesis is cheaper and easier, which is the prime objective of biosynthesis and is more preferable because purification and down streaming in this case are easier than the intracellular process (time-consuming and costly) (107).

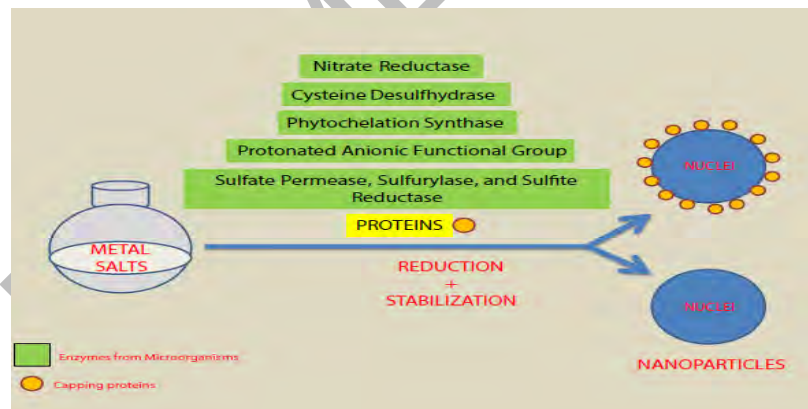


Figure 2.3. Various fungal enzymes for metal nanoparticle synthesis

#### 2.2.4.2 High throughput production

Various organisms, from simple prokaryotic bacterial cells to complex eukaryotes are used in nanoparticle synthesis (108). In fact, the ability of organisms has paved the path for the improvement of these natural nano-factories in metal nanoparticle production. Important factors which are worth considering for producing well-characterized and significantly stable nanoparticles are as under:

1. *Choice of the best organisms*: For selecting best organisms for nanoparticle synthesis, their essential intrinsic properties (e.g. biochemical pathways and enzyme activities) have been focused upon by the researchers.
2. *Optimal conditions for cell growth and enzyme activity*: Optimizing the growth conditions is of great significance. The mixing speed, inoculum size, temperature, light, nutrients, buffer strength and pH need to be optimized. If the substrates or related compounds in subtoxic levels are present from the beginning of the growth, the enzymes' activity increases.
3. *Optimal reaction conditions*: On industrial stage, crucial issue for using the organisms for metal nanoparticle synthesis is their yield rate as well as production rate. For that reason, in the reaction mixture, bioreduction conditions are needed to be optimized (109). The substrate concentration, the electron donor and its concentration, the biocatalyst concentration, buffer strength, mixing speed, exposure time, pH, light and temperature have to be controlled. These crucial factors, if optimized, could manage morphologies and other characteristics of nanoparticles. This exciting improvement toward production of nanoparticles with desired morphological sizes and characteristics might prove helpful to researchers for overcoming several limitations (95).

## **2.3 Biomedical application of NPs as antimicrobial agents**

### **2.3.1 Mechanism of antibacterial mode of action**

#### **2.3.1.1 Mode of Action of antibacterial drugs:**

The main antibiotics group being used recently, affect three major targets in bacterial cells i.e. DNA replication, translational machinery and cell wall synthesis (110). However, modes of bacterial resistance against these drugs (e.g. in case of vancomycin) might include antibiotic degrading, modification in cell components (e.g. cell wall), or enzymes (such as aminoglycosides,  $\beta$ -lactamases etc.) (110) and ribosomes in tetracyclines resistance, and eventually efflux pumps which offer multidrug resistance against several antibiotics (110).

#### **2.3.1.2 Mechanisms for antibacterial drug resistance:**

Bacterial resistance has turned out to be a serious issue because of the huge application of antibiotics, used without proper medical indications prophylactically or remedially; the repeated switching between antimicrobial treatments and the

inappropriate alternate antimicrobial selection. There are many causes for multidrug resistance in bacteria of extrinsic and intrinsic nature. The extrinsic factors include prolonged “selection pressure” of antimicrobial drugs and changes in the human microflora. Intrinsic factors are described here with respect to genetics at DNA level and from the level of protein biochemistry.

When we look at the gene level, it is seen that resistance can be of two types i.e. intrinsic and acquired resistance. Intrinsic resistance occurs when exogenous or existing genes undergo spontaneous mutation, while acquired resistance occurs due to transfer of resistance genes from outside (e.g. another organism). Particularly, the multidrug resistance (MDR) emerges when the same bacterial cell acquires drug resistance genes of various types (111). Intrinsic resistance, usually, is of secondary significance. There are three ways to transfer and spread resistance between bacteria, i.e. integrons (112), transposons (113) and plasmids (114). At the level of protein biochemistry resistance mechanisms involve alteration in cell surface targets and certain enzymes e.g. target alteration, inactivated or passivated enzymes generation, active efflux pump systems usage (115), obstacle presentation to antibiotic permeation, biofilms formation (116) and the elimination or emergence of a specific protein for instance BamA28, increased production of competitive inhibitor against antibiotic (117) or induction of an antagonist etc.

Consequently, the combination of several antibiotics, high-dose administration (118), the development of new drugs, were three methods applied to control antibiotic resistance, in the pre-nanoparticles era (119). The bacterial mutation, however, could not be challenged by the production of novel antibiotics, and high-dose treatment always gives rise to intolerable toxicity (120).

### **2.3.1.3 Mechanism of action of nanomaterials as antibacterial agent**

Studies concerning exploration of nanoparticles' prospective antibacterial mechanisms (Figure 2.4) has increased over the recent times, as the usage of NPs in medicine has grown (118). For instance, bacteria's metabolic activity can be changed by the metal nanoparticles (121). This facility turns out to be a massive advantage for the eradication of bacteria for curing certain diseases. Nanoparticles are able to penetrate biofilms and can inhibit biofilm formation by inhibiting gene expression (122). To accomplish their antibacterial role, nanoparticles have to be in contact with bacterial cells. There are certain forms of contact which are accepted e.g. van der

Waals forces (123), electrostatic attraction (124), hydrophobic (125) and receptor–ligand (126) interactions. After this nanoparticles, enter the cell membrane and affect its shape and function. Afterward, an interaction of NPs with the basic components (i.e. enzymes, ribosomes, lysosomes, and DNA) of the bacterial cell takes place, causing oxidative stress, permeability changes in cell membrane, heterogeneous alterations, disorders in electrolyte balance, protein deactivation, inhibition of enzymes, and changes in gene expression (127). Oxidative stress (128), non-oxidative mechanisms (129) and metal ion release (130) are among the most frequently projected mechanisms in contemporary research.

Oxidative stress induced by ROS, is the most significant of NPs' antibacterial mechanisms. ROS term is commonly used for reactive intermediates and molecules, whose potential positive redox is strong. The four types of ROS include, the hydroxyl radical ( $\cdot\text{OH}$ ), superoxide radical ( $\text{O}_2^{\cdot-}$ ), singlet oxygen ( $\text{O}_2$ ) and hydrogen peroxide ( $\text{H}_2\text{O}_2$ ).  $\text{O}_2^{\cdot-}$  can be generated by nanoparticles of calcium oxide and magnesium oxide but zinc oxide nanoparticles can only produce  $\text{OH}$  and  $\text{H}_2\text{O}_2$  and no  $\text{O}_2^{\cdot-}$ . Copper oxide nanoparticles are capable of producing reactive oxygen of all four types. Studies have shown that endogenous antioxidants (particularly superoxide enzymes and catalase) can neutralize  $\text{O}_2^{\cdot-}$  and  $\text{H}_2\text{O}_2$ , which cause less acute stress reactions, whereas  $\text{O}_2$  and  $\text{OH}$  may result in acute microbial death. ROS generation occurs due to oxygen vacancies in the crystal, defect sites and restructuring (131). Clearance and production of ROS, under normal conditions, in the bacterial cells are balanced. On the contrary, ROS are excessively produced, oxidation is preferred by cell's redox balance. This irregular situation produces oxidative stress, damaging bacterial cells' individual components (132).

Oxidative stress might damage the cell membrane of bacteria, as it has been established as a major contributor of varying the cell membrane's permeability (133). Nanosilver particles are used, in air or water, to turn on the oxygen, thus produce reactive oxygen ions and hydroxyl radicals, which kill the bacteria or avert their proliferation (134). ROS work by causing the interaction between bacterial cell and DNA (135), by increasing the level of gene expression for oxidative proteins (leading to cell apoptosis) (136), by attacking essential proteins and periplasmic enzymes in bacterial cells (137). Several mechanisms are involved in the production of ROS by

the nanoparticles. The present mainstream view is photocatalytic hypothesis according to which light energy stimulates the valence band electrons and hole is created in catalytic material which leads to interaction between  $H^+$  and  $H_2O$  or  $OH^-$ , which oxidizes to hydroxyl radical ( $\cdot OH$ ) which reduces to superoxide radical ( $O^{2-}$ ) after interacting with  $O_2$ . The active components are degraded due to generation of ROS. These active components maintain the microorganism's usual physiological and morphological functions (138). In addition, ultrasonic activation can induce the formation of ROS by dissociating nanoparticles and helping in the penetration through cell membrane.

From metal oxide, metal ions are released slowly and absorbed through the cell membrane, while interacting with functional groups of nucleic acids and proteins, e.g. carboxyl ( $-COOH$ ), amino ( $-NH$ ) and mercapto ( $-SH$ ) groups, causing damage in enzyme activity, altering cell structure and its physiological processes resulting in cell death. The pH in the lipid vesicles is minutely affected by the metal ions and it has a weak antimicrobial activity. That is why, dissolved metal ions cannot be regarded as the foremost antimicrobial mechanism for nanoparticles of the metal oxide (138).

For the study of antibacterial mechanisms of a magnesium oxide nanomaterial, various researchers have employed different techniques, such as flat cultivation liquid proteomics tools, chromatography-mass spectrometry, electron spin resonance, Fourier transform infrared analysis and transmission electron microscopy. The mechanisms are not associated with the membrane lipid peroxidation, or oxidative stress. In this case, instead of increase in the quantity of protein associated with ROS, in the cell, many critical cellular metabolic processes involving proteins, e.g. metabolisms of amino acid, energy, carbohydrate, and nucleotide, are considerably reduced (129).



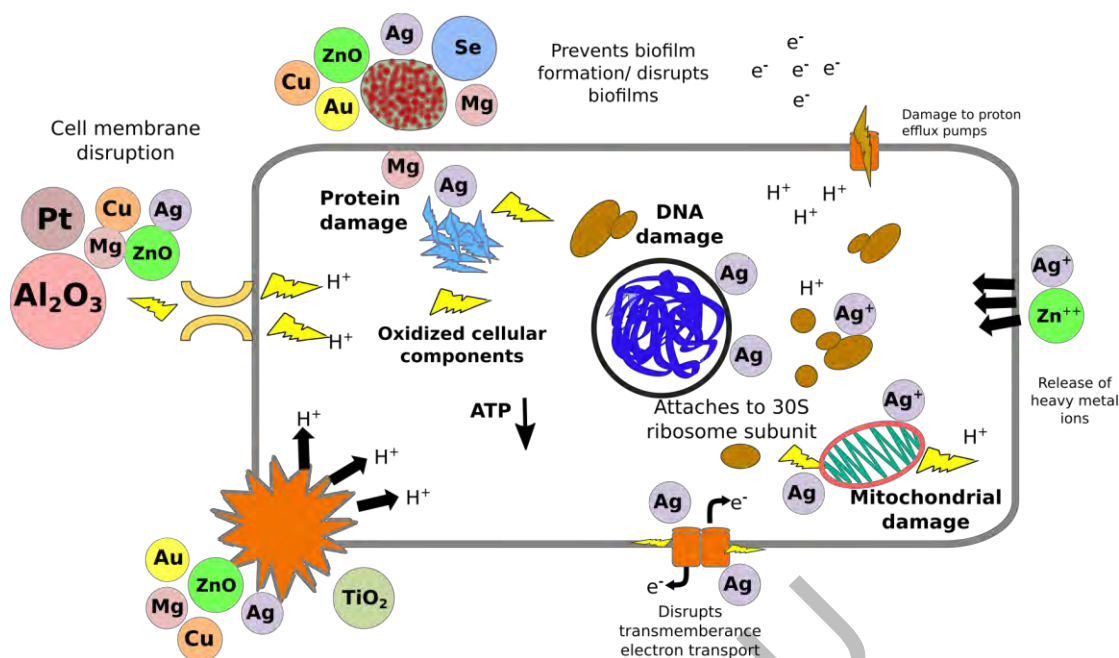


Figure 2.4. Proposed antibacterial effects caused by nanomaterials: inhibition of biofilm formation, generation of free radicals, disruption of cell signaling, damaging cell proteins, release of metal ions from nanomaterial.

### 2.3.2 Mechanism of antifungal mode of action

#### 2.3.2.1 Mode of Actions of antifungal drugs:

At present, the classes of anti-candidiasis drugs are restricted to a small number i.e including allylamines, azoles, echinocandins and polyenes (139). The antifungal targets include, synthesis of  $\beta(1,3)$ -D-glucan, mitochondria, mitosis, ergosterol, proteins and nucleic acids (Figure 2.5). Arylamidine, an antifungal, accumulates selectively in *C. albicans* by disrupted yeast mitochondrial function and transporter-mediated systems (140).

Griseofulvin, is used against skin/nails ringworm (fungal infection) in both humans and animals, was reported for binding with tubulin, affecting microtubule function and inhibiting mitosis in fungal cells (141) (142). Fungal cell wall which contains  $\alpha$  and  $\beta$  glucans, chitin, and mannan is also a well-known drug target, due to lack of any equivalent in mammalian cells. Echinocandins, by inhibiting  $\beta(1,3)$ -D-glucan synthesis and disrupting structure of cell wall, may result in death of fungal cell (143, 144).

Ergosterol, somewhat like human cholesterol, one of the major components of cell membrane of fungi, plays a key role in growth of fungal cell. Polyene drugs (like amphotericin B), develop channels on fungal cell membranes, bind to ergosterol,

resulting in release of inner components (145, 146). The antifungal class, azoles, targets ergosterol biosynthesis (147).

Sordarin as fungicide, in yeasts, can inhibit protein synthesis by stabilizing the ribosome/EF2 complex (148, 149). Synthesis of RNA and DNA is a potential target of antifungal agents. For example, a fluorinated pyrimidine analog, 5-fluorocytosin (5-FC), an antifungal drug, can enter into cells and convert into 5-fluorouracil triphosphate (5-FUTP) or 5-fluorodeoxyuridine monophosphate (5-FdUMP) to stop RNA/DNA synthesis (150).

### 2.3.2.2 Mechanism of action of nanomaterials as antifungal agent

In a previous study, silver nanoparticles were seen to have antifungal effect against *Candida albicans* by disrupting the cell membrane structure and inhibiting the budding process by destructing fungal membrane integrity (151). In another study, ZnO nanoparticles showed greater antifungal activity against *Colletotrichum gloeosporioides* that cause anthracnose in papaya and avocado. ZnO nanoparticles inhibited spore germination and caused hyphal deformation (152).

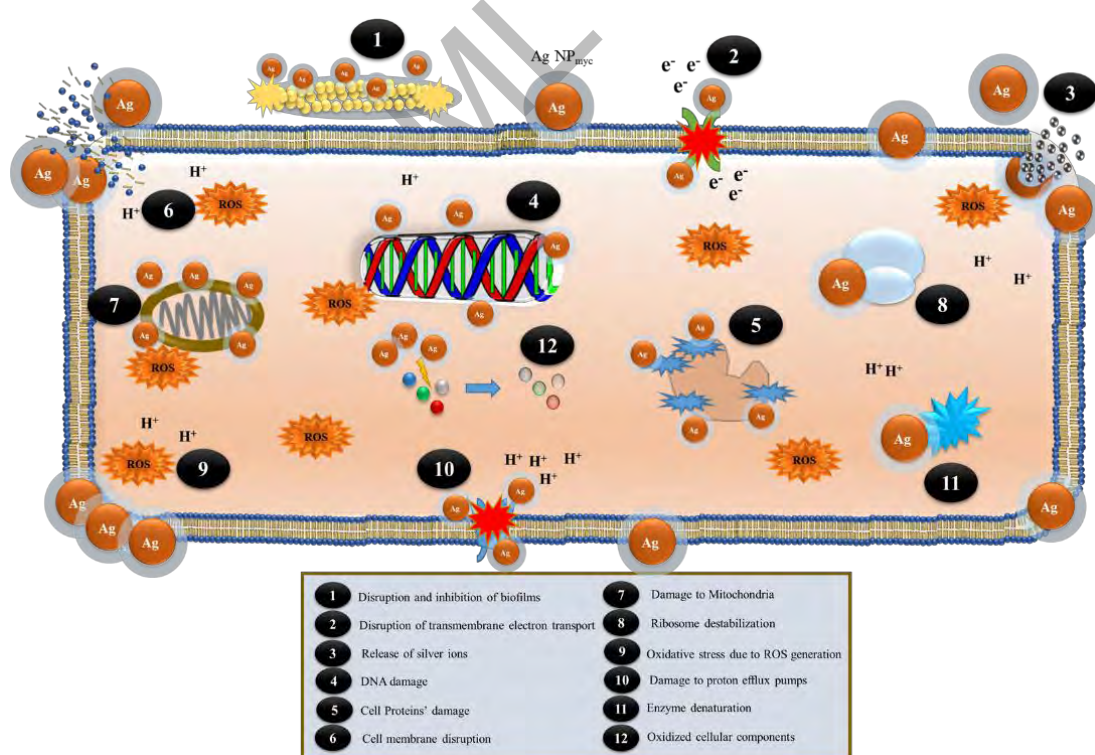


Figure 2.5. Antifungal drug resistance and drug target mechanisms by metal nanoparticles.

### 2.3.3 Mechanism of antibiofilm mode of action

#### 2.3.3.1 NPs inhibit the formation of bacterial biofilms

Bacterial high resistance to unfamiliar chemicals is because of biofilm structure. Past reports confirmed the interference of nanoparticles with biofilm integrity followed by an interaction with its extra-polymeric substances (153). Silver nanoparticles inhibit the EPSs formation, which acts against the drug-resistant strains biofilms of *Klebsiella pneumonia* and *E. coli* (154). The bacterial biofilms inhibition by NPs is related to the regulation of bacterial metabolism. For example, the role of potassium ion channels was recognized in bacterial long-distance conduction of electrical signal in biofilm (155). Moreover, the bacterial metabolic activities inside and outside the biofilm are organized by potassium ions diffusion. It was revealed that magnesium nanoparticles can adhere and diffuse to biofilms, which causes membrane potential disruption, DNA binding, and improved lipid peroxidation. Disorder in regular performance of these processes might lower bacterial ability of biofilm formation (156). It was seen in a study that the amounts of zinc oxide and silver nanoparticles were nearly equal for inhibition of growth and metabolic activity (120).

Although the exact mechanisms of action of AgNPs against infectious microbes are poorly understood but various mechanisms have been suggested as given in the following:

- i. Physical interference by altering the membrane permeability
- ii. Transport of nanoparticles inside microbial cells
- iii. Interference of silver with DNA replication machinery leading to DNA damage, mutation
- iv. Denaturation of proteins structural as well as functional leading to the inhibition of oxidative enzymes.
- v. Nanoparticles generating reactive oxygen species (ROS) causing cytotoxicity by oxidative stress

Interaction of bacterial membrane and intracellular organelles including proteins with silver particles, largely with the phosphorus-containing DNA and sulfur containing membrane proteins may lead to the interruption of cell division and consequently

death of the cell. Biocidal ionic silver is released from nanoparticle surfaces in control manner, its presence results in effective and long term inhibition (157).

### 2.3.3.2 Nanoparticles inhibit the formation of fungal biofilms

Biofilm development in yeast like fungi comprises the main phases of microbial cell adhesion, cell organization and discrete colony formation, phenotypic switching and EPS secretion, maturation into a three-dimensional structure and cell dispersal (158).

Combination of anti-*Candida* therapies, mouth rinses, denture cleansers and antifungal lock therapy, have been suggested as alternatives for disrupting candida biofilms on various substrates. Also for candidiasis management, the use of natural compounds is also a proposed approach, for example anti-*Candida* antibodies and vaccines, plants oils and extracts, antifungal quorum sensing molecules, probiotics, cytokine therapy, photodynamic therapy, nanoparticles and primed immune cells transfer (159).

In a study involving effect of silver nanoparticles on biofilms, it was noticed by SEM analysis that nanoparticles inhibited hyphal growth, affected secretion of exopolymeric substances, targeted cell walls causing cell disruption (40). Earlier work on biofilms of *C. albicans* also revealed morphological and EPS alternation by silver nanoparticles (160, 161). Silver nanoparticles also affect membrane permeability (162), inhibition of enzymes in respiratory and replication processes. Binding of nanoparticles to phosphorus-containing molecules (DNA) and sulfur-containing proteins in cellular membrane results in loss of intracellular functions (163). In another study, inhibitory effect of mycogenic AgNPs were explored in-vitro against biofilm growth and aspartyl proteinase enzyme (SAP) activity in *C. albicans* and non-*albicans* (164).

## 2.4 Safety and sustainability

Biosafety and biocompatibility are major aspects, taken into account, in almost all medical and biological applications. Nanotoxicology is the study of biological system- nanostructures interactions, explaining the relationship between the chemical and physical properties viz. surface chemistry, size, shape, composition and aggregation with induction of toxic biological responses (165). Nanotoxicological

studies are used to determine whether and to what degree these properties may cause a threat to the environment and to human health (166). In vivo toxicity analysis is studied through cell lines, brine shrimp larval hatching, larval morphological abnormalities, mitochondria damage, stress response, ROS generation, cellular apoptosis, cell growth, RBC lysis, reporter genes for sublethal effects, DNA damage, assessment of inflammation and hemolysis etc.

In this perspective, nanoparticle toxicity is the ability of the particles that enables them to affect the normal physiology badly and also to disturb the regular structure of tissues and organs of human and animal, directly. Toxicity is dependent on physicochemical parameters i.e. shape and size of the particle, surface charge and chemistry, stability and composition of nanoparticles (167).

Chemical composition determines the chemistry, energy and defects of the surface, potential of photoactivation, redox status, surface groups and charge that define “surface reactivity”, so its significance is definite. Foremost determinants of hazard generation are suspension stability, wettability, solubility, durability, and shedding of toxic ions, which are determined by material chemistry and surface coatings. Although the increase in surface area and nano size adds to surface reactivity, other physicochemical properties (e.g., shape, dimension, state of agglomeration, surface coating crystal structure and surface charge) are important modifiers of effects of composition and surface reactivity. Therefore, toxicity of nanomaterial can be attributed to non-specific biological responses to shape, size and bio-persistence of material, but can also result from specific biological interactions generated from a release of toxic ions, ligands or reactive surface impacting definite toxicological pathways (168).

Toxicity assessment is principally based on the structural complexity and physicochemical composition of the nanomaterial (Figure 2.6) (169). For example, studies have reported that for induction of toxic effects, dose-response relationship depends upon the number of functional groups on the particle surface (170), particle number (171) and surface area of nanomaterials (172) mainly for low toxicity and less soluble particles (173).

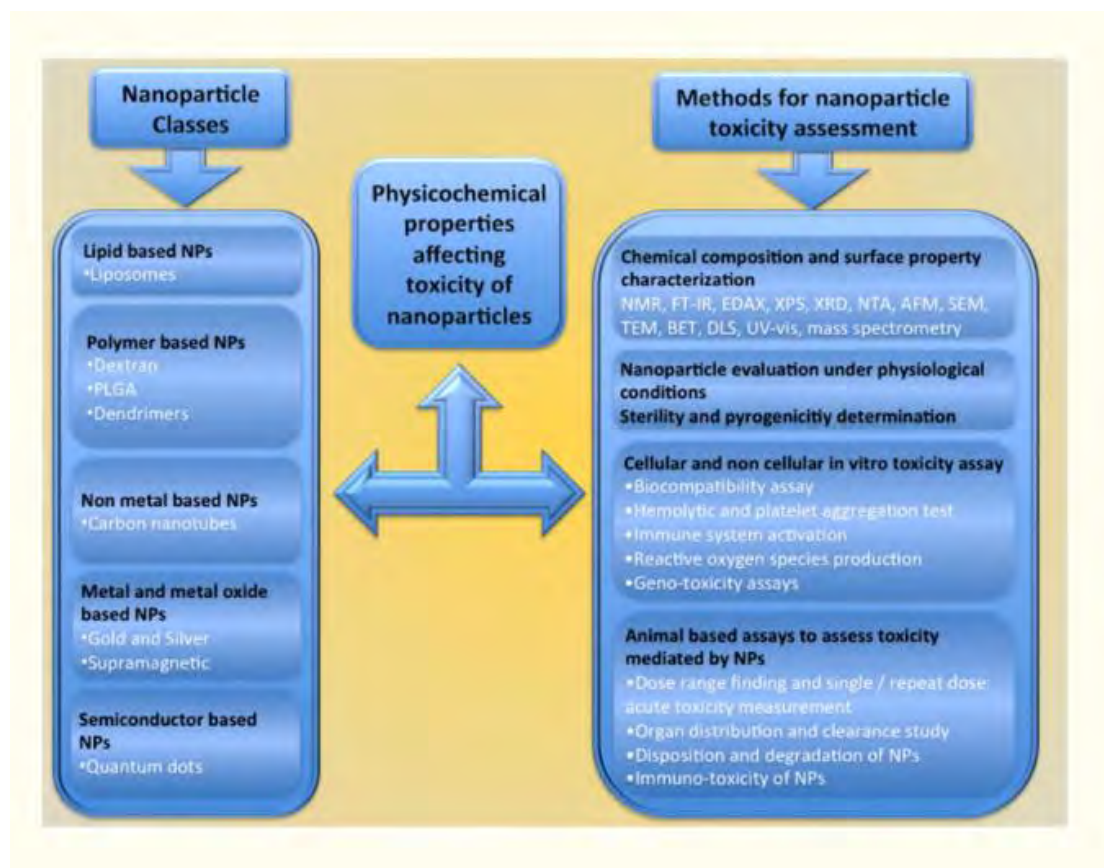


Figure 2.6. Diagram showing classes of nanoparticles, properties affecting nanoparticle toxicity and methods for assessing nanoparticle based toxicity.

Mechanisms behind the interaction between living systems and nanoparticles are poorly understood (174). The complication comes when particles bring change in the surface characteristics of the biological matter, after binding and interacting with them, depending on their environment. A good deal of scientific knowledge regarding mechanisms of nanoparticle cell interaction has been gathered in past few years, which demonstrate that nanoparticles are taken up by the cells via either active or passive mechanisms. Normally, characterization of toxicants in classical toxicology is protocolised with a well-established set of existing methodologies, based on dose metric. In case of nanotoxicology, the dose metric is not clear-cut. Though, in nanotoxicology the dose metric is not clear-cut, as discussed below. Additionally, the bioassays protocolization concerning nanomaterials is still under progress and generally not widely accepted on international level. While working with nanomaterials, several variables are taken into account, including material, surface, size, shape, coating, charge, dispersion, agglomeration, concentration, aggregation, and matrix. The complexity multiplies when moving from in vitro to in vivo models.

Hazard identification at in-vivo level, with respect to nanomaterials, is still on its initial stage.

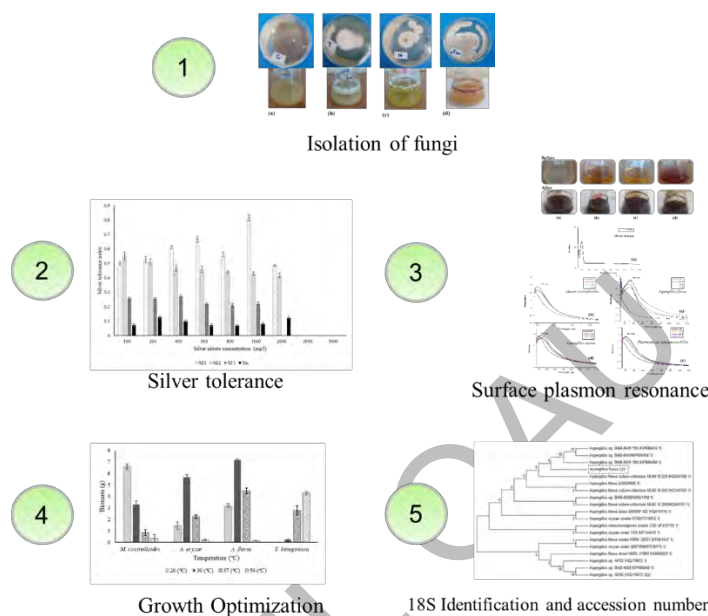
*Cytotoxicity.* The severity of toxicity varies, according to administration mode and deposition sites. Thus, in order to maintain medical relevance, a system-based approach is used to present information on toxicity, with focus on lung, liver, dermal, and nervous system targets.

*Neurotoxicity.* There are two parts of central nervous system: the brain and the spinal cord. Both must be protected from the injury to xenobiotics. Recent studies suggest that nanoparticles, e.g. pegylated PLA immunonanoparticles and polysorbate 80-coated PBCA nanoparticles, accumulate in the brain after crossing blood brain barrier (175) through intravenous administration. When nanoparticles enter the brain, their special physicochemical properties, (e.g. large surface area) may result in neurotoxicity. That is why, the potential neurotoxic effects of these NPs on CNS function are direly in need of evaluation, as exact pathways and mechanisms through which toxic effects of NPs may put forth, are mostly unidentified (167). Risk assessment needs a detailed study of properties, including: particle size, surface area, surface properties, solubility, stability, chemical reactivity etc. (176).

DRSML QAU

## Chapter 3: Isolation, screening and selection of fungi for silver nanoparticles' synthesis

### Graphical Abstract



### 3.1 Introduction

Due to their efficient antimicrobial potential, silver nanoparticles are widely used in biomedical applications such as implants, bandages, implants, coatings etc., clothing, water purification etc. (177) (178). Silver ions (free) are reported to have lower antimicrobial properties in comparison to silver nanoparticles (179). Many microbial species have been reported in literature for silver nanoparticles formation (180).

Fungi belong to versatile group of microorganisms who can withstand adverse life circumstances, sturdy thermal gaps, extreme temperatures, nutrient deficit and desiccation. However, the mechanisms developed by fungi to grow and survive under hostile environments of high metal concentrations make them a focal point to be applied in interesting research studies (181). Fungi are known to create around 6400 bioactive substances (182). Fungi can give an important route for nanoparticle synthesis due to their high binding capacity, secretion of significantly higher quantities of proteins while being more advantageous with respect to bacteria and



plants, due to higher ability to withstand agitation, high flow pressures (because of mesh-like mycelia), and adverse conditions in bioreactors (183).

Heavy metals in the extreme environments are considered as important stress factor (exogenous), and is area of active research on effect of metal ions on fungal physiology. Fungi develop specific biochemical/genetic resistance mechanisms when exposed to various types of metals (59). These mechanisms might include intracellular deposition, extracellular binding, complexation or precipitation, altering the redox state of metal ions, cellular efflux pumping system (60). For most of the metals, establishing this resistance and homeostasis involves combinations of the above mentioned mechanisms (68).

The present study aims to determine the potential of extracellular synthesis of silver nanoparticles and phylogenetic analysis of culturable isolates of metal resistant fungi isolated from soil samples of Neelam Valley, Khewra mines and metal industrial waste. This investigation provides a comparative study of culturable fungal diversity of different habitats. Objectives of current study are given below.

### **Objectives:**

- To isolate indigenous fungi from different soils, which will be efficient in silver tolerance.
- To screen and select fungi on the basis of high silver tolerance.
- To screen isolated fungi for silver transformation (reduction) extracellularly.
- To optimize the growth conditions of the separated strains for their optimum performance.
- To identify the fungi by 18S sequencing and perform phylogenetic analysis.

## **3.2 Material and methodology**

### **3.2.1 Collection of soil samples**

Strictly following to aseptic procedures, three samples were collected at 10 cm deep from each soil source using gloves and stored in polyethylene zipper bags (sterilized). and transported with care back to Department of Microbiology, Quaid-i-Azam University, Islamabad. Samples were kept at 4°C till further use.

In order to determine the metal ions concentration in soil samples, atomic absorption spectrometry was performed. First the soil samples were dried at room temperature then each sample (1 g) was acidified with 5 ml of HNO<sub>3</sub> and 10 ml of 70% HClO<sub>4</sub>. This mixture was digested by heating till white fumes emerged (RAURET 1998), cooled at room temperature, filtered and boiled again to remove oxides of chlorine and nitrogen. Finally, digested soil mixtures were sent for atomic absorption spectrophotometry using Perkin-Elmer 460 Spectrophotometer. In each sample, metal ion analysis of Ni<sup>+2</sup>, Cu<sup>+2</sup>, Zn<sup>+2</sup>, Cr<sup>+2</sup>, Pb<sup>+2</sup>, Mn<sup>+2</sup>, Fe<sup>+2</sup> and Cd<sup>+2</sup> was carried out.

### **3.2.2 Fungal isolation and selection based on metal tolerance**

Fungi were isolated from different geological conditions for studying the potential of silver tolerance and extracellular silver reduction. Following sites were selected for isolation of indigenous fungi.

#### **3.2.2.1 Salt mine**

Soil samples were collected from salt range Khewra, Chakwal, Pakistan and enriched in liquid culture media for 24 hours, serially diluted and inoculated on agar plates. Sabouraud dextrose broth culture media supplemented with NaCl (10%) and ampicillin (100 µg/ml) was used for enrichment and maintenance of isolates. Cultures were grown at 25 °C for two weeks. Colony morphology was observed on plates of Sabouraud dextrose agar (SDA) supplemented with NaCl (5%) and ampicillin (100 µg/ml) (184). The soil samples were named as KS (after Khewra Soil).

#### **3.2.2.2 Metal industrial waste:**

Soil samples were collected in sterilized polythene bags from the “Industrial waste of Hummak, Islamabad” and transported to laboratory. One gram of soil was serially diluted; the dilutions were used to spread on nutrient agar plates. The plates were incubated at 37°C for 24-48 hours. The soil samples were named as MS (after Metal Soil).

#### **3.2.2.3 Mountains Neelam Valley (Kashmir)**

Fungi were isolated by spreading soil on nutrient medium Sabouraud Dextrose Agar (SDA). The plates with growth medium were incubated at 4 and 15°C. From each plate, morphologically distinct colonies were subcultured. Later, fungal isolates were

inoculated for preservation on SDA slants and stored at 4°C for future use. The soil samples were named as NS (after Neelam Soil)

#### **3.2.2.4 Thermophilic fungus:**

*Thermomyces lanuginosus* STm was obtained from Department of Microbiology, Quaid-i-Azam University Islamabad which was previously isolated from garden soil samples from Multan city, Pakistan (185).

### **3.2.3 Silver resistance potential**

Stock solution of silver nitrate (1000 ppm) was prepared in deionized water. Effect of metal ions on fungal strains was determined by inoculating five mm disks of 4 days old pure fungal cultures on SDA agar plates supplemented with variable concentrations of silver nitrate solution (100, 200, 400, 600, 800, 1000, 2000, 3000 and 5000 mg/lit) and incubated at 30°C for 7 days. In parallel, cultures without metal salts were kept as control. The mean diameter of radial growth from triplicate cultures (in millimeters) was recorded for each plate after 7 days. Silver resistance of fungal isolates was determined by measuring minimum inhibitory concentration of silver ions and silver tolerance index (186).

The tolerance index ( $T_i$ ), an indication of the organism response to metal stress was calculated from the growth of strain exposed to the metals divided by the growth in the control plate. The higher the  $T_i$ , the greater the metal tolerance (187).

$$T_i = \text{Diameter of silver treated fungus} / \text{Diameter of untreated (control)} \times 100$$

Based on the highest silver tolerance, one fungal isolate (KS3, NS3, MS1) from each source was selected for further silver reduction test.

### **3.2.4 Optimization of growth conditions for metal tolerant fungi**

#### **3.2.4.1 pH optimization for fungal growth**

The fungal strains were grown in SDB media having different pH values (4, 5, 6, and 7 and 9) to analyze for optimum pH for their growth.

#### **3.2.4.2 Temperature optimization for fungal growth**

The fungal strains were grown at different temperatures; 20°C, 30°C, 37°C and 50°C to find the optimum temperature for their growth.

### **3.2.5 Extracellular screening of silver ions reduction**

Fungi-mediated extracellular reduction of silver ions was carried out using *in vitro* method by using fungal aqueous filtrate, where previously the mycelia was kept suspended (188). Fungal cultures were grown in nutrient rich MGYP media containing 0.3% malt extract, 1% glucose, 0.3% yeast extract and 0.5% peptone. pH of culture medium was adjusted using NaOH (1M). Culture media was incubated for 72 h at optimized temperatures according to the fungal strains. After incubation, mycelia were centrifuged at 5000 rpm and 4 °C for 20 min and washed with distilled water to remove media components. After washing, mycelia (20g) was suspended again in sterile water (100 ml) and was put onto a shaker at optimized temperatures according to the fungal strains at 200 rpm, 24 h. After this, fungal biomass was filtered using sterile filter paper to obtain cell free filtrate. This filtrate was added with an equal volume of AgNO<sub>3</sub> solution (final concentration 0.1 M) and was put onto a shaker at optimized temperatures according to the fungal strains for 96 h at 200 rpm. In order to screen the silver reduction, aliquots from reaction mixture were periodically subjected to UV–Vis spectroscopy.

### **3.2.6 Identification of fungal isolates**

Colony morphology of fungal colonies growing on Sabouraud dextrose agar plates were observed. Phase contrast microscopy was utilized to determine the structure of hyphae and fruiting bodies of living cells blue (usually contained in culture) after staining with lactophenol cotton (Labomed Lx400). The metal tolerant fungal isolates were inoculated on SDA culture plates with range of pH (4.0-7.0) and temperature (20-50°C), for 4 days to determine physiological characteristics in the form of optimum growth conditions.

### **3.2.7 Molecular identification using 18s rRNA gene sequencing technique**

#### **3.2.7.1 Fungal DNA extraction**

Approximately 200 mg of mycelia was frozen at -20°C and grounded in chilled pestle and mortar by adding 5.0–6.0 ml of CTAB buffer. It was then incubated at 65°C for 30 minutes. After incubation, mycelia were centrifuged at 10,000 rpm for 10 minutes. Supernatant was mixed with equal volume of chloroform-isoamyl alcohol (24:1) and centrifuged at 10,000 rpm for 10 minutes. Chloroform isoamyl alcohol acted as a

detergent and precipitated the proteins and lipids of the cell membrane to let the cell DNA dissolve into left-over aqueous phase. The lowest organic layer along with the precipitated protein-lipid white layer was discarded and upper aqueous supernatant was collected. In supernatant phenol-chloroform (1:1) was added and then it was centrifuged at 14000 rpm for 16 minutes. Phenol removed protein impurities and chloroform prevented DNA shearing during extraction procedure. Lower organic phase and interphase of precipitated proteins were discarded and upper aqueous phase was collected. In collected supernatant chilled isopropanol was added in equal volume to that of supernatant and centrifuged at 14000 rpm for 15 minutes. Centrifugation was carried out at lower temperature (4 °C) to let the pellet stick to the bottom wall of eppendorf. The purpose of using isopropanol was that it precipitated DNA from the solution in the form of a pellet. Supernatant was discarded and pellet was washed with absolute ethanol (500 µl). Then the pellet was re-dissolved in 50-100 µl 1x TE buffer and about 15-20 µg/ml (10 µl) RNase was added to remove the contamination of RNA and get pure DNA. The freshly isolated DNA was kept in refrigerator until future use.

### **3.2.7.2 Gel electrophoresis**

1X agarose gel (0.4 g agarose in 1X TBE buffer) was prepared to run fungal DNA bands at 100 volts, 400 milli-amperes current for 40 minutes.

### **3.2.7.3 Sequencing and Phylogenetic analysis of fungal isolates**

The selected organisms were identified on the basis of partial sequencing of their internally transcribed spacer (ITS) (189) regions (5.8S and 18S rRNA) in the extracted DNA. For sequencing, these ITS regions were identified with the help of universal primers i.e. ITS-1 (5'-TCCGTAGGTGAACCTGCGG-3') and ITS-4 (5'-TCCTCCGCTTATTGATATGC-3'). The procedure of Anderson *et al.* was used for extraction of genomic DNA (190). After purification of PCR product, the sequencing was carried out. Sequence alignment was carried out through NCBI BLAST tool and phylogeny was determined for homologs using Molecular Evolutionary Genetic Analysis (MEGA). Neighbor-joining tree was constructed on the basis of a maximum likelihood, to identify the isolated fungi. The gene sequences were submitted to NCBI GenBank for assigning of accession numbers.

### **3.2.8 Statistical analysis**

Statistics was applied on results of metal tolerance index and ionic silver reduction into nanoparticles. All values were expressed as mean ( $\pm$ ) standard deviation (SD) of triplicate samples in a representative experiment. All experiments were done independently at least three times.

### 3.3 Results

#### 3.3.1. Metal Analysis of Soil Samples

Large temperature oscillations were attributes of the sampling areas. Figure 3.1 presents concentration of heavy metals in soil (ppm) samples, collected from three different places. The samples from metal industrial waste showed higher concentration of  $Mn^{+2}$ ,  $Fe^{+2}$  and  $Zn^{+2}$ , samples from Neelam Valley showed high concentration of Zn and Cr and samples from Khewra mines showed high concentration of  $Mn^{+2}$ ,  $Fe^{+2}$  and  $Zn^{+}$  and  $Pb^{+2}$ .

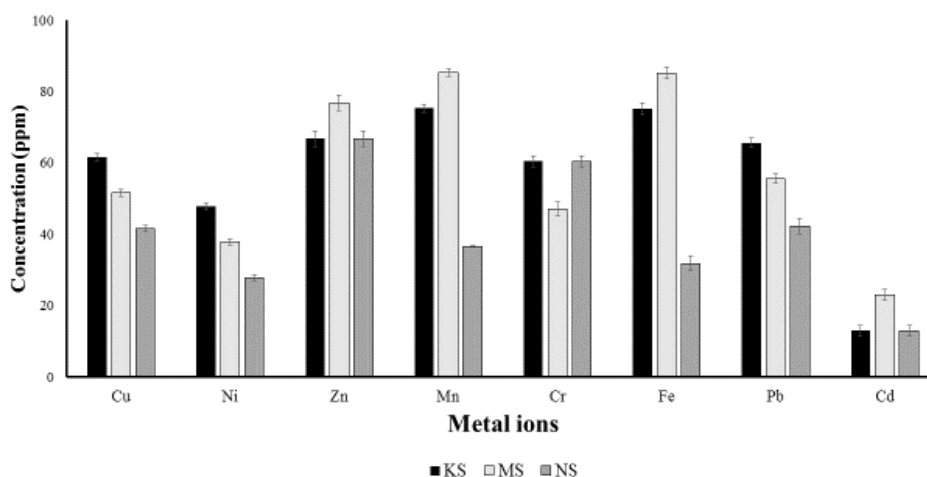


Figure 3.1. Concentration of metal ions (ppm) in samples from different soils.

Note: The bars represent the mean values of concentration of metal ions in parts per millions, the error bars represent standard error being calculated after taking average of three replicates of each sample and calculating standard deviation. KS: Khewra Soil, MS: Metal Soil, NS: Neelam Soil (details are given in section 3.2.2)

#### 3.3.2. Isolation of silver resistant fungi

To observe metal tolerance, fungal isolates were grown at different silver ion concentrations. The results demonstrated that different fungi showed different silver tolerance pattern. The majority of the fungal strains were sensitive to silver concentrations higher than 1000 mg/lit. Some were sensitive, moderately resistant and

resistant and behaved differently against different concentration. Fungi inhabiting soil are able to survive under metals' presence by physiological adaptation that gives metal sorption capacity to fungi. Based on the highest silver tolerance on solid growth media, one fungal isolate (KS3, NS3, MS1) from each source was selected and further silver reduction test in liquid media was performed.

Table 3.1. Location of site showing the name of isolates

Sr. No.	Location of isolates	No. of Isolates
1	Neelam Valley (Kashmir)	NS1, NS2, <b>NS3</b> , NS4
2	Khewra mines (Kalarkahar)	KS1, KS2, <b>KS3</b> , KS4, KS5
3	Metal/industrial waste	<b>MS1</b> , MS2, MS3, MS4, MS5
4	Department of Microbiology, Quaid-i-Azam University, Islamabad	<i>Thermomyces lanuginosus</i> STm

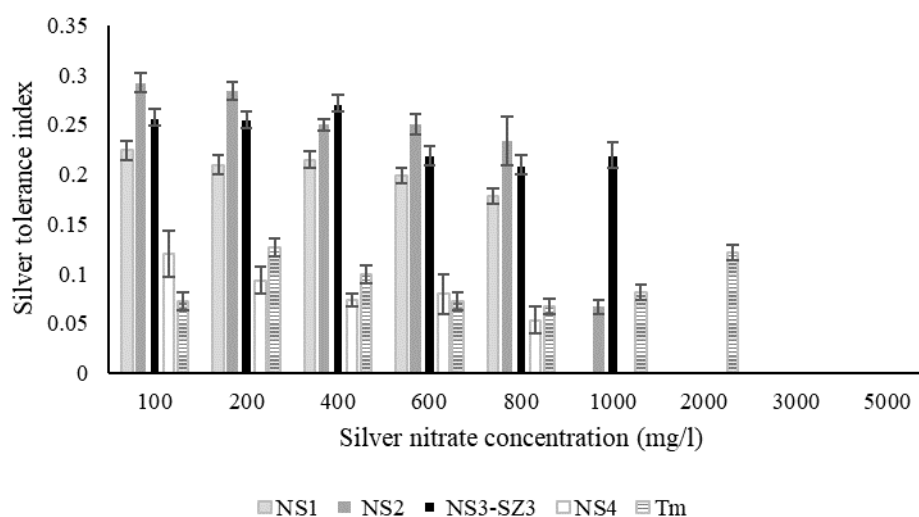


Figure 3. 2. Silver tolerance index for NS isolates

Note: The bars represent the mean values of silver tolerance index (it has no units), the error bars represent standard error being calculated after taking average of three replicates of each sample and calculating standard deviation. NS: Neelam Soil (details are given in section 3.2.2), Tm: *Thermomyces lanuginosus* STm.

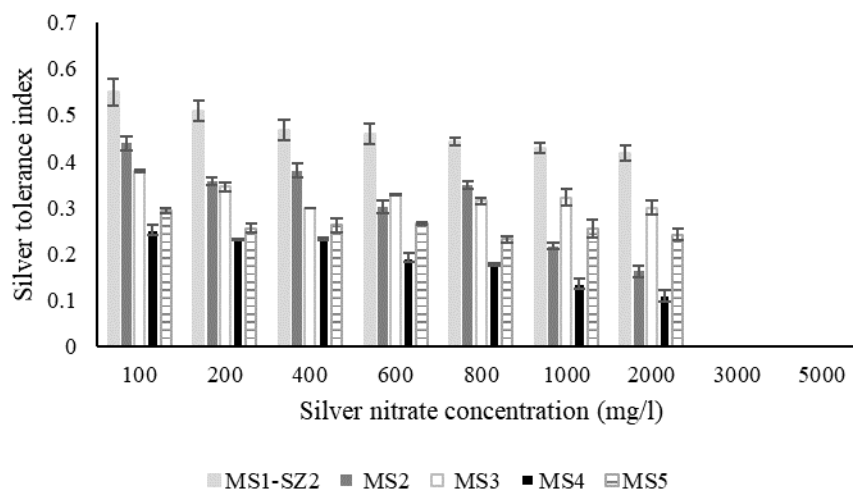


Figure 3.3. Silver tolerance index for MS isolates

Note: The bars represent the mean values of silver tolerance index (it has no units), the error bars represent standard error being calculated after taking average of three replicates of each sample and calculating standard deviation. MS: Metal Soil (details are given in section 3.2.2).

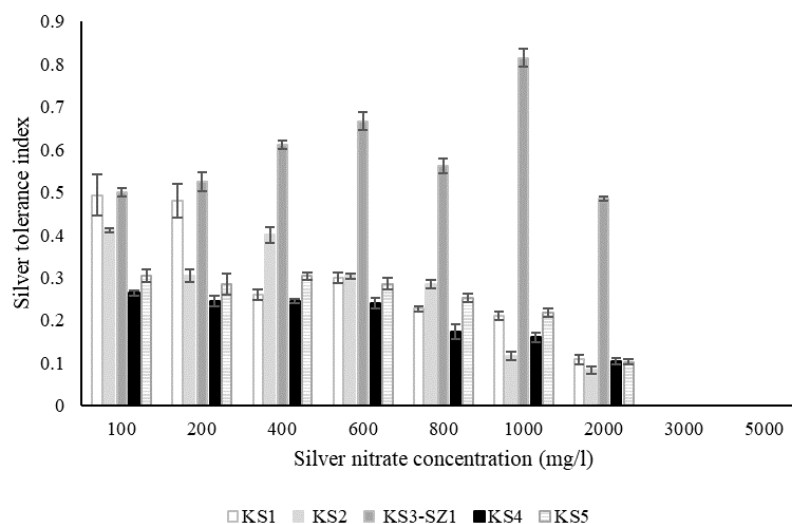


Figure 3.4. Silver tolerance index for KS isolates

Note: The bars represent the mean values of silver tolerance index (it has no units), the error bars represent standard error being calculated after taking average of three replicates of each sample and calculating standard deviation. KS: Khewra Soil (details are given in section 3.2.2).



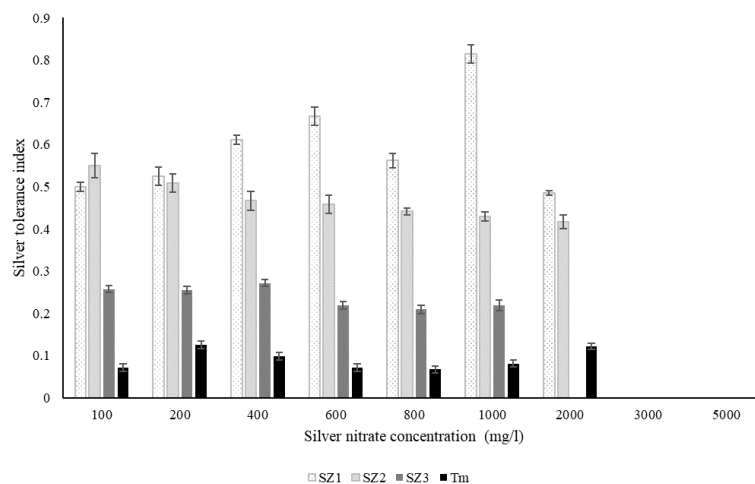
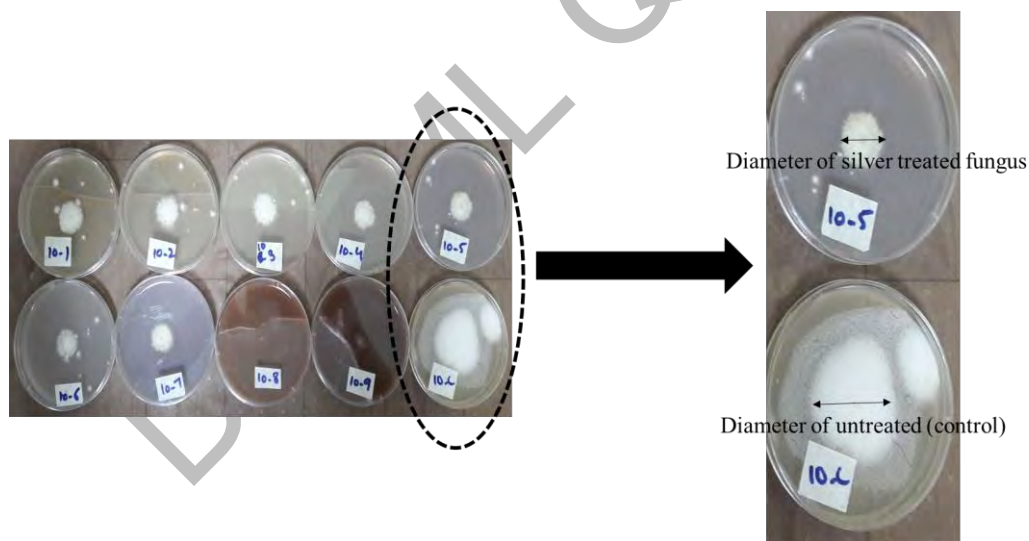


Figure 3.5. Silver tolerance index for selected fungal isolates

Note: The bars represent the mean values of silver tolerance index (it has no units), the error bars represent standard error being calculated after taking average of three replicates of each sample and calculating standard deviation. NS: Neelam Soil (details are given in section 3.2.2), Tm: *Thermomyces lanuginosus* STm. SZ1, SZ2 and SZ3 are culture codes (details are given in Table 3.2).



$$\text{Silver Tolerance Index (T}_i\text{)} = \frac{\text{Diameter of silver treated fungus}}{\text{Diameter of untreated (control)}} \times 100$$

Figure 3.6. Silver tolerance plate assay against selected fungal isolates. The fungus being shown in the figure is *Aspergillus flavus*.

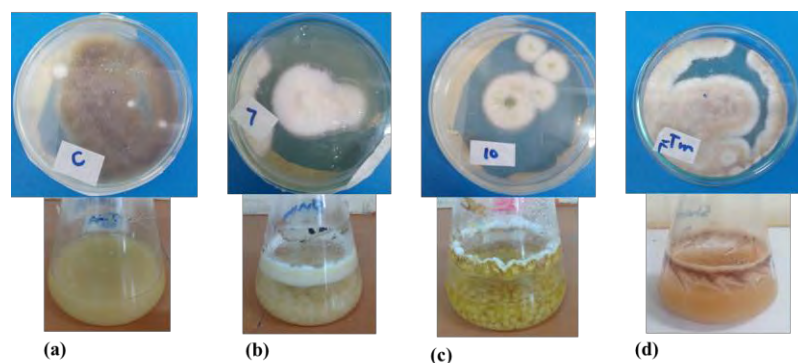


Figure 3.7. Growth of selected fungal isolates on solid and liquid media (a) *Mucor circinelloides* (b) *Aspergillus oryzae* (c) *Aspergillus flavus* (d) *Thermomyces lanuginosus*

### 3.3.4 Optimization of growth conditions for metal tolerant fungi

On optimization the growth conditions of selected fungi for this study, it was found that *M. circinelloides* showed optimum growth at pH 5, *A. oryzae* at pH 7, *A. flavus* at pH 7 and *T. lanuginosus* at pH 5 (Figure 3.8).

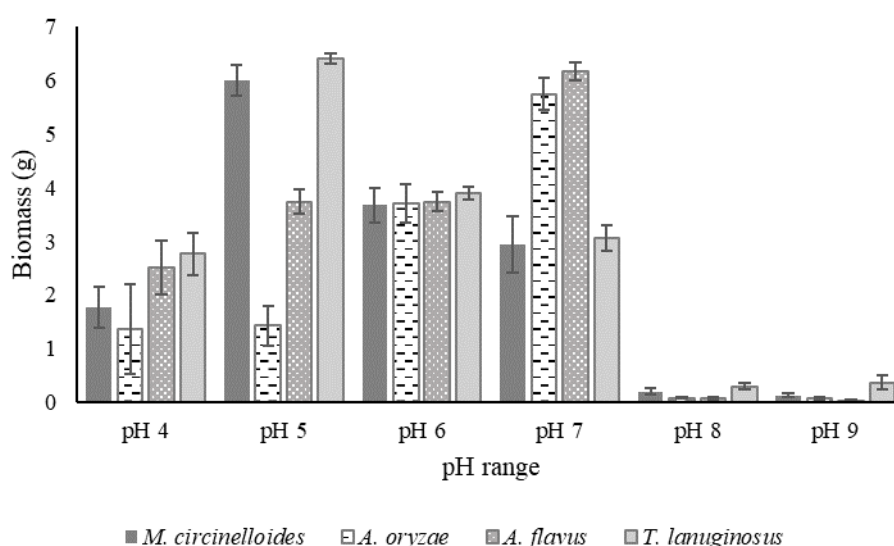


Figure 3.8. pH optimization for fungal growth

Note: The bars represent the mean values of fungal biomass in grams, the error bars represent standard error being calculated after taking average of three replicates of each sample and calculating standard deviation.

In case of temperature, the optimum values were found to be 20 °C for *M. circinelloides*, 30 °C for *A. oryzae* and *A. flavus* at pH 7 and 50 °C for *T. lanuginosus* (Figure 3.9).

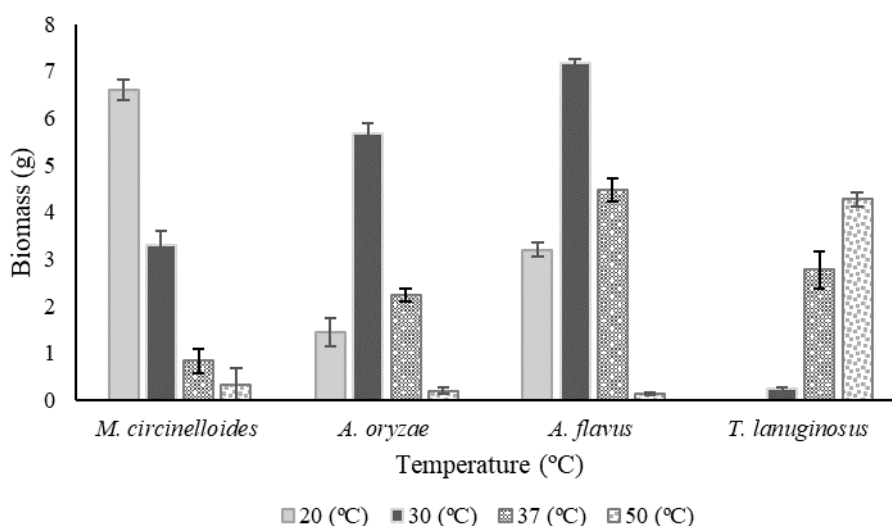


Figure 3.9. Temperature optimization for fungal growth

Note: The bars represent the mean values of fungal biomass in grams, the error bars represent standard error being calculated after taking average of three replicates of each sample and calculating standard deviation.

### 3.3.3 Extracellular screening of silver ions reduction

In order to screen the potential of selected fungi for synthesis of silver nanoparticles, extracellular screening of silver ions was carried out using extracellular fungal growth cultures in liquid medium. The combined solutions of silver ions with fungal extracellular growth media were mixed; incubated and surface plasmon resonance was measured using ultra violet spectroscopy by scanning the solutions between 400 to 500 nm wavelengths. Silver reduction is shown in Figure 3.10. Silver nitrate solution as control was also scanned at the same wavelengths (Figure 3.11a). Surface plasmon resonance results by *Mucor circinelloides* (3.11b) *Aspergillus oryzae* (3.11c) *Aspergillus flavus* (3.11d) *Thermomyces lanuginosus* (3.11e) showed the specific spectra characteristic to silver reduction.

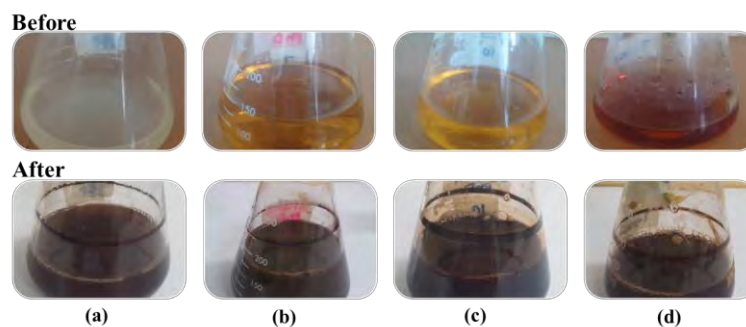


Figure 3.10. Extracellular silver reduction test by selected fungal isolates: (a) *Mucor circinelloides* (b) *Aspergillus oryzae* (c) *Aspergillus flavus* (d) *Thermomyces lanuginosus*

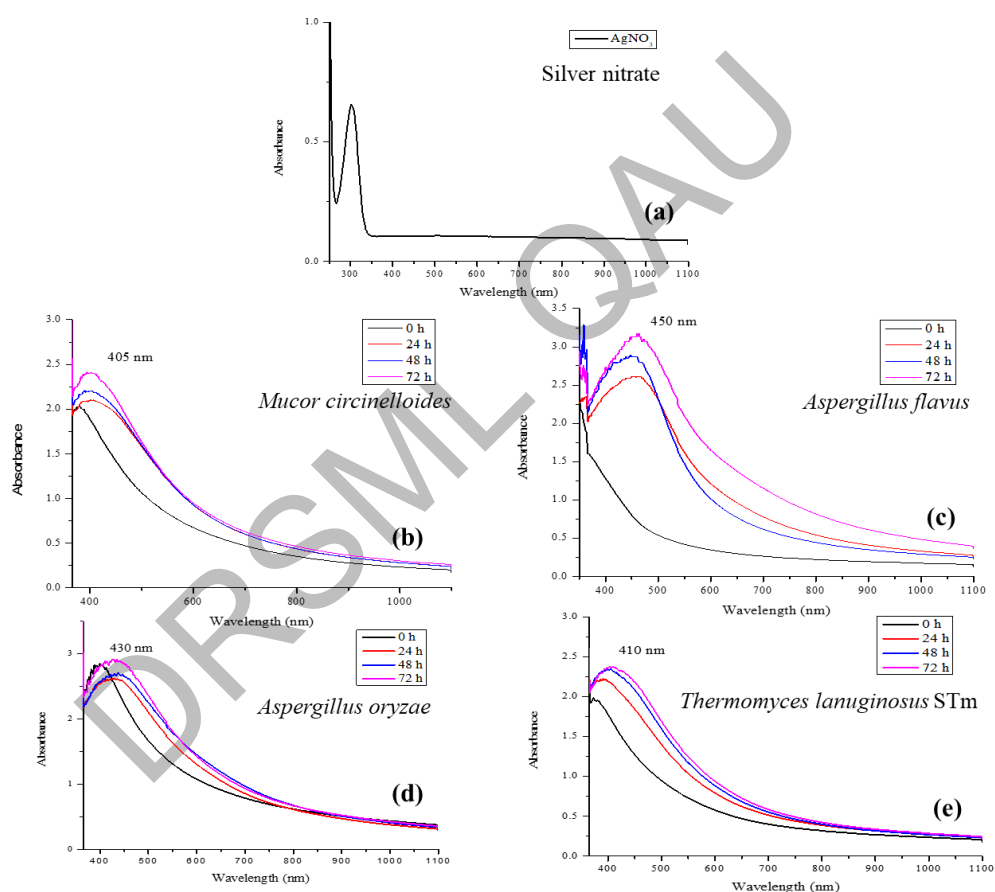


Figure 3.11. UV-Vis spectra for scanning silver reduction between 400-500 nm wavelengths  
Note: The lines represent the values of optical density/absorbance (no units) of samples.

### 3.3.5 Identification of fungal isolates

#### 3.4.5.1. Morphology

The morphology of selected fungi was carried out by observing microscopic and macroscopic growth features that is given in the Table 3.2.

Table 3.2. Growth of selected fungal isolates

Culture code	Selected Isolate	Location of soil	Colony Morphology		Microscopy
			Front	Reverse	
SZ1	KS3	Khewra mines (Kalarkahar)	White, yellowish green to olive green colonies	Saddle brown center with golden edges	Hyphae: hyaline and septate
SZ2	MS1	Metal industrial waste	Parrot green to deep green colonies with smaller conidia	Cream colored. woolly to cottony texture	Septate and hyaline hyphae. Yellow-green conidial colour, globose to sub-globose vesicles
SZ3	NS3	Neelam Valley (Kashmir)	Yellow greyish with raised mycelium	Black center with Off-white edges	Long cylindrical hyphae, globose yellowish brown sporangia
<i>T. lanuginosus</i> STm	-	Department of Microbiology, Quaid-i-Azam University, Islamabad	White and velvety at first, but soon turn dull dark brown when mature.	dark brown to reddish from centre with pink colored diffusing pigments on edges	Colorless un-branched hyphae of young colonies. Dark brown pigmented spores in later stage

### 3.4.5.2 Molecular Characterization and Phylogenetic Analysis of silver resistant fungi

Results of 18s gene PCR were sent for DNA sequencing to Macrogen, Seoul, South Korea. For phylogenetic analysis, sequence results from Korea were compared (Blastn program) with the available sequences of other fungi on the GenBank database of national centre for biotechnology information (NCBI) (191). Bootstrap analyses with 500 replicates were carried out to check the robustness of the trees. Finally, the phylogenetic trees were plotted using the Neighbour Joining plot program.

The partial 18S rRNA gene sequences of the isolated fungi were submitted to NCBI GenBank database and the fungi were identified as *Aspergillus oryzae* (Figure 3.13), *Aspergillus flavus* (Figure 3.14) and *Mucor circinelloides* (Figure 3.15) under the accession numbers MH664050, MH664051 and MH664052, respectively. (Table 3.3).

Table 3.3. 18S rRNA sequence based molecular homology, closest related species, gene bank accession number, growth conditions (pH and temperature) and silver ion reduction potential of metal resistant fungal isolates.

Selected Isolate	Culture Code	GenBank Accession Number	Closest related Species	pH	Temperature (°C)	Silver reduction
KS3	SZ1	MH664050	<i>Aspergillus oryzae</i> SZ1	5	30	Yes
MS1	SZ2	MH664051	<i>Aspergillus flavus</i> SZ2	6	30	Yes
NS3	SZ3	MH664052	<i>Mucor circinelloides</i> SZ3	5	37	Yes
<i>Thermomyces lanuginosus</i> STm	Tm	KJ432867	Previously identified	9	50	Yes

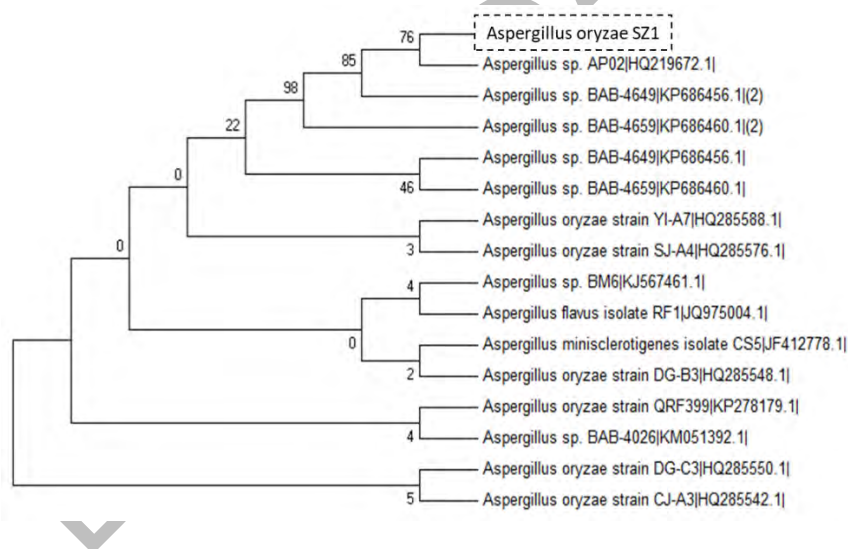


Figure 3.12. Phylogenetic analysis of *Aspergillus oryzae* SZ1 by using Mega 6.1 neighborhood joining method

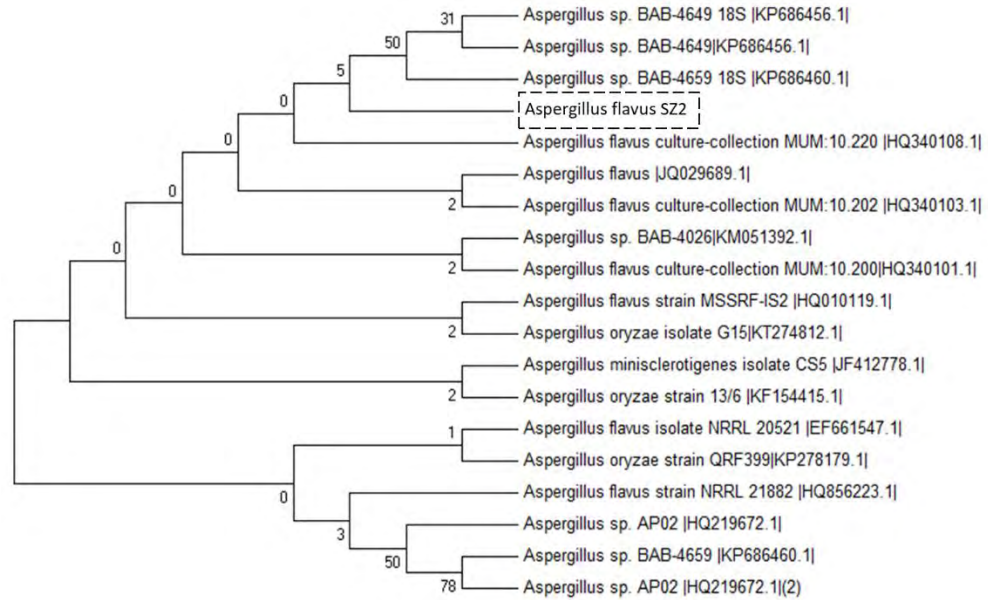


Figure 3. 13. Phylogenetic analysis of *Aspergillus flavus* SZ2 by using Mega 6.1 neighborhood joining method

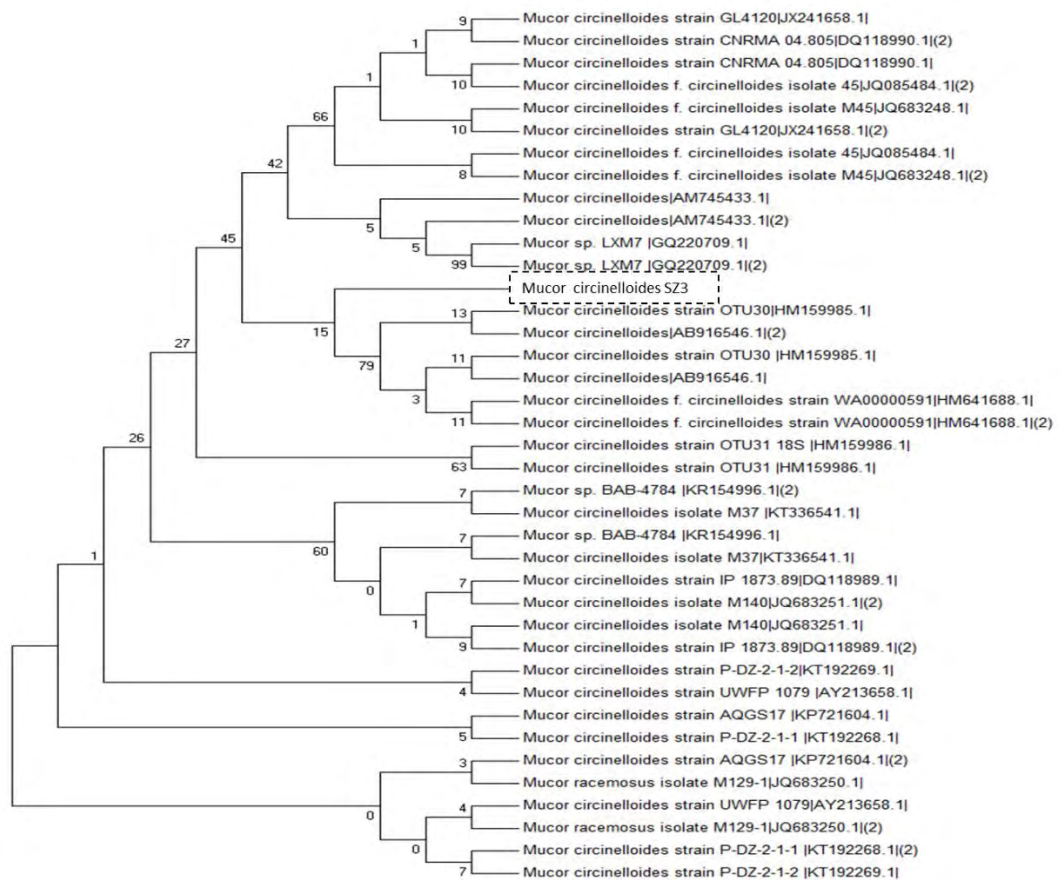


Figure 3. 14. Phylogenetic analysis of *Mucor circinelloides* SZ3 by using Mega 6.1 neighborhood joining method

### 3.4 Discussion

Considering the importance of filamentous fungi for involvement in metal nanoparticle synthesis, this study was planned to isolate and identify soil-borne indigenous filamentous fungi to observe their silver ions transformation potential. In this study fungi were isolated from salt mine, metal industrial waste, mountains of Neelam Valley to explore their potential to produce silver nanoparticles.

Soil has a combination of diverse conditions, from pleasant to extreme providing all types of environments for fungal growth making them ubiquitous in nature. Soil makes a relatively thin cover over the terrestrial land surface and has more microbial diversity than any other microbial ecosystem. Soils are formed by the microbial decomposition of living matter. Based on different physical characteristics, 26 different soil classes exist in nature. Due to presence of plant roots, more decomposition, incomplete breakdown products of biomass, complex spatial heterogeneity and presence of microenvironments, the topsoil is rich in organic material and thus contains high diversity of microbial community (192). Areas with extreme climates, geographical differentiation provide various altitudinal stresses like cold, drought, frost, low oxygen, salinity, intense UV radiations etc. thus exposing fungal communities to adapt survival mechanisms (193). About 80% of the Earth surface consists of hostile environments. Microorganisms surviving in such environments develop inductive force which can lead towards production of noteworthy metabolites with remarkable potential of useful properties (194).

Fungi have immense capability of physiological adaptation to diverse soil environments with greater potential of fast growth, high biomass, extensive hyphal spread and extracellular hydrolytic enzymes and secondary metabolites production. In the present study, fungal isolates were able to tolerate silver nitrate concentration upto 2000 mg/l. Different mechanisms are reported for metal resistance in fungi like iron, copper, manganese and zinc such as ion metallothionein, chelator binding, ion storage in hyphal cell walls, vacuole sequestration, deleting a metal ion importer etc. (29, 195). However, there is little known about the mechanisms behind silver resistance in filamentous fungi. Metals as micronutrients help in growth of fungi but higher concentrations increases the fungal-metal interaction and can cause stress conditions which lead to development of metal tolerance ability in fungi. In any metal-polluted habitat, diverse taxonomic groups of fungi can be found which can even survive under potentially toxic concentrations of metals (186).



The characteristic spectra of surface plasmon resonance (SPR) for silver reduction was observed as 405 nm for *Mucor circinelloides* (196), 430 nm for *Aspergillus oryzae*, 450 nm for *Aspergillus flavus* (197) and 410 nm in case of *Thermomyces lanuginosus* (198). Metallic nanoparticles exhibit specific optical properties which make them useful in sensing and imagine applications. Silver nanoparticles are considered suitable as their SPR can respond easily to any change in environment where these are dispersed. The response is observable in the form of shift in SPR which can be detected in the UV–vis spectrum (199). The reason behind this shift in SPR can possibly be due to presence of nanoparticle surface conjugation by variety of different organic ligands produced as extracellular fungal metabolites thus turning the particles for useful applications due to functionalized surfaces. Recently, silver nanoparticles have been used in many applications like detection of biomolecules (200), proteins (201), biosensing viruses (202), metal ions (203), biomedicine (204) etc.

### 3.5 Conclusion

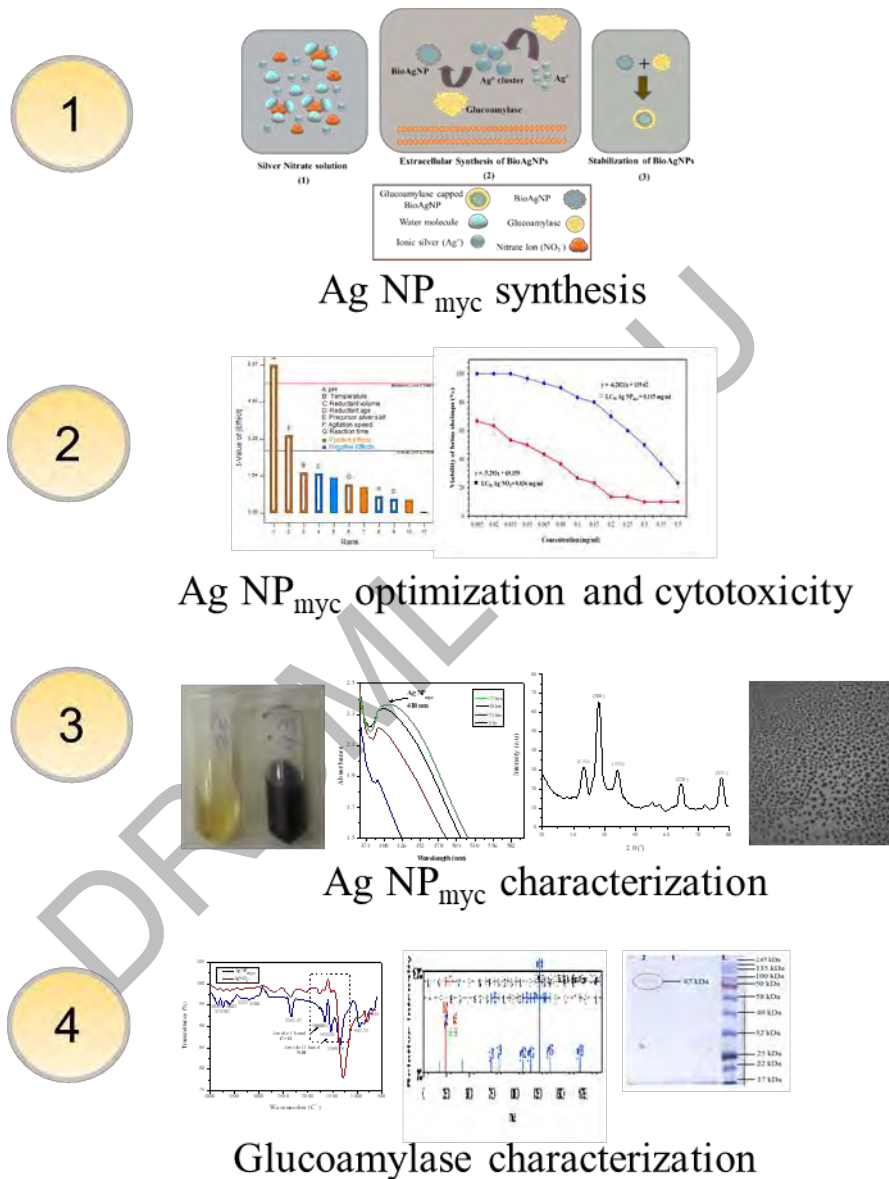
- Three indigenous fungi were isolated from different soils, *Aspergillus oryzae* SZ1, *Aspergillus flavus* SZ2, *Mucor circinelloides* SZ3, thermophilic fungus *Thermomyces lanuginosus* was obtained from department.
- The minimum inhibitory concentration in case of silver tolerance was found to be 2000 mg/l in case of *A. oryzae* SZ1, *A. flavus* SZ2 and *T. lanuginosus* whereas in case of *M. circinelloides* SZ3 wasn't able to grow beyond 1000mg/l.
- The characteristic spectra of surface plasmon resonance (SPR) for silver reduction was observed as 405 nm for *M. circinelloides* , 430 nm for *A. oryzae*, 450 nm for *A. flavus* and 410 nm in case of *Thermomyces lanuginosus*.
- The optimum growth conditions: *M. circinelloides* pH 5, for *A. oryzae* pH 7, for *A. flavus* pH 7 and for *T. lanuginosus* pH 5. In case of temperature, the optimum values were found to be 20 °C for *M. circinelloides*, 30 °C for *A. oryzae* and *A. flavus* at pH 7 and 50 °C for *T. lanuginosus*.

- To identify the fungi by after 18S sequencing, the fungi were given accession numbers from NCBI:, *A. oryzae* SZ1 (MH664050), *A. flavus* SZ2 (MH664051) and *M. circinelloides* SZ3 (MH664052).

DRSML QAU

## Chapter 4: Green synthesis of Ag NP<sub>myc</sub> and their stabilization by *Thermomyces lanuginosus*

### Graphical Abstract



### 4.1 Introduction

Silver nanoparticles (AgNPs) are extensively applied in therapeutic and industrial products due to their unique plasmonic properties and surface to volume ratio (102). In order to meet the sufficient amounts for commercial use, various chemical, physical, and biological methods are used to synthesize nanoparticles (NPs). The physical and chemical processes often yield small quantities of nanoparticles under harsh conditions (like high temperature) and the use of hazardous chemicals (205). Biosynthetic pathways for the production of metal nanoparticles are considered as relatively safer and less toxic (206). During last two decades extensive research has been carried out on application of microorganisms as factories for metal nanoparticles synthesis as this option is more environmentally friendly, cost-effective and suitable for large-scale synthesis of NPs.

Fungi are good candidates for production of NPs because of their high metal tolerance; detoxification capability and enhanced production of extracellular enzymes (207). Thermophilic enzymes produced by fungi can play a role in creating a protective layer on the surface of mycogenic metal nanoparticles hence provide stabilization (18). Identification of these surface layer macromolecules on metal nanoparticles can be useful to determine the possible synthesis mechanisms of NPs by microorganisms (208). The physical and biochemical interactions through electrostatic attraction and covalent bonds between proteins and mycogenic silver nanoparticles ( $\text{Ag NP}_{\text{myc}}$ ) may provide colloidal stability and can be utilized in specialized applications including therapeutic and industrial applications like biomedicine, biocatalysis, bioremediation and biosensing (209).

Capping molecules on the surface of  $\text{Ag NP}_{\text{myc}}$  of biological origin might be responsible for either  $\text{Ag NP}_{\text{myc}}$  synthesis or stabilization or both. Furthermore, immobilization of these fungal proteins on  $\text{Ag NP}_{\text{myc}}$  surface, reduces next steps of capping or stabilizing, required in case of chemical synthesis of nanoparticles for medical application (27). The industrial processes demand unique biocatalysing tendency under harsh conditions, therefore, the use of extremophiles which can grow under extreme geochemical and physical conditions, can be considered as an alternative (18). Due to their stability and adaptability under extreme conditions such as their tolerance for a broad range of pH (3-12), survival at temperatures up to 80 °C, thermophilic fungi can be a potential source for large-scale NPs synthesis (207).

Studies about identification of biomolecules covering biogenic silver nanoparticles are in their infancy and very less is known about identified capping molecules on the surface of biogenic silver nanoparticles synthesized from fungi.

These extracellular enzymes play important role in synthesis and stabilizing of metal ions and immobilization (210) of these enzymes on surface of nanoparticles is also carried out for optimum results. Excellent stability and homogeneity of nanomaterials can be achieved by using stabilizing agents which bind to nanoparticles via steric, electrostatic or some ligand interaction (211). The use of biocomponents fabricating nanomaterials are advantageous due to causing increased nanomaterial stability. A number of studies are reported on machineries and the mechanisms involved in biosynthesis of nanomaterials, but the nature of stabilizing agents on surface of nanomaterials still need to be explored (212). Ag NP<sub>myc</sub> stabilization results when nanoparticles interact with extracellular fungal proteins leading to the formation of capped structures (208) on the surface of nanoparticles that can be identified by various molecular techniques. The electrostatic interactions (213) and groups like amine H<sub>2</sub>N<sup>-</sup> and thiol HS<sup>-</sup> (Cys) in proteins when complexed with nanoparticles (214) can result in stability of nanoparticles.

Herein we report the extracellular synthesis of Ag NP<sub>myc</sub>, formation and identification of capping proteins by employing *Thermomyces lanuginosus*, a thermophilic fungus, along with the evaluation of the Ag NP<sub>myc</sub> cytotoxicity against eukaryotic animal model *Artemia salina* (brine shrimp) larvae. *T. lanuginosus* is an alkalotolerant, thermophilic fungus that belongs to genus *Thermomyces* which produces many heat stable hydrolytic enzymes. A previous study reported production of highly monodispersed Ag NP<sub>myc</sub> production from *T. lanuginosus* (198) however, to understand the involvement of fungal proteins in the synthesis and/or stabilization of Ag NP<sub>myc</sub>, the nanoparticle capping was removed and identified in current study along with the factors affecting Ag NP<sub>myc</sub> production. Objectives of this study was carried are given below.

- To optimize the process variables for the mycosynthesis of silver nanoparticles using statistical experimental design of Plackett Berman model.

- To characterize the bio-nanoparticles using microscopic (TEM) and spectroscopic (FTIR, UV-Vis spectrometry and XRD) techniques.
- To find the synthesis mechanism involving protein capping on mycogenic nanoparticles using SDS PAGE and LCMS/mass spectrometry.
- To perform the biological activities of nanoparticles (cytotoxicity).

## **4.2 Material and methodology**

### **4.2.1 Materials**

The material used in the study include, silver nitrate (Sigma Aldrich) salt, glucose (Oxoid), peptone (Oxoid), yeast extract (Oxoid), malt extract (Oxoid) and were of analytical grade.

### **4.2.2 Fungal strain**

Fungal strain, *Thermomyces lanuginosus* STm (GenBank: KJ432867) was stored on potato dextrose agar (PDA) slants at 4 °C. The fungus was re-grown by inoculating in culture medium containing 1% glucose, 0.3% malt extract, 0.5% peptone and 0.3% of yeast extract. The conditions for fungal growth include 50 °C, pH 9 and four days' incubation.

### **4.2.3 Silver resistance**

To determine fungal tolerance against silver ions, fungus was grown on MGYP (Malt Glucose Yeast Peptone) agar plates (in triplicate) each supplemented with increasing concentration of silver nitrate from 100 to 5000 mg/L. The inoculated plates were incubated at 50 °C for 10 days. Control cultures were incubated in the absence of any silver ion source. The radial growth was observed from these plates on the final day (10th) of experiment (187).

### **4.2.4 Mycosynthesis of nanosilver (Ag NP<sub>myc</sub>)**

For mycogenesis of Ag NP<sub>myc</sub>, *T. lanuginosus* STm was grown in 100 ml of MGYP liquid culture medium containing 1 % glucose, 0.3% malt extract, 0.5 % peptone and 0.3 % of yeast extract (Figure 4.1). pH was initially adjusted at 8.5 by using 1M

NaOH. These culture flasks were incubated at 50 °C for 96 hours. After incubation, fungal biomass was separated by centrifuging at 5000 rpm for about 15 min and washed with distilled water then resuspended in 100 ml sterile water and incubated in a shaker (at 200 rpm) at 50 °C for 24 hours to remove the culture media components. Later, fungal cells were separated by centrifugation. The supernatant obtained, was added with an equal volume of AgNO<sub>3</sub> solution to synthesize Ag NP<sub>myc</sub>. Periodically (0, 24, 48, 72 hrs), small amounts of reaction mixture were removed for spectral analysis to screen the mycosynthesis of Ag NP<sub>myc</sub>.

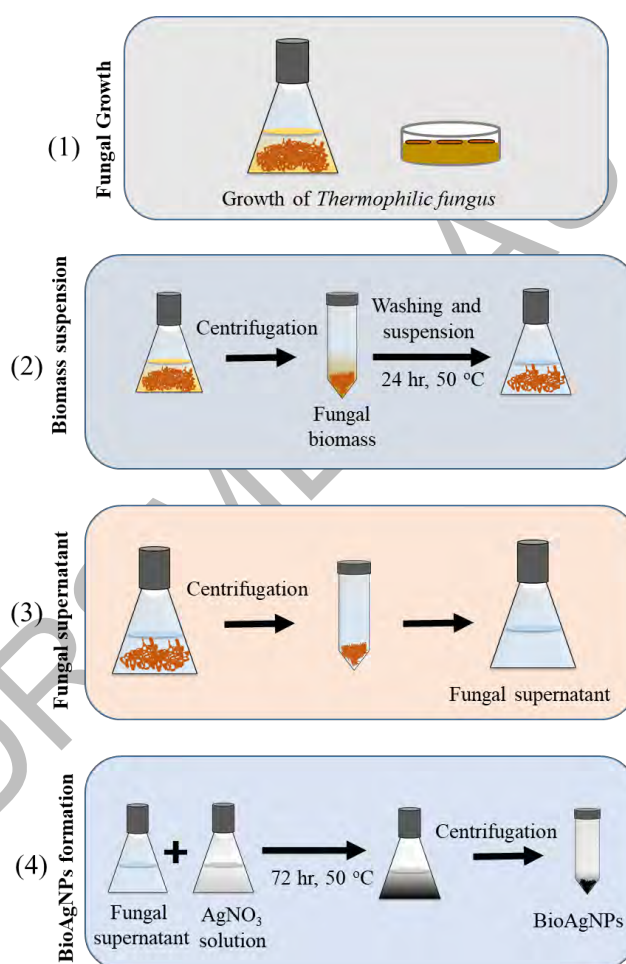


Figure 4.1. Schematic illustration of Ag NP<sub>myc</sub> synthesis procedure

#### 4.2.5 Screening of Parameters by Plackett–Burman (PB) Design

To identify the significant parameters affecting bio-synthesis process of Ag NP<sub>myc</sub>, Plackett–Burman design was used for screening the reaction pH, temperature,

reductant volume, reductant age, agitation time, stirring rate and concentration of precursor silver salt. Plackett–Burman (PB) has been frequently used and well suited to screen the vital parameters affecting a process. PB design is useful in terms of highlighting the role of most effective variables for optimizing the whole process with the least number of runs as possible (215). PB design is based on two factorial experimental design and in current study, it was used to identify the most effective physical and chemical variables needed for synthesis of Ag NP<sub>myc</sub> (216). Table 1 describes the experimental designing for current study by showing the factors for each experimental run. All the variables were investigated at two levels i.e., low level (-1) and high level (+1). In this case, eleven variables comprising of seven independent variables and four dummy variables [H, J, K and L] were organized in 12 runs of triplicates set of experiments. Design Expert (7.0.0 Trial) software was used to analyze the experimental design. The experiments were carried out in random order. The dependent variables, i.e. absorbance of Ag NP<sub>myc</sub> at 420 nm was selected as the response of the results of experiments (217). The following first order polynomial equation was used in this design:

$$Y=A_0 + A_1X_1 + A_2X_2 + A_3X_3 + A_4X_4 + \dots\dots\dots A_nX_n$$

Here, Y is the response being measured, A<sub>0</sub> is the coefficient of model, A<sub>1</sub> represents as linear coefficient, while X<sub>1</sub> shows level for independent variable (218).

#### 4.2.6 Characterization methods for Ag NP<sub>myc</sub>

Surface plasmon resonance of Ag NP<sub>myc</sub> was measured using Shimadzu UV-Vis spectrophotometer (UV-1601) The Ag NP<sub>myc</sub> film on carbon-coated copper was subjected to TEM analysis (JEOL JEM-1010, Japan) at 80 kV. In case of XRD (PANalytical X'pert PRO XRD, Netherlands) analysis, nanoparticle-coated film on silica was analyzed using Cu K  $\alpha$  radiation, the intensities of diffraction peaks (2 $\theta$  angles) were noted from 20-80 degrees with transmission mode of 20 mA and 30 kV. The mean diameter values were calculated using *Debye-Scherrer* equation (219) which is a derivative of Bragg's law given as follows:

$$D = \frac{57.3.k.\lambda}{\beta \cos\theta}$$



Where  $D$  is the diameter of nanoparticle, 57.3 is used to convert  $\beta$  from degrees to radians,  $k$  is the shape factor (0.9nm),  $\lambda$  is X-Ray wavelength (0.1541 nm),  $\beta$  is broadening of peaks at half maximum (FWHM) and  $\theta$  is angle of diffraction.

#### **4.2.7 Characterization methods for capping proteins on Ag NP<sub>myc</sub>.**

**4.2.7.1 Fourier Transform Infrared Spectroscopy (FTIR):** To investigate presence of capping moieties on the surface of Ag NP<sub>myc</sub>, FTIR spectrometer (Perkin Elmer-Spectrum 100) equipped with an Attenuated Total Reflectance (ATR) was used. Ag NP<sub>myc</sub> sample was placed uniformly, and spectra were recorded from 4,000-500 cm<sup>-1</sup>.

**4.2.7.2 SDS-PAGE:** To identify proteins potentially involved in the stabilization of Ag NP<sub>myc</sub>, SDS-PAGE was performed. The assumption inherent in this approach is that proteins involved in nanoparticles' formation are tightly associated with the Ag NP<sub>myc</sub> and should be dissociated and identified. For this purpose a modified method was used as described by (220). Briefly, the pellet of nanoparticles was mixed with sodium dodecyl sulphate (1% w/v) (SDS) and boiled for 20 minutes to remove the attached surface protein on Ag NP<sub>myc</sub>. The mixture was centrifuged (10,000 rpm) for 25 minutes. The supernatant containing the SDS-protein complex was subjected to protein quantification using Bradford method. According to this method, the pellet containing Ag NP<sub>myc</sub> was boiled with Tris-Cl (1 ml at pH 8.0) for 15 minutes to remove traces of SDS bound to Ag NP<sub>myc</sub>. Dialysis was performed against Milli-Q water to completely remove SDS, by changing water three times.

**4.2.7.3 Liquid chromatography–mass spectrometry (LC-MS) analysis:** LC-MS/MS was performed at Interdisciplinary Center for Biotechnology Research (ICBR), Proteomics Division, University of Florida, USA using hybrid quadrupole-TOF mass spectrometer (QSTAR elite, Applied Biosystems, Framingham, MA). The protein bands were cut and analyzed by Mass Spectrometry using method which involves denaturation of protein segments, trypsin digestion, desalting and finally concentrating the protein. The trypsin digested sample was injected to a capillary trap (LC Packings PepMap) and desalted with acetic acid (0.1% v/v) at flow rate of 3  $\mu$ l/min for 5 minutes. After desalting, the sample was loaded on nanoflow HPLC column (LC Packing® C18 Pep Map). LC-MS/MS analysis was carried out on a hybrid quadrupole-TOF mass spectrometer (QSTAR elite, Applied Biosystems,

Framingham, MA). For each IDA cycle, spectra for survey and MS/MS analyses, were recorded at 1 and 3 sec, respectively. ABI Analyst (version 2.0) was used to extract tandem mass spectra for protein search algorithm. The MS/MS sample was analyzed on Mascot (Matrix Science, London, UK; version 2.2.2). Mascot was set on NCBI search portal with Fungi taxonomy database assuming protein digestion using trypsin enzyme. To identify proteins and to validate MS/MS peptides, Scaffold (Proteome Software Inc., Portland) was used. Protein identification was accepted if there was 99.0% similarity with peptides being obtained in sample (221).

#### 4.2.8 Cytotoxic assay

Brine shrimp viability assay was used to measure the concentration (50% lethal concentration-LC<sub>50</sub>) required to kill half of a group of brine shrimp larvae (*Artemia salina*). Toxicity testing was carried by plotting the dose–response curve by adding different doses of Ag NP<sub>myc</sub> to small numbers of *A. salina* larvae and measuring their viability (%) according to the procedure previously described (222) with some modifications. The viability (%) of *A. salina* against different concentrations of AgNO<sub>3</sub> was also determined to compare the difference between Ag NP<sub>myc</sub> and ionic silver (223). In this method, dried eggs of *A. salina* were introduced to saline solution prepared with sea salt (Instant Ocean®). Within 24 hours, *A. salina* larvae hatched and were subjected to experimental trials. Ten *A. salina* larvae along with saline solution were individually shifted to test tube (5 ml) containing 5, 20, 35, 50, 65, 80, 100, 150, 200, 250, 300, 350 and 500 µg/ml of aqueous suspension of Ag NP<sub>myc</sub> serially diluted with saline water. The assay was performed in triplicates. After 24 hours, number of living shrimps were calculated and viability (%) was determined for each dose (224). Following formula was used to determine the viability of *A. salina*:

$$\% \text{ viability} = [(Number \text{ of live brine shrimps in test}) / (Number \text{ of live shrimps in control})] \times 100.$$

#### 4.2.9 Statistical analysis

Statistics was applied on results of metal tolerance, screening of physicochemical factors, viability (%) of brine shrimps and distribution of nanoparticles. All values were expressed as mean (±) standard deviation (SD) of triplicate samples in a

representative experiment. All experiments were done independently at least three times.

## 4.3 Results

### 4.3.1 Silver tolerance

Metal tolerance ability of the fungus *T. lanuginosus* STm was screened against silver nitrate salt, the thermophilic fungus was able to tolerate silver concentration up to 2000 mg/ml.

### 4.3.2 Screening of parameters

To evaluate the impact of various parameters (reaction pH, temperature, reductant volume, reductant age, agitation time, stirring rate and concentration of precursor silver salt) on synthesis of Ag NP<sub>myc</sub> using *T. lanuginosus* STm, Plackett–Burman model was designed with 11 factors (7 independent and 4 dependent variables) in 12 experimental runs of triplicate set (given in Table 4.1). Absorbance of Ag NP<sub>myc</sub> at 410 nm was recorded as the response. Out of 12 runs, higher response Ag NP<sub>myc</sub> synthesis was seen in runs 1, 3, 9, 10, 11 and 12. In experimental run no. 10, the highest absorbance was recorded as 2.2 at 410 nm wavelength, and the lowest absorbance was recorded in experimental run no. 7 as 1.64 (Table 4.1). First-order regression equation was used to measure the effect of each parameter on Ag NP<sub>myc</sub> synthesis.

$$\text{Absorbance}_{410\text{nm}} = 1.919 + 0.130_A + 0.037_B + (-0.035_C) + (-0.010_D) + 0.067_E + 0.022_G$$

Statistical evaluation of the results (Table 4.2) was used to develop the standardized main effect Pareto chart (Figure 4.2) which shows the contribution (%) of each variable in synthesis of Ag NP<sub>myc</sub>. This indicates a minimum t-value limit of 2.77 at a confidence level of 95.0% and Bonferroni limit of 5.74 (Figure 4.2). In this chart, effects below t-value limit are not significant whereas the significant effects are shown higher than Bonferroni limit and effects shown higher than t-value limit are nearly significant. Other points in Figure 4.2 are either insignificant or dummy variables. According to the relative influence of each parameter on synthesis process, the sequence order is pH, precursor (silver nitrate) concentration, temperature and

reaction time (Figure 4.2). The statistical significance (at significance level  $p < 0.05$ ) of the model and parameters was determined by ANOVA and  $F$ -test. The model  $p$  value of 0.02 indicates the statistical significance. The model  $F$ -value (9.11) indicates the model significance with only 2.48% chance that  $F$ -value could occur due to noise. In case of “Prob  $> F$ ”, the values (less than 0.0500) show the significance of model terms. The significant model terms of this model include, pH (0.0028), precursor concentration (0.0261), temperature (0.1491) and reaction time (0.2769) (Table 4.2).

Table 4.1. Statically designed experimental model (Plackett–Burman) for Ag NP<sub>myc</sub> synthesis

Std	Run	pH	Temperature °C	Reductant volume ml	Reductant age days	Precursor silver salt mM	Agitation speed rpm	Reaction time hours	Response OD <sub>410 nm</sub> (Standard error)
7	1	9	30	50	2	100	100	72	2.1 (±0.05)
2	2	6	50	100	2	100	150	72	1.84 (±0.002)
4	3	6	50	50	4	100	100	72	1.96 (±0.002)
12	4	6	30	50	2	50	100	24	1.72 (±0.002)
5	5	6	30	100	2	100	150	24	1.82 (±0.009)
10	6	6	50	100	4	50	100	24	1.64 (±0.005)
6	7	6	30	50	4	50	150	72	1.75 (±0.005)
3	8	9	30	100	4	50	150	72	1.9 (±0.02)
8	9	9	50	50	2	50	150	24	2 (±0.05)
1	10	9	50	50	4	100	150	24	2.2 (±0.09)
9	11	9	50	100	2	50	100	72	2.1 (±0.05)
11	12	9	30	100	4	100	100	24	2 (±0.02)

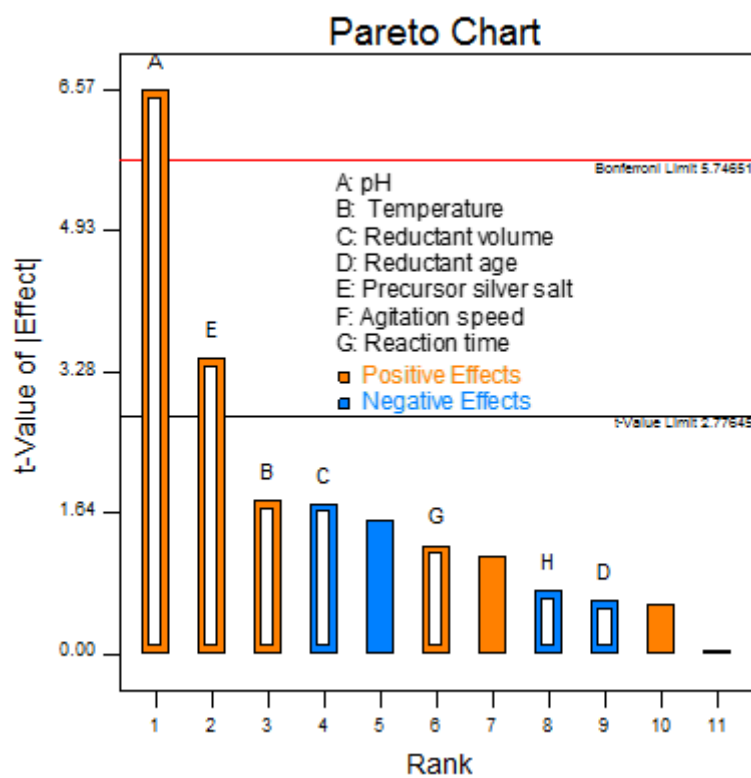


Figure 4.2. The Pareto chart, indicating the influence (by their t value) of important factors on Ag NP<sub>myc</sub> synthesis

Table 4.2. ANOVA and *F*-test) of Plackett–Burman experimental model

Model Terms	Sum of Squares	df	Mean Square	p-value Prob > F	F Value
Model	0.016	7	2.243E-003	0.0248	9.11
A-pH	0.011	1	0.011	0.0028	43.16
B- Temperature	7.833E-004	1	7.833E-004	0.1491	3.18
C-Reductant volume	7.483E-004	1	7.483E-004	0.1563	3.04
D-Reductant age	9.376E-005	1	9.376E-005	0.5706	0.38
E-Precursor silver salt	2.927E-003	1	2.927E-003	0.0261	11.88
G-Reaction time	3.896E-004	1	3.896E-004	0.2769	1.58

### 4.3.3 Characterization of Ag NP<sub>myc</sub>

#### 4.3.3.1 Change in color:

After screening for silver tolerance, the fungus was screened to determine the potential for extracellular mycogenesis of Ag NP<sub>myc</sub> which initially, was observed in

the form of gradual color change of reaction mixture containing cell-free supernatant of *T. lanuginosus* STm (Figure 4.3A). During the incubation period of 72 hours, the reaction mixture in flask containing cell-free supernatant and silver ions showed gradual color transition from colorless to blackish brown indicating the formation of Ag NP<sub>myc</sub>.

#### 4.3.3.2 Ultraviolet-Visible spectroscopy:

Mycogenesis of Ag NP<sub>myc</sub> is coupled with development of plasmonic properties which were initially scanned between 200 to 800 nm wavelength of ultraviolet and visible region. In the present study, gradual increase in optical density was observed at 410 nm wavelength after 0, 24, 48 and 72 hours of incubation of the fungus (Figure 4.3A) which confirmed the existence of Ag NP<sub>myc</sub>. The absorbance showed the transformation of precursor silver ions into Ag NP<sub>myc</sub> through reduction. Figure 4.3B shows the precursor silver nitrate solution which showed no change in absorbance of silver and nitrate ions over period of 72 hours. The Ag NP<sub>myc</sub> suspension was weekly monitored for absorption at 410 nm wavelength to screen its stability till 3 months, and it showed stability in aqueous solution at room temperature.

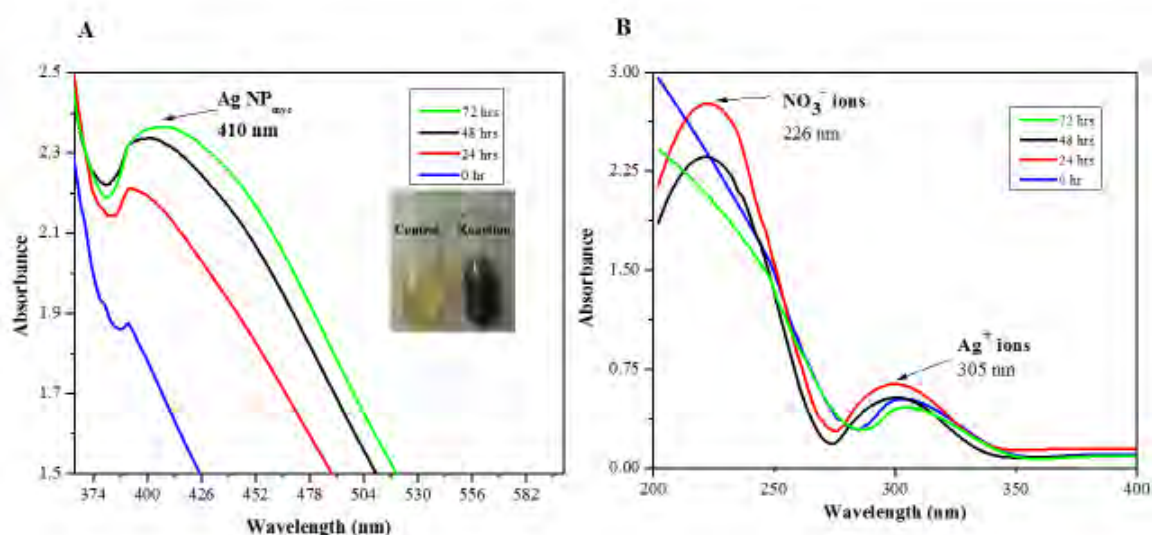


Figure 4.3. A: UV-Vis spectrum of reaction vessel for Ag NP<sub>myc</sub> synthesis showing absorbance near 410 nm. Change in color as indication of Ag NP<sub>myc</sub> synthesis as compared to control and reaction vessels, is also shown. B: UV-Vis spectrum for control vessel with silver and nitrate ions.

Note: The lines represent the values of optical density/absorbance (no units) of samples.

### 4.3.3.3 X-Ray diffraction (XRD):

The XRD analysis of Ag NP<sub>myc</sub> resulted with  $2\theta$  values of  $33.41^\circ$ ,  $38.13^\circ$ ,  $44.46^\circ$ ,  $64.52^\circ$  and  $77.50^\circ$  (Figure 4.4C) corresponds to respective silver planes of 111, 200, 111, 220 and 311. *Debye-Scherrer* equation was used to calculate the diameters of the Ag NP<sub>myc</sub> with the average diameter of these Ag NP<sub>myc</sub> was 3-24 nm (Table 4.3).

Table 4.3. XRD data for the mycogenic silver nanoparticles

Sr. No	Peak position $2(\theta)$ (Degrees)	Theta (Degrees)	FWHM (Degrees)	Mean Diameter (nm)
1	33.4127	16.70635	0.7872	11.01
2	38.1318	19.0659	0.7085	12.4
3	44.4675	22.23375	1.2595	7.12
4	64.5235	32.26175	0.3936	24.94
5	72.3443	36.17215	0.9446	10.88
6	77.5035	38.75175	0.48	22.17

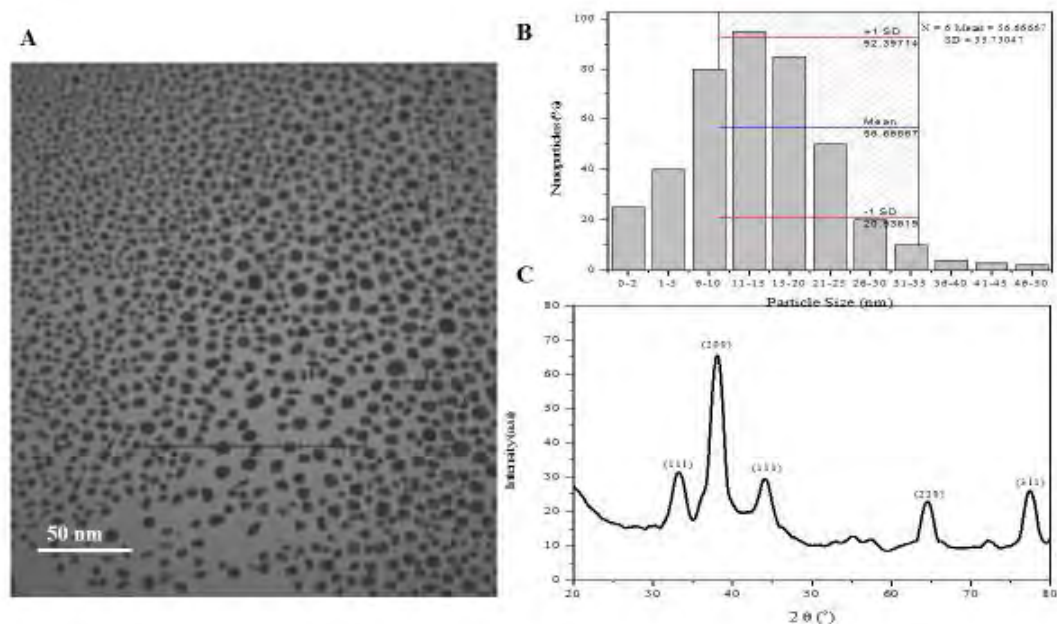


Figure 4.4. A: Representative TEM micrograph of Ag NP<sub>myc</sub> and B: particle size distribution of Ag NP<sub>myc</sub> C: XRD pattern for the mycogenic silver nanoparticles. Note: The bars in 4.4. B represent the values of number of nanoparticles at different size scale.

#### 4.3.3.4 Electron microscopy:

Transmission electron microscopy (TEM) was used to determine the size and morphology. TEM image shows Ag NP<sub>myc</sub> (Figure 4.4A) to be monodispersed with spherical shape. It can be seen from Figure 4.4B that the particle size is between 1-50 nm. It also shows that 54% ±35 of Ag NP<sub>myc</sub> lies in 5-35 nm range.

### 4.3.4 Characterization of capping agents on Ag NP<sub>myc</sub>

#### 4.3.4.1 FTIR analysis:

To screen the presence of fungal moieties as capping agents on the surface Ag NP<sub>myc</sub>, FTIR analysis was performed. FTIR spectrum showed specific bending and stretching



vibrations at 1660, 1531 and 1359 and 2341  $\text{cm}^{-1}$ , respectively (Figure 4.5). The carbonyl and amine linkages (amide I and amide II) in amino acids of proteins show characteristic peaks due to conformational changes in secondary structure after absorbing electromagnetic radiation from infrared region. In the present study, FTIR spectrum exhibited characteristic vibrations (bending and stretching) of the amide I (at 1660 and 3321  $\text{cm}^{-1}$ ) and amide II peaks (1531 and 3180  $\text{cm}^{-1}$ ) (Figure 4.5). The spectra showed intensive bands at 644, 941.21, 1359.75, 1531.41, 1660.63, 2341.47, 3180, 3321, 3602, 3737.87 and 3849  $\text{cm}^{-1}$  which were corresponding to C-H (methylene), =C-H (alkenes),  $-\text{CH}_3$ , O-H bending mode, phenols, N-H (amines), N-HCO, C=O (carbonyl), C-O-H respectively.

Figure 4.5. FTIR spectrum of mycogenic silver nanoparticles. Note: The lines represent the percent transmittance of each sample.

#### 4.3.4.2 SDS-PAGE:

In order to detach the surface attached (capping) protein(s), Ag NP<sub>myc</sub> were boiled with SDS (1%). The supernatant of boiled and unboiled samples were run on SDS-PAGE, the supernatant of boiled sample showed 67 kDa band of (lane 2, Figure

4.6A). The supernatant of unboiled sample did not show presence of any band (lane 1, Figure 4.6A).

#### 4.3.4.3 LC-MS/MS analysis:

The protein band being found in SDS-PAGE analysis Ag NP<sub>myc</sub> dispersion was identified by tryptic lysis followed by LC-MS/MS analysis (Figure 4.6B, 4.6C). From peptide chromatogram, the most intense signals were chosen for further fragmentation and their MS spectra were obtained to associate the fragmentation pattern with amino acid sequence, as shown in Figure 4.6B, 4.6C. Two peptide sequences (LQTVENPSGSLSSGGLGEPK, QVVDSFR) were identified in the Ag NP<sub>myc</sub> dispersion. Their molecular masses varied from 66.6 to 67 kDa. The capping protein was identified as glucoamylase (EC 3.2.1.3).

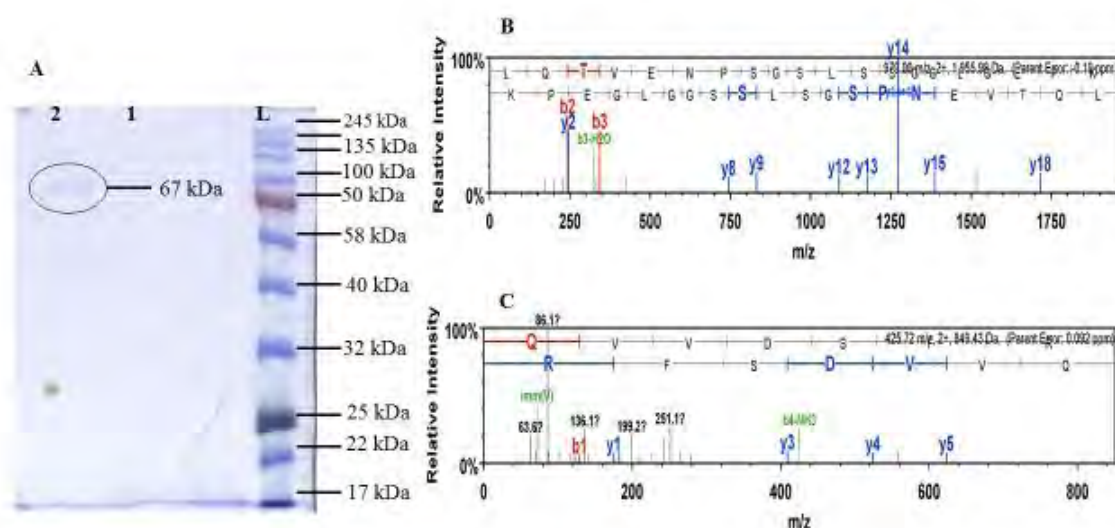


Figure 4.6. A: SDS-PAGE results depicting the size of capping protein glucoamylase on Ag NP<sub>myc</sub>; B and C: MS/MS data for identification of the capping protein's peptide sequences.

#### 4.3.5 Cytotoxic assay

In vitro cytotoxic assay against brine shrimp (*A. salina*) was performed to screen the acute toxicity of various concentrations of Ag NP<sub>myc</sub> in comparison with Ag NO<sub>3</sub>. The cytotoxic effect was measured against brine shrimp larvae in the form of LC<sub>50</sub>. The assay revealed that the LC<sub>50</sub> value for Ag NP<sub>myc</sub> was 0.115 mg/ml against eukaryotic

animal model (brine shrimps) after 24 hours. Whereas silver in ionic form showed cytotoxic effect with LC<sub>50</sub> value of 0.036 mg/ml (Figure 4.7).

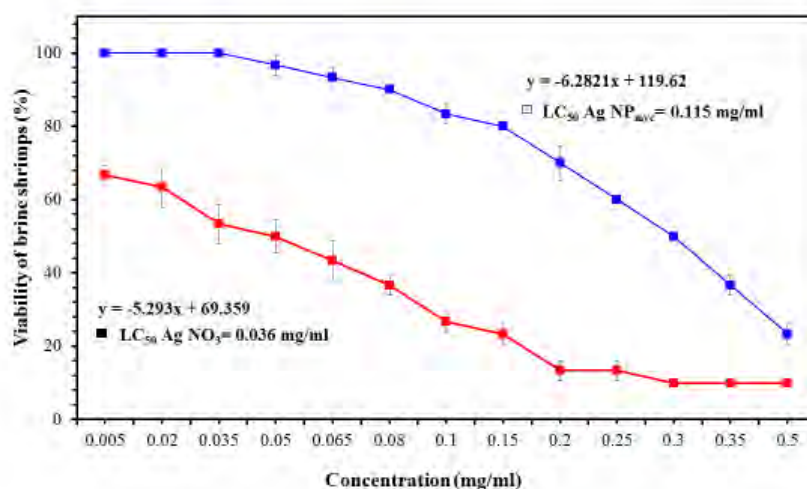


Figure 4.7. Dose-response plot showing viability (%) and LC<sub>50</sub> of *A. salina* at different concentrations of Ag NP<sub>myc</sub> (blue line) and Ag NO<sub>3</sub> (red line) after 24 hours. Note: The lines represent the mean values of percentage of alive brine shrimps. The error bars represent standard error being calculated after taking average of three replicates of each sample and calculating standard deviation.

## 4.4 Discussion

Recently there is an increased interest in the microbial reduction processes of transforming metal ions to nanosized metal particles which have potential usefulness. The metallic nanoparticles formation by microbial reduction of noble metal ions, e.g. platinum, palladium, gold and silver has already been reported in literature (225). Thermophiles counteract metal toxicity via their unique enzymes; metabolic and cell wall factors; metal efflux, metal sequestration by metallochaperones and metallothioneins and metal-based redox transformations. This thermophilic metal tolerating behavior may be due to presence of genes encoded on chromosomes, plasmids or transposons (226).

Screening of parameters revealed that alkaline pH condition played more important role for synthesis of mycogenic AgNPs as reported earlier (227). With color transition in flasks, oxidation state of AgNPs changed and detected by UV-Visible spectra in the form of surface plasmon resonance (SPR) (228) a characteristic feature of silver nanoparticles. The gradual increase in absorption spectrum at 410 nm showed rise in

the surface plasmon excitation. The absorption peaks from the silver nitrate solution are shown in inset graph at wavelengths of 226 and 305 nm indicating the presence of nitrate (229) and silver ions (230), respectively. XRD spectra obtained, confirmed the crystalline structure of Ag NP<sub>myc</sub> in nano-size range of 3-24 nm (231, 232). These results were in agreement with the TEM studies.

The FTIR results show that *T. lanuginosus* STm secrete different bioactive molecules (such as protein residues) thus making the reported strain more suitable for the biosynthesis of silver nanoparticles (233, 234). The surface protein (capping) of Ag NP<sub>myc</sub> was detached and separated as a protein band in SDS-PAGE was further identified as glucoamylase (EC 3.2.1.3), after tryptic lysis followed by LC-MS/MS analysis (221). This is proposed that glucoamylase might be acting as reducing agent converting ionic silver to Ag NP<sub>myc</sub> and capping agent (Figure 4.8) at the same time contrary to another thermophilic microbe *Thermomonospora* where capping and reducing agents were found to be two different proteins (235). Glucoamylase (EC 3.2.1.3), also known as amyloglycosidase contains some useful properties like high thermostability which make it a suitable candidate for industrial applications (236). Glucoamylase is identified to constitute the secretome of *T. lanuginosus* (237) and its thermostability has been reported in literature (238, 239). Previously, some important fungal (*Aspergillus tubingensis*) proteins have been identified on surface of silver nanoparticles including glycoamilase, acid phosphatase, serine carboxipeptidase and glucanosyltransferase (213).

The LC<sub>50</sub> results for Ag NP<sub>myc</sub> and ionic silver revealed that the more the LC<sub>50</sub>, the less is the toxicity. Compared to silver in ionic form in accordance with the previous studies, our Ag NP<sub>myc</sub> showed less cytotoxicity (240) (223).

These extracellular enzymes play important role in synthesis and stabilizing of metal ions and immobilization (210) of these enzymes on surface of nanoparticles is also carried out for optimum results.

So, this study not only identifies the protein coating around nanoparticles enhancing its stability but also proposes the idea that fungal biosynthesis of nanoparticles might exclude the need of extra steps involved in immobilization of enzymes on the surface of nanoparticles required during the industrial processes. The nature of protein-

nanoparticle attachment and enzyme's stability on the nanoparticle surface can be analyzed further by measuring its residual activity for pH, thermal and storage stability for biocatalytic bioremediation and biosensing application.

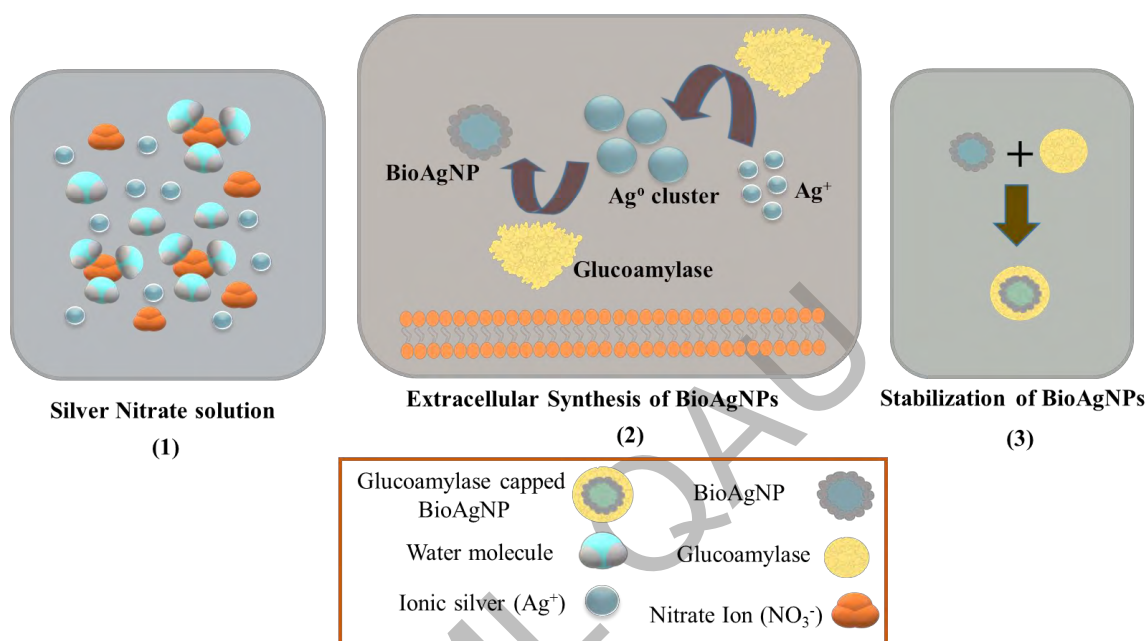


Figure 4.8. Glucoamylase capped silver nanoparticles production mechanism

## 4.5 Conclusions

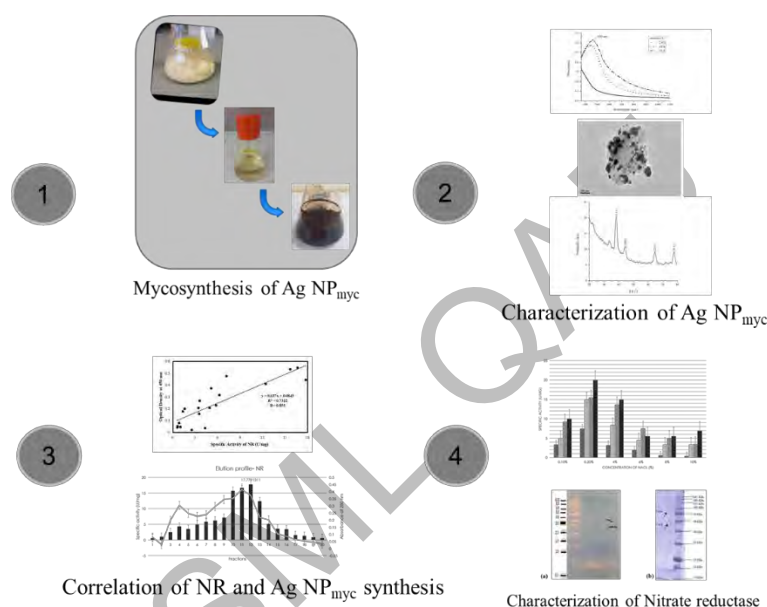
In the present study, bottom up method of myco-reduction of silver ions by glucoamylase protein secreted extracellularly by *T. lanuginosus* STM was utilized which resulted in spherical shaped thermostable mycogenic silver nanoparticles. The SPR band was observed at 410 nm. Under transmission electron microscope, monodispersity of Ag NP<sub>myc</sub> was seen which predicts the role of thermostable capping protein in nucleation and growth of Ag NP<sub>myc</sub>. SDS-PAGE and LC-MS/MS analysis confirmed that nascent Ag NP<sub>myc</sub> were strongly coated with glucoamylase (67 kDa). Ag NP<sub>myc</sub> when acted against brine shrimp larvae, found to be less toxic as compared to ionic form of silver. It is interesting to note that in case of Ag NP<sub>myc</sub> synthesized by extracellular titer of thermophilic fungus, the adsorbed protein thermostable glucoamylase can possibly help in resuming activity of Ag NP<sub>myc</sub> at high temperatures. The properties of the protein coated Ag NP<sub>myc</sub> can be further studies in

terms of stability and reusability and comparison of free and attached form of enzyme can be explored further.

DRSML QAU

## Chapter 5: Identification of the role of nitrate reductase involvement in nano-silver mycogenesis using *Aspergillus* sp.

### Graphical Abstract



### 5.1 Introduction

In nanoscience, an important domain of research is the nanoparticles' fabrication pathways resulting in nanoparticles with different sizes, controlled dispersity, shapes and variety of chemical compositions. It is a big challenge to develop experimental protocols for these fabrication pathways. For this purpose, various fabricating techniques are employed at atomic and molecular level in liquid media or vacuum (241). The drawbacks of many such bottom up or top down techniques are being inefficient in energy and use of materials and being capital intensive (18). Therefore, to develop eco-safe methods using green synthesis are highly required. In case of green biological methods, various biomolecules are involved in synthesis of nanomaterial which may include proteins, amides, terpenoids, amines, flavones, carbonyl groups, phenolic which exist in microbial or plant extracts (65).

Evolution has resulted in emergence of range of inorganic structures. Every species has unique mechanisms for biogenesis of specific minerals. Unicellular microorganisms like magnetotactic bacteria, diatoms and calcareous algae are suitable to examples. The complex structures of composites and crystals of amorphous inorganic polymers and proteins are synthesized in these microorganisms (18). In case of multicellular organisms, hard-form organic-inorganic complexes are produced e.g. spicules, shells and bones etc. (242). The S-layer (surface layer) bacteria produce calcium carbonate and gypsum layers (243). These examples from nature encouraged nonscientists to employ biological systems for nanomaterials' synthesis. The eco-friendly, nontoxic and clean synthesis by the microbial systems to fabricate metal nanoparticles is of profound importance in development of bionanotechnology (18). Silver nanoparticles have developed huge research interest due to their wide applications in fields like antimicrobial fibers (244), integrated circuits (245), fuel cell electrodes (246), biosensors, antimicrobial filters, biolabelling (247). Due to antimicrobial potential of nanosilver particles, these are employed in various areas like health, packaging, medicine, cosmetics and various industries (248).

The objectives of current study are given below.

**Objectives:**

- To synthesize mycogenic silver nanoparticles using metal tolerant *Aspergillus flavus* SZ2 extracellularly.
- To characterize mycogenic silver nanoparticles using spectroscopy and electron microscopy.
- To screen the role of nitrate reductase in synthesis of mycogenic silver nanoparticles.
- To purify and characterize nitrate reductase using molecular methods of PCR and SDS-PAGE

## **5.2 Material and methodology**

### **5.2.1 Isolation from soil**

*Aspergillus flavus* SZ2 was isolated from metal industrial waste as mentioned in chapter 3 under section 3.2.2.2.



### **5.2.2 Silver resistance**

Effect of silver ions on fungal strains was determined as mentioned in the chapter 3 under section 3.2.3.

### **5.2.3 Growth optimization**

The pH and temperature of the growth media were optimized using methods given in chapter 3 under section 3.2.4.1 and 3.2.4.2.

### **5.2.4 Molecular Identification**

*Aspergillus flavus* SZ2 was molecularly identified by amplification and sequencing of internal transcribed spacer (ITS) regions of 18s rRNA gene as mentioned in chapter 3 under section 3.2.7 and the accession number was given as MH664051 after submission to NCBI.

### **5.2.5 Mycosynthesis of Ag NP<sub>myc</sub>**

Mycosynthesis of Ag NP<sub>myc</sub> was carried out using *Aspergillus flavus* SZ2 (NCBI accession number: MH664051) using the method given in section 3.2.5.

### **5.2.6 Characterization of Ag NP<sub>myc</sub>**

Characterization of Ag NP<sub>myc</sub> was carried out as given in section 4.2.6.

### **5.2.7 Mechanistic study of myconanosilver synthesis**

#### **5.2.7.1 Screening of nitrate reductase activity**

Nitrate reductase activity was determined in both aqueous culture filtrates with AgNO<sub>3</sub> according to the procedure followed by (249). An aliquot (0.10 ml) of 4-day fungal filtrate was mixed with 1.8 ml of assay medium (10 mM KNO<sub>3</sub> with 0.1 M phosphate buffer of pH 7.3 and 0.05 mM Ethylenediaminetetraacetic Acid) and incubated at 30 °C for 1 hr in dark condition. After incubation, nitrites formed in the assay mixture were estimated by adding 1 ml of 58mM sulphanilamide and NEED (N-(1-naphthyl) ethylene diamine dihydrochloride) solutions in to it. The developed pink color was measured in an UV–vis spectrophotometer at 540 nm. A control beside the reaction mixture was also run. The enzyme activity was finally expressed in terms of μM of nitrite/min/ml.

#### **5.2.7.2 Standard curves development and enzyme unit calculation**

Standard curve of known concentration of the nitrite was prepared

***Nitrite standard curve:***

Different molar concentrations of standard solution of nitrite were prepared, then all other reagents of enzyme assay other than enzyme and substrate and O.D was taken at 540 nm. From this curve, enzymes units per milliliter were determined.

***Protein Estimation:*** For the estimation of protein contents Bradford method (250) was used by taking the Bovine serum albumin (BSA) as a standard. 0.5 ml of the sample was taken in test tube and 0.5 ml of the buffer or distilled water and then 1ml of 1X Bradford reagent was added and incubated at 30 C for 15 minutes. Optical density was measured using spectrophotometer (Agilent 8453) at 595 nm. Total content of protein was calculated using the BSA standard curve.

***BSA standard curve:*** Stock solution (1mg/ml) of Bovine Serum Albumin (BSA) was prepared and its different dilutions were prepared ranging from 50 µg to 900 µg in distilled water and then adding the Bradford reagent. Optical density (O.D) was noted at 595 nm wavelength and was plotted against the concentration of BSA.

***Nitrate reductase specific Activity***

One unit of nitrate reductase is the amount of nitrate reductase that release 1µmol of nitrite per minute using standard procedure. Specific activity of the nitrate reductase enzyme was calculated by dividing the enzyme activity by total protein.

Specific Activity = Unit per ml of enzyme activity/mg per ml of total protein

Its unit is U/mg.

**5.2.7.3 Correlation between silver reduction and NR Assay**

***Use of enzyme specific inhibitors:*** In order to determine the effect of enzyme specific inhibitors on the mycogenic nanoparticle synthesis, the inhibitor study was carried out with a slight modification of (251). Among these inhibitors included ethylene diamine tetra acetic acid (EDTA), phenyl methane sulphonyl fluoride (PMSF), sodium azide, iodoacetate and p-chloromercuribenzoate (PCMB). Total protein content was obtained from fungal aqueous supernatant by precipitating with ice cold acetone (100%) and centrifugation of mixture was carried out at 4 °C, 10,000×g for 10 min. The protein pellet was suspended in water for further use in nanoparticle synthesis. The positive control contained the fungal aqueous supernatant, the negative control contained protein pellets along with 0.1 M AgNO<sub>3</sub> and the experimental sample contained protein pellets along with a mixture of 0.1 M AgNO<sub>3</sub> and 1 mM of each inhibitor. The

experiments were performed in triplicates for each inhibitor. The percentage inhibition by each inhibitor was calculated as compared with negative control.

**Use of chromatographic enzyme fractions for silver reduction and NR assay:** Gel permeation chromatography (252) using Sephadex gel was used to partially purify the nitrate reductase enzyme from precipitated protein content. Sephadex G-100 (10 g) was kept overnight at pH 7.5 in phosphate buffer (500ml) with sodium azide (0.1 g) as bacteriostatic agent. The gel was homogenized by sonicating (20 minutes) in a sonicator and then filled in a 0.9×60 cm size glass column. Phosphate buffer (pH 7.5) was run through the Sephadex gel continuously using till it settled down completely. Precipitated proteins (2 ml) sample was loaded subjected to the sephadex gel and eluted by continuous addition of phosphate buffer (pH 7.4) and 3 ml fraction was collected with an average speed of 15 min/fraction. Enzyme assay and protein estimation (Bradford assay) was carried out for each eluted fraction. Each purified fraction was treated with equal volumes of 0.1 M AgNO<sub>3</sub> solution to evaluate the reducing capability of nitrated reductase for synthesis of silver nanoparticles. Each fraction was incubated for 24 h at 37°C and silver reduction was measured at 420 nm.

#### **5.2.7.4 Optimization of nitrate reductase production**

Growth conditions for nitrate reductase production were optimized by submerged fermentation method. Inoculum was prepared by inoculation of 72 hours fresh cultures in Sabouraud dextrose broth and incubated at 30°C for 72 hours in shaker incubator at 150 rpm.

**Optimization of temperature:** The fungal strain *Aspergillus flavus* SZ2 (NCBI accession number: MH664051) was grown at different temperatures; 25°C, 30°C, 40°C, 45°C and 50°C. Crude nitrate reductase activity and specific activity was calculated after 12, 24, 48 and 72 hours by collecting supernatants at respective time and processed for enzyme assay and protein estimation as described previously.

**Optimization of pH:** The fungal strain was grown in media having different pH values (4, 5, 6, 7, 8, and 9) and analyzed for nitrate reductase production. Crude nitrate reductase activity and specific activity was calculated after 12, 24, 48 and 72 hours by collecting supernatants at respective time and processed for enzyme assay and protein estimation

**Optimization of Nutritional Factors:** Nutritional components of a medium were optimized including NaCl, carbon sources (glucose, starch, glycerol), nitrogen sources (yeast extract, peptone) and substrate concentration (KNO<sub>3</sub>, NaNO<sub>3</sub>). Different concentration of these nutritional components include: NaCl (0.1, 0.2, 4, 6, 8, and 10 %), glucose (1%), starch (1%), glycerol (1%), yeast extract, peptone (0.5, 1, 1.5, and 2 %), KNO<sub>3</sub> (0.5, 1, 2 and 4 %) and NaNO<sub>3</sub> (0.5, 1, 2 and 4 %). Nitrate reductase activity and specific activity was calculated after 12, 24, 48 and 72 hours.

#### 5.2.7.5 Purification of nitrate reductase

Purification of nitrate reductase enzyme from *A. flavus* SZ2 was performed through ammonium sulphate precipitation and gel permeation (Sephadex G-100) chromatography. All the steps were performed at 4°C.

**Ammonium sulphate precipitation:** Required amount of ammonium sulfate was first calculated via online calculator of EnCor Biotechnology Inc. The precipitation of crude enzyme nitrate reductase (100 ml aliquot per tube) was carried out at different concentrations of ammonium sulfate (NH<sub>4</sub>)<sub>2</sub> SO<sub>4</sub> (30, 40, 50, 60, 70 and 90%). Precipitation was carried out by slowly adding ammonium sulfate to cell free supernatant at 4°C using magnetic stirrer. Precipitates were collected at 4°C from each tube at 10,000 rpm using centrifuge (Kokusan Model H-251) for 10 minutes. Pellet was dissolved in potassium phosphate buffer (pH 7.4). NR activity and protein quantification (Bradford method) was carried out in the pellet and supernatant for each tube for calculating specific activity of enzyme in pellet and supernatant. On the basis of maximum nitrate reductase activity in pellet, optimum concentration of ammonium sulfate was determined and bulk precipitation was carried out.

**Gel filtration chromatography:** Sephadex G-100 was used to carry out gel filtration chromatography. Sephadex G-100 gel (3g) was soaked with 0.04 g sodium azide and 0.04 g fluconazole in 200 ml of potassium phosphate buffer (pH 7.4) and stored (4°C, 24 hours). Before chromatography, gel in buffer was sonicated for 30 minutes for degassing and loaded in 27 cm long column up to 21 cm and remaining part was filled with buffer. The flow rate of column was maintained at 0.33 ml per minute. NR extract (2 ml) was loaded to the chromatography column and flow of sample was aided by continuously adding potassium phosphate buffer slowly. At least 30 fractions were collected and absorbance was measured at 280 nm of each fraction

using UV–Visible spectrophotometer (Shimadzu) for an estimate about protein content in different fractions. Enzyme activity and protein estimation of the each fractions was measured. Fractions with higher nitrate reductase activity were combined and kept at 4°C for further study.

#### **5.2.4.5 Physiological characterization of nitrate reductase**

Purified nitrate reductase was characterized by calculating its relative activity of NR, by using the given formula:

Residual Activity (%) = Activity (U/mg) of enzyme/Activity (U/mg) of the original enzyme X 100

**Temperature:** NR activity was noted at temperature range (25, 30, 40, 45 and 50 °C) for ten minutes, and the residual/relative activity was measured.

**pH:** NR activity at pH range (4, 5, 6, 7, 8 and 9) was noted by using phosphate buffer. At optimum temperature for NR, activity was noted for 10 minutes and residual/relative activity was measured.

**Thermo-stability:** NR was incubated with substrate at different temperatures (25, 30, 40, 45 and 50°C) for 0, 30, 60, 90, 120, 150 and 180 min) and its residual/relative activity was measured.

**pH stability:** pH stability was determined by incubating NR (without substrate at 4°C) at different pH values (4, 5, 6, 7, 8, 9 and 10) for 0, 30, 60, 90, 120, 150 and 180 min, substrate was added and residual/relative activity was measured.

**Metal ions:** Effect of metal ions (10 and 20 mM) on NR activity was measured using metal salts: copper chloride, calcium chloride, zinc chloride, ferrous chloride, cobalt chloride, manganese chloride, nickel chloride, mercuric sulfate, magnesium chloride and potassium sulphate and residual/relative activity was measured.

**Surfactants and detergents:** Purified nitrate reductase was incubated with surfactants cetyl trimethyl ammonium bromide (CTAB), Triton X-100, Polyoxyethylene (20) sorbitan monooleate (Tween 80) and sodium dodecyl sulfate (SDS) at a concentration of 0.5 and 1.0 % and residual/relative activity was measured.

**Organic solvents:** Effect of different organic solvents (methanol, ethanol, propanol, butanol, benzene, DMSO, acetone and formaldehyde) at a concentration of 10% was analyzed by incubating with nitrate reductase and residual/relative activity was measured.

**Nitrate reductase kinetics:**  $V_{max}$  and  $K_m$  of nitrate reductase were measured with substrate concentrations i.e. 5, 10, 15, 20, 25, 30 and 35 mg/ml. Enzyme assay was performed under optimum condition for 5 minutes with one minute interval followed by enzyme activity calculations.

The kinetic parameters were calculated based on Lineweaver–Burke plots of the double reciprocal of the Michaelis–Menten equation, as follows:

$$1/V = (K_m/V_{max}) \times 1/[S] + 1/V_{max}$$

Where  $V$  is the initial reaction rate,  $V_{max}$  is the maximum reaction rate,  $[S]$  is the substrate concentration, and  $K_m$  is the Michaelis–Menten constant.

#### **5.2.4.6 Molecular identification of nitrate reductase protein and gene**

##### ***Sodium dodecyl sulfate-polyacrylamide gel electrophoresis (SDS-PAGE)***

From gel permeation chromatography, the fractions with higher nitrate reductase activity were combined and concentrated by freeze-drying (Labconco Freezone). The dried sample was analyzed on SDS-PAGE for relative molecule mass determination on a polyacrylamide gel (12%) (253). Coomassie Brilliant Blue R-250 was used to stain the gel. Protein ladder was used with size range of molecular mass markers from 10–250 kDa (NewEngland Biolab).

**DNA extraction:** Fungal DNA was extracted as mentioned in chapter 3 under section 3.2.6.1.

**PCR optimization:** Eight primer sets were designed to identify the correct sequence of nitrate reductase gene of *A. flavus* (as shown in the Table 5.1). Among these sets, primer set no. 4 identified the gene of *A. flavus* nitrate reductase with the sequences: 5'-ATGGCAACCATCACCGAGGT-3' (forward primer), 5'-TGAAGGTCTGATTCTTTCCATCCT-3' (reverse primer). The gene was amplified using gradient PCR. The PCR conditions to detect NR genes included 30–35 cycles with initial temperature 98 °C for 30 sec, annealing temp 55 °C for 30 sec and extension for 72 °C for 5 min. Extension time: 5 min,  $T_m$ : 50°degree Celsius, PCR volume was 10 µl which included master mix: Quick load 5 µl, forward primer: 0.5 µl, reverse primer: 0.5 µl, DNA Template: 1 µl and water: 3 µl. To eliminate equipment variability, triplicates were run. PCR product was separated on agarose gel electrophoresis and then quantified.

Table 5.1. Set of primer designed for NR gene of *A. flavus*

Sr. No	Gene size	Primer set	Primer sequence
01	2973 bp	Gene 1	F 5' ATGGCGGCGTCCACATACGA 3'
			R 5' TCAGCAGCGTAGATATCCCGACA 3'
02	1728 bp	Gene 2	F 5' ATGTCATTTGAGGAAGCGGC 3'
			R 5' CTATAATACACTCTGCACTATAGCC 3'
03	2624 bp	Gene 3	F 5' ATGGCAACCATCACCGAG 3'
			R 5' GAAGAAGTGAAGGTCTGATTC 3'
04	2607 bp	Gene 4	F 5' ATGGCAACCATCACCGAGGT 3'
			R 5' TGAAGGTCTGATTCTTTCCATCCT 3'
05	2982 bp	Gene 5	F 5' ATGCCGCTCACGAGCCAA 3'
			R 5' TCAGAAACCGAACAAGTTCTTATCTTCG 3'
06	2973 bp	Gene 6	F 5' ATGCTCTATCCAGGATGTTTACGGTGA 3'
			R 5' GCAGCGTAGATATCCCGACAAA 3'
07	2006 bp	Gene 7	F 5' ATGTCCCCTTGAAGAAATTCGAACGG 3'
			R 5' ACCATAAAGCACTATTAACCATCCCCA 3'
08	1104bp	Gene 8	F 5' ATGGACATTCTATATACCGGGTGATTC 3'
			R 5' ACTTCTGCCTACATGTATCCGC 3'

### 5.3 Statistical analysis

Statistics was applied on data in the form of mean, standard deviation (SD) and standard error of triplicate samples in a representative experiment. All experiments were done independently at least three times.

### 5.4 Results

#### 5.4.1. Silver tolerance screening:

Effect of silver ions on fungal strains was determined as mentioned in the chapter 3 under section 3.3.2. The fungus was able to grow at 2000 mg/l as minimum inhibitory concentration of silver ions.

#### 5.4.2 Characterization of synthesized Ag NP<sub>myc</sub>

The Ag NP<sub>myc</sub> formation by fungus *A. flavus* SZ2 was initially monitored by gradual color change of reaction mixture Figure 5.1 during 72 hours. The color changed from

colorless to blackish brown. In contrast, silver nitrate solution did not show any color change.

UV–Visible spectral analysis confirmed the formation of Ag NP<sub>myc</sub> production through detection of surface plasmon resonance (SPR) peak at 450 nm (Figure 5.1). The SPR peaks showd regular rise. SPR are characteristic feature of noble metal nanoparticles. The absorption peaks at 226 and 305 nm from the silver nitrate solution indicate presence of nitrate (229) and silver ions (254), respectively.

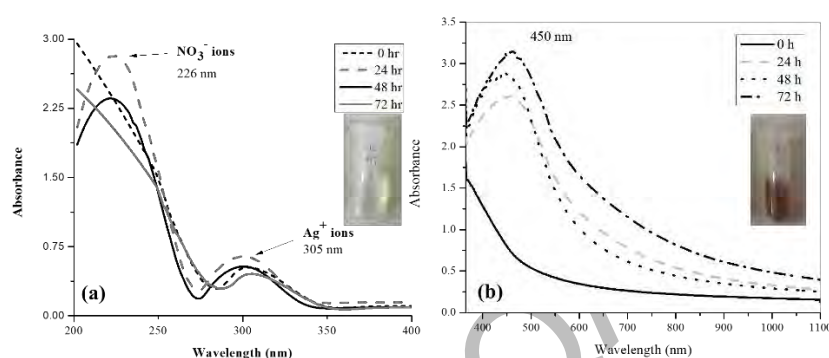


Figure 5.1. UV–Visible spectrum for the (a) silver nitrate solution and (b) mycogenic silver nanoparticles

The size and morphology Ag NP<sub>myc</sub> were determined by TEM micrograph (Figure 5.2a), which revealed to be spherical shaped. The Ag NP<sub>myc</sub> particle size histogram shows a size range of 1 to 70 nm (Figure 5.2b). Ag NP<sub>myc</sub> distribution frequency was observed as 30-40% ± 36 particles in the size range of 1 to 40 nm. Ag NP<sub>myc</sub> exhibited X-ray diffraction (2 $\theta$ ) peaks at 38.56°, 44.33°, 64.52°, and 77.60°, corresponding to silver planes of 111, 200, 220 and 311, respectively (Figure 5.2c).

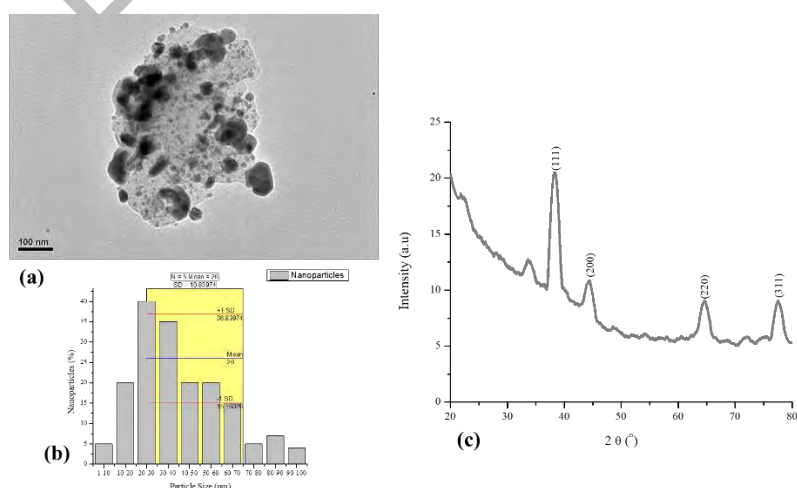


Figure 5.2. Representative (a, b) TEM micrographs and (c) XRD pattern for Ag NP<sub>myc</sub>.

### 5.4.3 Correlation between silver reduction and NR Assay



To find out the underlying mechanistic pathway of mycosynthesis of Ag NP<sub>myc</sub>, evaluation of nitrate reductase inhibition was observed along with silver reduction. In addition, the fractions obtained during the purification step were also compared in terms of NR activity and silver reduction.

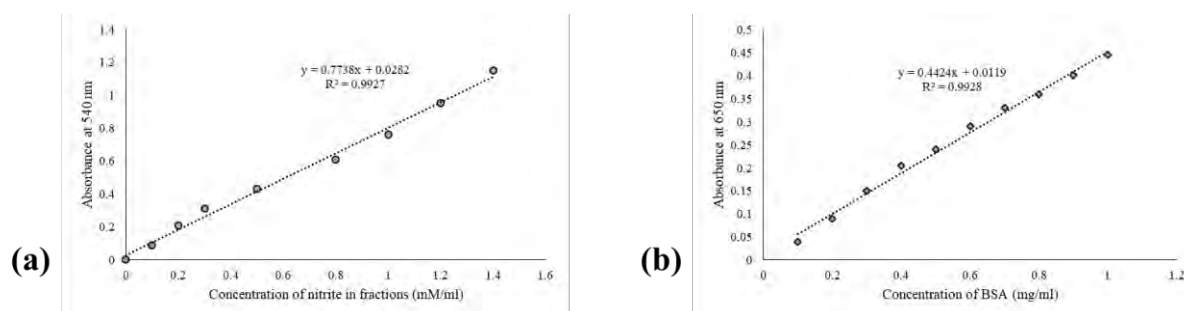


Figure 5.3. Standard curves of (a) Nitrite for NR assay and (b) Bovine serum albumin for protein quantification

#### 5.4.3.1 Use of enzyme specific inhibitors

To confirm the involvement of nitrate reductase in the mycosynthesis of AgNPs, inhibitors were used to measure inhibition in NR activity and silver reduction at 450 nm. The fungal mycelial filtrates after treating with 1 mM AgNO<sub>3</sub> turned brown from colorless after 24 hours, indicated synthesis of nanoparticles, whereas the fractions interacting with AgNO<sub>3</sub> along with inhibitors (10 mM) depicted range of inhibition in nanoparticles' formation.

Among these inhibitors, ethylene diamine tetra acetic acid (EDTA), phenyl methane sulphonyl fluoride (PMSF), sodium azide, iodoacetate and p-chloromercuribenzoate (PCMB) resulted in 44%, 26%, 67%, 22.5% and 14% inhibition in NR specific activity, respectively. In case of silver reduction at 450 nm, 45% inhibition was observed in case of sodium azide which is highest among all inhibitors.

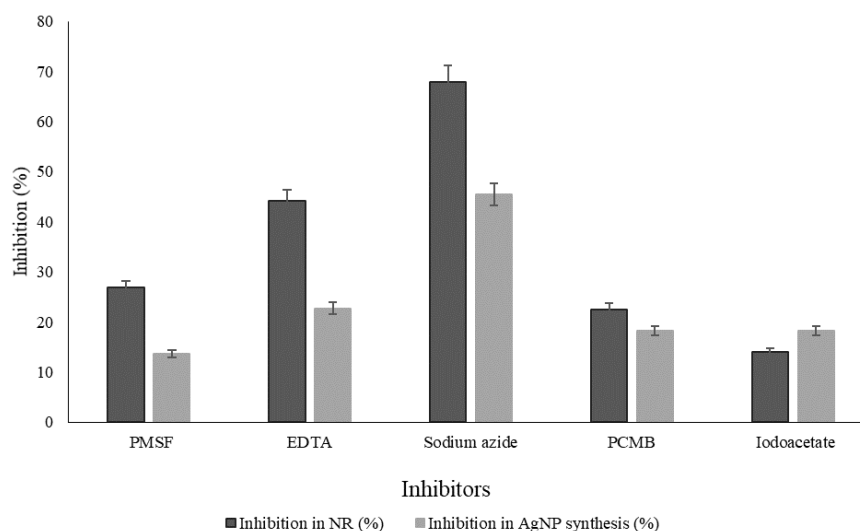


Figure 5.4. The in-vitro effect of various inhibitors on activity of nitrate reductase from *Aspergillus flavus* SZ2. Note: The bars represent the mean values, while the error bars represent standard error of triplicate samples after calculating standard deviation.

#### 5.4.3.2 Use of chromatographic enzyme fractions for silver reduction and NR assay

The synthesis mechanism was further supported by finding the correlation between silver reduction and NR activity in chromatographic enzyme fractions for fungus *A. flavus* SZ2 nitrate reductase on Sephadex G-100 chromatography (Figure 5.5).

The nitrate reductase assay was performed to screen crude fungal mycelial filtrate. Positive correlation ( $R = 0.855$ ) indicated the involvement of nitrate reductase in partially purified protein fractions in mycosynthesis of Ag NP<sub>myc</sub> by reducing silver nitrate (Figure 5.6).

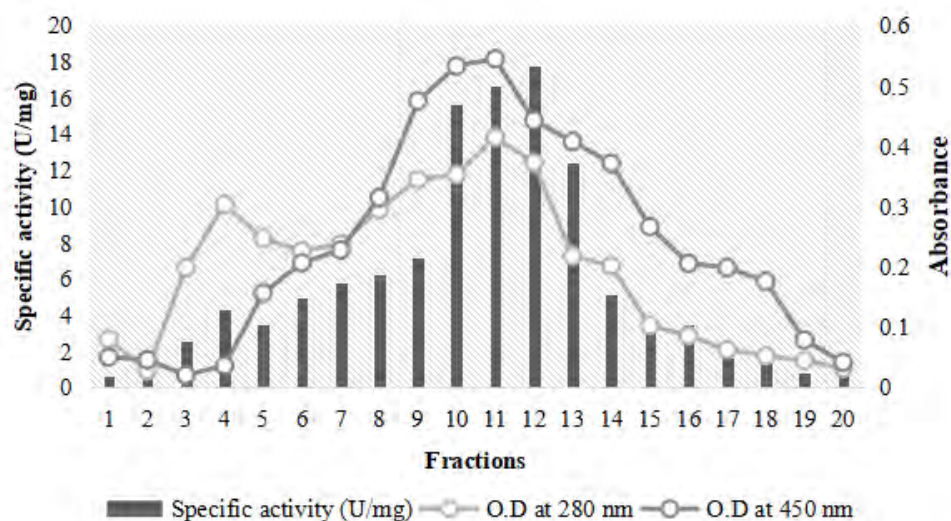


Figure 5.5. Using gel-filtration chromatography, partially purified fractions with protein activity and specific activity of nitrate reductase enzyme in total extracellular protein content from filtrate of *Aspergillus flavus* SZ2

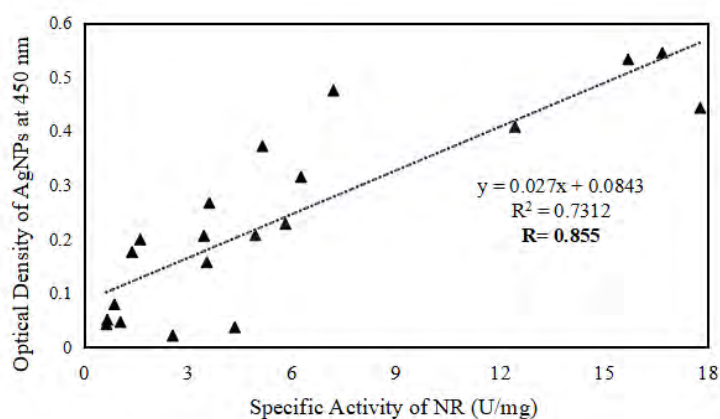


Figure 5.6. Positive correlation ( $R = 0.855$ ) indicating the involvement of nitrate reductase in the mycosynthesis of AgNPs by reducing silver nitrate.

## 5.4.4 Optimization of nitrate reductase production

### 5.4.4.1 Optimization of temperature

Effect of temperature on production of nitrate reductase from *A. flavus* SZ2 was analyzed at different temperatures (25, 30, 40, 45, 50°C) at intervals of 12, 24, 48, 72 hours. Maximum activity was seen at 30°C (16.662 U/mg) after 72 hours (Fig. 5.7).

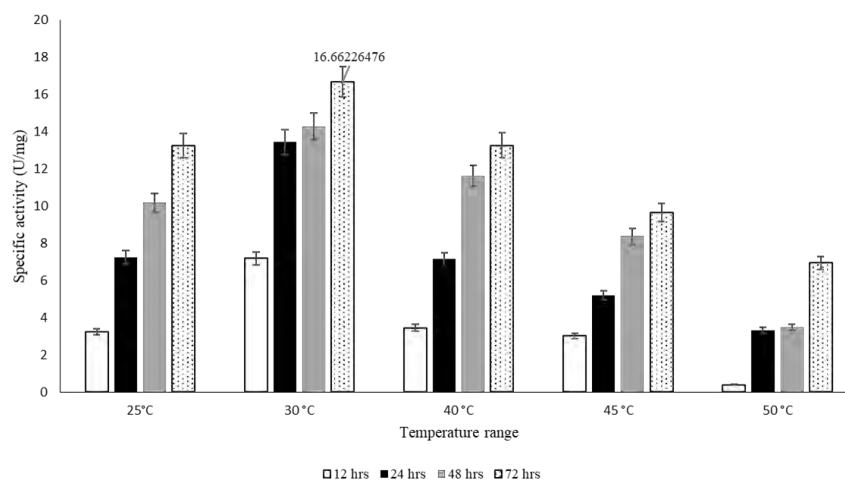


Figure 5.7. Effect of temperature on production of nitrate reductase from *A. flavus* SZ2. Note: The bars represent the mean values, while the error bars represent standard error of triplicate samples after calculating standard deviation.

#### 5.4.4.2 Optimization of pH

Production of nitrate reductase was also analyzed at different pH values (4.0– 9.0). Optimum temperatures (30°C) along with other conditions were kept constant. Highest activity was seen at pH 7.0 (14.1 U/mg) while production was good at wide range of pH (6.0–9.0) (Figure 5.8).

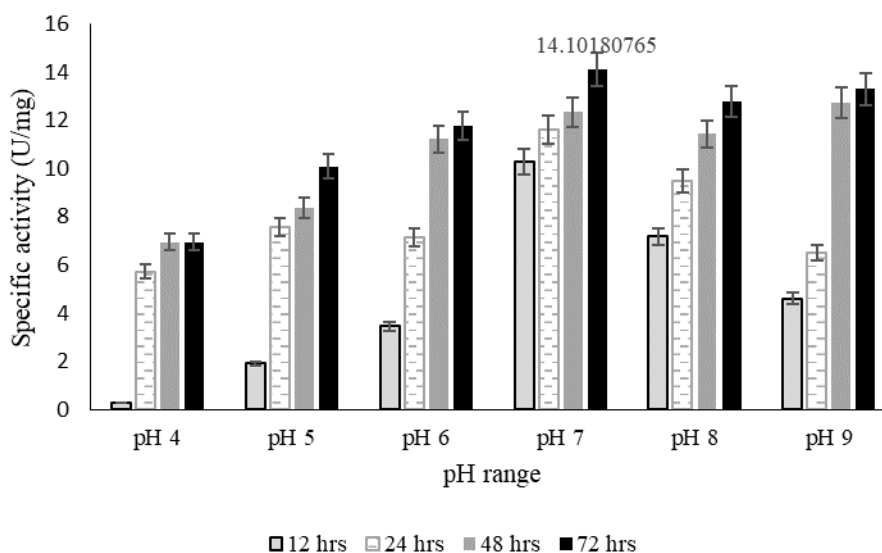


Figure 5.8. Effect of different pH on production of nitrate reductase from *A. flavus* SZ2. Note: The bars represent the mean values, while the error bars represent standard error of triplicate samples after calculating standard deviation.

#### 5.4.4.3 Optimization of nutritional factors

Nutritional components of a medium were optimized including NaCl (Figure 5.9), carbon sources (glucose, starch, glycerol) (Figure 5.10) and nitrogen sources (yeast extract, peptone) (Figure 5.11). 0.2 % NaCl showed good activity of nitrate reductase, among carbon sources glucose showed the highest NR activity and among nitrogen sources, use of yeast extract showed higher NR activity. Nitrate reductase activity and specific activity was calculated after 12, 24, 48 and 72 hours.

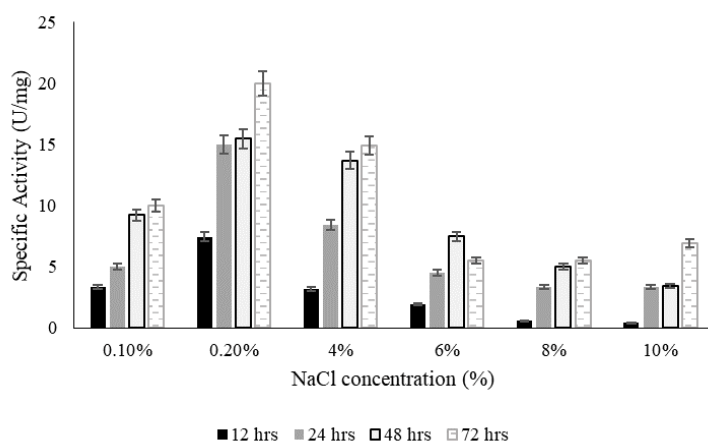


Figure 5.9. Effect of NaCl on NR production by *A. flavus* SZ2

Note: The bars represent the mean values, while the error bars represent standard error of triplicate samples after calculating standard deviation.

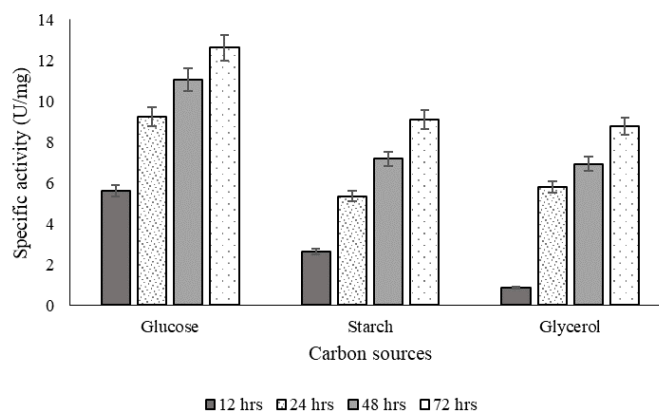


Figure 5. 10. Effect of carbon sources on NR production by *A. flavus* SZ2

Note: The bars represent the mean values, while the error bars represent standard error of triplicate samples after calculating standard deviation.

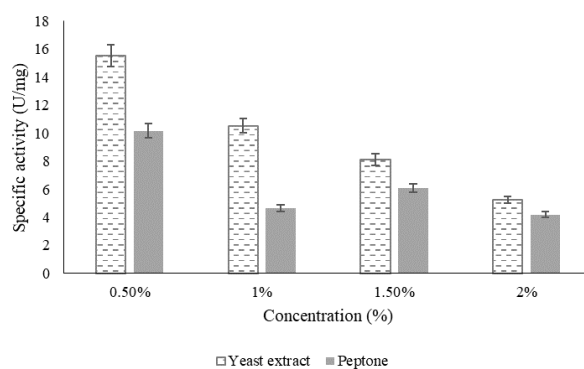


Figure 5. 11. Effect of nitrogen sources on NR production by *A. flavus* SZ2

Note: The bars represent the mean values, while the error bars represent standard error of triplicate samples after calculating standard deviation.

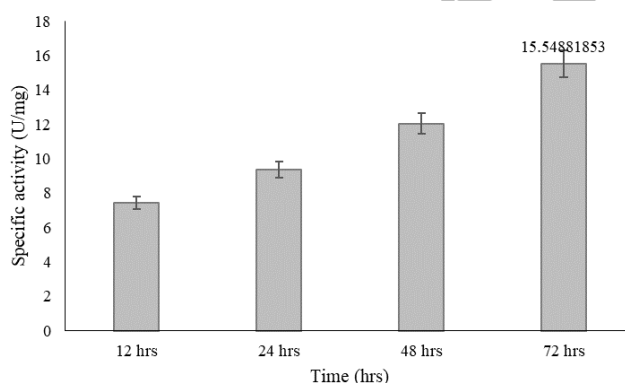


Figure 5. 12. Optimized value of NR produced by *A. flavus* SZ2

Note: The bars represent the mean values, while the error bars represent standard error of triplicate samples after calculating standard deviation.

## 5.4.5 Purification of nitrate reductase

### 5.4.5.1 Ammonium Sulfate Precipitation of Crude nitrate reductase

Ammonium sulfate was carried out for total proteins precipitation. Maximum NR precipitation was observed in the precipitate of solution with 40% ammonium sulfate with maximum specific activity of 17.106 U/mg (Figure 5.13).

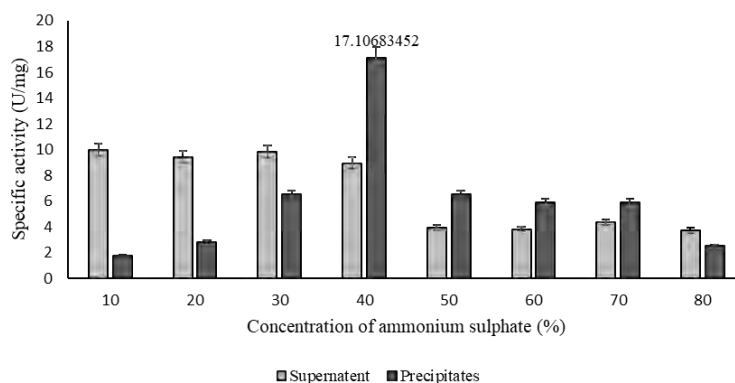


Figure 5. 13. Ammonium Sulfate precipitation of crude nitrate reductase from *A. flavus* SZ2 showing comparison of specific activities of pellets and supernatants at different concentrations of ammonium sulfate (10-80%)

Note: The bars represent the mean values, while the error bars represent standard error of triplicate samples after calculating standard deviation.

#### 5.4.5.2 Gel filtration Chromatography

Partially purified sample of *A. flavus* SZ2 nitrate reductase was further purified by Sephadex G-100 gel chromatography. Maximum specific activity of NR was seen at fraction 12 17.779 U/mg, 8 – 14 number fractions showed higher NR specific activity (Figure 5.14).

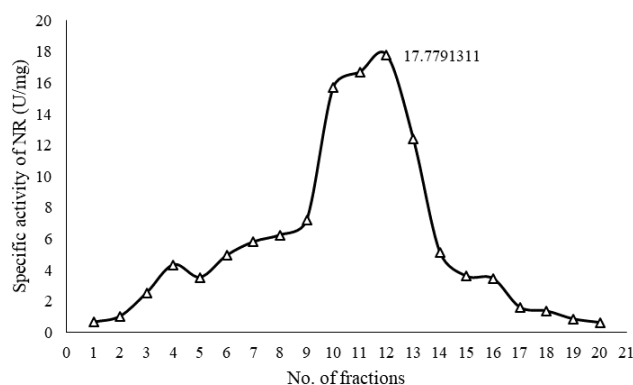


Figure 5.14. The elution profile of fungus *A. flavus* SZ2 nitrate reductase on Sephadex G-100 chromatography.

#### 5.4.5.3 Total yield of Purified nitrate reductase from *A. flavus* SZ2

The total yield and purification fold for precipitated and gel filtered nitrate reductase from *A. flavus* SZ2 was calculated as 1.10 and 89.94% (Table 5.2).

Table 5.2. Purification steps of nitrate reductase from *A. flavus* SZ2

Purification step	Enzyme activity (U/ml)	Total protein (mg/ml)	Specific activity (U/mg)	Purification fold	Yield (%)
Supernatant (Crude extract)	26.36	1.69	15.54	1	100
Ammonium sulphate precipitation	26.10	1.52	17.10	1.10	89.94
Gel filtration (Sephadex-100)	15.63	0.879	17.77	1.14	52.01

### 5.4.6 Characterization of nitrate reductase

Purified nitrate reductase (NR) from *A. flavus* SZ2 was measured to see the effect of different parameters on NR activity.

#### 5.4.6.1 Temperature

At 30°C, NR showed optimum activity and more than 60 % of initial NR activity was retained at 25 to 40°C (Figure 5.15).

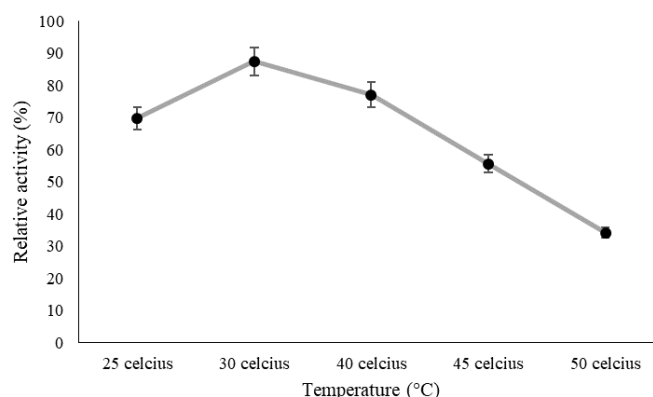


Figure 5.15. Effect of temperature on specific activity of nitrate reductase from *A. flavus* SZ2

Note: The line represents the mean values, while the error bars represent standard error of triplicate samples after calculating standard deviation.

#### 5.4.6.2 Effect of pH on activity of nitrate reductase from *A. flavus* SZ2

The optimum pH for nitrate reductase from *A. flavus* SZ2 was observed 7.0 at its optimum temperatures (Figure 5.16). Nitrate reductase retained more than 80% activity at pH 7.0 – 8.0.



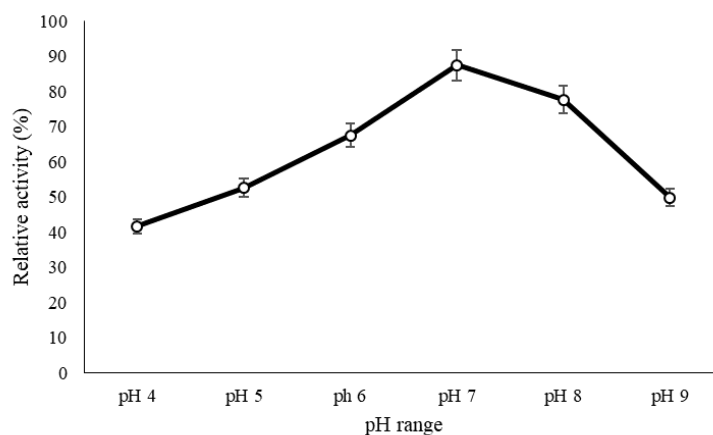


Figure 5.16. Effect of pH on specific activity of nitrate reductase from *A. flavus* SZ2

Note: The line represents the mean values, while the error bars represent standard error of triplicate samples after calculating standard deviation.

#### 5.4.6.3 Temperature stability profile

Nitrate reductase from *A. flavus* SZ2 retained 90% initial activity after three hours incubation at 30°C while lowest activity (<20%) was observed at 50°C (Figure 5.17).

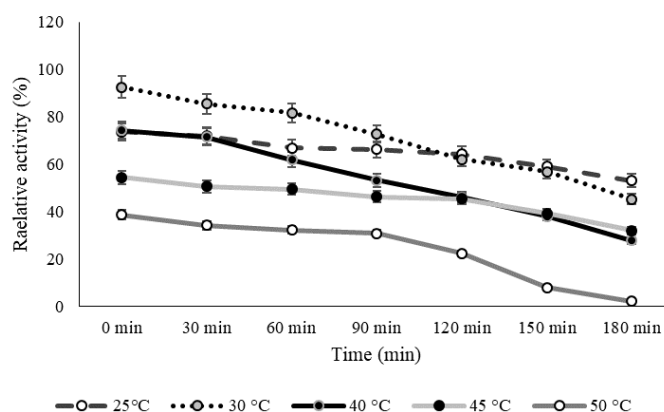


Figure 5.17. Temperature stability of nitrate reductase from *A. flavus* SZ2

Note: The lines represent the mean values, while the error bars represent standard error of triplicate samples after calculating standard deviation.

#### 5.4.6.4 pH stability profile

Nitrate reductase from *A. flavus* SZ2 was stable at pH 7.0 and retained 80% to 70% activity for three hours while showed approximately 20% activity at pH 4 (Figure 5.18).

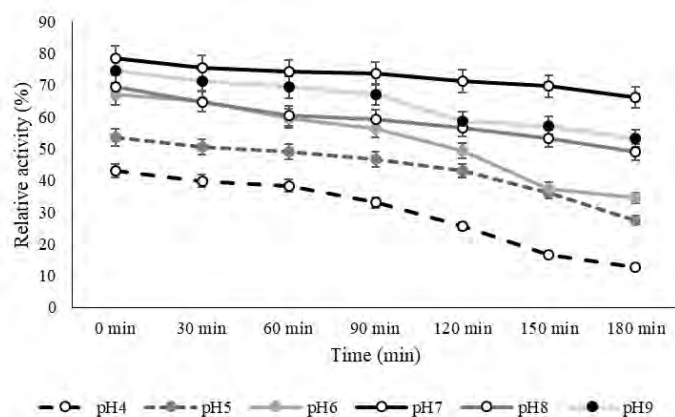


Figure 5.18. pH stability profile of nitrate reductase from *A. flavus* SZ2

Note: The lines represent the mean values, while the error bars represent standard error of triplicate samples after calculating standard deviation.

#### 5.4.6.5 Effect of metal ions

Effect of different metal ions on nitrate reductase of *A. flavus* SZ2 was analyzed at concentration of 10 and 20 mM (Figure 5.19). Hg and Ni ions showed high inhibitory effect at both concentrations while K have shown high activity for NR.

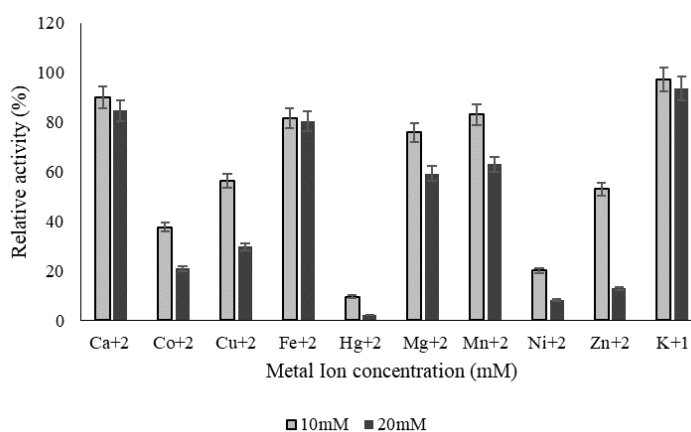


Figure 5.19. Effect of metals on activity of nitrate reductase from *A. flavus* SZ2

Note: The bars represent the mean values, while the error bars represent standard error of triplicate samples after calculating standard deviation.

#### 5.4.6.6 Effect of surfactants

Effect of surfactant was analyzed at 0.05 and 1 % concentration for nitrate reductase from *A. flavus* SZ2 (Figure 5.20). The lowest NR activity was observed at with Trinton X-100 whereas highest activity was observed with SDS.

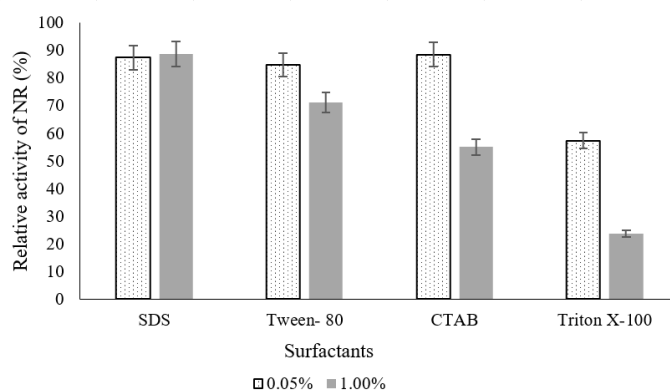


Figure 5.20. Effect of surfactant and detergents on activity of nitrate reductase from *A. flavus* SZ2

Note: The bars represent the mean values, while the error bars represent standard error of triplicate samples after calculating standard deviation.

#### 5.4.6.7 Effect of organic solvents

Effect of organics solvent was analyzed on nitrate reductase from *A. flavus* SZ2 (Figure 5.21). The highest activity was observed with methanol whereas lowest activity was observed with DMSO.

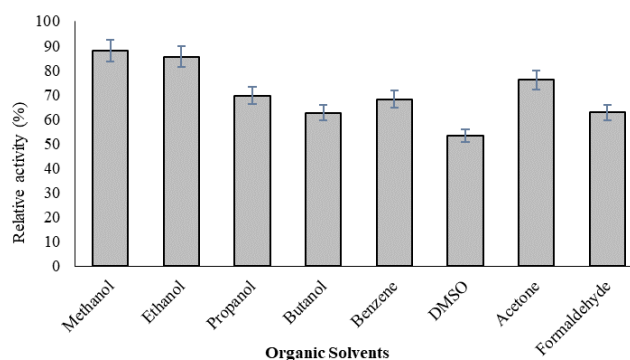


Figure 5.21. Effect of organics solvent on activity of nitrate reductase from *A. flavus* SZ2

Note: The bars represent the mean values, while the error bars represent standard error of triplicate samples after calculating standard deviation.

#### 5.4.6.8 Kinetic parameter of nitrate reductase from *A. flavus* SZ2

The  $K_m$  and  $V_{max}$  value for nitrate reductase (NR) from *A. flavus* SZ2 were calculated by Lineweaver and Burk (1934) plot using the Michaelis–Menten equation (Figure 5.22). The NR was incubated with substrate  $KNO_3$  at different concentrations activity (U/ml) was measured. Kinetic parameters  $K_m$  and  $V_{max}$  were calculated as 13.18 mg/ml and 0.07 U/ml ( $\mu\text{mol}/\text{ml}/\text{min}$ ).

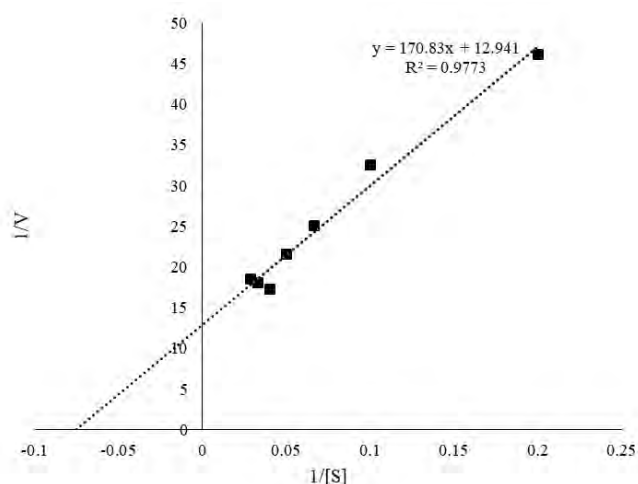


Figure 5. 22. Kinetics analysis (Lineweaver Burk plot) of nitrate reductase from *A. flavus* SZ2

## 5.4.7 Molecular characterization of nitrate reductase Gene

### 5.4.7.1 PCR and agarose gel electrophoresis

In the present study, the size of the PCR product was found to be 2604 bp.

### 5.4.7.2 Molecular Weight determination

SDS-PAGE was performed after precipitating total fungal proteins and fractionised by Sephadex G-100 gel-filtration chromatography. Fractions with the highest specific activity were combined and used in sodium dodecyl sulfate polyacrylamide gel electrophoresis (SDS-PAGE) analysis. The molecular weight of nitrate reductase from *A. flavus* SZ2 was seen in the form of 70 and 45 KDa bands in SDS-PAGE gel (Fig. 5.23). The double bands obtained indicate dimeric nature of the enzyme.

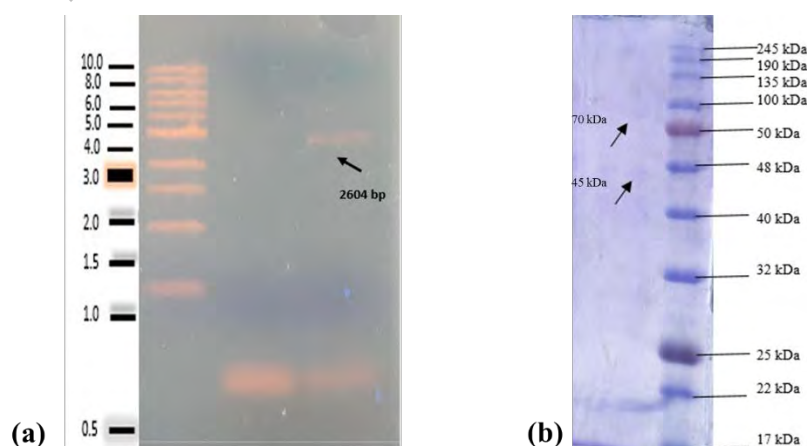


Figure 5. 23. (a) PCR results for identification of nitrate reductase gene of *A. flavus* SZ2 (b) SDS-PAGE of nitrate reductase of *A. flavus* SZ2 showing two bands of 70 and 45 kDa.

## 5.5 Discussion

The silver nanoparticle synthesis was confirmed through color change of reaction mixture and surface plasmon resonance value, and that extracellular fungal components might be involved in the process (255). The noble metal nanoparticles formation of microbial origin such as gold, silver, palladium, platinum etc. has been reported previously with applications in the fields of catalysis, photonics, bioleaching etc. (225). The plane values from XRD spectrum confirmed the crystal structure for silver nanoparticles (231).

Enzyme inhibition assays are usually performed to screen and identify metals in environmental samples (256). Five inhibitors of nitrate reductase were studied in this work. Comparable inhibition in silver reduction along with NR reduction in case of sodium azide suggested the involvement of NR in Ag NP<sub>myc</sub> production. There is a possibility that nitrate reductase might have performed the role of an electron shuttle by taking electrons from nitrate reduction to nitrite and thus transferring these electrons to silver ion, converting it to silver nanoparticle (257).

The nitrate reductase enzyme is considered an important biomolecules in the mycosynthesis of silver nanoparticles (258-260). Nitrate reductase was reported in case of other fungi (261). like *Aspergillus japonicus* PJ01, *Botryosphaeria rhodina* (262, 263). *Aspergillus brunneoviolaceus* (264), *Aspergillus niger* (265) *Aspergillus fumigatus*, *Fusarium oxysporum*, *Penicillium bellutanum* and *Beauveria baaiana*, as responsible biomolecule for bioreduction of silver ions to nanoparticles. The optimum activity of nitrate reductase was attained at pH 7-9, 0.2% salinity, and 30 °C (266). Higher NR activity was observed with carbon source glucose and nitrogen source yeast extract (251). Thermal stability of NR was observed as <20% residual activity at 50°C (267). Metal ions of mercury, nickle, cobalt and zinc caused highest reduction the NR activity (256). The values of NR activity and its kinetic parameters *Km* and *Vmax* were found to be higher than other reported cases (255, 267).

The size (2604 kb) of the NR gene of *A. flavus* SZ2 was in agreement with the previous findings (268). Molecular weight of nitrate reductase protein were also found in case of other fungi involved in biosynthesis of silver nanoparticles (269, 270).

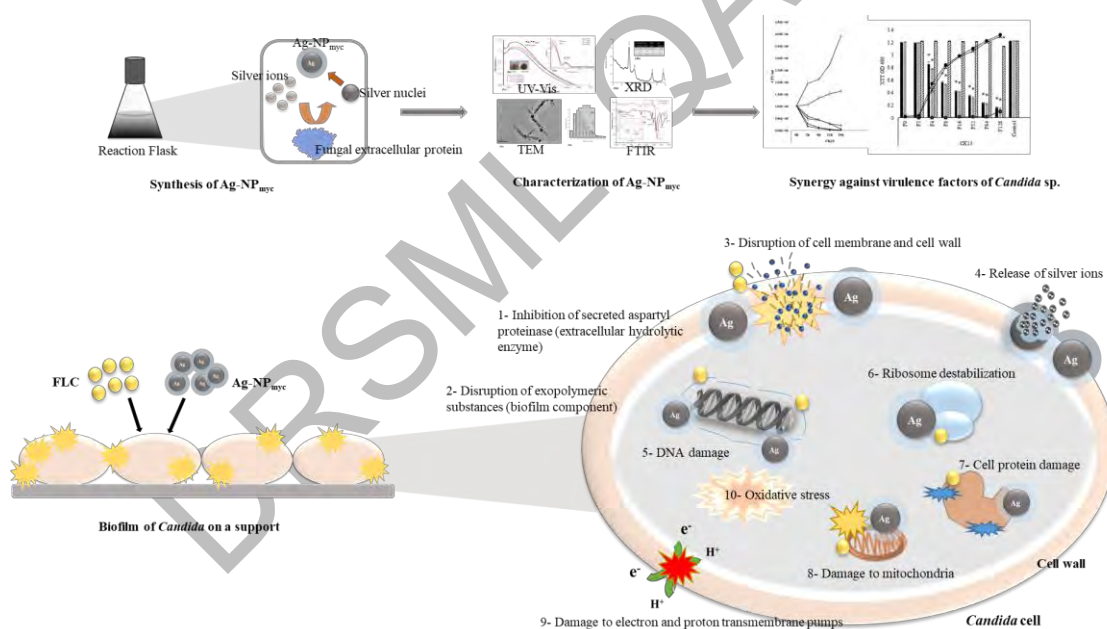
## 5.6 Conclusion

- The change in color of reaction mixture and surface plasmon resonance value (450 nm) suggest the transformation of the oxidation state of silver ions, and that extracellular fungal components might be involved in the process.
- The size and morphology Ag NP<sub>myc</sub> were determined by TEM micrograph, which revealed to be spherical shaped. The Ag NP<sub>myc</sub> particle size histogram shows a size range of 1 to 70 nm.
- The XRD spectrum showed that the plane values confirm the crystal structure for silver to be face-centered cubic (fcc).
- Five inhibitors of nitrate reductase (NR) were studied in this work. Comparable inhibition in silver reduction along with NR reduction in case of sodium azide suggested the involvement of NR in Ag NP<sub>myc</sub> production.
- Positive correlation ( $R = 0.855$ ) indicating the involvement of nitrate reductase in the mycosynthesis of Ag NP<sub>myc</sub> by reducing silver nitrate specific activity of NR and optical density at 450 nm.
- Specific activity was improved from 15.54 to 17.77 U/mg after Sephadex-100 gel filtration.
- The  $K_m$  and  $V_{max}$  of NR were found to be 13.18 mg/ml and 0.07 U/ml ( $\mu\text{mol/ml/min}$ ).
- The size of the NR gene product was found to be 2604 bp.
- SDS-PAGE of nitrate reductase of *A. flavus* SZ2 showing two bands of 70 and 45 kDa.

# Chapter 6: Fluconazole and Biogenic Silver Nanoparticles-based Nano-fungicidal System for Highly Efficient Elimination of Multi-drug Resistant *Candida* Biofilms

**Status:** Contents out of this study have been published in the journal of Materials Chemistry and Physics (<https://doi.org/10.1016/j.matchemphys.2021.125451>): Zainab, S., et al. (2022). "Fluconazole and biogenic silver nanoparticles-based nano-fungicidal system for highly efficient elimination of multi-drug resistant *Candida* biofilms." *Materials Chemistry and Physics* 276: 125451.

## Graphical Abstract



## 6.1 Introduction

Pathogenic eukaryotes including protists and fungi are distributed worldwide with high rates of morbidity and mortality in clinic. Among these eukaryotic pathogens, *C. albicans*, is of the most importance being ranked as the fourth-highest cause of human blood infections (271). Candidiasis-associated diseases are of great concern because of the prevalence of related risk factors, such as antibiotic treatment, neutropenia, long-term stay of intensive care unit (ICU) and organ transplantation etc. (272).

Currently, the therapeutic drugs to treat candidiasis are limited to few classes including azoles, polyenes, echinocandins and allylamines (273). Most of antifungal drug agents, target the distinct synthesis pathways and functions of ergosterol, beta (1-3)-D-glucan, nucleic acids, protein, mitochondria and mitosis. Among antifungal drugs, azoles such as itraconazole (ITC), fluconazole (FLC), voriconazole (VOR) and posaconazole (POS) are considered as first-line drug agents to treat refractory fungal diseases.

The efficacy of antifungal drugs is compromised by the strong ability of *Candida* sp. in biofilm formation on the surfaces of teeth, mucosa and artificial implanted devices (274) and the emergence of drug resistant fungal strains. Compared to antibacterial drugs, antifungals drugs are not very effective as the fungi develop the drug resistance within a very short time (275). Drug resistant mechanisms of various kind were seen in *C. albicans* e.g. target alteration with decreased antifungal binding affinity, over expression of drug targets, drug sequestration by keeping drugs into sub-cell structures (276), blocking of antifungal drug entry by phenotype transition and chromosome aneuploidy (e.g. increase target gene copy on some chromosome (277), enhanced drug efflux with the help of drug efflux pumps e.g. CDR (Candida Drug-Resistance) pump and MFS (Major Facilitator Superfamily) efflux pump in *C. albicans* (274).

The metallic nanoparticles formation by microbial reduction of noble metal ions, e.g. those of platinum, palladium, gold and silver has been reported in literature with potential usefulness in technological applications (278) such as energy, industry, agriculture, medicine, environmental protection, photonics, catalysis, in the bioleaching from metal ores etc. (225, 279, 280). Due to their surface moieties, specific size and shape, catalytic, electron transfer and redox active properties (281), biogenic noble metal-based nanomaterials display antimicrobial properties (282), making them suitable for dental and biomedical implants and bandages (283-285). Previous studies on biofilms of *C. albicans* to study the effect of silver nanoparticles, showed how nanoparticles caused cell disruption by targeting cell wall, affected secretion of exopolymeric substances (EPS) and inhibited hyphal growth (161). Silver nanoparticles also found to affect the membrane permeability by binding to sulfur-containing proteins in cellular membranes and phosphorus-containing molecules



resulting in inhibition of respiratory enzymes and replication (162). But with increasing pathogenic resistant forms, new alternative drugs are required. For this purpose, synergistic drug therapy has been proved to be a pragmatic and valid strategy to seek novel drugs with unique mode of action.

Secreted aspartyl proteinases (SAP) are the important virulence factors in *Candida* species which help the pathogenicity towards host cells (286, 287). Till now, no data is available for combined efficacy of mycogenic silver nanoparticles Ag NP<sub>myc</sub> and fluconazole causing inhibition of SAP produced by resistant *Candida* species. This study uses the synergistic combination of mycogenic silver nanoparticles and antifungal drug as a way for discovering new potential agent for anti-biofilm and anti-virulence against fungal pathogens. In a previous study, our research team carried out the potential antifungal role of Ag NP<sub>myc</sub> alone to control biofilms of clinical isolates of *Candida* sp., (40). In order to understand the mechanism behind the inhibition of biofilm formation, this study was extended to encompass, the combined effect of fluconazole and Ag NP<sub>myc</sub> on planktonic and biofilm forms of six *Candida* species along with their virulence factors including exopolymeric substances as biofilm component and secreted aspartyl proteinases as hydrolytic enzymes.

### Objectives

- To synthesize and characterize mycogenic silver nanoparticles (Ag NP<sub>myc</sub>) using *Aspergillus oryzae* SZ1.
- To study the cytotoxic effects of mycogenic silver nanoparticles against brine shrimp lethality assay.
- To investigate the potent synergistic effect of Ag NP<sub>myc</sub> along with antifungal fluconazole on planktonic growth and biofilm formation on six fluconazole resistant clinical isolates of *Candida* species (*C. albicans*, *C. galabrata*, *C. parapsilosis*, *C. krusei*, *C. tropicalis*, *C. albicans* ATCC 24433).
- To investigate combined effect of fluconazole and Ag NP<sub>myc</sub> on exopolymeric substance (EPS) of planktonic and biofilm matrix composition of six *Candida* sp.
- To evaluate combined effect of fluconazole and Ag NP<sub>myc</sub> on secretion of S aspartyl proteinases in planktonic and biofilm forms of *Candida* sp.

## 6.2 Material and methods

### 6.2.1. Microorganisms

For the synthesis of Ag NP<sub>myc</sub>, the fungus *Aspergillus oryzae* SZ1 (NCBI accession number: MH664050) was used. The fungus was maintained on Sabouraud dextrose agar (SDA, Oxoid) slants after culturing the fungus at 30 °C, pH 6 and 3 days. For Ag NP<sub>myc</sub> synthesis, actively growing subcultures were used as the starting material.

For Anti-*Candida* study, clinical isolates from urine (n= 5) including *C. albicans* (CA115), *C. glabrata* (CG55), *C. parapsilosis* (CP100), *C. krusei* (CK13), *C. tropicalis* (CT51) were provided by Immunology and Medical Microbiology lab, Quaid-i-Azam University, Islamabad. To compare biofilm studies, American Type Culture Collection culture of *C. albicans* (ATCC 24433) was utilized as a control. The isolates were resistant against voriconazole, amphotericin B and fluconazole. The isolates were cultured on Sabouraud dextrose agar (Oxoid) for 24–48 hours at 37 °C and stored at 4 °C.

### 6.2.2 Silver tolerance screening assay

Heavy metal ions can impact fungi by causing morphological and physiological and changes, in order to tolerate these changes, fungi may develop stress response as defense mechanism to protect the cellular constituents. These mechanisms may include production of enzymes and other biochemical resulting in metal tolerant fungi. Metal tolerance index (TI), is often used as indication of the response to metal stress that tells the minimum inhibitory concentration of a metal which an organism can tolerate.

Stock solution (1000 ppm) of silver nitrate (Ag<sup>+</sup>) was prepared in deionized, filter-sterilized water. Effect of metal ions on *A. oryzae* SZ1 was determined by inoculating five mm disks of 4 days old pure fungal cultures on SDA agar plates supplemented with different metals at variable concentrations (100, 200, 400, 600, 800, 1000, 2000, 3000 and 5000 mg/lit) and incubated at 30°C for 7 days. In parallel, culture without metal salts was kept as control. The mean diameter of radial growth from triplicate cultures (in millimeters) was recorded for each plate on the day 7th. Silver resistance of *A. oryzae* SZ1 was determined by measuring minimum inhibitory concentration of

silver ions and silver tolerance index (186). The tolerance index ( $T_i$ ), an indication of the organism response to metal stress was calculated from the growth of *A. oryzae* SZ1 exposed to the metals divided by the growth in the control plate. The higher the  $T_i$ , the greater the metal tolerance (187).

$T_i = \text{Diameter of colony of metal treated fungus} / \text{Diameter of colony of untreated fungus (control)} \times 100$

### 6.2.3. Molecular identification of the fungal isolate

The selected fungus was identified by partial sequencing of their internally transcribed spacer (ITS) region in the extracted DNA. For sequencing, the ITS regions of 5.8S and 18S rRNA were identified by using the universal primers ITS-1 and ITS-4 (189).

### 6.2.4. Mycosynthesis of Ag NP<sub>myc</sub>

Mycosynthesis of Ag NP<sub>myc</sub> was carried out using *A. oryzae* SZ1 (NCBI accession number: MH664050). Fungus was cultured in nutrient rich MGY media containing 0.3% malt extract, 1 % glucose, 0.3 % yeast extract and 0.5% peptone. pH of culture medium was adjusted to 9 using NaOH (1M). Culture media was then incubated in shaker incubator at rotation of 150 rpm at 72 h at 30 °C. After incubation of 72 h, mycelia were centrifuged at 5000 rpm and 4 °C for 20 min to separate the mycelium from the culture media. Later, mycelia were washed well to remove the culture media components, with autoclaved distilled water, funnel and filter paper under sterile conditions. 20 g of washed mycelia was suspended in sterile water (100 ml) and was put onto a shaker at 30 °C (200 rpm) for 24 h to obtain extracellular fungal enzymes' secretions. After this, fungal biomass was filtered again using sterile filter paper and distilled water to obtain cell free filtrate. This filtrate (as a source of fungal enzymes) was added with an equal volume of AgNO<sub>3</sub> solution (final concentration 0.1 M) and was put onto a shaker at 30 °C (200 rpm) for a period of 96 h. In order to screen the fabrication process of Ag NP<sub>myc</sub>, aliquots from reaction mixture were periodically collected and subjected to UV–Vis spectroscopy.

### 6.2.5. Characterization of Ag NP<sub>myc</sub>

The UV–Vis spectroscopy measurements were performed on a Shimadzu dual-beam spectrophotometer (model UV-1601 PC) operating at a resolution of 1 nm. To obtain X-ray Diffraction (XRD) patterns, instrument Philips PW 1830 Cu K $\alpha$  radiation ( $k = 1.5404 \text{ \AA}$ ) was used. The operating conditions were 30 mA current and 40 kV voltage. Ag NP<sub>myc</sub> solution was casted as a drop on a copper grid (carbon-coated) for high-resolution transmission electron microscopy (HRTEM) using JEM-2100F field emission electron microscope at an accelerating voltage of 200 kV. To investigate presence of capping moieties on the surface of Ag NP<sub>myc</sub>, an ATR (Attenuated Total Reflectance) equipped FTIR spectrometer (Perkin Elmer Inc. Spectrum 100. Wellesley, MA, United States) was used. Spectra were recorded after 32 scans of wavenumbers from 4,000 to 500  $\text{cm}^{-1}$  at 4  $\text{cm}^{-1}$  resolution. All FTIR graphs represented wavenumber in  $\text{cm}^{-1}$  on the x-axis and transmittance on the y-axis.

#### **6.2.6. Cytotoxicity analysis of Ag NP<sub>myc</sub>**

Brine shrimp lethality assay was used to measure the dose (50% lethality dose-LD50) required to kill half of a group of brine shrimp (*Artemia salina*) larvae. Lethality or viability is a commonly used indicator to measure toxicity, here it was assessed by noticing brine shrimp movement in the medium. Brine shrimp (aquatic zooplankton, microcrustacean) is being used extensively as a model organism in toxicology studies of nanomaterial due to their distinct characteristics such as small body size, rapid hatching, cost-effective and simple growth conditions (222). Toxicity testing was carried out by letting *A. salina* larvae growing in vials containing different concentrations of Ag NP<sub>myc</sub> (288). In this study, organismic-level acute (289) toxicity of Ag NP<sub>myc</sub> was determined; acute toxicity refers to the adverse effects of a substance with a short exposure in little period of time.

Dried eggs of brine shrimps were bred in sea salt medium (Instant Ocean®) for 48 h in a container with two partitions connected through holes in the central barrier. After adding eggs to one part of the container, it was covered and whole container was placed under lamp as a light source. After hatching, the brine shrimp larvae were swimming towards the part under light and could be observed with fast movement. 10 larvae per vial (24 h old) were transferred to triplicate vial set containing saline solution along with 0.005, 0.02, 0.035, 0.05, 0.065, 0.08, 0.1, 0.15, 0.2, 0.25, 0.3, 0.35, 0.5 mg/ml of Ag NP<sub>myc</sub> suspension, serially diluted with sea salt solution. After

24 and 48h, percentage lethality for each dose was calculated by counting the number of dead brine shrimps in each vial (224) using following formula:

% Lethality = [(Number of dead brine shrimps in experimental vials)/Number of total brine shrimps in the control] × 100.

LD50 was calculated from the regression equation in dose–response curve.

### **6.2.7. Planktonic cells inhibition study:**

#### **6.2.7.1 MIC**

The minimum inhibitory concentrations (MIC) of fluconazole (FLC) (2–128 µg/ml) and mycogenic silver nanoparticles (Ag NP<sub>myc</sub>) (12.5-800 µg/ml) alone and combined was determined against planktonic forms of fluconazole resistant clinical isolates of *Candida* species: *C. albicans*, *C. galabrata*, *C. parapsilosis*, *C. krusie*, *C. tropicalis* and *C. albicans* ATCC 24433.

The MIC of FLC (2–128 µg/ml) and Ag NP<sub>myc</sub> (12.5-800 µg/ml) alone and combined was measured in sabouraud dextrose broth (SDB, Oxoid) as test medium using modified broth micro-dilution procedure. First, the inoculum was prepared using standard method, then dilutions of drugs alone and in combinations were introduced to the wells in micro-titer plate resulting in eighty drug combinations.

#### **6.2.7.2 FICI**

The results of MIC were explained after finding values for fractional inhibitory concentration index (FICI). FICI describes its values for drug combinations as: synergy ( $\leq 0.5$ ), no interaction ( $>0.5$  to 4.0), antagonism ( $\geq 4.0$ ) (290). To determine individual FICI values, MIC values of nanoparticles and FLC were noted alone and in combination, after 24 hours as the lowest concentrations which caused decrease in turbidity with respect to the control growth with no drugs. Final FICI of the drug combination was then calculated by adding up the individual FICI values of nanoparticles and FLC for each *Candida* species (Table 3).

#### **6.2.7.3 Time-kill studies of drug combinations**

For time-dependent fungistatic or fungicidal analysis, *Candida* cells (CFU/ml:  $1 \times 10^6$ ) were inoculated in SDB with Ag NP<sub>myc</sub> alone or in combination with FLC at previously determined MIC values. Aliquots were taken and inoculated on SDA at time points of 0, 2, 6, 12, 24 hours and incubated for 24 hours at 37°C. Control growth of contained no drug (291).

## **6.2.8. Biofilm inhibition study**

### **6.2.8.1 Biofilm formation**

For biofilm formation, *Candida sp.* were grown in flat-bottomed plates (96-wells) as described previously (40). *Candida* cell suspensions (volume:200  $\mu$ l , CFU:  $1.0 \times 10^6$  cells/ml), were prepared glucose (10%) supplemented sabouraud dextrose broth (SDB, Oxoid) by growing at 37 °C under shaking incubation (120 rpm). After 24 hours, the medium above formed biofilms was removed and wells were rinsed with PBS to remove non-adherent cells.

### **6.2.8.2 Anti-biofilm activity**

To determine anti-biofilm activity, SDB (200  $\mu$ l), containing Ag NP<sub>myc</sub> alone (15 or 25  $\mu$ g/ml) and combinations with FLC (serial twofold dilutions from 2-128  $\mu$ g/ml), was introduced, and incubation was carried out at 37°C for 24 hours. Growth controls wells contained cell suspension without compound additions.

### **6.2.8.3 Quantification of biofilm metabolic activity (XTT assay)**

To quantify viability, biofilm metabolic activity, XTT reduction assay was performed after treating and incubating with drugs. For this purpose, stock solutions of phenazine methosulfate (PMS) and 2,3-bis[2-Methoxy-4-nitro-5-sulfophenyl]-2H-tetrazolium-5-carboxanilide inner salt (XTT) were prepared freshly (40). Briefly, suspensions above biofilms formed in wells were removed and biofilm cells were washed gently with PBS two times. Then, 10  $\mu$ l of PMS and 90 $\mu$ l of XTT were added to each well. Microtiter plates were incubated (37°C) in dark for two hours. Optical density (at 492 nm) of suspensions in wells was measured under a microtiter plate reader (Platos, R492) (292). Assays were performed in triple replicates at three different times.

## **6.2.9. Study of extracellular polymeric substances (EPS) as Virulence Factor**

### 6.2.9.1 EPS evaluation in planktonic cells

#### 6.2.9.1.1 EPS extraction from planktonic growth:

EPS are important component of biofilm forms of pathogenic fungi and can be evaluated in order to study the effect of potent drugs against biofilm resistance. First, EPS matrix was extracted from planktonic growth. In case of planktonic growth, loop full of culture was transferred into test-tubes having 5 ml of SDB medium supplemented with 10% glucose. Each culture was subjected to treatment with 200  $\mu$ l of Ag NP<sub>myc</sub> alone (15, 25 ppm) and in combinations with fluconazole (2, 4, 8, 16, 32, 64 and 128  $\mu$ g/ml) whereas cultures without drugs served as control and incubated at 37 °C under shaking conditions. After 72 hours of incubation, cell free supernatant was obtained by centrifugation (10,000 rpm) at 4°C for 10 min thereby removing *Candida* cells. EPS was precipitated from supernatant using by chilled absolute ethanol followed by overnight incubation (4°C). EPS pellet was obtained by centrifuging (10,000 rpm, at 4°C for 20 min), dried and weight was measured at room temperature (293).

### 6.2.9.2. EPS evaluation in Biofilms

#### 6.2.9.2.1 EPS extraction from biofilm growth:

In case of biofilm growth, biofilms were developed in eppendorf tubes by inoculating 100 $\mu$ l of standard *Candida* suspensions in 1.5 ml of SDB supplemented with glucose (10%) and incubated at 120 rpm and 37°C for 2 h for initial adherence to tube walls. Then, suspensions were carefully removed and tubes were washed twice with sterile PBS in order to remove non-adherent or weakly adherent cells. Afterwards, the tubes were filled with fresh SDB and kept in incubation for 24 hours at 37 °C. Later, the growth medium was aspirated and biofilms were washed with PBS. Additions of 100  $\mu$ L mycogenic silver nanoparticle suspension (15, 25 ppm) alone and in combinations with antifungal agent (2, 4, 8, 16, 32, 64, 128 ppm) to biofilms were made after 24 h of growth and incubated for further period 72 h at 37 °C. After 72 hours of incubation, biofilms were sonicated to remove the EPS, and cell free supernatant was obtained by centrifugation (10,000 rpm) at 4°C for 10 min. EPS was precipitated using chilled absolute ethanol followed by overnight incubation at 4°C. EPS was obtained by centrifuging (10,000 rpm) at 4°C for 20 min. EPS pellet was dried at room temperature dry weight was measured (293).

### **6.2.10. Evaluation of extracellular SAP activity as virulence factor**

Inocula were prepared by inoculating loopful of each one of six *Candida* strains into sabouraud dextrose broth (SDB) and incubated for 24 h at 35 °C in an orbital incubator. The cells were then harvested by centrifugation and suspended in sterile saline (8.5 g/L NaCl), vortexed and diluted using saline to yield standard *Candida* suspensions with cell density of  $10^6$  cells/ml (OD530 nm, by a 0.5 McFarland standard).

#### **6.2.10.1 Evaluation of extracellular SAP activity in planktonic cells**

##### ***6.2.10.1.1 SAP induction in planktonic forms:***

In order to induce SAP secretion in planktonic forms, cultures were grown under proteinase-inducing conditions by inoculating 100µl of standard *Candida* suspension in 1.5 ml of yeast peptone dextrose broth (YPD) (1% w/v yeast extract, 2% w/v peptone, 2% w/v dextrose), supplemented with BSA (1%) in eppendorf tubes and incubated for 24 h at 37°C at 120 rpm. Later, the cells were washed with PBS twice and centrifuged (3000 rpm/5 min) and then inoculated ( $10^6$  cells) into new YPD medium.

##### ***6.2.10.1.2 Drug treatment in planktonic forms:***

Next step is the drug treatment in planktonic forms. Additions of 100 µL mycogenic silver nanoparticle suspension (15, 25 ppm) alone and in combinations with antifungal agent (2, 4, 8, 16, 32, 64, 128 ppm) to planktonic cells were made after 24 h of growth and incubated for further period of 4 and 24 h at 37 °C. Next, the planktonic suspensions were centrifuged (3000 rpm/5 min) and the supernatants were submitted to SAP determination assay.

#### **6.2.10.2 Evaluation of extracellular SAP activity in biofilm forms**

##### ***6.2.10.2.1 SAP induction in biofilm forms:***

To induce SAP activity in sessile forms of *Candida* spp, biofilms were developed in eppendorf tubes by inoculating 100µl of standard *Candida* suspensions in 1.5 ml of yeast peptone dextrose broth (YPD), supplemented with glucose (10%) and BSA (1%) and incubated at 120 rpm and 37°C for 2 h for initial adherence to tube walls. Then, suspensions were carefully removed and tubes were washed twice with sterile PBS in order to remove non-adherent or weakly adherent cells. Afterwards, the tubes



were filled with fresh growth medium, incubated and after that, medium was carefully aspirated and cells were rinsed with PBS centrifuged for five minutes at 5000 rpm and fresh YPD medium was used to inoculate the cell suspension (CFU:  $10^6$  cells/ml).

#### **6.2.10.2.2 Drug treatment in biofilm forms:**

For drug treatment in biofilm forms, 100  $\mu$ L of mycogenic Ag NP<sub>myc</sub> suspensions, alone and in combinations with antifungal agent (as described above) were introduced *Candida* cell suspensions and incubation (37 °C) was carried out for further 24 h. The suspensions after incubation, were centrifuged (3000 rpm/5 min) and the supernatants were used to determine SAP activity.

#### **6.2.10.2.3. SAP assay:**

SAP activity was measured based on a modification of a previously described procedure (164). Briefly, after incubation with drug combinations, 0.1 ml of supernatant from planktonic cells and biofilm containing tubes was shifted to other eppendorf tubes and BSA (1% w/v) containing sodium citrate buffer (0.1 M, 0.4 ml, pH 3.2) was added and tubes were incubated at 37°C for 1 h. After incubation, 0.5 ml of ice cold 5% trichloroacetic acid (TCA) was added to stop the reaction. The mixture was centrifuged at 5000 rpm for 10 min to remove precipitated material and absorbance (at 280 nm) was noted. SAP activity was determined in the culture supernatant as amount ( $\mu$ M) of released tyrosine per ml per min.

### **6.3. Statistical analysis**

Statistical analysis was performed using one-way ANOVA and Tukey's test by Origin 8.0. All values were expressed as mean ( $\pm$ ) standard deviation (SD) of triplicate samples in a representative experiment. All experiments were done independently at least three times. A *P*-value less than 0.05 was considered as statistical significance.

### **6.4. Results and Discussion**

#### **6.4.1. Silver tolerance screening:**

Silver tolerance ability of the fungus *Aspergillus oryzae* SZ1 (NCBI accession number: MH664050) was screened against ionic silver. The fungus was able to grow till silver concentration of 2000 mg/ml.

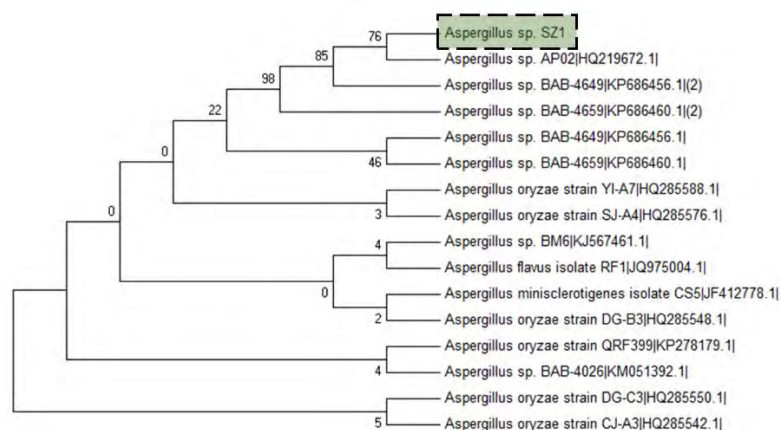


Figure 6.1. Phylogenetic tree of *Aspergillus oryzae* SZ1

#### 6.4.2 Ag NP<sub>myc</sub> formation

The extra-cellular production of Ag NP<sub>myc</sub> (schematic illustration shown in Figure 6.2) was initially determined by monitoring gradual color change of reaction mixture containing silver ions with cell-free filtrate of *A. oryzae* SZ1. Figure 6.3b shows Erlenmeyer flasks showing the color change in reaction mixture of ionic silver and mycelia-free filtrate during 72 hours interval. During the incubation of silver ions with mycelia free filtrate, it showed color transition from colorless to blackish brown (Figure 6.3b). In contrast, the positive (containing the reducing agent i.e. mycelia-free filtrate) and negative (without reducing agent i.e. ionic silver) controls did not display any characteristic color change which suggested that extracellular filtrate components might be involved in nanofabrication process.

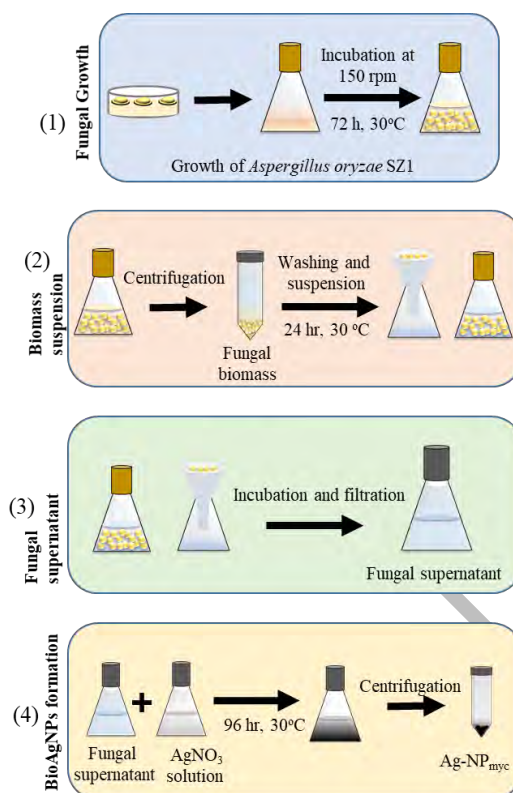


Figure 6.2. Schematic illustration of Ag NP<sub>myc</sub> synthesis procedure

The change in color of reaction mixture in Figure 6.3b reflects the fungal ability to transform the oxidation state of silver metal ions. Table 6.1 shows some examples of silver nanoparticles from other fungi.

Table 6.1. Other examples of mycogenic silver nanoparticles from literature.

Serial no.	Fungal source	Mechanism of synthesis	Reference
1.	<i>Fusarium oxysporum</i>	$\alpha$ -NADPH-dependent nitrate reductase	(294)
2.	<i>Lentinus edodes</i>	Laccase	(295)
3.	<i>Macrophomina phaseolina</i>	Signal peptides	(296)
4.	<i>Aspergillus tubingensis</i>	Glycoamilase, acid phosphatase, glucanosyltransferase and serine carboxipeptidase	(213)
5.	<i>Aspergillus oryzae</i> SZ1 (This study)	Nitrate reductase	-

### 6.4.3 Ag NP<sub>myc</sub> characterization:

UV-Visible spectroscopy is used commonly to characterize Ag NP by detecting the absorption spectra due to surface plasmon resonance which is characteristic feature of

noble metal nanoparticles. The gradual increase in absorption spectrum at 430 nm showed rise in the surface plasmon excitation. A gradual increase in absorption was observed at 430 nm wavelength at various time intervals (till 48 h) with same peak position (Figure 6.3a) (297). The regular rise in absorbance shows transformation of precursor silver ions into Ag NP<sub>myc</sub> through reduction (233). The absorption peaks from the silver nitrate solution are shown in inset graph (Figure 3c) at wavelengths of 226 and 305 nm indicate presence of nitrate (229) and silver ions (254), respectively.

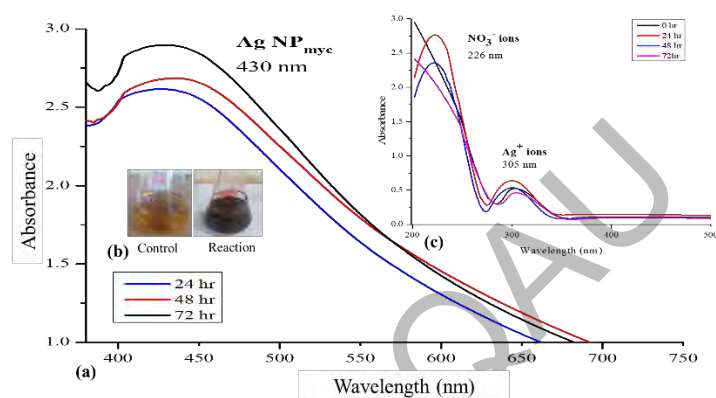


Figure 6.3. UV-Vis spectrum for the mycogenic silver nanoparticles

Ag NP<sub>myc</sub> film showed defined X-ray diffraction ( $2\theta$ ) peaks at  $13.96^\circ$ ,  $20.79^\circ$ , and  $33.87^\circ$ , corresponding to metallic silver crystal planes of 111, 200, 220 and 311, respectively (Figure 6.4). These planes confirm the crystal structure for silver to be face-centered cubic (fcc) (ICDD reference code. 01-087-0717). In a previous study by our research group using different a similar XRD pattern was observed for Ag NP<sub>myc</sub> produced by *Aspergillus* species (298).

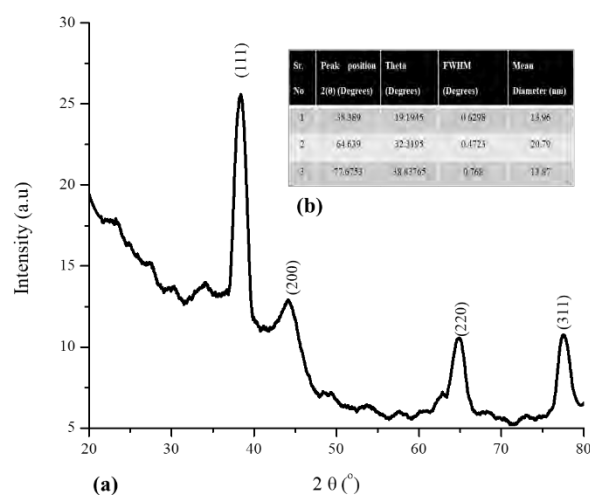


Figure 6.4. XRD pattern and data for the mycogenic silver nanoparticles

The size and morphology Ag NP<sub>myc</sub> were determined by TEM micrographs (Figure 5a), which revealed to be uniform, spherical shaped and monodispersed without any prominent flocculation. The Ag NP<sub>myc</sub> size ranges from 1 to 50 nm as shown by the particle size histogram (Figure 6.5b).

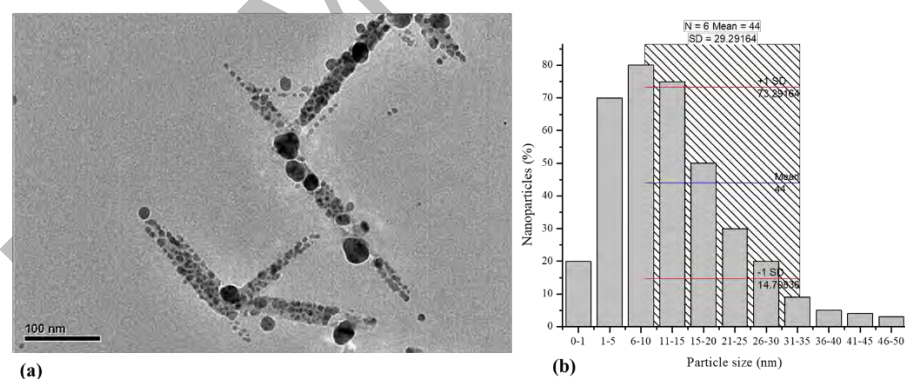


Figure 6.5. Representative TEM micrographs of mycogenic silver nanoparticles produced from *A. oryzae* SZ1

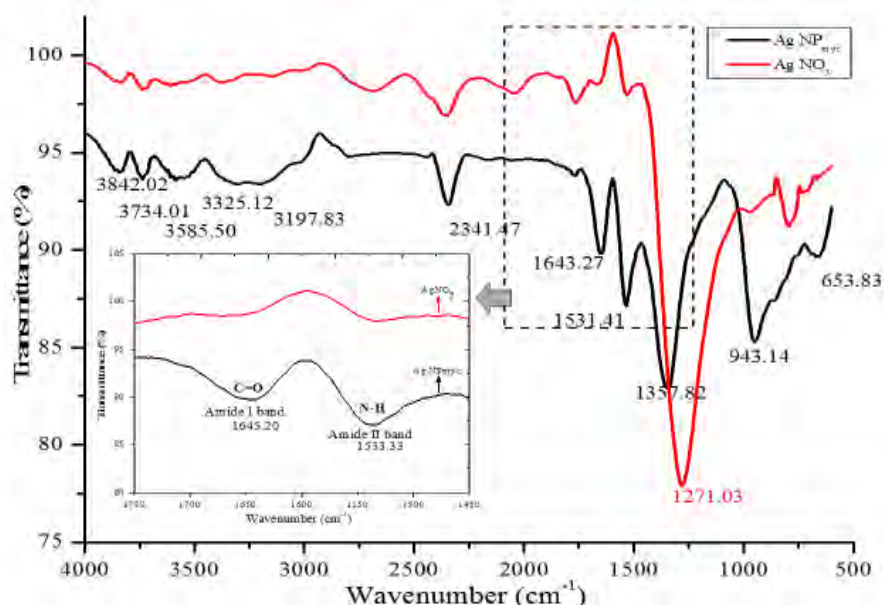


Figure 6. 6. FTIR spectrum of mycogenic silver nanoparticles produced from *A. oryzae* SZ1

The Ag NP<sub>myc</sub> were subjected to FTIR analysis to identify the presence of capping ligands involved in stabilization of the Ag NP<sub>myc</sub> surface. Carbonyl and amine linkages (amide I and amide II) in amino acids of proteins show characteristic peaks due to conformational changes in secondary structure after absorbing electromagnetic radiation from infrared region. In this study, FTIR spectrum exhibited characteristic bending ( $1643\text{ cm}^{-1}$ ) and stretching vibrations ( $3325\text{ cm}^{-1}$ ) of amide I and amide II bands ( $1531$  and  $3197\text{ cm}^{-1}$ ) (Figure 6.6) (233). The spectra showed intensive bands at  $653.83$ ,  $943.14$ ,  $1357.82$ ,  $1531$ ,  $1643$ ,  $3197$ ,  $3325$ ,  $3585.50$ ,  $3734$  and  $3842\text{ cm}^{-1}$  which were corresponding to C-H (methylene), =C-H (alkenes), -CH<sub>3</sub>, O-H bending mode, phenols, N-H (amines), N-HCO, C=O (carbonyl), C-O-H respectively (234). Previous FTIR studies of biogenic silver nanoparticles revealed the involvement of amine, cysteine and carboxylate residues from proteins (233) polyphenols, flavanones or terpenoids, and carbohydrate in capping and stabilization of silver nanoparticles (234). These results indicate that *A. oryzae* SZ1 (NCBI accession number: MH664050) secretes different bioactive molecules in much higher amounts which make them desirable for the biosynthesis of silver nanoparticles.

For the synthesis of silver nanoparticles by *Aspergillus oryzae* SZ1, the proposed mechanism is given in Figure 11. The reduction reaction which governs mechanisms of most types of biogenic synthesis of nanoparticles involves cellular polysaccharides and peptides, both intra and extracellular, leading to enzymatic oxido-reduction,

chelation, and sorption. In case of *Fusarium oxysporum* (291), NADPH-dependent nitrate reductase, silver ions were reduced by an electron transfer involving NADP (co-factor). Quinine derivatives of naphthoquinones and anthraquinones are also known to produce silver nanoparticles (102). In *Verticillium* sp., extracellular process of silver nanoparticle synthesis involved trapping of silver ions on the cell wall and reduction by reductase enzyme to silver nuclei (103). During intracellular way of synthesis, trapping of ions, their reduction, and finally capping of the nuclei takes place. While in case of extracellular biosynthesis, enzyme secretion, reduction, nucleation, growth and particle capping takes place. For most of cases in silver nanoparticle synthesis, nitrate reductase is the enzyme most commonly isolated so far (106).

#### **6.4.4. Cytotoxicity analysis of Ag NP<sub>myc</sub>:**

In vitro cytotoxicity assays against brine shrimps (*Artemia salina*) have been performed to preliminary screen the toxicity of test samples (Figure 6.7). Ag NP<sub>myc</sub> did not show any cytotoxic effect on *A. salina* larvae, as measured by cell viability which was more than 50% even after 48 hours, however, the maximum cytotoxicity was achieved after 0.3 mg/ml concentration which exhibited 100% mortality (Table 6.2). Ag NP<sub>myc</sub> exhibit toxicity (LD50 0.114 to 0.049 mg/ml) against eukaryotic animal model (brine shrimps) after 24 and 48 hours. Vijayan et al. (299) screened the effect of silver nanoparticles against *A. salina* mortality (24 h) and found the lethal effect (LC50) at concentration of  $89 \pm 5$  mg/l. Kumar et al. (300) assessed the effects of biogenic silver nanoparticles (synthesized from *Sargassum ilicifolium* extracts) against *A. salina* and LC50 was found to be 1.08 mg/l.

Table 6.2. Cytotoxicity (% mortality and LD50) of Ag NP<sub>myc</sub> in brine shrimps

Time	Concentration of Ag-NP <sub>myc</sub> (mg/ml)													LD50
	0.005	0.02	0.035	0.05	0.065	0.08	0.1	0.15	0.2	0.25	0.3	0.35	0.5	
24 hr	13 ±2	13 ±2	33 ±2	33 ±2	33 ±2	53 ±2	63 ±2	73 ±2	76 ±2	83 ±2	86 ±2	93 ±2	100 ±0	0.114
48 hr	16 ±2	23 ±2	36 ±2	36 ±2	43 ±2	56 ±2	66 ±2	76 ±2	86 ±2	86 ±2	96 ±2	100 ±0	100 ±0	0.049

Note: The values are shown as percentage mortality (%) with S.E (standard errors) (±). The units for LD50 are expressed in mg/ml.

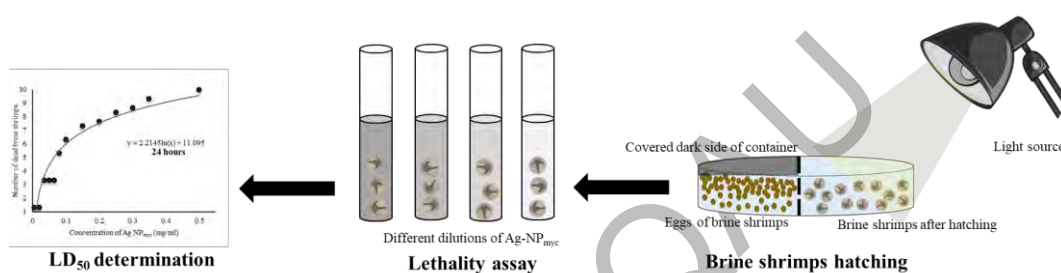


Figure 6.7. In vitro acute toxicity analysis - brine shrimp mortality assay

#### 6.4.5. Planktonic cells inhibition study

In this study, Ag NP<sub>myc</sub> synthesized by *A. oryzae* SZ1 were screened for antifungal capability against drug resistant clinical isolates of six *Candida species* (*C. albicans*, *C. galabrata*, *C. parapsilosis*, *C. krusie*, *C. tropicalis*, *C. albicans* ATCC 24433). It can be seen that the combined effect of FLC and Ag NP<sub>myc</sub> on planktonic cells of all six *Candida* species caused gradual decrease in CFU (Figure 6.8a, 6.8b). The MIC of FLC (2–128 µg/ml) and Ag NP<sub>myc</sub> (12.5–800 µg/ml) alone and in combination were determined in SDB as test medium by the standard broth microdilution method. Table 6.3 shows the minimum inhibitory concentrations (MICs) and fractional inhibitory concentration index (FICs) of Ag NP<sub>myc</sub>/FLC against planktonic cells by drug without as well as in combination with Ag NP<sub>myc</sub>. Ag NP<sub>myc</sub> exhibited an antifungal effect against planktonic form of *Candida* spp. Fractional inhibitory concentration index (FICI) was used to interpret the results of MIC (291). The results showed that combination use of Ag NP<sub>myc</sub> with FLC exhibit strong *in vitro* antifungal synergy (FICI values ranged from 0.2812 to 0.375) against the majority of the *Candida* strains tested (301). Lower antifungal effect was displayed when FLC (64 to 128 µg/ml) and Ag NP<sub>myc</sub> (50 to 100 µg/ml) were used independently.



The resistance in fungal pathogens results in use of high dosage of antifungal drug. The minimum inhibitory concentration was determined to find if there any reduction dosage of fluconazole and nanoparticles take place or not. The use of combination of FLC and Ag NP<sub>myc</sub> caused a significant reduction in MIC of FLC for all resistant *Candida* strains (302). For example, in case of *C. albicans*, the MIC of fluconazole was reduced from 128 µg/ml (when used alone) to 8 µg/ml (when used in combination with nanoparticles) and same in case of other *Candida* species.

Table 6.3. Antifungal effect of Ag NP<sub>myc</sub> alone/or in combination with fluconazole (FLC) against *Candida sp.*

<i>Candida sp.</i>	MIC (µg/ml)			FICI		
	FLC	Ag NP <sub>myc</sub>	FLC/Ag NP <sub>myc</sub>	FLC	Ag NP <sub>myc</sub>	FLC/Ag NP <sub>myc</sub>
CA115 ( <i>C. albicans</i> )	128	50	8/12.5	0.0625	0.25	0.3125
CG55 ( <i>C. glabrata</i> )	64	100	16/12.5	0.25	0.125	0.375
CP100 ( <i>C. parapsosis</i> )	128	50	16/12.5	0.125	0.25	0.375
CK13 ( <i>C. krusei</i> )	64	100	4/12.5	0.0625	0.125	0.1875
CT51 ( <i>C. tropicalis</i> )	128	50	8/12.5	0.0625	0.25	0.3125
ATCC 24433 ( <i>C. albicans</i> )	64	50	2/12.5	0.03125	0.25	0.2812

Note: FICI: Fractional inhibitory concentration index

The time-kill studies by CFU were performed to evaluate the nature of drug interaction (fungistatic or fungicidal) with *Candida sp.* In case of *C. albicans*, FLC and Ag NP<sub>myc</sub> (15 and 25 ppm) alone showed fungistatic growth whereas the combinations of FLC and Ag NP<sub>myc</sub> showed the synergistic fungicidal effects as indicated by gradual decrease in CFU. Whereas in other species of *Candida*, treatments with 15 and 25 ppm Ag NP<sub>myc</sub> alone, showed fungicidal effect (291). These results again showed the advantage of use of combination of nanoparticles with antifungal drugs to reduce the growth of resistant *Candida* species.

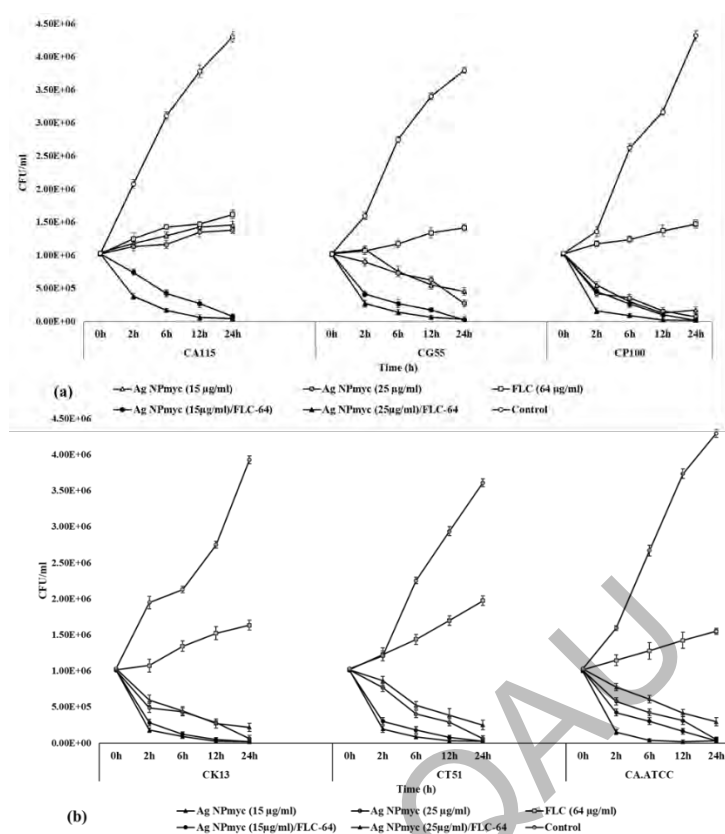


Figure 6.8. Combined effect of Ag NP<sub>myc</sub> and FLC alone or in combination on planktonic cells of *Candida sp.* for time-kill curve analysis (CFU) at 0, 2, 6, 12, 24 hours at 37°C.  $1 \times 10^6$ . CFU values are represented with mean  $\pm$  SE of three independent experiments.

#### 6.4.6. Biofilm inhibition study

In FLC resistant *Candida sp.*, reduction of metabolic activity in biofilms (24 hours old) by Ag NP<sub>myc</sub> was observed. Overall, >60% reduction of metabolic activity was observed in different *Candida sp.* at 16 µg/ml FLC in combination with Ag NP<sub>myc</sub>. The highest reduction was observed in *C. parapsilosis* (CP100) and *C. tropicalis* (CT51) at 25 ppm Ag NP<sub>myc</sub> and in *C. glabrata* (CG55) at 15 ppm Ag NP<sub>myc</sub> and shown to be >80% and >90% respectively (Figure 9a, 9b). The anti-biofilm effect was comparable with a previous study of Ag NP<sub>myc</sub> synthesized with *Fusarium oxysporum* (291). When Ag NP<sub>myc</sub> (15 and 25 ppm) were tested on biofilm alone, no significant effect was observed, however, in combination with the fluconazole drug (15 ppm, 25 ppm Ag NP<sub>myc</sub> with FLC) the cell viability decreased significantly ( $P < 0.05$ ) within 24 hours (Figure 6.9a, 6.9b). The reduction in metabolic activity of fungal pathogen again proved the advantage of use of combination of antifungal drug with the nanoparticles against *Candida* species.

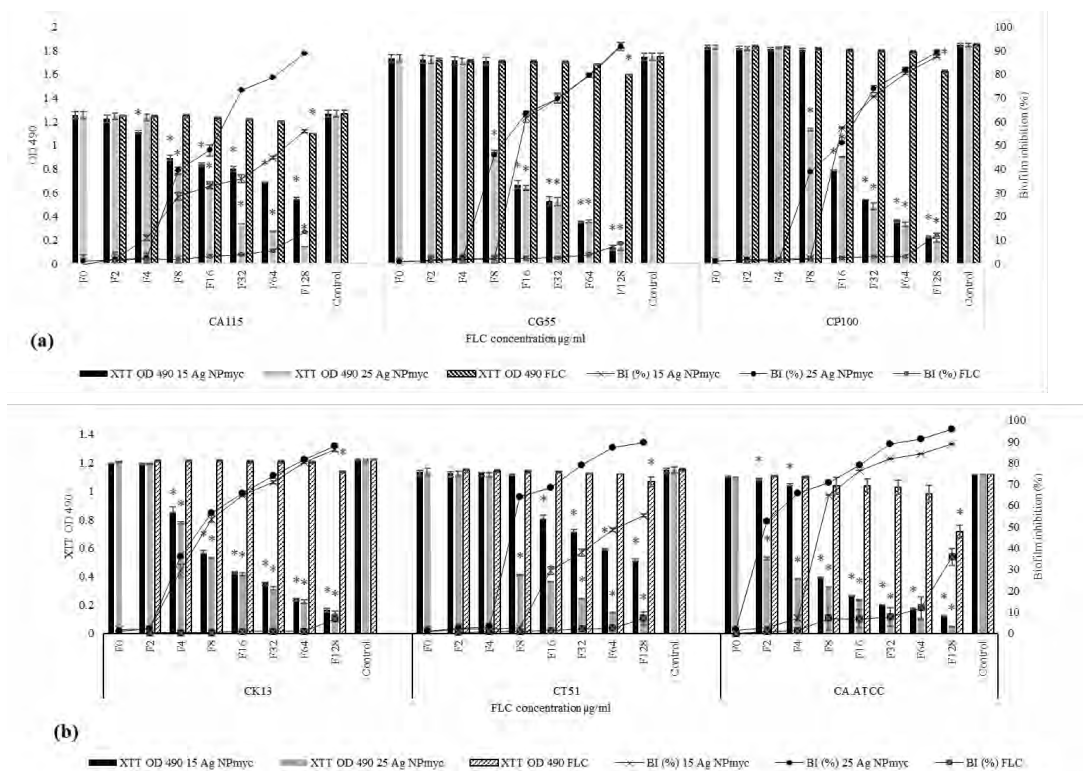


Figure 6.9. Combined effect of different concentrations of fluconazole (FLC) alone and in combination with Ag NP<sub>myc</sub> (15 ppm) (Figure a) and Ag NP<sub>myc</sub> (25 ppm) (Figure b) on percentage inhibition in biofilm metabolic activity (XTT) of six *Candida* species.

Note: The graph values are written as percentage inhibition (\*statistical significance,  $\pm$ standard deviation of  $P < 0.005$ , Tukey's test, one-way ANOVA) of treated compared to untreated-biofilms of six *Candida* species.

It was found in the literature that, FLC resistance is being promoted by morphological transition alteration of targets, enhanced efflux (274) sequestration and blocking of drug entry (303). It has been recently discovered that many nanomaterials affect the microbial growth by disrupting the cell walls or cell membranes (304). So the decrease in the drug dosage, enhanced fungicidal effect of the drug combination and reduced metabolic activity of pathogenic strains, are seen as an advantage of the current study where nanoparticles might have helped in the drug entry to the fluconazole resistant fungal cells. (305) Synergistic combined drug therapy strategy potentially reduce the usage dose of drug thus lowering drug toxicity with increase in drug-efficacy. Moreover, multi-target strategy slows down the development of drug resistance (303).

## 6.4.7. Study of Virulence Factors in planktonic cells and Biofilms

### 6.4.7.1. Extracellular polymeric substances (EPS) study

The combined effect of Ag NP<sub>myc</sub> (at 15 and 25 ppm) and FLC on EPS inhibition in planktonic and biofilm forms of FLC resistant *Candida* spp. was monitored. The EPS inhibition (%) in planktonic cells ranged from 2–73, 3–82 and 1–19 by 15 ppm Ag NP<sub>myc</sub>/FLC, 25 ppm Ag NP<sub>myc</sub>/FLC and FLC alone, respectively (Figure 6.10a, 6.10b). Whereas in case of biofilms, EPS inhibition (%) ranged from 1–84, 1–93 and 1–32 by 15 ppm Ag NP<sub>myc</sub>/FLC, 25 ppm Ag NP<sub>myc</sub>/FLC and FLC alone, respectively (Figure 10c, 10d).

The EPS present in the planktonic and biofilm forms mainly consists of protein, carbohydrate, hexosamine and phosphorus. The greater inhibition in EPS in case of biofilm could be due to lower carbohydrate content in biofilm as compared to planktonic form (306). Exposure to FLC did not have any noticeable effect on EPS which could be due to activation of resistance mechanism e.g. production of extracellular  $\beta$ -1,3-glucan matrix which binds to drug thus hindering its entry (307). Planktonic cells, in a homogenous environment, perform uniform metabolic activity, EPS production and gene expression as compared to biofilms. With the abundant -OH, -NH, and -COOH groups in EPS as well as the hydrophobic regions in polysaccharides, they act as a barrier and hinder the diffusion of antibiotics (308).

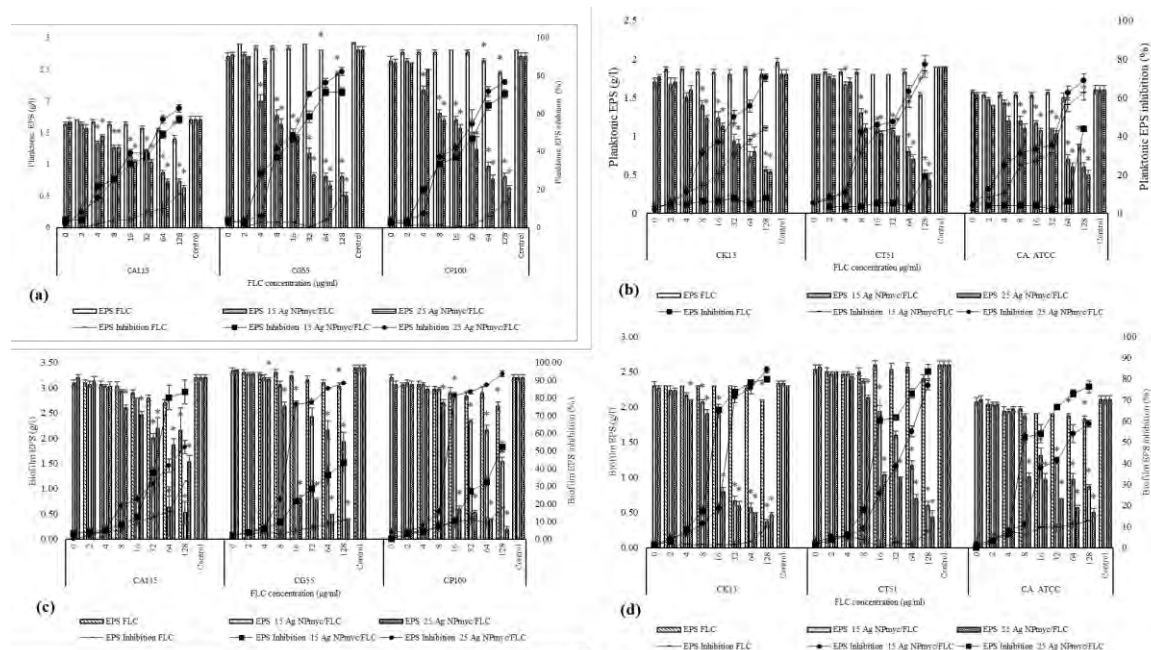


Figure 6.10. Effect of FLC alone and in combination with Ag NP<sub>myc</sub> (15 ppm) and Ag NP<sub>myc</sub> (25 ppm) on percentage inhibition in EPS of planktonic (a, b) and biofilm (c, d) forms of six *Candida* species

Note: The graph values are written as percentage inhibition (\*statistical significance,  $\pm$ standard deviation of  $P < 0.005$ , Tukey's test, one-way ANOVA) of treated compared to untreated-biofilms of six *Candida* species.

The combined use of antifungal fluconazole with the nanoparticles against *Candida* species was found effective in reducing the amount of EPS in resistant biofilm forms of fungal pathogens. The possible reasons behind this decrease in EPS can be the exopolymeric antiadhesion strategy which might have targeted either cell dispersion or caused biofilm matrix elimination (303). Synergistic combination of a drug along with nanoparticles as an anti-virulence agent could provide innovative solutions to elimination of fungal biofilms.

#### 6.4.7.2. Secreted aspartyl proteases (SAP) activity

The results showed that combinations of 15 ppm and 25 ppm Ag NP<sub>myc</sub> with FLC effectively inhibited the SAP in *Candida* spp. with an inhibition range of 1–82% and 1–79%, respectively in case of planktonic cells (Figure 6.11a, 6.11b). Whereas 1–78% and 2–92% in case of biofilm cells (Figure 11c, 11d) as compared to less inhibition seen in case of FLC treated *Candida* spp. planktonic (1–15%) (Figure 6.11a, 6.11b) and biofilm (1–14%) cells (Figure 11c, 11d).

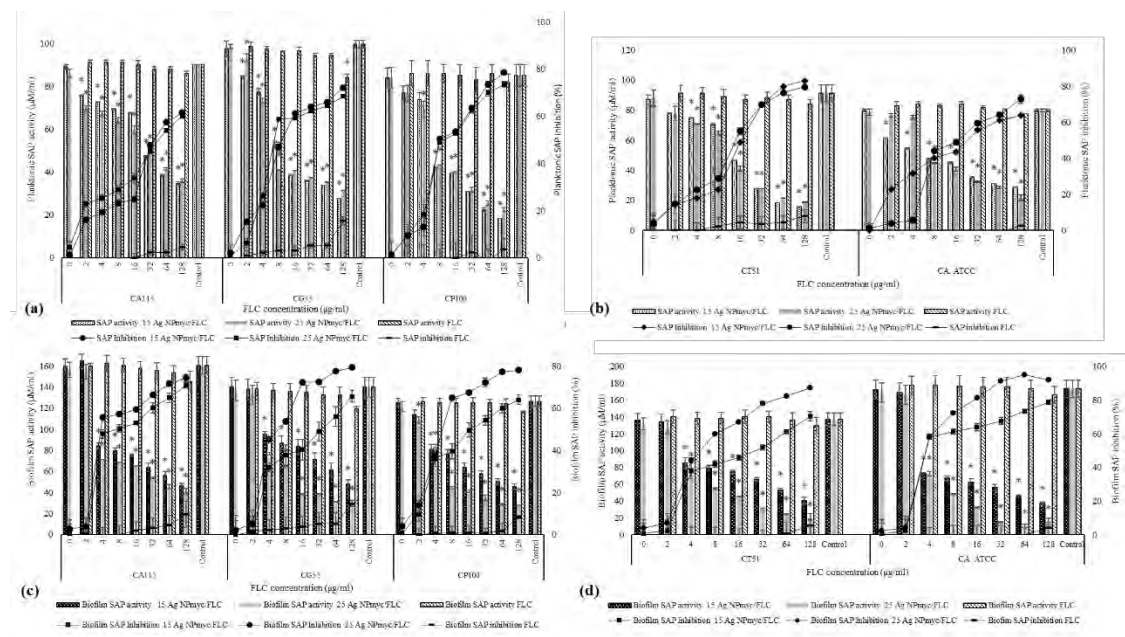


Figure 6.11. Effect of FLC alone and in combination with Ag NP<sub>myc</sub> (15 ppm) and Ag NP<sub>myc</sub> (25 ppm) on percentage inhibition in SAP of planktonic (a, b) and biofilm (c, d) forms of six *Candida* species after 24 hours

*Note:* The graph values are written as percentage inhibition (\*statistical significance,  $\pm$ standard deviation of  $P < 0.005$ , Tukey's test, one-way ANOVA) of treated compared to untreated-biofilms of six *Candida* species.

In resistant strains of *Candida* sp., secretion of hydrolytic enzymes such as secreted aspartyl proteinases (SAP) and exopolymeric substances (EPS) as biofilm component are considered as important virulence determinants which facilitate the pathogenicity towards host cells. With limited number of antifungal drugs and high dosage, new methods are required to reduce the dose and increase the efficacy of these drugs. Nanoparticles are gaining importance due to their antimicrobial potential. As antibacterial agents, an interaction of nanoparticles with the basic cellular components of the bacterial cell takes place, causing oxidative stress, permeability changes in cell membrane, heterogeneous alterations, inhibition of enzymes, and changes in gene expression (127). Nanoparticles are able to penetrate biofilms and can inhibit biofilm formation by inhibiting gene expression (122).

This study shows a clear link between exposure of cells to drug combinations and expression of SAP as virulence factor. At different stages of infections, different types of SAPs are generated (286). Extracellular hydrolytic enzymes of *Candida* species, facilitate in many different ways including the adherence, colonization, nutrition,

penetration of host cells, escape from immune responses, invasion and dissemination (287). To combat the resistant mechanisms of *Candida*, anti-virulence agents (such as nanoparticles) with strategies such as anti-morphogenesis, anti-secreted hydrolytic enzymes and anti-adhesion (309) can be a potential alternative.

In this case, the two drugs, separately exhibiting resistance, is an obvious and straightforward reason to use a combination of agents. Synergistic activity of mycogenic silver nanoparticles along with antifungal fluconazole can involve different mechanisms like inhibition of secreted aspartyl proteinase (extracellular hydrolytic enzyme), disruption of exopolymeric substances (biofilm components), disruption of cell membrane and cell wall, release of silver ions, DNA damage, ribosome destabilization, cell protein damage, damage to mitochondria, damage to electron and proton transmembrane pumps and oxidative stress (48) (128) (129).

To date, information is not available regarding the synergistic effect of Ag NP<sub>myc</sub> and fluconazole on SAP activity of biofilm forming clinical isolates of *Candida* species. The possible reasons behind the enhanced action of combined drugs against SAP can be numerous, ranged from enzyme disruption to activation of quorum sensing, time of interaction with aspartyl residues within active site of SAP altering the substrate-binding capacity, sequence variation in SAP's structures. The reduction in metabolic activity of *Candida* species by Ag NP<sub>myc</sub> in a dose dependent manner prove to be potent antifungal agent.

The main pathogenic determinants for *Candida* sp. include secretion of extracellular enzymes and biofilm formation. To target these virulence factors should be one of the goal of research while developing antifungal drugs or synergistic combination. Evaluation of underlying antifungal mechanism of action at molecular level is very crucial. To determine the exact therapeutic potential of nanoparticles alone or in combination against resistant *Candia* sp., in vivo studies on various cell lines are necessary in order to understand their pharmacokinetics, biodistribution, bioavailability and stability.

Antifungal mechanism of action of silver nanoparticles combined with other drugs has many missing research gaps which need to be studied for future. There are only a limited number of reports in which Ag NP/antifungal drug combination have been

evaluated on the basis of their silver release in aqueous medium, reusability, durability, release of free radicals, long-term antimicrobial efficacy, long term organismic level toxicity on developmental stages of model organisms and cytotoxic effects on human or mammalian cells.

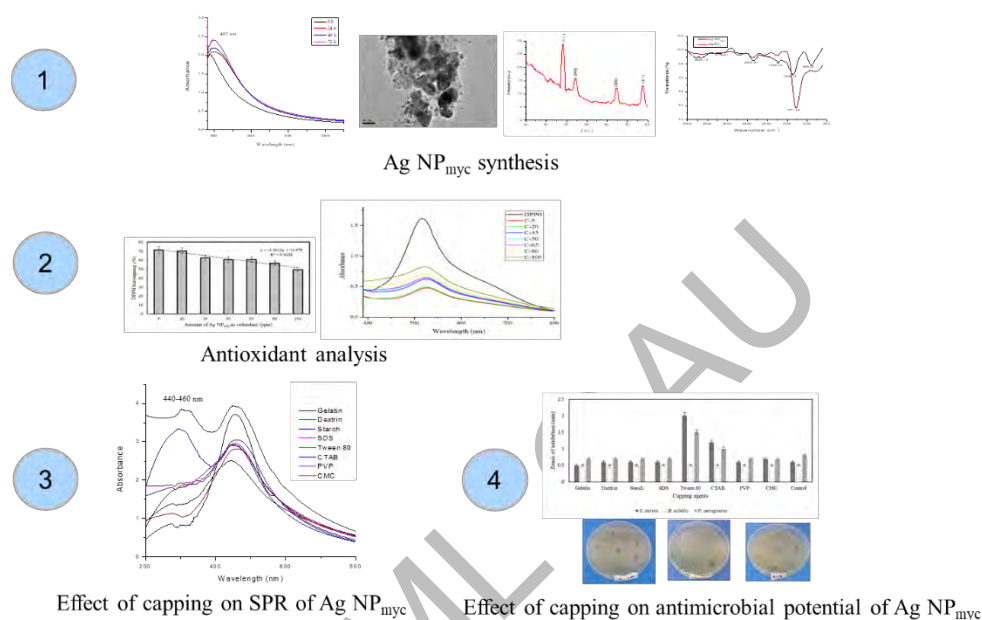
## 6.5 Conclusion

Fungus *Aspergillus oryzae* SZ1 (NCBI accession number: MH664050) was used to synthesize mycogenic silver nanoparticles (Ag NP<sub>myc</sub>) which in combination with fluconazole (FLC), promoted significant reduction in virulence factors (SAP-secreted aspartyl proteinase and EPS-exopolymeric substances) in resistant forms of *Candida* sp. All concentrations of Ag NP<sub>myc</sub>, alone or in combination with FLC, were not cytotoxic to brine shrimps. In order to study the effect of reduced amount of antifungal, against resistant forms of *Candida* sp., combination therapy was utilized. Currently, no data related to combined effect of mycogenic silver nanoparticles and fluconazole, in SAP inhibition by resistant *Candida* spp. has been described. In this study, synergistic combination along with anti-virulence was used as a way for discovering new antifungal potential of mycogenic silver nanoparticles (Ag NP<sub>myc</sub>). The decrease in the drug dosage, enhanced fungicidal effect of the drug combination and reduced metabolic activity of pathogenic strains are seen as advantages of the current study where, as mechanism of synergy against resistant *Candida* strains, nanoparticles might have helped in the drug entry (by disrupting cell membranes) to the fluconazole resistant fungal cells. Synergistic combined drug therapy along with multi-target strategy, potentially reduce the usage dose of drug thus lowering its toxicity and resistance against it thus increasing the drug-efficacy. Synergistic antifungal mechanism of action of silver nanoparticles (Ag NPs) with other drugs at molecular level need to be studied further. To determine the exact therapeutic potential of nanoparticles alone or in combination against resistant *Candia* sp., in vivo studies are required to understand their pharmacokinetics and biodistribution.



## Chapter 7: Mycosynthesis of nanosilver particles using exocellular secretions of silver tolerant oleaginous fungus *Mucor circinelloides* SZ3

### Graphical Abstract



### 7.1 Introduction

Nanosilver particles due to their potential antimicrobial effects, have been used extensively in various biomedical applications such as bone substitute biomaterials, coatings on surgical instruments, implants and wound dressings, antibacterial surgical sutures, dental implants, burn healing ointments, contraceptive devices etc. (310). To increase the biocompatibility and safety of silver nanoparticles for biomedical applications, use of natural capping agents for synthesis and stabilization of NPs has gained more attention (311).

Silver nanoparticles can be formed using chemical, physical but these routes involve consumption of hazardous and toxic chemicals along with high amounts of energy (26). As an alternative, use of green methods in the form fungi provide safer and natural way with high biocompatibility (258). Among all types of metal nanoparticles, silver nanoparticles are most frequently biosynthesized (174). Bio

silver nanoparticles are considered as more biocompatible and stable due to bioactive surface with suitable covering by microbial-derived capping molecules (312).

The surface-associated biomolecules on silver nanoparticles has been observed to affect the stability and behavior of nanoparticles. These biomolecules with unique functionalities can enable different types of surface modifications and can be helpful in attachment of other compounds on the surface of nanoparticle. Interaction between biomolecules and silver nanoparticles can play an important role in biocompatibility and antimicrobial property of nanoparticles (27).

Metal nanoparticles are stabilized using a range of capping materials, from ligands to surfactants to polymers. Major classes of commonly used capping agents include polymers, long chain hydrocarbons, polysaccharides and small molecules etc (313) (310).

*Mucor circinelloides* is a valuable oleaginous filamentous fungus (314), commonly used as the model microbe to investigate lipid production (315) especially  $\gamma$ -linolenic acid (GLA) (316). It produces high amounts of lipids in its mycelium (317), therefore studied for biodiesel production (318), it gives good biomass yield in submerged batch fermenters with a wide range of carbon sources (319), has capacity to grow in large industrial stirred-tank bioreactors to produce  $\gamma$ -linolenic acid rich oil (320). The key genes and regulation of lipid accumulation in this fungus has been have been identified (321) (315). Oleaginous fungi have short life cycle, easily grow, utilize waste carbon sources, are cost-effective, give easy scale-up production with economic value (322). The major fatty acids produced by fungi are oleic acid, palmitic acid, and linoleic acid. linolenic acid, Palmitoleic acid and stearic acid are also produced in small amounts. Gamma-linoleic acid is produced uniquely by Mucorales. (323, 324).

In this study we used silver tolerant oleaginous fungus *Mucor circinelloides* SZ3 (NCBI accession number: MH664052) synthesize mycogenic silver nanoparticles (Ag NP<sub>myc</sub>). To study the biocompatibility, antioxidant activity was observed. For enhanced stability studies, effect of different capping agents on surface plasmon resonance (SPR) was observed along with antibacterial activity of Ag NP<sub>myc</sub> against *Staphylococcus aureus*, *Bacillus subtilis* and *Pseudomonas aeruginosa* was studied. Capping agents included gelatin, dextrin, starch; surfactants such as sodium dodecyl sulfate (SDS), Polyoxyethylene (20) sorbitan monooleate (Tween 80), cetyl trimethyl

ammonium bromide (CTAB), polymers such as polyvinylpyrrolidone (PVP) and carboxy methyl cellulose (CMC) were used. Objectives of this study are given below:

**Objectives:**

- To synthesize extracellular mycogenic silver nanoparticles (Ag NP<sub>myc</sub>) using silver tolerant oleaginous fungus *Mucor circinelloides* SZ3 (NCBI accession number: MH664052).
- To characterize Ag NP<sub>myc</sub> using UV-Visible spectroscopy, X-Ray diffraction, Transmission electron microscopy and FT-IR.
- To study biocompatibility of Ag NP<sub>myc</sub> through antioxidant properties.
- To study the effect of different capping agents on stability (by observing surface plasmon resonance) and antibacterial potential of Ag NP<sub>myc</sub>.

## **7.2 Material and methodology**

### **7.2.1 Isolation from soil**

*Mucor circinelloides* SZ3 was isolated from metal industrial waste as mentioned in chapter 3 under section 3.2.2.3.

### **7.2.2 Silver resistance**

Effect of silver ions on fungal strains was determined as mentioned in the chapter 3 under section 3.2.3.

### **7.2.3 Growth optimization**

The pH and temperature of the growth media were optimized using methods given in chapter 3 under section 3.2.4.1 and 3.2.4.2.

### **7.2.4 Molecular Identification**

*Mucor circinelloides* SZ3 was molecularly identified by amplification and sequencing of internal transcribed spacer (ITS) regions of 18s rRNA gene as mentioned in chapter 3 under section 3.2.7 and the accession number was given as MH664052 after submission to NCBI.

### **7.2.5 Synthesis of Ag NP<sub>myc</sub>**

Mycosynthesis of Ag NP<sub>myc</sub> was carried out using *Mucor circinelloides* SZ3 (NCBI accession number: MH664052) using the method given in section 3.2.5.

### 7.2.6 Characterization of Ag NP<sub>myc</sub>

Characterization of Ag NP<sub>myc</sub> was carried out as given in section 4.2.6.

## 7.2.5 Bioassays of mycogenic silver nanoparticles

### 7.2.5.1 Antioxidant assay

Antioxidants gives protection to cells against the oxidation caused by free radicals. by neutralization the radicals and themselves get oxidized. The use of 2,2-diphenyl-1-picrylhydrazyl-hydrate (DPPH) to measure the antioxidant activity of biogenic silver nanoparticles is a quick, easy method which involves the measurement of radical scavenging activity of nanoparticles. DPPH is a purple color, organic radical whose color fades during the antioxidant activity analysis of tested sample. (325)

Antioxidant activity of different concentrations (5 ppm, 20 ppm, 35 ppm, 50ppm, 65 ppm, 80ppm, 100 ppm) of Ag NP<sub>myc</sub> was determined using the DPPH (2, 2-diphenyl-picrylhydrazyl ) free radical scavenging assay, with the protocol of (326). For the assay, 50 µL of Ag NP<sub>myc</sub> solution was mixed with 5 ml of DPPH (0.004%) dissolved in methanol. After shaking and 30 minutes of incubation, absorbance was measured at 515 nm. Similar concentrations of ascorbic acid in place of silver nanoparticles were run as standard. Percent inhibition or scavenging effect (% remaining) of DPPH was calculated using the following formula:

$$\text{DPPH scavenging effect (\%)} = [(A_0 - A_1)/A_0] \times 100$$

Where, A<sub>0</sub> is absorbance of blank solution (solution with all components except the compound to be tested) and A<sub>1</sub> is absorbance of sample (Ag NP<sub>myc</sub> concentrations).

### 7.2.5.2 Effect of capping agents on stability of Ag NP<sub>myc</sub>

In order to study the effect of different capping/stabilizing agents on stability of Ag NP<sub>myc</sub>, eight different capping agents *polypeptides* such as gelatin, *polysaccharides* such as dextrin, starch, *surfactants* such as sodium dodecyl sulfate (SDS), polyoxyethylene (20) sorbitan monooleate (Tween 80), cetyl trimethyl ammonium bromide (CTAB) and *polymers* such as polyvinylpyrrolidone (PVP) and carboxy

methyl cellulose (CMC) were used. For this purpose, surface plasmon resonance was measured using UV-Visible spectroscopy at regular intervals of time.

1- *Gelatin*: Gelatin is a collagen as heat-denatured protein, contains many proline, glycine and 4-hydroxyproline amino acid residues and have been shown to be biodegradable (310). For synthesis of gelatin stabilized Ag NP<sub>myc</sub>, 2.0 g of gelatin was added to 190 mL of fungal extract and mixed, then 10 ml of 0.1 M silver nitrate solution was added to the mixture and incubated under shaking conditions at 20 °C (327) (328).

2- *Dextrin*: For synthesis of dextrin stabilized Ag NP<sub>myc</sub>, maltodextrin with 3 % concentration was used to stabilize nanoparticles (329).

3- *Starch*: For synthesis of starch stabilized Ag NP<sub>myc</sub>, starch solution (1 g dissolved in 100 ml of fungal cell free filtrate) was mixed with silver nitrate (final concentration 0.1 M) (330).

4- *Sodium dodecyl sulfate (SDS)*: For synthesis of SDS-stabilized Ag NP<sub>myc</sub>, 0.4 mM solution of SDS was used (331).

5- *Polyoxyethylene (20) sorbitan monooleate (Tween 80)*: To synthesize Tween-80 stabilized Ag NP<sub>myc</sub>, 2 ml of Tween 80 was used with modification in this protocol (332).

6- *Cetyl trimethyl ammonium bromide (CTAB)*: To synthesize CTAB stabilized Ag NP<sub>myc</sub>, 2 ml of 0.01 M solution of CTAB was used (333).

7- *Polyvinylpyrrolidone (PVP)*: To synthesize PVP-stabilized Ag NP<sub>myc</sub>, 1 mM PVP was utilized (334).

8- *Carboxy methyl cellulose (CMC)*: To synthesize CMC-stabilized Ag NP<sub>myc</sub>, 0.1mM CMC was used using modified protocol of (335).

#### **7.2.5.3 Effect of capping agents on antibacterial activity of Ag NP<sub>myc</sub>**

The antibacterial activity of mycogenic silver nanoparticles against *S. aureus*, *B. subtilis* and *P. aeruginosa* with the zone of inhibitions, was conducted using the disc diffusion method (325). Petri plates with Mueller Hinton agar were swabbed with bacterial cultures. The discs (6 mm) saturated with biosynthesized silver nanoparticles

(100 µg/ml) were seeded on upper surface of agar, incubated at 37 °C for 24 h. After incubation, the diameters (mm) of the zones of inhibition were measured for each bacterial strain.

## 7.4 Statistical analysis

Statistics was applied on data in the form of mean, standard deviation (SD) and standard error of triplicate samples in a representative experiment. All experiments were done independently at least three times.

## 7.5 Results

### 7.5.1 Silver resistance

Effect of silver ions on *Mucor circinelloides* SZ3 was determined as mentioned in the chapter 3 under section 3.3.2. The fungus was able to grow at 1000 mg/l as minimum inhibitory concentration of silver ions.

### 7.5.2 Growth optimization

The pH and temperature of the growth media were optimized as pH 5 and 20 °C respectively, as given in chapter 3 under section 3.3.4.

### 7.5.3 Synthesis and characterization of Ag NP<sub>myc</sub>

During 72 hours of reaction time, the Ag NP<sub>myc</sub> formed by fungus *M. circinelloides* SZ3 changed the color from colorless to blackish brown. The surface plasmon resonance (SPR) peak was observed at 405 nm using UV–Visible spectral analysis (Figure 7.1)

Figure 7.1. UV–Vis spectrum for the Ag NP<sub>myc</sub> synthesized by fungus *M. circinelloides* SZ3

TEM micrograph (Figure 7.2a) revealed the Ag NP<sub>myc</sub> size range 1-100 nm and morphology as spherical and triangular shaped. From, particle size histogram, Ag NP<sub>myc</sub> distribution frequency was observed as 40-50% ± 38 particles with size range of 1 to 50 nm (Figure 7.2b).

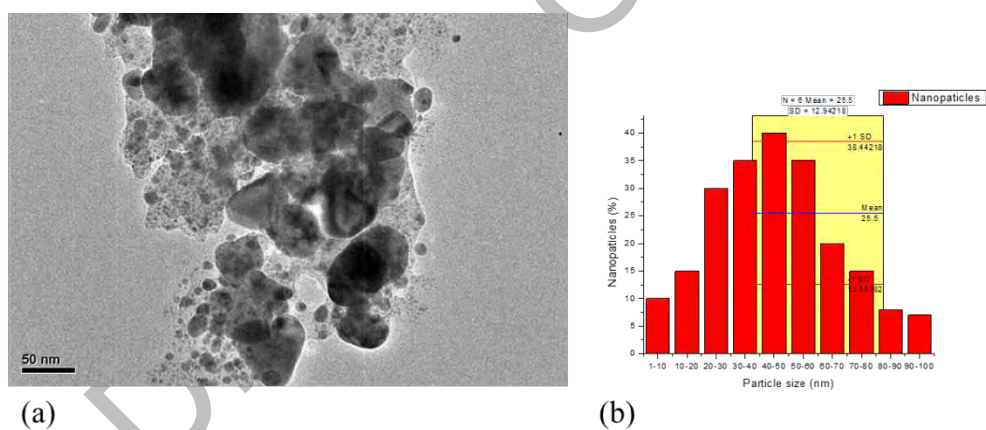


Figure 7.2. Representative TEM micrograph (a) and size distribution (b) for Ag NP<sub>myc</sub> synthesized by fungus *M. circinelloides* SZ3.

X-ray diffraction ( $2\theta$ ) peaks of Ag NP<sub>myc</sub> were noted at  $38.24^\circ$ ,  $44.35^\circ$ ,  $64.55^\circ$ , and  $77.57^\circ$ , corresponding to silver planes of 111, 200, 220 and 311, respectively (Figure 7.3).

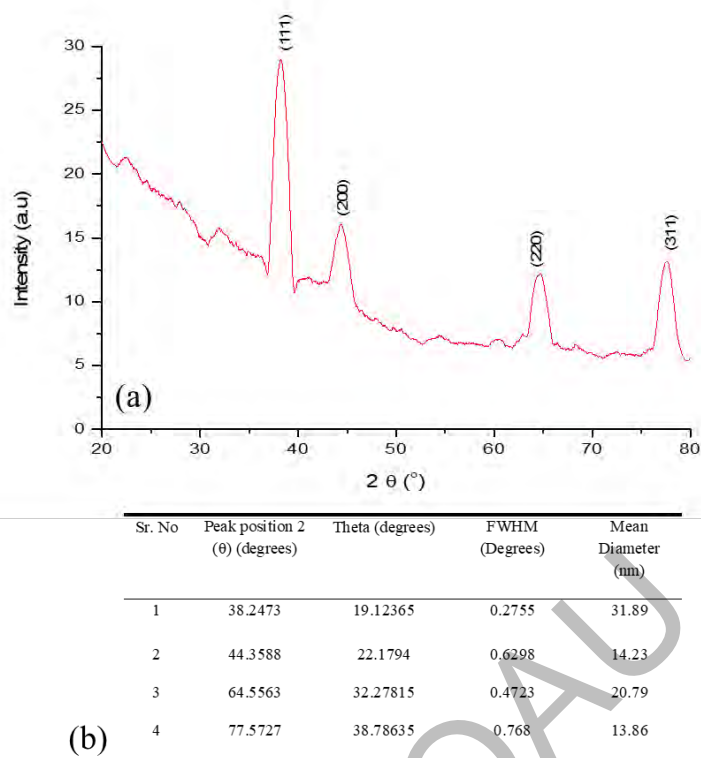


Figure 7.3. XRD pattern (a) and data (b) for Ag NP<sub>myc</sub> synthesized by fungus *M. circinelloides* SZ3

To observe the presence of capping molecules, on surface of Ag NP<sub>myc</sub>, FTIR analysis was carried out (Figure 7.4). In this FTIR spectrum, the characteristic molecular vibrations observed with peaks include -C-H stretching at 2910.45 cm<sup>-1</sup>, N-H stretching at 3176.61 cm<sup>-1</sup>, -C=O stretching at 1722.35 cm<sup>-1</sup>, P-O-P stretching at 885.28 cm<sup>-1</sup>, -C=O stretching (amide I) at 1652.92 cm<sup>-1</sup>, C-N-H deformation (amide-II) at 1523.69 cm<sup>-1</sup> and C-O-C stretching at 1082.01 cm<sup>-1</sup>.



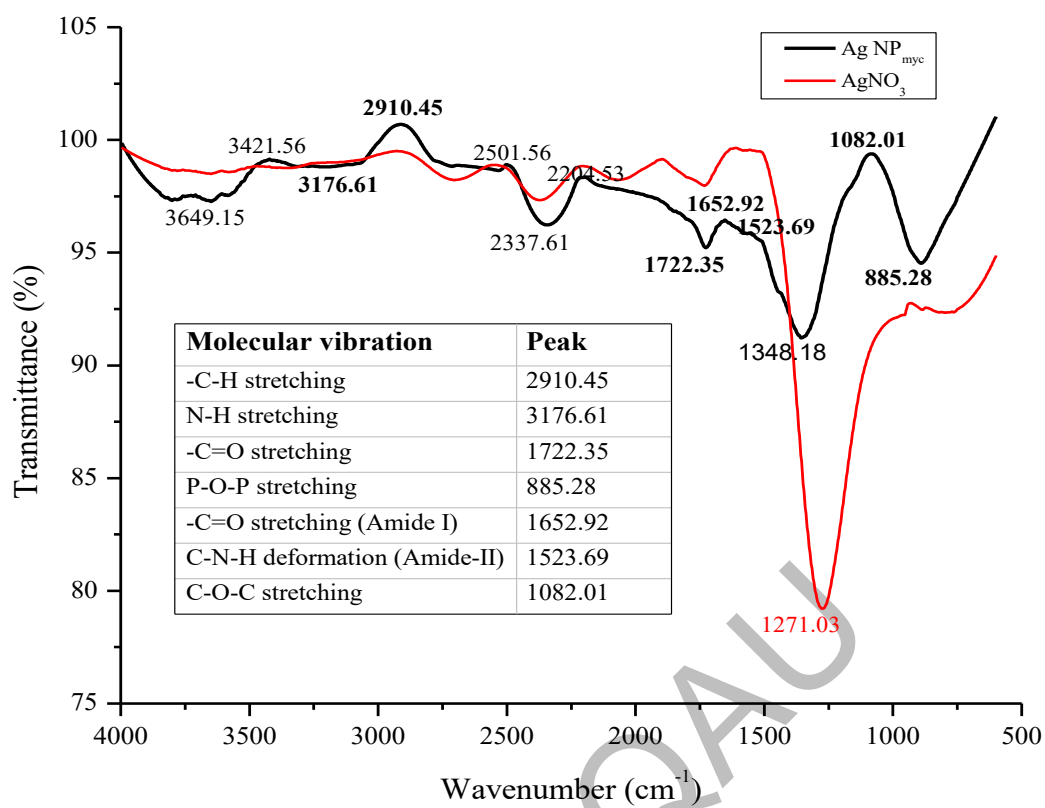


Figure 7.4. FTIR spectrum of Ag NP<sub>myc</sub> synthesized by fungus *M. circinelloides* SZ3

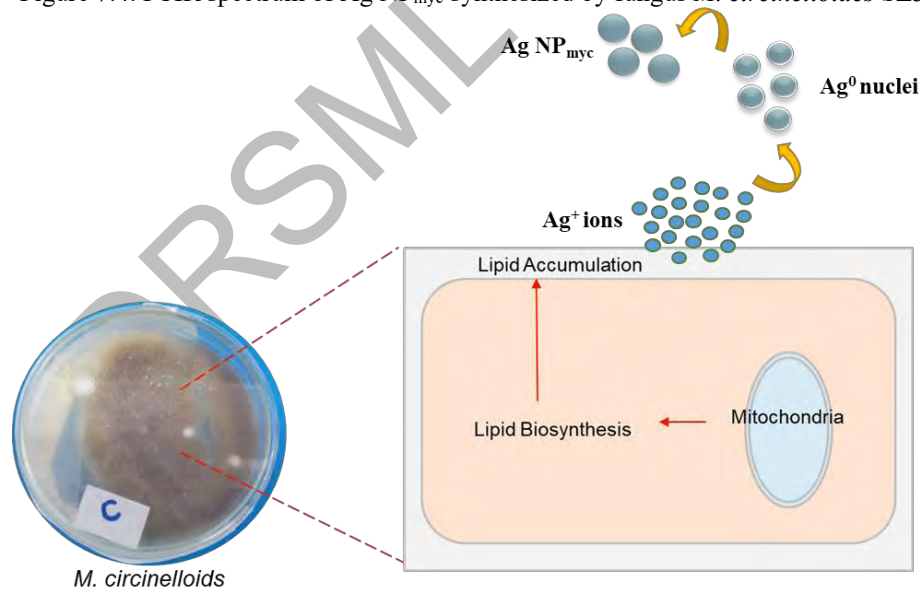


Figure 7.5. Proposed mechanism of synthesis of Ag NP<sub>myc</sub> by fungus *M. circinelloides* SZ3

## 7.5.6 Bioassays/Application of mycogenic silver nanoparticles

### 7.5.6.1 Antioxidant assay

UV-Vis absorbance spectrum of different concentrations of Ag NP<sub>myc</sub> to observe the antioxidant activity was investigated in the form of 2,2-diphenyl-1-picrylhydrazyl-hydrate (DPPH) scavenging as shown in Figure 7.6a. The antioxidant activity of nanoparticles DPPH is represented by the percentage DPPH scavenging (inhibition) (Figure 7.6b). 5 ppm Ag NP<sub>myc</sub> sample showed highest free radical scavenging activity (70%).

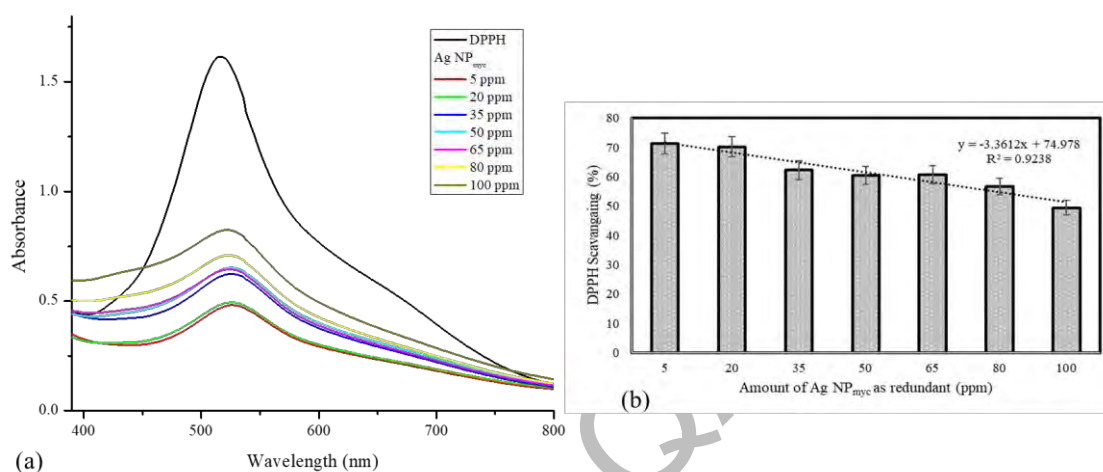


Figure 7.6. UV-Vis absorbance spectrum of different concentrations of Ag NP<sub>myc</sub> to observe DPPH scavenging. **(b)** Anti-oxidant effect (%) of different concentrations of Ag NP<sub>myc</sub>. Note: The bars in 7.6 (b) represent the mean values with the error bars representing standard error being calculated after taking average of three replicates of each sample and calculating standard deviation.

Ag NP<sub>myc</sub> showed comparable results of DPPH inhibition (%) with ascorbic acid (Figure 7.7a). The DPPH scavenging activity of Ag NP<sub>myc</sub> at different time intervals for 30 minutes was observed and 67.59% significant activity was found even after 30 minutes with ascorbic acid as standard (Figure 7.7b).

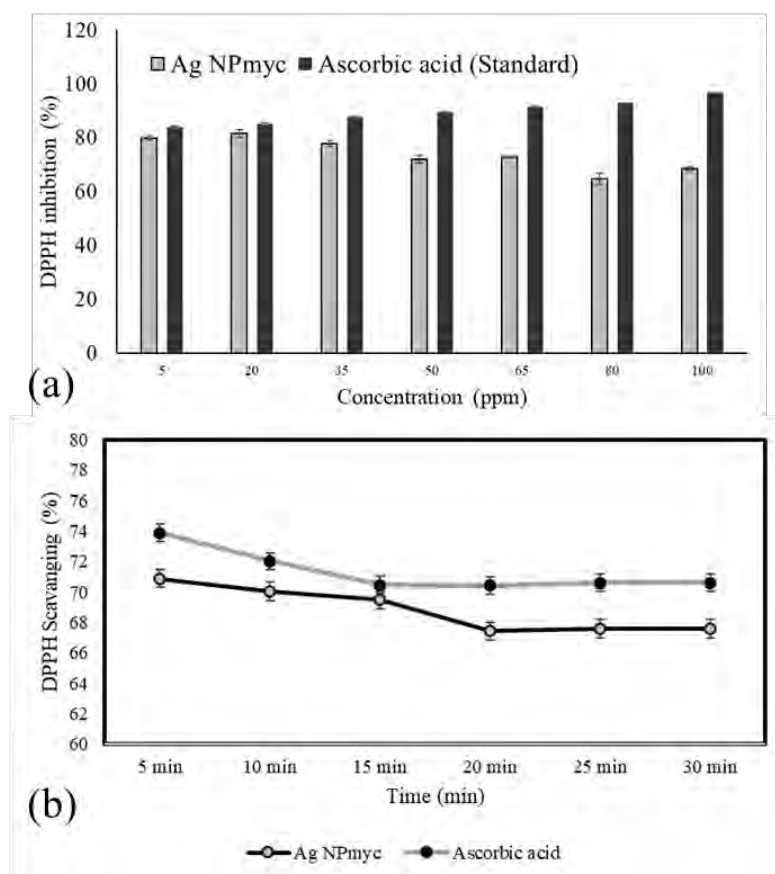


Figure 7. 7. Anti-oxidant effect of Ag NP<sub>myc</sub> as compared with ascorbic acid (b) Kinetic curve of DPPH inhibition by Ag NP<sub>myc</sub> for 30 min with ascorbic acid as positive control. Note: The bars and lines represent the mean values with the error bars representing standard error being calculated after taking average of three replicates of each sample and calculating standard deviation.

### 7.5.6.2 Effect of capping agents on surface plasmon resonance of Ag NP<sub>myc</sub>

Stability of Ag NP<sub>myc</sub> was assessed with different capping agents in the form of surface plasmon resonance (SPR) peaks (Figure 7.8). The initial SPR peak of Ag NP<sub>myc</sub> i.e. 405 nm was shifted towards right from 440 nm to 460 nm with the use of different capping agents. The SPR peak values at 2, 24 and 48 hours are given in Table 7.1. The absorbance was increased with time, highest absorbance was observed in case of Tween 80, CTAB and PVP at 455 nm, 467 nm and 457 nm respectively.

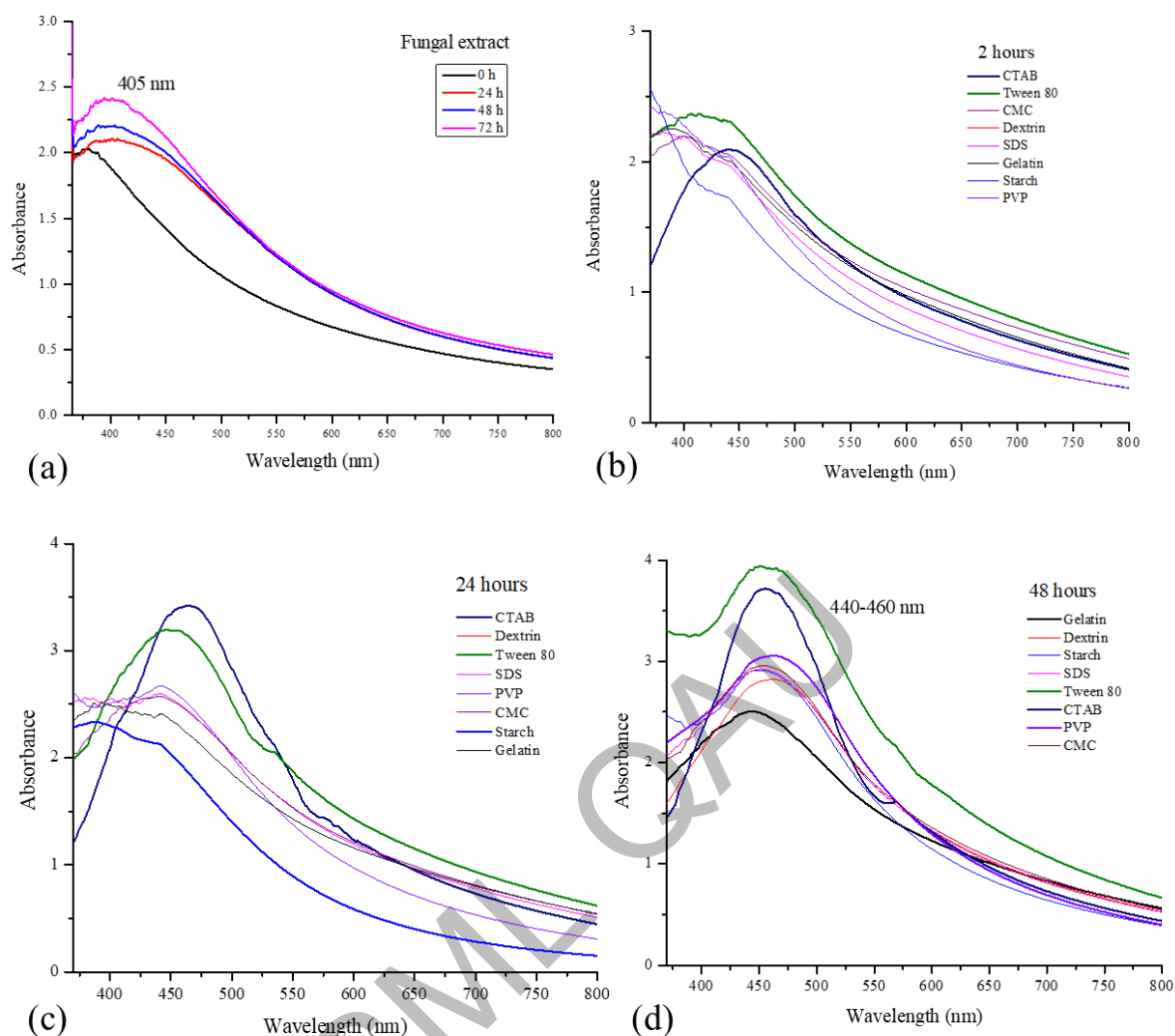


Figure 7.8. Effect of different capping agents on surface plasmon resonance of Ag NP<sub>myc</sub> (a) fungal extract (b) 2 hours (c) 24 hours (d) 48 hours with capping agents.

Table 7.1. SPR peaks of Ag NP<sub>myc</sub> using different capping agents at 2, 24 and 48hr.

Sr. No	Type of capping agent	SPR (nm)		
		48 hrs	24 hrs	2 hrs
1	Gelatin	443	445	443
2	Dextrin	461	443	443
3	Starch	451	440	438
4	SDS	451	443	443
5	Tween 80	455	455	438
6	CTAB	467	467	441
7	PVP	457	446	439
8	CMC	454	442	441
9	Control (fungal extract)	405	404	400

### 7.5.6.3 Antibacterial assay

To find the antibacterial efficiency of capped-Ag NP<sub>myc</sub>, Gram negative bacterial strain *Pseudomonas aeruginosa* and Gram positive bacterial strains, *Staphylococcus*

*aureus*, *Bacillus subtilis* were used. Zones of inhibitions (mm) of capped-Ag NP<sub>myc</sub> were measured by using the disc diffusion method (Figure 7.9). Highest antibacterial activity was observed by Tween-80 and CTAB-capped Ag NP<sub>myc</sub>.

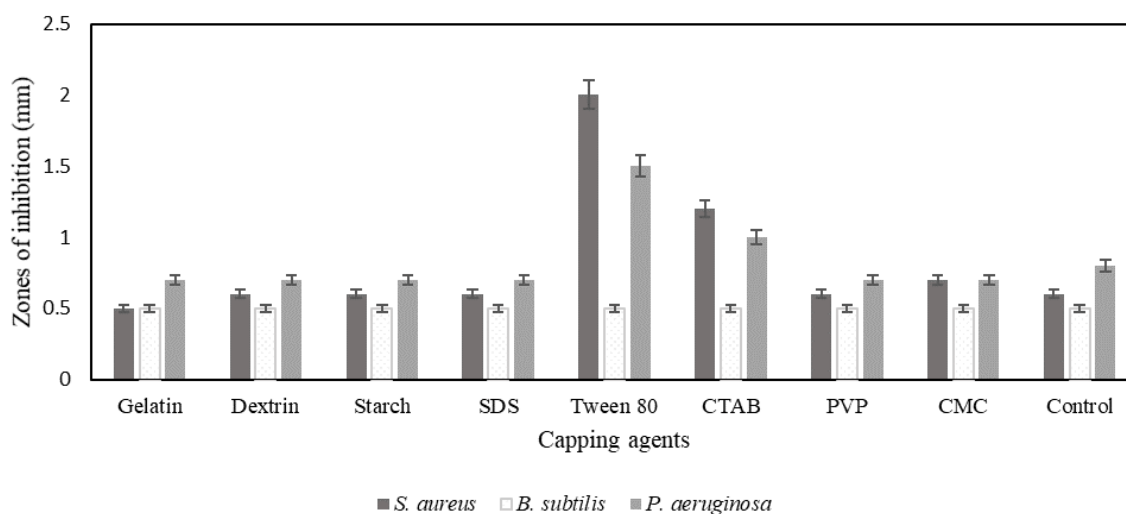


Figure 7.9. Effect of different capping agents on antibacterial activity of Ag NP<sub>myc</sub>. Note: The bars represent the mean values with the error bars representing standard error being calculated after taking average of three replicates of each sample and calculating standard deviation.

## 7.6 Discussion

The change in color of reaction mixture from colorless to blackish brown was indicated by shift in UV-visible absorption peaks, maximum peak was observed at 405 nm. The appearance of peak in the range of 400-500 nm is the characteristic surface plasmon peak of silver nanoparticles (183). The XRD peaks of Ag NP<sub>myc</sub> displayed four characteristic diffraction signals robust peaks which were confirmed with ICDD reference code. 01-087-0717) (182). TEM micrographs proved the synthesis of nanocrystalline Ag NP<sub>myc</sub> (264).

The results of FTIR indicated that by fungus *M. circinelloides* SZ3 (NCBI accession number: MH664052) might be secreting different bioactive molecules which are involved in mycosynthesis of silver nanoparticles. The analysis of FTIR spectrum showed, the absorption bands of 1722.35 cm<sup>-1</sup> (carbonyl compounds) indicate the presence of lipids, whereas 1652.92 cm<sup>-1</sup> indicated the presence of chitin/chitosan, 885.28 cm<sup>-1</sup> P-O-P stretching indicated the presence of polyphosphates. *M. circinelloides* produces various types of fatty acids including  $\gamma$ -linolenic acid,

palmitoleic, myristic, oleic, palmitic, stearic, linoleic etc. (336) (337) (338). It is assumed that the lipids might have acted as a reducing agent and transformed ionic silver form to Ag NP<sub>myc</sub>. In current work, it is possible that the lipids and the metabolites secreted by the fungus into the broth could have induced the reduction of Ag<sup>+</sup> into Ag NP<sub>myc</sub> (339). The formation of the silver nanoparticles might involve the coupling of the Ag NP<sub>myc</sub> with the lipid molecules via either weak covalent interaction or coordination bond formation (338).

Ag NP<sub>myc</sub> showed notable radical scavenging activity against 2,2-diphenyl-1-picrylhydrazyl-hydrate (DPPH) in a dose-dependent manner with significant inhibition (70%). The lower the concentration of Ag NP<sub>myc</sub>, greater the antioxidant activity which was maintained for 30 min of incubation. The mechanism of this antioxidant ability might involve the size of Ag NP<sub>myc</sub> or it might be due to presence of fungal functional groups (340) on surface of Ag NP<sub>myc</sub> as shown by FTIR analysis.

In the present work, with use of different capping agents, shifts in SPR spectra were observed with time. The change in absorbance wavelength from left to right in the spectrum showed a red shift or bathochromic shift (higher wavelengths) towards visible range which means bandgap was decreasing, which was harvesting more visible light thus giving more stability for biological activity of Ag NP<sub>myc</sub>. The shift in SPR peaks in UV-Vis spectra depend on the shape, particle size, nature of the adjacent dielectric medium and aggregation of particles (311). Studies have reported that optical properties of nanoparticles depend on their size, large particles will show absorbance at longer wavelengths and smaller particles at short wavelengths (341). UV-vis absorption spectra are most commonly used for detecting the optical properties of metal nanoparticles, as the absorption peaks are related to their diameter and aspect ratio. At nanoscale, on the particle surface, the electron cloud can absorb electromagnetic radiation and can change its energy level while oscillations. This absorbance, which is also called plasmon absorbance or surface plasmon resonance, is caused by the size of nanoparticles or its surface functionalizations. This surface effect influence the peak intensity and width (342).

The antibacterial efficiency of Ag NP<sub>myc</sub> revealed that Tween 80 and CTAB-stabilized silver nanoparticles showed greater antibacterial activity as compared to other capped nanoparticles. Tween 80 (343) and CTAB-capped (344) nanoparticles

showed more antibacterial activity against Gram-positive *Staphylococcus aureus* and Gram-negative bacterial strain *Pseudomonas aeruginosa*. The antimicrobial potential of silver is broad and well known, and it had wide applications in the field of medicine. The mechanism behind the antimicrobial effect of silver nanoparticles involve their interaction with bacterial proteins of cell membrane, DNA synthesis and respiratory chain (345).

## 7.7 Conclusion

- The change in color of reaction mixture and surface plasmon resonance value (405 nm) suggest the transformation of the oxidation state of silver ions, and that extracellular fungal components might be involved in the process. The TEM micrograph revealed to be spherical and triangular shaped Ag NP<sub>myc</sub> with particle size range of 10 to 50 nm.
- The XRD spectrum showed that the plane values confirm the crystal structure for silver to be face-centered cubic (fcc).
- The FTIR spectra revealed the peaks for Amide I, Amide II, lipids, chitin/chitosan, and polyphosphate.
- The antioxidant activity of silver nanoparticles at different concentrations time intervals was studied and found that 100 µl sample of 5 ppm Ag NP<sub>myc</sub> showed a very good radical scavenging activity with time.
- Colloidal silver nanoparticles of different sizes were prepared using 8 capping agents, The SPR peak is found to be shifted towards the high wavelength, red shift with increase in particle size, broad absorption peaks, greater stability.
- Tween 80 and CTAB gave highest intensity peaks of surface plasmon resonance and highest antibacterial activity.

## Conclusions

- This work involves the mycosynthesis of silver nanoparticles using fungal species and the assessment of these mycogenic silver nanoparticles (Ag NP<sub>myc</sub>) as antimicrobial agents. The subject is interesting and important in the area of nanobiotechnology towards sustainable production of silver nanoparticles. In this work, cell-free culture supernatant of different fungi isolated from different sources including *Aspergillus oryzae* SZ1, *Aspergillus flavus* SZ2, *Mucor circinelloides* SZ3 and *Thermomyces lanuginosus* were used for biosynthesis of silver nanoparticles. This method is an economical and simple one-step approach to synthesize Ag NP<sub>myc</sub>.
- Three fungi from different sources were selected in the study after screening for silver tolerance, their 18s DNA sequences were submitted to NCBI and accession numbers were assigned. UV-Vis spectrophotometry, FTIR, XRD and TEM results confirmed the biosynthesis of Ag NP<sub>myc</sub>.
- Ag NP<sub>myc</sub> did not show any cytotoxic effect on brine shrimps (*Artemia salina*), as measured by cell viability.
- Glucoamylase was found as a capping agent during mycosynthesis of Ag NP<sub>myc</sub> by *Thermomyces lanuginosus* resulted in formation of highly monodispersed nanoparticles.
- Nitrate reductase was identified for nano-silver mycogenesis by *Aspergillus flavus* SZ2 (NCBI accession number: MH664051).
- Combinational antibiofilm efficacy of Ag NP<sub>myc</sub> synthesized by *Aspergillus oryzae* SZ1 (NCBI accession number: MH664050) with fluconazole was proved to be a suitable nanofungicide for deterrence of virulence factors (Hydrolytic enzyme- secreted aspartyl proteinase (SAP) and biofilm component-exopolymeric substances (EPS) in multidrug resistant *Candida* biofilms. The decrease in the drug dosage, enhanced fungicidal effect of the drug combination and reduced metabolic activity of pathogenic strains are seen as advantages of the this study.



## Conclusions

---

- Good antioxidant activity of low concentration of Ag NP<sub>myc</sub> oleaginous fungus *Mucor circinelloides* SZ3 was observed.

DRSML QAU

## Future Prospects

- Exploration of soil enzymes and metagenomic fungal DNA analysis for microbial metal nanoparticle synthesis.
- Exploration of thermozymes which can possibly be responsible in nucleation, growth and stability of biogenic nanoparticles, might help in resuming their activity at high industrial temperatures.
- To explore the metal-organic hybrid systems through mycosynthesis of nanoparticles as natural way of immobilization of enzymes on nanoparticles' surfaces thus eliminating the extra steps require for immobilizing for commercial purposes.
- To determine the therapeutic potential (antifungal mechanism of action) of mycogenic nanoparticles alone or with other drugs, in-vivo studies along with pharmacokinetics, biodistribution, studies at molecular level need to be studied further.
- Determination of the mechanisms of possible development of microbial resistance against metal nanoparticles.
- Molecular recognition/biosensing by synthesis and conjugating silver nanoparticles with fungal secondary metabolites for environmental detection of pollutants.
- To explore the oleaginous fungi's potential of nanoparticle synthesis for biodiesel production.

## References

1. Bayda S, Adeel M, Tuccinardi T, Cordani M, Rizzolio F. The history of nanoscience and nanotechnology: from chemical–physical applications to nanomedicine. *Molecules*. 2020;25(1):112.
2. Whitesides GM. The 'right' size in nanobiotechnology. *Nature Biotechnology*. 2003;21(10):1161-5.
3. Khan I, Saeed K, Khan I. Nanoparticles: Properties, applications and toxicities. *Arabian Journal of Chemistry*. 2019;12(7):908-31.
4. Kii TM, Park S. Physical properties of nanoparticles do matter. *Journal of Pharmaceutical Investigation*. 2021;51(1):35-51.
5. Gaffney EM, Minter SD. A silver assist for microbial fuel cell power. *Science*. 2021;373(6561):1308-9.
6. Khalifa Z, Zahran M, Zahran MA, Azzem MA. Mucilage-capped silver nanoparticles for glucose electrochemical sensing and fuel cell applications. *RSC Advances*. 2020;10(62):37675-82.
7. Ibrahim S, Ahmad Z, Manzoor MZ, Mujahid M, Faheem Z, Adnan A. Optimization for biogenic microbial synthesis of silver nanoparticles through response surface methodology, characterization, their antimicrobial, antioxidant, and catalytic potential. *Scientific Reports*. 2021;11(1):1-18.
8. Lee SH, Jun B-H. Silver Nanoparticles: Synthesis and Application for Nanomedicine. *International Journal of Molecular Sciences*. 2019;20(4):865.
9. Nasrollahzadeh M, Sajadi SM, Sajjadi M, Issaabadi Z. Chapter 4 - Applications of Nanotechnology in Daily Life. In: Nasrollahzadeh M, Sajadi SM, Sajjadi M, Issaabadi Z, Atarod M, editors. *Interface Science and Technology*. 28: Elsevier; 2019. p. 113-43.
10. Pirzada M, Altintas Z. Nanomaterials for Healthcare Biosensing Applications. *Sensors*. 2019;19(23):5311.
11. Wang Y, Pan J-A, Wu H, Talapin DV. Direct wavelength-selective optical and electron-beam lithography of functional inorganic nanomaterials. *ACS nano*. 2019;13(12):13917-31.
12. Qi K, Selvaraj R, Wang L. Functionalized Inorganic Semiconductor Nanomaterials: Characterization, Properties, and Applications. *Frontiers in Chemistry*. 2020;8.
13. Xu Y, Cao M, Zhang Q. Recent advances and perspective on heterogeneous catalysis using metals and oxide nanocrystals. *Materials Chemistry Frontiers*. 2021;5(1):151-222.
14. Pandey RP, Mukherjee R, Priyadarshini A, Gupta A, Vibhuti A, Leal E, et al. Potential of nanoparticles encapsulated drugs for possible inhibition of the antimicrobial resistance development. *Biomedicine & Pharmacotherapy*. 2021;141:111943.
15. Lee Y-C, Moon J-Y. *Introduction to bionanotechnology*: Springer; 2020.
16. Zahoor M, Nazir N, Iftikhar M, Naz S, Zekker I, Burlakovs J, et al. A Review on Silver Nanoparticles: Classification, Various Methods of Synthesis, and Their Potential Roles in Biomedical Applications and Water Treatment. *Water*. 2021;13(16):2216.
17. Nejati K, Dadashpour M, Gharibi T, Mellatyar H, Akbarzadeh A. Biomedical Applications of Functionalized Gold Nanoparticles: A Review. *Journal of Cluster Science*. 2022;33(1):1-16.
18. Tiquia-Arashiro S, Rodrigues DF. *Extremophiles: Applications in Nanotechnology*: Springer; 2016.
19. Staicu LC, Stolz JF. Editorial: microbes vs. metals: harvest and recycle. *FEMS Microbiology Ecology*. 2021;97(5).
20. Sharma P, Kumar S. Bioremediation of heavy metals from industrial effluents by endophytes and their metabolic activity: Recent advances. *Bioresource Technology*. 2021;339:125589.

21. Keshavarz S, Faraji F, Rashchi F, Mokmeli M. Bioleaching of manganese from a low-grade pyrolusite ore using *Aspergillus niger*: Process optimization and kinetic studies. *Journal of Environmental Management*. 2021;285:112153.
22. Mazumder P, Sharma SK, Taki K, Kalamdhad AS, Kumar M. Microbes involved in arsenic mobilization and respiration: a review on isolation, identification, isolates and implications. *Environmental Geochemistry and Health*. 2020;42(10):3443-69.
23. Ejileugha C, Ezealisiji KM, Ezejiofor AN, Orisakwe OE. Microbiologically Influenced Corrosion: Uncovering Mechanisms and Discovering Inhibitor—Metal and Metal Oxide Nanoparticles as Promising Biocorrosion Inhibitors. *Journal of Bio-and Tribo-Corrosion*. 2021;7(3):1-21.
24. Ghosh S, Ahmad R, Zeyaulah M, Khare SK. Microbial Nano-Factories: Synthesis and Biomedical Applications. *Frontiers in Chemistry*. 2021;9.
25. Huang J, Lin L, Sun D, Chen H, Yang D, Li Q. Bio-inspired synthesis of metal nanomaterials and applications. *Chemical Society Reviews*. 2015;44(17):6330-74.
26. Saravanan A, Kumar PS, Karishma S, Vo D-VN, Jeevanantham S, Yaashikaa PR, et al. A review on biosynthesis of metal nanoparticles and its environmental applications. *Chemosphere*. 2021;264:128580.
27. Wypij M, Jędrzejewski T, Ostrowski M, Trzcińska J, Rai M, Golińska P. Biogenic silver nanoparticles: assessment of their cytotoxicity, genotoxicity and study of capping proteins. *Molecules*. 2020;25(13):3022.
28. Salvadori MR, Nascimento CAO, Corrêa B. Nickel oxide nanoparticles film produced by dead biomass of filamentous fungus. *Scientific Reports*. 2014;4(1):6404.
29. Priyadarshini E, Priyadarshini SS, Cousins BG, Pradhan N. Metal-Fungus interaction: Review on cellular processes underlying heavy metal detoxification and synthesis of metal nanoparticles. *Chemosphere*. 2021;274:129976.
30. Aslam B, Wang W, Arshad MI, Khurshid M, Muzammil S, Rasool MH, et al. Antibiotic resistance: a rundown of a global crisis. *Infect Drug Resist*. 2018;11:1645-58.
31. Ojemaye MO, Adefisoye MA, Okoh AI. Nanotechnology as a viable alternative for the removal of antimicrobial resistance determinants from discharged municipal effluents and associated watersheds: A review. *Journal of Environmental Management*. 2020;275:111234.
32. Roy A, Bulut O, Some S, Mandal AK, Yilmaz MD. Green synthesis of silver nanoparticles: biomolecule-nanoparticle organizations targeting antimicrobial activity. *RSC Advances*. 2019;9(5):2673-702.
33. Beyth N, Houri-Haddad Y, Domb A, Khan W, Hazan R. Alternative Antimicrobial Approach: Nano-Antimicrobial Materials. *Evidence-Based Complementary and Alternative Medicine*. 2015;2015:246012.
34. Skóra B, Krajewska U, Nowak A, Dziedzic A, Barylyak A, Kus-Liśkiewicz M. Nontoxic silver nanoparticles as a new antimicrobial strategy. *Scientific Reports*. 2021;11(1):13451.
35. Crisan CM, Mocan T, Manolea M, Lasca LI, Tăbăran F-A, Mocan L. Review on Silver Nanoparticles as a Novel Class of Antibacterial Solutions. *Applied Sciences*. 2021;11(3):1120.
36. Arroyo GV, Madrid AT, Gavilanes AF, Naranjo B, Debut A, Arias MT, et al. Green synthesis of silver nanoparticles for application in cosmetics. *Journal of Environmental Science and Health, Part A*. 2020;55(11):1304-20.
37. Biswal AK, Misra PK. Biosynthesis and characterization of silver nanoparticles for prospective application in food packaging and biomedical fields. *Materials Chemistry and Physics*. 2020;250:123014.
38. Mathur P, Jha S, Ramteke S, Jain NK. Pharmaceutical aspects of silver nanoparticles. *Artificial Cells, Nanomedicine, and Biotechnology*. 2018;46(sup1):115-26.
39. Zhang H. Application of silver nanoparticles in drinking water purification. 2013.
40. Hamid S, Zainab S, Faryal R, Ali N. Deterrence in metabolic and biofilms forming activity of *Candida* species by mycogenic silver nanoparticles. *Journal of Applied Biomedicine*. 2017;15(4):249-55.

41. Nakamura S, Sato M, Sato Y, Ando N, Takayama T, Fujita M, et al. Synthesis and Application of Silver Nanoparticles (Ag NPs) for the Prevention of Infection in Healthcare Workers. *International Journal of Molecular Sciences*. 2019;20(15):3620.
42. Vance ME, Kuiken T, Vejerano EP, McGinnis SP, Hochella MF, Jr., Rejeski D, et al. Nanotechnology in the real world: Redeveloping the nanomaterial consumer products inventory. *Beilstein Journal of Nanotechnology*. 2015;6:1769-80.
43. Nagamune T. Biomolecular engineering for nanobio/bionanotechnology. *Nano Convergence*. 2017;4(1):9.
44. McWilliams A. Nanotechnology: a realistic market assessment. BCC Research. 2010.
45. Vance ME, Kuiken T, Vejerano EP, McGinnis SP, Hochella Jr MF, Rejeski D, et al. Nanotechnology in the real world: Redeveloping the nanomaterial consumer products inventory. *Beilstein journal of nanotechnology*. 2015;6:1769.
46. Yaqoob AA, Ahmad H, Parveen T, Ahmad A, Oves M, Ismail IMI, et al. Recent Advances in Metal Decorated Nanomaterials and Their Various Biological Applications: A Review. *Frontiers in Chemistry*. 2020;8.
47. Dhand C, Dwivedi N, Loh XJ, Ying ANJ, Verma NK, Beuerman RW, et al. Methods and strategies for the synthesis of diverse nanoparticles and their applications: a comprehensive overview. *Rsc Advances*. 2015;5(127):105003-37.
48. Hemeg HA. Nanomaterials for alternative antibacterial therapy. *International journal of nanomedicine*. 2017;12:8211.
49. Wei L, Lu J, Xu H, Patel A, Chen Z-S, Chen G. Silver nanoparticles: synthesis, properties, and therapeutic applications. *Drug discovery today*. 2015;20(5):595-601.
50. Morgan KA, Tang T, Zeimpekis I, Ravagli A, Craig C, Yao J, et al. High-throughput physical vapour deposition flexible thermoelectric generators. *Scientific reports*. 2019;9(1):1-9.
51. Bhuyan RK, Mohapatra RK, Nath G, Sahoo BK, Das D, Pamu D. Influence of high-energy ball milling on structural, microstructural, and optical properties of Mg<sub>2</sub>TiO<sub>4</sub> nanoparticles. *Journal of Materials Science: Materials in Electronics*. 2020;31(1):628-36.
52. Sakar N, Gergeroglu H, Akalin SA, Oguzlar S, Yildirim S. Synthesis, structural and optical characterization of Nd: YAG powders via flame spray pyrolysis. *Optical Materials*. 2020;103:109819.
53. Uhl AM, Mills SC, Andrew JS. Synthesis of cobalt ferrite nanoparticles via electrospraying into a liquid collector. *Journal of Materials Research*. 2020;35(8):864-71.
54. Tommalieh M, Ibrahim HA, Awwad NS, Menazea A. Gold nanoparticles doped polyvinyl alcohol/chitosan blend via laser ablation for electrical conductivity enhancement. *Journal of Molecular Structure*. 2020;1221:128814.
55. Zhu X, ten Brink GH, de Graaf S, Kooi BJ, Palasantzas G. Gas-phase synthesis of tunable-size germanium nanocrystals by inert gas condensation. *Chemistry of Materials*. 2020;32(4):1627-35.
56. Yu CH, Tam K, Tsang ESC. Chapter 5 Chemical Methods for Preparation of Nanoparticles in Solution. In: Blackman JA, editor. *Handbook of Metal Physics*. 5: Elsevier; 2008. p. 113-41.
57. Kulkarni SK. *Nanotechnology: principles and practices*: Springer; 2015.
58. Boroumand Moghaddam A, Namvar F, Moniri M, Azizi S, Mohamad R. Nanoparticles biosynthesized by fungi and yeast: a review of their preparation, properties, and medical applications. *Molecules*. 2015;20(9):16540-65.
59. Deshpande LM, Chopade BA. Plasmid mediated silver resistance in *Acinetobacter baumannii*. *Biomaterials*. 1994;7(1):49-56.
60. Durán N, Marcato PD, Durán M, Yadav A, Gade A, Rai M. Mechanistic aspects in the biogenic synthesis of extracellular metal nanoparticles by peptides, bacteria, fungi, and plants. *Applied microbiology and biotechnology*. 2011;90(5):1609-24.
61. Lemire JA, Harrison JJ, Turner RJ. Antimicrobial activity of metals: mechanisms, molecular targets and applications. *Nature Reviews Microbiology*. 2013;11(6):371.

62. Annear D, Mee B, Bailey M. Instability and linkage of silver resistance, lactose fermentation, and colony structure in *Enterobacter cloacae* from burn wounds. *Journal of clinical pathology*. 1976;29(5):441-3.
63. Li X-Z, Nikaido H, Williams KE. Silver-resistant mutants of *Escherichia coli* display active efflux of Ag<sup>+</sup> and are deficient in porins. *Journal of bacteriology*. 1997;179(19):6127-32.
64. Slawson RM, Trevors JT, Lee H. Silver accumulation and resistance in *Pseudomonas stutzeri*. *Archives of microbiology*. 1992;158(6):398-404.
65. Klaus T, Joerger R, Olsson E, Granqvist C-G. Silver-based crystalline nanoparticles, microbially fabricated. *Proceedings of the National Academy of Sciences*. 1999;96(24):13611-4.
66. Shakibaie MR, Dhakephalkar B, Kapadnis BP, Chopade BA. Silver resistance in *Acinetobacter baumannii* BL54 occurs through binding to a Ag-binding protein. *Iranian Journal of Biotechnology*. 2003;1(1):41-6.
67. Parikh RY, Singh S, Prasad B, Patole MS, Sastry M, Shouche YS. Extracellular synthesis of crystalline silver nanoparticles and molecular evidence of silver resistance from *Morganella* sp.: towards understanding biochemical synthesis mechanism. *ChemBioChem*. 2008;9(9):1415-22.
68. Singh R, Shedbalkar UU, Wadhvani SA, Chopade BA. Bacteriogenic silver nanoparticles: synthesis, mechanism, and applications. *Applied microbiology and biotechnology*. 2015;99(11):4579-93.
69. Wang H, Chen H, Wang Y, Huang J, Kong T, Lin W, et al. Stable silver nanoparticles with narrow size distribution non-enzymatically synthesized by *Aeromonas* sp. SH10 cells in the presence of hydroxyl ions. *Current Nanoscience*. 2012;8(6):838-46.
70. Debabov V, Voeikova T, Shebanova A, Shaitan K, Emel'yanova L, Novikova L, et al. Bacterial synthesis of silver sulfide nanoparticles. *Nanotechnologies in Russia*. 2013;8(3-4):269-76.
71. Prakash A, Sharma S, Ahmad N, Ghosh A, Sinha P. Synthesis of AgNps By *Bacillus cereus* bacteria and their antimicrobial potential. *Journal of Biomaterials and Nanobiotechnology*. 2011;2(02):155-61.
72. Jha AK, Prasad K. Biosynthesis of metal and oxide nanoparticles using *Lactobacilli* from yoghurt and probiotic spore tablets. *Biotechnology journal*. 2010;5(3):285-91.
73. Kalimuthu K, Babu RS, Venkataraman D, Bilal M, Gurnathan S. Biosynthesis of silver nanocrystals by *Bacillus licheniformis*. *Colloids and Surfaces B: Biointerfaces*. 2008;65(1):150-3.
74. Karthik C, Radha K. Biosynthesis and characterization of silver nanoparticles using *Enterobacter aerogenes*: a kinetic approach. *Dig J Nanomater Biostruct*. 2012;7(3):1007-14.
75. Gaidhani S, Singh R, Singh D, Patel U, Shevade K, Yeshvekar R, et al. Biofilm disruption activity of silver nanoparticles synthesized by *Acinetobacter calcoaceticus* PUCM 1005. *Materials Letters*. 2013;108:324-7.
76. Brayner R, Barberousse H, Hemadi M, Djedjat C, Yéprémian C, Coradin T, et al. Cyanobacteria as bioreactors for the synthesis of Au, Ag, Pd, and Pt nanoparticles via an enzyme-mediated route. *Journal of nanoscience and nanotechnology*. 2007;7(8):2696-708.
77. Shahverdi AR, Fakhimi A, Shahverdi HR, Minaian S. Synthesis and effect of silver nanoparticles on the antibacterial activity of different antibiotics against *Staphylococcus aureus* and *Escherichia coli*. *Nanomedicine: Nanotechnology, Biology and Medicine*. 2007;3(2):168-71.
78. Prasad K, Jha AK, Prasad K, Kulkarni A. Can microbes mediate nano-transformation? *Indian Journal of Physics*. 2010;84(10):1355-60.
79. Sintubin L, De Windt W, Dick J, Mast J, van der Ha D, Verstraete W, et al. Lactic acid bacteria as reducing and capping agent for the fast and efficient production of silver nanoparticles. *Applied Microbiology and Biotechnology*. 2009;84(4):741-9.
80. Hosseini-Abari A, Emtiazi G, Ghasemi SM. Development of an eco-friendly approach for biogenesis of silver nanoparticles using spores of *Bacillus athrophaeus*. *World Journal of Microbiology and Biotechnology*. 2013;29(12):2359-64.

81. Liu C, Yang D, Wang Y, Shi J, Jiang Z. Fabrication of antimicrobial bacterial cellulose–Ag/AgCl nanocomposite using bacteria as versatile biofactory. *Journal of Nanoparticle Research*. 2012;14(8):1084-95.
82. Naik RR, Stringer SJ, Agarwal G, Jones SE, Stone MO. Biomimetic synthesis and patterning of silver nanoparticles. *Nature materials*. 2002;1(3):169-72.
83. Nam KT, Lee YJ, Krauland EM, Kottmann ST, Belcher AM. Peptide-mediated reduction of silver ions on engineered biological scaffolds. *ACS Nano*. 2008;2(7):1480-6.
84. Selvakannan P, Swami A, Srisathiyarayanan D, Shirude PS, Pasricha R, Mandale AB, et al. Synthesis of aqueous Au core– Ag shell nanoparticles using tyrosine as a pH-dependent reducing agent and assembling phase-transferred silver nanoparticles at the air–water interface. *Langmuir*. 2004;20(18):7825-36.
85. Si S, Mandal TK. Tryptophan-based peptides to synthesize gold and silver nanoparticles: A mechanistic and kinetic study. *Chemistry–A European Journal*. 2007;13(11):3160-8.
86. Banerjee K, Rai VR. A review on mycosynthesis, mechanism, and characterization of silver and gold nanoparticles. *BioNanoScience*. 2018;8(1):17-31.
87. Durán N, Marcato PD, Alves OL, De Souza GI, Esposito E. Mechanistic aspects of biosynthesis of silver nanoparticles by several *Fusarium oxysporum* strains. *Journal of nanobiotechnology*. 2005;3(1):8.
88. Bhainsa KC, D'souza S. Extracellular biosynthesis of silver nanoparticles using the fungus *Aspergillus fumigatus*. *Colloids and surfaces B: Biointerfaces*. 2006;47(2):160-4.
89. Vahabi K, Mansoori GA, Karimi S. Biosynthesis of silver nanoparticles by fungus *Trichoderma reesei* (a route for large-scale production of AgNPs). *Insciences J*. 2011;1(1):65-79.
90. Mukherjee P, Ahmad A, Mandal D, Senapati S, Sainkar SR, Khan MI, et al. Bioreduction of AuCl<sub>4</sub><sup>-</sup> ions by the fungus, *Verticillium* sp. and surface trapping of the gold nanoparticles formed. *Angewandte Chemie International Edition*. 2001;40(19):3585-8.
91. Chandrappa C, Govindappa M, Chandrasekar N, Sarkar S, Ooha S, Channabasava R. Endophytic synthesis of silver chloride nanoparticles from *Penicillium* sp. of *Calophyllum apetalum*. *Advances in Natural Sciences: Nanoscience and Nanotechnology*. 2016;7(2):025016.
92. Alghuthaymi MA, Almoammar H, Rai M, Said-Galiev E, Abd-Elsalam KA. Myconanoparticles: synthesis and their role in phytopathogens management. *Biotechnology & Biotechnological Equipment*. 2015;29(2):221-36.
93. Thakkar KN, Mhatre SS, Parikh RY. Biological synthesis of metallic nanoparticles. *Nanomedicine: nanotechnology, biology and medicine*. 2010;6(2):257-62.
94. Akhtar MS, Panwar J, Yun Y-S. Biogenic synthesis of metallic nanoparticles by plant extracts. *ACS Sustainable Chemistry & Engineering*. 2013;1(6):591-602.
95. Iravani S. Green synthesis of metal nanoparticles using plants. *Green Chemistry*. 2011;13(10):2638-50.
96. Avery KN, Schaak JE, Schaak RE. M13 bacteriophage as a biological scaffold for magnetically-recoverable metal nanowire catalysts: combining specific and nonspecific interactions to design multifunctional nanocomposites. *Chemistry of Materials*. 2009;21(11):2176-8.
97. Lee LA, Nguyen HG, Wang Q. Altering the landscape of viruses and bionanoparticles. *Organic & biomolecular chemistry*. 2011;9(18):6189-95.
98. Blum AS, Soto CM, Wilson CD, Cole JD, Kim M, Gnade B, et al. Cowpea mosaic virus as a scaffold for 3-D patterning of gold nanoparticles. *Nano letters*. 2004;4(5):867-70.
99. Hou L, Gao F, Li N. T4 Virus-Based Toolkit for the Direct Synthesis and 3D Organization of Metal Quantum Particles. *Chemistry–A European Journal*. 2010;16(48):14397-403.
100. Zhou JC, Soto CM, Chen M-S, Bruckman MA, Moore MH, Barry E, et al. Biotemplating rod-like viruses for the synthesis of copper nanorods and nanowires. *Journal of nanobiotechnology*. 2012;10(1):18.

101. Dujardin E, Peet C, Stubbs G, Culver JN, Mann S. Organization of metallic nanoparticles using tobacco mosaic virus templates. *Nano Letters*. 2003;3(3):413-7.
102. Narayanan KB, Sakthivel N. Biological synthesis of metal nanoparticles by microbes. *Advances in colloid and interface science*. 2010;156(1-2):1-13.
103. Mukherjee P, Ahmad A, Mandal D, Senapati S, Sainkar SR, Khan MI, et al. Fungus-mediated synthesis of silver nanoparticles and their immobilization in the mycelial matrix: a novel biological approach to nanoparticle synthesis. *Nano Letters*. 2001;1(10):515-9.
104. Krumov N, Oder S, Perner-Nochta I, Angelov A, Posten C. Accumulation of CdS nanoparticles by yeasts in a fed-batch bioprocess. *Journal of biotechnology*. 2007;132(4):481-6.
105. Apte M, Girme G, Bankar A, RaviKumar A, Zinjarde S. 3, 4-dihydroxy-L-phenylalanine-derived melanin from *Yarrowia lipolytica* mediates the synthesis of silver and gold nanostructures. *Journal of nanobiotechnology*. 2013;11(1):2.
106. Hulkoti NI, Taranath T. Biosynthesis of nanoparticles using microbes—a review. *Colloids and Surfaces B: Biointerfaces*. 2014;121:474-83.
107. Singh OV. *Bio-nanoparticles: biosynthesis and sustainable biotechnological implications*: John Wiley & Sons; 2015.
108. Korbekandi H, Ashari Z, Iravani S, Abbasi S. Optimization of biological synthesis of silver nanoparticles using *Fusarium oxysporum*. *Iranian journal of pharmaceutical research: IJPR*. 2013;12(3):289.
109. Ahmad A, Mukherjee P, Senapati S, Mandal D, Khan MI, Kumar R, et al. Extracellular biosynthesis of silver nanoparticles using the fungus *Fusarium oxysporum*. *Colloids and surfaces B: Biointerfaces*. 2003;28(4):313-8.
110. Magiorakos AP, Srinivasan A, Carey R, Carmeli Y, Falagas M, Giske C, et al. Multidrug-resistant, extensively drug-resistant and pandrug-resistant bacteria: an international expert proposal for interim standard definitions for acquired resistance. *Clinical microbiology and infection*. 2012;18(3):268-81.
111. Aung MS, Zi H, Nwe KM, Maw WW, Aung MT, Min W, et al. Drug resistance and genetic characteristics of clinical isolates of staphylococci in Myanmar: high prevalence of PVL among methicillin-susceptible *Staphylococcus aureus* belonging to various sequence types. *New microbes and new infections*. 2016;10:58-65.
112. Moghaddam MJM, Mirbagheri AA, Salehi Z, Habibzade SM. Prevalence of class 1 integrons and extended spectrum beta lactamases among multi-drug resistant *Escherichia coli* isolates from north of Iran. *Iranian biomedical journal*. 2015;19(4):233-9.
113. Tsutsui M, Kawakubo H, Hayashida T, Fukuda K, Nakamura R, Takahashi T, et al. Comprehensive screening of genes resistant to an anticancer drug in esophageal squamous cell carcinoma. *International journal of oncology*. 2015;47(3):867-74.
114. Coetzee J, Corcoran C, Prentice E, Moodley M, Mendelson M, Poirel L, et al. Emergence of plasmid-mediated colistin resistance (MCR-1) among *Escherichia coli* isolated from South African patients. *SAMJ: South African Medical Journal*. 2016;106(5):449-50.
115. Daury L, Orange F, Taveau J-C, Verchère A, Monlezun L, Gounou C, et al. Tripartite assembly of RND multidrug efflux pumps. *Nature communications*. 2016;7:10731.
116. Andersson DI, Hughes D, Kubicek-Sutherland JZ. Mechanisms and consequences of bacterial resistance to antimicrobial peptides. *Drug Resistance Updates*. 2016;26:43-57.
117. Khameneh B, Diab R, Ghazvini K, Bazzaz BSF. Breakthroughs in bacterial resistance mechanisms and the potential ways to combat them. *Microbial Pathogenesis*. 2016;95:32-42.
118. Huh AJ, Kwon YJ. “Nanoantibiotics”: a new paradigm for treating infectious diseases using nanomaterials in the antibiotics resistant era. *Journal of controlled release*. 2011;156(2):128-45.
119. Koul A, Arnoult E, Lounis N, Guillemont J, Andries K. The challenge of new drug discovery for tuberculosis. *Nature*. 2011;469(7331):483-90.
120. Wang L, Hu C, Shao L. The antimicrobial activity of nanoparticles: present situation and prospects for the future. *International journal of nanomedicine*. 2017;12:1227.
121. Chatzimitakos TG, Stalikas CD. Qualitative alterations of bacterial metabolome after exposure to metal nanoparticles with bactericidal properties: A comprehensive workflow



- based on <sup>1</sup>H NMR, UHPLC-HRMS, and metabolic databases. *Journal of proteome research*. 2016;15(9):3322-30.
122. Zhao L, Ashraf M. Influence of silver-hydroxyapatite nanocomposite coating on biofilm formation of joint prosthesis and its mechanism. *The West Indian Medical Journal*. 2015;64(5):506.
123. Armentano I, Arciola CR, Fortunati E, Ferrari D, Mattioli S, Amoroso CF, et al. The Interaction of Bacteria with Engineered Nanostructured Polymeric Materials: A Review. *The Scientific World Journal*. 2014;2014:18.
124. Li H, Chen Q, Zhao J, Urmila K. Enhancing the antimicrobial activity of natural extraction using the synthetic ultrasmall metal nanoparticles. *Scientific reports*. 2015;5:11033.
125. Luan B, Huynh T, Zhou R. Complete wetting of graphene by biological lipids. *Nanoscale*. 2016;8(10):5750-4.
126. Gao W, Thamphiwatana S, Angsantikul P, Zhang L. Nanoparticle approaches against bacterial infections. *Wiley Interdisciplinary Reviews: Nanomedicine and Nanobiotechnology*. 2014;6(6):532-47.
127. Xu Y, Wei M-T, Ou-Yang HD, Walker SG, Wang HZ, Gordon CR, et al. Exposure to TiO<sub>2</sub> nanoparticles increases *Staphylococcus aureus* infection of HeLa cells. *Journal of nanobiotechnology*. 2016;14(1):34.
128. Gurunathan S, Han JW, Dayem AA, Eppakayala V, Kim J-H. Oxidative stress-mediated antibacterial activity of graphene oxide and reduced graphene oxide in *Pseudomonas aeruginosa*. *International journal of nanomedicine*. 2012;7:5901-14.
129. Leung YH, Ng AM, Xu X, Shen Z, Gethings LA, Wong MT, et al. Mechanisms of antibacterial activity of MgO: non-ROS mediated toxicity of MgO nanoparticles towards *Escherichia coli*. *Small*. 2014;10(6):1171-83.
130. Zakharova OV, Godymchuk AY, Gusev AA, Gulchenko SI, Vasyukova IA, Kuznetsov DV. Considerable Variation of Antibacterial Activity of Cu Nanoparticles Suspensions Depending on the Storage Time, Dispersive Medium, and Particle Sizes. *BioMed Research International*. 2015;2015:11.
131. Malka E, Perelshtein I, Lipovsky A, Shalom Y, Naparstek L, Perkas N, et al. Eradication of multi-drug resistant bacteria by a novel Zn-doped CuO nanocomposite. *Small*. 2013;9(23):4069-76.
132. Li Y, Zhang W, Niu J, Chen Y. Mechanism of photogenerated reactive oxygen species and correlation with the antibacterial properties of engineered metal-oxide nanoparticles. *ACS nano*. 2012;6(6):5164-73.
133. Cheloni G, Marti E, Slaveykova VI. Interactive effects of copper oxide nanoparticles and light to green alga *Chlamydomonas reinhardtii*. *Aquatic Toxicology*. 2016;170:120-8.
134. Shrivastava S, Bera T, Roy A, Singh G, Ramachandrarao P, Dash D. Characterization of enhanced antibacterial effects of novel silver nanoparticles. *Nanotechnology*. 2007;18(22):225103.
135. Pramanik A, Laha D, Bhattacharya D, Pramanik P, Karmakar P. A novel study of antibacterial activity of copper iodide nanoparticle mediated by DNA and membrane damage. *Colloids and Surfaces B: Biointerfaces*. 2012;96:50-5.
136. Wu B, Zhuang W-Q, Sahu M, Biswas P, Tang YJ. Cu-doped TiO<sub>2</sub> nanoparticles enhance survival of *Shewanella oneidensis* MR-1 under Ultraviolet Light (UV) exposure. *Science of the total environment*. 2011;409(21):4635-9.
137. Padmavathy N, Vijayaraghavan R. Interaction of ZnO nanoparticles with microbes—a physio and biochemical assay. *Journal of biomedical nanotechnology*. 2011;7(6):813-22.
138. Yu J, Zhang W, Li Y, Wang G, Yang L, Jin J, et al. Synthesis, characterization, antimicrobial activity and mechanism of a novel hydroxyapatite whisker/nano zinc oxide biomaterial. *Biomedical Materials*. 2014;10(1):015001.
139. Robbins N, Cowen LE. Antifungal drug resistance: Deciphering the mechanisms governing multidrug resistance in the fungal pathogen *Candida glabrata*. *Current Biology*. 2021;31(23):R1520-R3.

140. Nishikawa H, Yamada E, Shibata T, Uchihashi S, Fan H, Hayakawa H, et al. Uptake of T-2307, a novel arylamidine, in *Candida albicans*. *Journal of antimicrobial chemotherapy*. 2010;65(8):1681-7.
141. Singh S, Chandra U, Anchan V, Verma P, Tilak R. Limited effectiveness of four oral antifungal drugs (fluconazole, griseofulvin, itraconazole and terbinafine) in the current epidemic of altered dermatophytosis in India: results of a randomized pragmatic trial. *British Journal of Dermatology*. 2020;183(5):840-6.
142. Borgers M. Mechanism of action of antifungal drugs, with special reference to the imidazole derivatives. *Reviews of infectious diseases*. 1980;2(4):520-34.
143. Holt SL, Drew RH. Echinocandins: addressing outstanding questions surrounding treatment of invasive fungal infections. *American Journal of Health-System Pharmacy*. 2011;68(13):1207-20.
144. Ibe C, Munro CA. Fungal cell wall: An underexploited target for antifungal therapies. *PLoS Pathogens*. 2021;17(4):e1009470.
145. Hirano M, Takeuchi Y, Matsumori N, Murata M, Ide T. Channels formed by amphotericin B covalent dimers exhibit rectification. *The Journal of membrane biology*. 2011;240(3):159-64.
146. Cavassin FB, Baú-Carneiro JL, Vilas-Boas RR, Queiroz-Telles F. Sixty years of Amphotericin B: An overview of the main antifungal agent used to treat invasive fungal infections. *Infectious Diseases and Therapy*. 2021;10(1):115-47.
147. Lupetti A, Danesi R, Campa M, Del Tacca M, Kelly S. Molecular basis of resistance to azole antifungals. *Trends in molecular medicine*. 2002;8(2):76-81.
148. Domínguez JM, Kelly VA, Kinsman OS, Marriott MS, de las Heras FG, Martín JJ. Sordarins: a new class of antifungals with selective inhibition of the protein synthesis elongation cycle in yeasts. *Antimicrobial Agents and Chemotherapy*. 1998;42(9):2274-8.
149. Shao Y, Molestak E, Su W, Stankevič M, Tchórzewski M. Sordarin—the antifungal antibiotic with a unique modus operandi. *British Journal of Pharmacology*. 2021.
150. Morschhäuser J. Regulation of multidrug resistance in pathogenic fungi. *Fungal Genetics and Biology*. 2010;47(2):94-106.
151. Kim KJ, Sung WS, Suh BK, Moon SK, Choi JS, Kim JG, et al. Antifungal activity and mode of action of silver nano-particles on *Candida albicans*. *Biometals : an international journal on the role of metal ions in biology, biochemistry, and medicine*. 2009;22(2):235-42.
152. Rosa-Garc DL, #x00ED, a SC, Mart, #x00ED, nez-Torres P, et al. Antifungal Activity of ZnO and MgO Nanomaterials and Their Mixtures against *Colletotrichum gloeosporioides* Strains from Tropical Fruit. *Journal of Nanomaterials*. 2018;2018:9.
153. Su H-L, Chou C-C, Hung D-J, Lin S-H, Pao I-C, Lin J-H, et al. The disruption of bacterial membrane integrity through ROS generation induced by nanohybrids of silver and clay. *Biomaterials*. 2009;30(30):5979-87.
154. Ansari MA, Khan HM, Khan AA, Sultan A, Azam A. Synthesis and characterization of the antibacterial potential of ZnO nanoparticles against extended-spectrum  $\beta$ -lactamases-producing *Escherichia coli* and *Klebsiella pneumoniae* isolated from a tertiary care hospital of North India. *Applied microbiology and biotechnology*. 2012;94(2):467-77.
155. Lundberg ME, Becker EC, Choe S. MstX and a putative potassium channel facilitate biofilm formation in *Bacillus subtilis*. *PloS one*. 2013;8(5):e60993.
156. Lellouche J, Friedman A, Lellouche J-P, Gedanken A, Banin E. Improved antibacterial and antibiofilm activity of magnesium fluoride nanoparticles obtained by water-based ultrasound chemistry. *Nanomedicine: Nanotechnology, Biology and Medicine*. 2012;8(5):702-11.
157. Seil JT, Webster TJ. Antimicrobial applications of nanotechnology: methods and literature. *International journal of nanomedicine*. 2012;7:2767.
158. Seneviratne C, Jin L, Samaranyake L. Biofilm lifestyle of *Candida*: a mini review. *Oral diseases*. 2008;14(7):582-90.
159. Bandara H, Matsubara V, Samaranyake L. Future therapies targeted towards eliminating *Candida* biofilms and associated infections. Expert review of anti-infective therapy. 2017;15(3):299-318.

160. Lara HH, Romero-Urbina DG, Pierce C, Lopez-Ribot JL, Arellano-Jimenez MJ, Jose-Yacamán M. Effect of silver nanoparticles on *Candida albicans* biofilms: an ultrastructural study. *Journal of nanobiotechnology*. 2015;13(1):91.
161. Monteiro D, Silva S, Negri M, Gorup L, de Camargo E, Oliveira R, et al. Silver colloidal nanoparticles: Effect on matrix composition and structure of *Candida albicans* and *Candida glabrata* biofilms. *Journal of applied microbiology*. 2013;114(4):1175-83.
162. Monteiro DR, Takamiya AS, Feresin LP, Gorup LF, de Camargo ER, Delbem ACB, et al. Silver colloidal nanoparticle stability: influence on *Candida* biofilms formed on denture acrylic. *Sabouraudia*. 2014;52(6):627-35.
163. Sule P, Wadhawan T, Carr NJ, Horne SM, Wolfe AJ, Prüss BM. A combination of assays reveals biomass differences in biofilms formed by *Escherichia coli* mutants. *Letters in applied microbiology*. 2009;49(3):299-304.
164. Hamid S, Zainab S, Faryal R, Ali N, Sharafat I. Inhibition of secreted aspartyl proteinase activity in biofilms of *Candida* species by mycogenic silver nanoparticles. *Artificial cells, nanomedicine, and biotechnology*. 2018;46(3):551-7.
165. Srivastava V, Gusain D, Sharma YC. Critical review on the toxicity of some widely used engineered nanoparticles. *Industrial & Engineering Chemistry Research*. 2015;54(24):6209-33.
166. Ai J, Biazar E, Jafarpour M, Montazeri M, Majdi A, Aminifard S, et al. Nanotoxicology and nanoparticle safety in biomedical designs. *International journal of nanomedicine*. 2011;6:1117-27.
167. Li X, Wang L, Fan Y, Feng Q, Cui F-z. Biocompatibility and toxicity of nanoparticles and nanotubes. *Journal of Nanomaterials*. 2012;2012:6.
168. Nel A, Xia T, Meng H, Wang X, Lin S, Ji Z, et al. Nanomaterial toxicity testing in the 21st century: use of a predictive toxicological approach and high-throughput screening. *Accounts of chemical research*. 2013;46(3):607-21.
169. Sharma A, Madhunapantula SV, Robertson GP. Toxicological considerations when creating nanoparticle-based drugs and drug delivery systems. *Expert opinion on drug metabolism & toxicology*. 2012;8(1):47-69.
170. Warheit DB, Sayes CM, Reed KL, Swain KA. Health effects related to nanoparticle exposures: environmental, health and safety considerations for assessing hazards and risks. *Pharmacology & therapeutics*. 2008;120(1):35-42.
171. Wittmaack K. In search of the most relevant parameter for quantifying lung inflammatory response to nanoparticle exposure: particle number, surface area, or what? *Environmental health perspectives*. 2006;115(2):187-94.
172. Stoeger T, Takenaka S, Frankenberger B, Ritter B, Karg E, Maier K, et al. Deducing in vivo toxicity of combustion-derived nanoparticles from a cell-free oxidative potency assay and metabolic activation of organic compounds. *Environmental Health Perspectives*. 2008;117(1):54-60.
173. Rao V. Systems Approach to Biosafety and Risk Assessment of Engineered Nanomaterials. *Applied Biosafety*. 2014;19(1):11-9.
174. Dang F, Huang Y, Wang Y, Zhou D, Xing B. Transfer and toxicity of silver nanoparticles in the food chain. *Environmental Science: Nano*. 2021;8(6):1519-35.
175. Olivier J-C. Drug transport to brain with targeted nanoparticles. *NeuroRx*. 2005;2(1):108-19.
176. SCENIHR. Risk Assessment of Products of Nanotechnologies. European Commission, Scientific Committee on Emerging and Newly Identified Health Risks (SCENIHR): Brussels, Belgium. 2009.
177. Ali SM, Yousef NM, Nafady NA. Application of biosynthesized silver nanoparticles for the control of land snail *Eobania vermiculata* and some plant pathogenic fungi. *Journal of Nanomaterials*. 2015;2015:3.
178. Murphy M, Ting K, Zhang X, Soo C, Zheng Z. Current development of silver nanoparticle preparation, investigation, and application in the field of medicine. *Journal of Nanomaterials*. 2015;2015:5.

179. Shahzad A, Saeed H, Iqtedar M, Hussain SZ, Kaleem A, Abdullah R, et al. Size-Controlled Production of Silver Nanoparticles by *Aspergillus fumigatus* BTCB10: Likely Antibacterial and Cytotoxic Effects. *Journal of Nanomaterials*. 2019;2019.
180. Ghosh S, Ahmad R, Banerjee K, AlAjmi MF, Rahman S. Mechanistic Aspects of Microbe-Mediated Nanoparticle Synthesis. *Frontiers in Microbiology*. 2021;12(867).
181. Garcia-Hernandez M, Villarreal-Chiu J, Garza-González M. Metallophilic fungi research: an alternative for its use in the bioremediation of hexavalent chromium. *International Journal of Environmental Science and Technology*. 2017;14(9):2023-38.
182. Ameen F, Al-Homaidan AA, Al-Sabri A, Almansob A, AlNadhari S. Anti-oxidant, anti-fungal and cytotoxic effects of silver nanoparticles synthesized using marine fungus *Cladosporium halotolerans*. *Applied Nanoscience*. 2021.
183. Osorio-Echavarría J, Osorio-Echavarría J, Ossa-Orozco CP, Gómez-Vanegas NA. Synthesis of silver nanoparticles using white-rot fungus *Anamorphous Bjerkandera* sp. R1: influence of silver nitrate concentration and fungus growth time. *Scientific Reports*. 2021;11(1):3842.
184. Evans S, Hansen RW, Schneegurt MA. Isolation and Characterization of Halotolerant Soil Fungi from the Great Salt Plains of Oklahoma. *Cryptogam Mycol*. 2013;34(4):329-41.
185. Sikandar S, Ujor VC, Ezeji TC, Rossington JL, Michel Jr FC, McMahan CM, et al. *Thermomyces lanuginosus* STm: A source of thermostable hydrolytic enzymes for novel application in extraction of high-quality natural rubber from *Taraxacum kok-saghyz* (Rubber dandelion). *Industrial Crops and Products*. 2017;103:161-8.
186. Iram S, Parveen K, Usman J, Nasir K, Akhtar N, Arouj S, et al. Heavy metal tolerance of filamentous fungal strains isolated from soil irrigated with industrial wastewater. *Biologija*. 2012;58(3).
187. Fazli MM, Soleimani N, Mehrasbi M, Darabian S, Mohammadi J, Ramazani A. Highly cadmium tolerant fungi: their tolerance and removal potential. *Journal of Environmental Health Science and Engineering*. 2015;13(1):19.
188. Molnár Z, Bódai V, Szakacs G, Erdélyi B, Fogarassy Z, Sáfrán G, et al. Green synthesis of gold nanoparticles by thermophilic filamentous fungi. *Scientific Reports*. 2018;8(1):3943.
189. Rättö M, Chatani M, Ritschkoff A-C, Viikari L. Screening of micro-organisms for decolorization of melanins produced by bluestain fungi. *Applied microbiology and biotechnology*. 2001;55(2):210-3.
190. Anderson MJ, Gull K, Denning DW. Molecular typing by random amplification of polymorphic DNA and M13 southern hybridization of related paired isolates of *Aspergillus fumigatus*. *J Clin Microbiol*. 1996;34(1):87-93.
191. Altschul SF, Madden TL, Schäffer AA, Zhang J, Zhang Z, Miller W, et al. Gapped BLAST and PSI-BLAST: a new generation of protein database search programs. *Nucleic acids research*. 1997;25(17):3389-402.
192. Wessner D, Dupont C, Charles T, Neufeld J. *Microbiology: John Wiley & Sons; 2020*.
193. Ahmad KS, Hameed M, Fatima S, Ashraf M, Ahmad F, Naseer M, et al. Morpho-anatomical and physiological adaptations to high altitude in some *Aveneae* grasses from Neelum Valley, Western Himalayan Kashmir. *Acta physiologiae plantarum*. 2016;38(4):93.
194. Ibrar M, Ullah MW, Manan S, Farooq U, Rafiq M, Hasan F. Fungi from the extremes of life: an untapped treasure for bioactive compounds. *Applied Microbiology and Biotechnology*. 2020;104(7):2777-801.
195. Robinson JR, Isikhuemhen OS, Anike FN. Fungal–Metal Interactions: A Review of Toxicity and Homeostasis. *Journal of Fungi*. 2021;7(3):225.
196. Aziz N, Pandey R, Barman I, Prasad R. Leveraging the Attributes of *Mucor hiemalis*-Derived Silver Nanoparticles for a Synergistic Broad-Spectrum Antimicrobial Platform. *Frontiers in Microbiology*. 2016;7(1984).
197. Sulaiman GM, T HUSSIEN H, Saleem MM. Biosynthesis of silver nanoparticles synthesized by *Aspergillus flavus* and their antioxidant, antimicrobial and cytotoxicity properties. *Bulletin of Materials Science*. 2015;38(3):639-44.

198. Syed A, Saraswati S, Kundu GC, Ahmad A. Biological synthesis of silver nanoparticles using the fungus *Humicola* sp. and evaluation of their cytotoxicity using normal and cancer cell lines. *Spectrochimica Acta Part A: Molecular and Biomolecular Spectroscopy*. 2013;114:144-7.
199. ul Ain N, Anis I, Ahmed F, Shah MR, Parveen S, Faizi S, et al. Colorimetric detection of amoxicillin based on querecetagetin coated silver nanoparticles. *Sensors and Actuators B: Chemical*. 2018;265:617-24.
200. Sahu S, Sharma S, Kant T, Shrivastava K, Ghosh KK. Colorimetric determination of L-cysteine in milk samples with surface functionalized silver nanoparticles. *Spectrochimica Acta Part A: Molecular and Biomolecular Spectroscopy*. 2021;246:118961.
201. Nycz M, Arkusz K, Pijanowska DG. Fabrication of Electrochemical Biosensor Based on Titanium Dioxide Nanotubes and Silver Nanoparticles for Heat Shock Protein 70 Detection. *Materials*. 2021;14(13):3767.
202. Ibrahim N, Jamaluddin ND, Tan LL, Mohd Yusof NY. A Review on the Development of Gold and Silver Nanoparticles-Based Biosensor as a Detection Strategy of Emerging and Pathogenic RNA Virus. *Sensors*. 2021;21(15):5114.
203. Rathnakumar S, Bhaskar S, Rai A, Saikumar DV, Kambhampati NSV, Sivaramakrishnan V, et al. Plasmon-coupled silver nanoparticles for mobile phone-based attomolar sensing of Mercury ions. *ACS Applied Nano Materials*. 2021;4(8):8066-80.
204. Barveen NR, Wang T-J, Chang Y-H. Photochemical decoration of silver nanoparticles on silver vanadate nanorods as an efficient SERS probe for ultrasensitive detection of chloramphenicol residue in real samples. *Chemosphere*. 2021;275:130115.
205. Poulouse S, Panda T, Nair PP, Theodore T. Biosynthesis of silver nanoparticles. *Journal of nanoscience and nanotechnology*. 2014;14(2):2038-49.
206. Khalil AT, Iqbal J, Shah A, Haque MZ, Khan I, Ayaz M, et al. The bio-nano interface as an emerging trend in assembling multi-functional metal nanoparticles. 2021.
207. Molnár Z, Bódai V, Szakacs G, Erdélyi B, Fogarassy Z, Sáfrán G, et al. Green synthesis of gold nanoparticles by thermophilic filamentous fungi. *Scientific reports*. 2018;8(1):3943.
208. Barwal I, Ranjan P, Kateriya S, Yadav SC. Cellular oxido-reductive proteins of *Chlamydomonas reinhardtii* control the biosynthesis of silver nanoparticles. *Journal of Nanobiotechnology*. 2011;9(1):56.
209. Wen Y, Geitner NK, Chen R, Ding F, Chen P, Andorfer RE, et al. Binding of cytoskeletal proteins with silver nanoparticles. *Rsc Advances*. 2013;3(44):22002-7.
210. Karthik V, Senthil Kumar P, Vo D-VN, Selvakumar P, Gokulakrishnan M, Keerthana P, et al. Enzyme-loaded nanoparticles for the degradation of wastewater contaminants: a review. *Environmental Chemistry Letters*. 2021;19(3):2331-50.
211. Roucoux A, Schulz J, Patin H. Reduced transition metal colloids: a novel family of reusable catalysts? *Chemical reviews*. 2002;102(10):3757-78.
212. Tiquia-Arashiro S, Rodrigues DF. *Extremophiles: Applications in Nanotechnology*. 2016.
213. Ballottin D, Fulaz S, Souza ML, Corio P, Rodrigues AG, Souza AO, et al. Elucidating Protein Involvement in the Stabilization of the Biogenic Silver Nanoparticles. *Nanoscale Research Letters*. 2016;11(1):313.
214. Christakopoulos P, Kekos D, Macris B, Claeysens M, Bhat M. Purification and mode of action of a low molecular mass endo-1, 4- $\beta$ -D-glucanase from *Fusarium oxysporum*. *Journal of biotechnology*. 1995;39(1):85-93.
215. Nezhadali A, Mojarrab M. Computational study and multivariate optimization of hydrochlorothiazide analysis using molecularly imprinted polymer electrochemical sensor based on carbon nanotube/polypyrrole film. *Sensors and Actuators B: Chemical*. 2014;190:829-37.
216. Montgomery DC. *Design and analysis of experiments*: John Wiley & sons; 2017.
217. Yousefi N, Pazouki M, Alikhani Hesari F, Alizadeh M. Statistical Evaluation of the Pertinent Parameters in Bio-synthesis of Ag/MWf-CNT Composites Using Plackett-Burman

- Design and Response Surface Methodology. Iranian Journal of Chemistry and Chemical Engineering (IJCCE). 2016;35(2):51-62.
218. Kuchekar AB, Pawar AP. Screening of factors using Plackett Burman design in the preparation of Capecitabine-loaded nano polymeric micelles. *Int J Pharm Pharm Sci*. 2014;6(5):489-96.
219. Ciupină V, Zamfirescu S, Prodan G. Evaluation of mean diameter values using Scherrer equation applied to electron diffraction images. *Nanotechnology–Toxicological Issues and Environmental Safety and Environmental Safety*: Springer; 2007. p. 231-7.
220. Chowdhury S, Basu A, Kundu S. Green synthesis of protein capped silver nanoparticles from phytopathogenic fungus *Macrophomina phaseolina* (Tassi) Goid with antimicrobial properties against multidrug-resistant bacteria. *Nanoscale research letters*. 2014;9(1):365.
221. Bocsanczy AM, Achenbach UC, Mangravita-Novo A, Chow M, Norman DJ. Proteomic comparison of *Ralstonia solanacearum* strains reveals temperature dependent virulence factors. *BMC genomics*. 2014;15(1):280.
222. Maurer-Jones MA, Love SA, Meierhofer S, Marquis BJ, Liu Z, Haynes CL. Toxicity of Nanoparticles to Brine Shrimp: An Introduction to Nanotoxicity and Interdisciplinary Science. *Journal of Chemical Education*. 2013;90(4):475-8.
223. Bondarenko O, Juganson K, Ivask A, Kasemets K, Mortimer M, Kahru A. Toxicity of Ag, CuO and ZnO nanoparticles to selected environmentally relevant test organisms and mammalian cells in vitro: a critical review. *Archives of toxicology*. 2013;87(7):1181-200.
224. Bucker A, Falcao-Bucker NC, Nunez CV, Pinheiro CCdS, Tadei WP. Evaluation of larvicidal activity and brine shrimp toxicity of rhizome extracts of *Zingiber zerumbet* (L.) Smith. *Revista da Sociedade Brasileira de Medicina Tropical*. 2013;46(3):377-80.
225. Wing-Shan Lin I. Biosynthesis of silver nanoparticles from silver (i) reduction by the periplasmic nitrate reductase c-type cytochrome subunit NapC in a silver-resistant *E. coli*. *Chemical Science*. 2014;5(8):3144-50.
226. Ranawat P, Rawat S. Metal-tolerant thermophiles: metals as electron donors and acceptors, toxicity, tolerance and industrial applications. *Environmental science and pollution research international*. 2018;25(5):4105-33.
227. El-Naggar NE-A, Hussein MH, El-Sawah AA. Bio-fabrication of silver nanoparticles by phycoyanin, characterization, in vitro anticancer activity against breast cancer cell line and in vivo cytotoxicity. *Scientific Reports*. 2017;7(1):10844.
228. Choukade R, Jaiswal A, Kango N. Characterization of biogenically synthesized silver nanoparticles for therapeutic applications and enzyme nanocomplex generation. *3 Biotech*. 2020;10(11):1-13.
229. Edwards AC, Hooda PS, Cook Y. Determination of nitrate in water containing dissolved organic carbon by ultraviolet spectroscopy. *International Journal of Environmental Analytical Chemistry*. 2001;80(1):49-59.
230. Ahmed AA, Allah EWA. Origin of Absorption Bands Observed in the Spectra of Silver Ion-Exchanged Soda–Lime–Silica Glass. *Journal of the American Ceramic Society*. 1995;78(10):2777-84.
231. Naqvi SH, Zainab S, Hameed A, Ahmed S, Ali N. Mycogenesis of silver nanoparticles by different *Aspergillus* species. *Scientia Iranica Transaction F, Nanotechnology*. 2014;21(3):1143.
232. Nikaeen G, Yousefinejad S, Rahmdel S, Samari F, Mahdavinia S. Central Composite Design for Optimizing the Biosynthesis of Silver Nanoparticles using *Plantago major* Extract and Investigating Antibacterial, Antifungal and Antioxidant Activity. *Scientific Reports*. 2020;10(1):1-16.
233. Jain N, Bhargava A, Majumdar S, Tarafdar J, Panwar J. Extracellular biosynthesis and characterization of silver nanoparticles using *Aspergillus flavus* NJP08: a mechanism perspective. *Nanoscale*. 2011;3(2):635-41.
234. El-Moslamy SH, Elkady MF, Rezk AH, Abdel-Fattah YR. Applying Taguchi design and large-scale strategy for mycosynthesis of nano-silver from endophytic *Trichoderma*

- harzianum SYA. F4 and its application against phytopathogens. *Scientific reports*. 2017;7:45297.
235. Khan SA, Ahmad A. Enzyme mediated synthesis of water-dispersible, naturally protein capped, monodispersed gold nanoparticles; their characterization and mechanistic aspects. *RSC Advances*. 2014;4(15):7729-34.
236. Mishra RS, Maheshwari R. Amylases of the thermophilic fungus *Thermomyces lanuginosus*: Their purification, properties, action on starch and response to heat. *Journal of Biosciences*. 1996;21(5):653-72.
237. Thorsen TS, Johnsen AH, Josefsen K, Jensen B. Identification and characterization of glucoamylase from the fungus *Thermomyces lanuginosus*. *Biochimica et Biophysica Acta (BBA)-Proteins and Proteomics*. 2006;1764(4):671-6.
238. Basaveswara Rao V, Sastri N, Subba Rao P. Purification and characterization of a thermostable glucoamylase from the thermophilic fungus *Thermomyces lanuginosus*. *Biochemical journal*. 1981;193(2):379-87.
239. Rao VB, Maheshwari R, Sastry N, Rao PS. A thermostable glucoamylase from the thermophilic fungus *Thermomyces lanuginosus*. *Current Science*. 1979;48(3):113-5.
240. Lekange S, Miranda AF, Abraham A, Li V, Shukla R, Bansal V, et al. The Toxicity of Silver Nanoparticles (AgNPs) to Three Freshwater Invertebrates With Different Life Strategies: *Hydra vulgaris*, *Daphnia carinata*, and *Paratya australiensis*. *Frontiers in Environmental Science*. 2018;6(152).
241. Daniel M-C, Astruc D. Gold nanoparticles: assembly, supramolecular chemistry, quantum-size-related properties, and applications toward biology, catalysis, and nanotechnology. *Chemical reviews*. 2004;104(1):293-346.
242. Lowenstam HA. Minerals formed by organisms. *Science*. 1981;211(4487):1126-31.
243. Pum D, Sleytr UB. The application of bacterial S-layers in molecular nanotechnology. *Trends in Biotechnology*. 1999;17(1):8-12.
244. Zhang W-z, Wang G. Research and development for antibacterial materials of silver nanoparticle. *New Chem Mater*. 2003;31(2):42-4.
245. Kotthaus S, Gunther BH, Hang R, Schafer H. Study of isotropically conductive bondings filled with aggregates of nano-sited Ag-particles. *IEEE Transactions on Components, Packaging, and Manufacturing Technology: Part A*. 1997;20(1):15-20.
246. Klaus-Joerger T, Joerger R, Olsson E, Granqvist C-G. Bacteria as workers in the living factory: metal-accumulating bacteria and their potential for materials science. *TRENDS in Biotechnology*. 2001;19(1):15-20.
247. Cao G. *Nanostructures & nanomaterials: synthesis, properties & applications*: Imperial college press; 2004.
248. Cho K-H, Park J-E, Osaka T, Park S-G. The study of antimicrobial activity and preservative effects of nanosilver ingredient. *Electrochimica Acta*. 2005;51(5):956-60.
249. Manjunath S, Thiagarajan P. Exploring the mechanism for mycobiosynthesis of silver nanoparticles from *Aspergillus* spp. and optimisation of synthesis parameters. *Micro & Nano Letters*. 2014;9(9):600-4.
250. Bradford MM. A rapid and sensitive method for the quantitation of microgram quantities of protein utilizing the principle of protein-dye binding. *Analytical biochemistry*. 1976;72(1-2):248-54.
251. Vaidyanathan R, Gopalram S, Kalishwaralal K, Deepak V, Pandian SRK, Gurunathan S. Enhanced silver nanoparticle synthesis by optimization of nitrate reductase activity. *Colloids and surfaces B: Biointerfaces*. 2010;75(1):335-41.
252. Determann H. *Gel Chromatography: Gel Filtration · Gel Permeation · Molecular Sieves: A Laboratory Handbook*: Springer Berlin Heidelberg; 2013.
253. Laemmli UK. Cleavage of Structural Proteins during the Assembly of the Head of Bacteriophage T4. *Nature*. 1970;227(5259):680-5.
254. A. AA, Abd AEW. Origin of Absorption Bands Observed in the Spectra of Silver Ion-Exchanged Soda-Lime-Silica Glass. *Journal of the American Ceramic Society*. 1995;78(10):2777-84.

255. El-Bendary MA, Moharam ME, Hamed SR, Abo El-Ola SM, Khalil SKH, Mounier MM, et al. Mycosynthesis of silver nanoparticles using *Aspergillus caespitosus*: Characterization, antimicrobial activities, cytotoxicity, and their performance as an antimicrobial agent for textile materials. *Applied Organometallic Chemistry*. 2021;35(9):e6338.
256. Aiken AM, Peyton BM, Apel WA, Petersen JN. Heavy metal-induced inhibition of *Aspergillus niger* nitrate reductase: applications for rapid contaminant detection in aqueous samples. *Analytica Chimica Acta*. 2003;480(1):131-42.
257. Martínez-Espinosa RM, Marhuenda-Egea FC, Bonete MaJ. Assimilatory nitrate reductase from the haloarchaeon *Haloferax mediterranei*: purification and characterisation. *FEMS Microbiology Letters*. 2001;204(2):381-5.
258. Annamalai J, Murugan K, Shanmugam J, Boopathy U. Mycosynthesis of silver nanoparticles: Mechanism and applications. *Green Synthesis of Silver Nanomaterials*: Elsevier; 2022. p. 391-411.
259. Hamedi S, Ghaseminezhad M, Shokrollahzadeh S, Shojaosadati SA. Controlled biosynthesis of silver nanoparticles using nitrate reductase enzyme induction of filamentous fungus and their antibacterial evaluation. *Artificial Cells, Nanomedicine, and Biotechnology*. 2017;45(8):1588-96.
260. Zomorodian K, Pourshahid S, Sadatsharifi A, Mehryar P, Pakshir K, Rahimi MJ, et al. Biosynthesis and Characterization of Silver Nanoparticles by *Aspergillus* Species. *BioMed Research International*. 2016;2016:5435397.
261. Guilger-Casagrande M, Lima Rd. Synthesis of silver nanoparticles mediated by fungi: a review. *Frontiers in bioengineering and biotechnology*. 2019;7:287.
262. Li P-J, Pan J-J, Tao L-J, Li X, Su D-L, Shan Y, et al. Green Synthesis of Silver Nanoparticles by Extracellular Extracts from *Aspergillus japonicus* PJ01. *Molecules*. 2021;26(15):4479.
263. Akther T, Vabeiryureilai M, Nachimuthu Senthil K, Davoodbasha M, Srinivasan H. Fungal-mediated synthesis of pharmaceutically active silver nanoparticles and anticancer property against A549 cells through apoptosis. *Environmental Science and Pollution Research*. 2019;26(13):13649-57.
264. Mistry H, Thakor R, Patil C, Trivedi J, Bariya H. Biogenically proficient synthesis and characterization of silver nanoparticles employing marine procured fungi *Aspergillus brunneoviolaceus* along with their antibacterial and antioxidative potency. *Biotechnology Letters*. 2021;43(1):307-16.
265. Ratvijitvech T, Na Pombejra S. Antibacterial efficiency of microporous hypercrosslinked polymer conjugated with biosynthesized silver nanoparticles from *Aspergillus niger*. *Materials Today Communications*. 2021;28:102617.
266. Roy S, Das TK. Biosynthesis of Silver Nanoparticles by *Aspergillus foetidus*: Optimization of Physicochemical Parameters. *Nanoscience and Nanotechnology Letters*. 2014;6(3):181-9.
267. Sachdeva V, Hooda V. Effect of changing the nanoscale environment on activity and stability of nitrate reductase. *Enzyme and Microbial Technology*. 2016;89:52-62.
268. Kitamoto N, Kimura T, Kito Y, Ohmiya K, Tsukagoshi N. The Nitrate Reductase Gene from a Shoyu Koji Mold, *Aspergillus oryzae* KBN616. *Bioscience, Biotechnology, and Biochemistry*. 1995;59(9):1795-7.
269. Ma L, Lv S, Tang J, Liu J, Li W, Deng J, et al. Study on bioactive molecules involved in extracellular biosynthesis of silver nanoparticles by *Penicillium aculeatum* Su1. *Materials Express*. 2019;9(5):475-83.
270. Gholami-Shabani M, Akbarzadeh A, Norouzian D, Amini A, Gholami-Shabani Z, Imani A, et al. Antimicrobial Activity and Physical Characterization of Silver Nanoparticles Green Synthesized Using Nitrate Reductase from *Fusarium oxysporum*. *Applied Biochemistry and Biotechnology*. 2014;172(8):4084-98.
271. Kett DH, Azoulay E, Echeverria PM, Vincent J-L. *Candida* bloodstream infections in intensive care units: analysis of the extended prevalence of infection in intensive care unit study. *Critical care medicine*. 2011;39(4):665-70.



272. Cheng S-C, Joosten LA, Kullberg B-J, Netea MG. Interplay between *Candida albicans* and the mammalian innate host defense. *Infection and immunity*. 2012;80(4):1304-13.
273. Shrestha SK, Fosso MY, Garneau-Tsodikova S. A combination approach to treating fungal infections. *Scientific reports*. 2015;5:17070.
274. Cowen LE. The evolution of fungal drug resistance: modulating the trajectory from genotype to phenotype. *Nature Reviews Microbiology*. 2008;6(3):187-98.
275. Pierce CG, Lopez-Ribot JL. Candidiasis drug discovery and development: new approaches targeting virulence for discovering and identifying new drugs. *Expert opinion on drug discovery*. 2013;8(9):1117-26.
276. Mitchell K, Taff H, Cuevas M, Reinicke E, Sanchez H, Andes D. Role of matrix  $\beta$ -1, 3 glucan in antifungal resistance of non-*albicans* *Candida* biofilms. *Antimicrobial agents and chemotherapy*. 2013;57(4):1918-20.
277. Selmecki A, Forche A, Berman J. Aneuploidy and isochromosome formation in drug-resistant *Candida albicans*. *Science*. 2006;313(5785):367-70.
278. Bourzac K. Nanotechnology: carrying drugs. *Nature*. 2012;491(7425):S58-S60.
279. Şahin B, Aygün A, Gündüz H, Şahin K, Demir E, Akocak S, et al. Cytotoxic effects of platinum nanoparticles obtained from pomegranate extract by the green synthesis method on the MCF-7 cell line. *Colloids and Surfaces B: Biointerfaces*. 2018;163:119-24.
280. Aygün A, Özdemir S, Gülcan M, Cellat K, Şen F. Synthesis and characterization of Reishi mushroom-mediated green synthesis of silver nanoparticles for the biochemical applications. *Journal of pharmaceutical and biomedical analysis*. 2020;178:112970.
281. Chambers BA, Afrooz AN, Bae S, Aich N, Katz L, Saleh NB, et al. Effects of chloride and ionic strength on physical morphology, dissolution, and bacterial toxicity of silver nanoparticles. *Environmental science & technology*. 2013;48(1):761-9.
282. Elmusa F, Aygun A, Gulbagca F, Seyrankaya A, Göl F, Yenikaya C, et al. Investigation of the antibacterial properties of silver nanoparticles synthesized using *Abelmoschus esculentus* extract and their ceramic applications. *International Journal of Environmental Science and Technology*. 2021;18(4):849-60.
283. Chen X, Schluesener H. Nanosilver: a nanoparticle in medical application. *Toxicology letters*. 2008;176(1):1-12.
284. Saleh NB, Chambers B, Aich N, Plazas-Tuttle J, Phung-Ngoc HN, Kirisits MJ. Mechanistic lessons learned from studies of planktonic bacteria with metallic nanomaterials: implications for interactions between nanomaterials and biofilm bacteria. *Frontiers in microbiology*. 2015;6.
285. Gulbagca F, Aygün A, Gülcan M, Ozdemir S, Gonca S, Şen F. Green synthesis of palladium nanoparticles: Preparation, characterization, and investigation of antioxidant, antimicrobial, anticancer, and DNA cleavage activities. *Applied Organometallic Chemistry*. 2021:e6272.
286. Naglik JR, Challacombe SJ, Hube B. *Candida albicans* secreted aspartyl proteinases in virulence and pathogenesis. *Microbiology and molecular biology reviews*. 2003;67(3):400-28.
287. Sardi J, Scorzoni L, Bernardi T, Fusco-Almeida A, Giannini MM. *Candida* species: current epidemiology, pathogenicity, biofilm formation, natural antifungal products and new therapeutic options. *Journal of medical microbiology*. 2013;62(1):10-24.
288. Asadi Dokht Lish R, Johari SA, Sarkheil M, Yu IJ. On how environmental and experimental conditions affect the results of aquatic nanotoxicology on brine shrimp (*Artemia salina*): A case of silver nanoparticles toxicity. *Environmental Pollution*. 2019;255:113358.
289. Malik NH, Zain H, Ali N. Organismic-level acute toxicology profiling of reactive azo dyes. *Environmental monitoring and assessment*. 2018;190(10):1-12.
290. Odds FC. Synergy, antagonism, and what the checkerboard puts between them. *Journal of Antimicrobial Chemotherapy*. 2003;52(1):1-.
291. Longhi C, Santos JP, Morey AT, Marcato PD, Durán N, Pinge-Filho P, et al. Combination of fluconazole with silver nanoparticles produced by *Fusarium oxysporum*

- improves antifungal effect against planktonic cells and biofilm of drug-resistant *Candida albicans*. *Sabouraudia*. 2015;54(4):428-32.
292. Nett JE, Cain MT, Crawford K, Andes DR. Optimizing a *Candida* biofilm microtiter plate model for measurement of antifungal susceptibility by tetrazolium salt assay. *Journal of clinical microbiology*. 2011;49(4):1426-33.
293. Abraham KP, Sreenivas J, Venkateswarulu TC, Indira M, Babu DJ, Diwakar T, et al. Investigation of the potential antibiofilm activities of plant extracts. *International Journal of Pharmacy and Pharmaceutical Sciences*. 2012;4(4):282-5.
294. Kumar SA, Abyaneh MK, Gosavi S, Kulkarni SK, Pasricha R, Ahmad A, et al. Nitrate reductase-mediated synthesis of silver nanoparticles from AgNO<sub>3</sub>. *Biotechnology letters*. 2007;29(3):439-45.
295. Lateef A, Adeeyo AO. Green synthesis and antibacterial activities of silver nanoparticles using extracellular laccase of *Lentinus edodes*. *Notulae Scientia Biologicae*. 2015;7(4):405-11.
296. Spagnoletti FN, Kronberg F, Spedaliere C, Munarriz E, Giacometti R. Protein corona on biogenic silver nanoparticles provides higher stability and protects cells from toxicity in comparison to chemical nanoparticles. *Journal of Environmental Management*. 2021;297:113434.
297. Korkmaz N, Ceylan Y, Hamid A, Karadağ A, Bülbül AS, Aftab MN, et al. Biogenic silver nanoparticles synthesized via *Mimusops elengi* fruit extract, a study on antibiofilm, antibacterial, and anticancer activities. *Journal of Drug Delivery Science and Technology*. 2020;59:101864.
298. Naqvi S, Zainab S, Hameed A, Ahmed S, Ali N. Mycogenesis of silver nanoparticles by different *Aspergillus* species. *Scientia Iranica*. 2014;21(3):1143-50.
299. Vijayan SR, Santhiyagu P, Singamuthu M, Kumari Ahila N, Jayaraman R, Ethiraj K. Synthesis and characterization of silver and gold nanoparticles using aqueous extract of seaweed, *Turbinaria conoides*, and their antimicrofouling activity. *The Scientific World Journal*. 2014;2014.
300. Kumar P, Selvi SS, Praba AL, Selvaraj M, Rani LM, Suganthi P, et al. Antibacterial activity and in-vitro cytotoxicity assay against brine shrimp using silver nanoparticles synthesized from *Sargassum ilicifolium*. *Digest Journal of Nanomaterials and Biostructures*. 2012;7(4):1447-55.
301. Sun L, Liao K, Li Y, Zhao L, Liang S, Guo D, et al. Synergy Between Polyvinylpyrrolidone-Coated Silver Nanoparticles and Azole Antifungal Against Drug-Resistant *Candida albicans*. *Journal of nanoscience and nanotechnology*. 2016;16(3):2325-35.
302. Monteiro DR, Silva S, Negri M, Gorup LF, de Camargo ER, Oliveira R, et al. Antifungal activity of silver nanoparticles in combination with nystatin and chlorhexidine digluconate against *Candida albicans* and *Candida glabrata* biofilms. *Mycoses*. 2013;56(6):672-80.
303. Cui J, Ren B, Tong Y, Dai H, Zhang L. Synergistic combinations of antifungals and anti-virulence agents to fight against *Candida albicans*. *Virulence*. 2015;6(4):362-71.
304. Mikhailova EO. Silver Nanoparticles: Mechanism of action and probable bio-application. *Journal of Functional Biomaterials*. 2020;11(4):84.
305. Mba IE, Nweze EI. The use of nanoparticles as alternative therapeutic agents against *Candida* infections: an up-to-date overview and future perspectives. *World Journal of Microbiology and Biotechnology*. 2020;36(11):163.
306. Lal P, Agarwal V, Pruthi P, Pereira BM, Kural M, Pruthi V. Biofilm formation by *Candida albicans* isolated from intrauterine devices. *Indian journal of microbiology*. 2008;48(4):438.
307. Nett J, Lincoln L, Marchillo K, Massey R, Holoyda K, Hoff B, et al. Putative role of  $\beta$ -1, 3 glucans in *Candida albicans* biofilm resistance. *Antimicrobial agents and chemotherapy*. 2007;51(2):510-20.
308. Cheng Q, Jiang H, Jin Z, Jiang Y, Hui C, Xu L, et al. Effects of Fe<sub>2</sub>O<sub>3</sub> nanoparticles on extracellular polymeric substances and nonylphenol degradation in river sediment. *Science of The Total Environment*. 2021;770:145210.

309. Nett J, Andes D. *Candida albicans* biofilm development, modeling a host–pathogen interaction. *Current opinion in microbiology*. 2006;9(4):340-5.
310. Srivastava P, Gunawan C, Soeriyadi A, Amal R, Hoehn KL, Marquis CP. In vitro coronal protein signatures and biological impact of silver nanoparticles synthesized with different natural polymers as capping agents. *Nanoscale Advances*. 2021.
311. Restrepo CV, Villa CC. Synthesis of silver nanoparticles, influence of capping agents, and dependence on size and shape: A review. *Environmental Nanotechnology, Monitoring & Management*. 2021;15:100428.
312. Chowdhury S, Basu A, Kundu S. Green synthesis of protein capped silver nanoparticles from phytopathogenic fungus *Macrophomina phaseolina* (Tassi) Goid with antimicrobial properties against multidrug-resistant bacteria. *Nanoscale research letters*. 2014;9(1):1-11.
313. Duan H, Wang D, Li Y. Green chemistry for nanoparticle synthesis. *Chemical Society Reviews*. 2015;44(16):5778-92.
314. Vellanki S, Navarro-Mendoza MI, Garcia A, Murcia L, Perez-Arques C, Garre V, et al. *Mucor circinelloides*: growth, maintenance, and genetic manipulation. *Current protocols in microbiology*. 2018;49(1):e53.
315. Yang J, Li S, Kabir Khan MA, Garre V, Vongsangnak W, Song Y. Increased lipid accumulation in *Mucor circinelloides* by overexpression of mitochondrial citrate transporter genes. *Industrial & Engineering Chemistry Research*. 2019;58(6):2125-34.
316. Tang X, Chen H, Gu Z, Zhang H, Chen YQ, Song Y, et al. Role of g 6 pdh and leuB on Lipid Accumulation in *Mucor circinelloides*. *Journal of agricultural and food chemistry*. 2020;68(14):4245-51.
317. Wynn JP, Hamid AA, Li Y, Ratledge C. Biochemical events leading to the diversion of carbon into storage lipids in the oleaginous fungi *Mucor circinelloides* and *Mortierella alpina*. *Microbiology*. 2001;147(10):2857-64.
318. Rodrigues Reis CE, Bento HB, Carvalho AK, Rajendran A, Hu B, De Castro HF. Critical applications of *Mucor circinelloides* within a biorefinery context. *Critical reviews in biotechnology*. 2019;39(4):555-70.
319. Wei H, Wang W, Yarbrough JM, Baker JO, Laurens L, Van Wycken S, et al. Genomic, proteomic, and biochemical analyses of oleaginous *Mucor circinelloides*: evaluating its capability in utilizing cellulolytic substrates for lipid production. *PloS one*. 2013;8(9):e71068.
320. Ratledge C. Single cell oils—have they a biotechnological future? *Trends in biotechnology*. 1993;11(7):278-84.
321. Vongsangnak W, Kingkaw A, Yang J, Song Y, Laoteng K. Dissecting metabolic behavior of lipid over-producing strain of *Mucor circinelloides* through genome-scale metabolic network and multi-level data integration. *Gene*. 2018;670:87-97.
322. Al-Zaban MI, AlHarbi MA, Mahmoud MA, Bahatheq AM. Production of biodiesel from oleaginous fungal lipid using highly catalytic bimetallic gold-silver core-shell nanoparticle. *J Appl Microbiol*. 2022;132(1):381-9.
323. Niu Y, Fan L, Gu D, Wu J, Chen Q. Characterization, enhancement and modelling of mannosylerythritol lipid production by fungal endophyte *Ceriporia lacerate* CHZJU. *Food chemistry*. 2017;228:610-7.
324. Zininga JT. Production of chitosan and lipids from a newly isolated *Mucor circinelloides* 2018.
325. Ibrahim S, Ahmad Z, Manzoor MZ, Mujahid M, Faheem Z, Adnan A. Optimization for biogenic microbial synthesis of silver nanoparticles through response surface methodology, characterization, their antimicrobial, antioxidant, and catalytic potential. *Scientific Reports*. 2021;11(1):770.
326. Kumbhare M, Guleha V, Sivakumar T. Estimation of total phenolic content, cytotoxicity and in–vitro antioxidant activity of stem bark of *Moringa oleifera*. *Asian Pacific Journal of Tropical Disease*. 2012;2(2):144-50.

327. Darroudi M, Ahmad MB, Abdullah AH, Ibrahim NA. Green synthesis and characterization of gelatin-based and sugar-reduced silver nanoparticles. *International Journal of Nanomedicine*. 2011;6:569-74.
328. Tagar ZA, Sirajuddin M, Kalhor M, Kalwar NH, Junejo Y, Sara Hassan S. Facile synthesis, characterization and catalytic function of gelatin stabilized gold nanoparticles. *Pak J Anal Environ Chem*. 2012;13(1):70-7.
329. Reyes-Esparza J, Martínez-Mena A, Gutiérrez-Sancha I, Rodríguez-Fragoso P, de la Cruz GG, Mondragón R, et al. Synthesis, characterization and biocompatibility of cadmium sulfide nanoparticles capped with dextrin for in vivo and in vitro imaging application. *Journal of Nanobiotechnology*. 2015;13(1):1-14.
330. Yakout SM, Mostafa AA. A novel green synthesis of silver nanoparticles using soluble starch and its antibacterial activity. *International Journal of Clinical and Experimental Medicine*. 2015;8(3):3538-44.
331. Kora AJ, Rastogi L. Enhancement of Antibacterial Activity of Capped Silver Nanoparticles in Combination with Antibiotics, on Model Gram-Negative and Gram-Positive Bacteria. *Bioinorganic Chemistry and Applications*. 2013;2013:7.
332. Li H-J, Zhang A-Q, Hu Y, Sui L, Qian D-J, Chen M. Large-scale synthesis and self-organization of silver nanoparticles with Tween 80 as a reductant and stabilizer. *Nanoscale Research Letters*. 2012;7(1):612-.
333. Khan Z, Bashir O, Hussain JI, Kumar S, Ahmad R. Effects of ionic surfactants on the morphology of silver nanoparticles using Paan (Piper betel) leaf petiole extract. *Colloids and Surfaces B: Biointerfaces*. 2012;98:85-90.
334. Chen R, Wu J, Li H, Cheng G, Lu Z, Che C-M. Fabrication of gold nanoparticles with different morphologies in HEPES buffer. *Rare Metals*. 2010;29(2):180-6.
335. Bae E-J, Park H-J, Park J-S, Yoon J-Y, Kim Y-H, Choi K-H, et al. Effect of chemical stabilizers in silver nanoparticle suspensions on nanotoxicity. *Bulletin of the Korean Chemical Society*. 2011;32(2):613-9.
336. Dzurendova S, Zimmermann B, Tafintseva V, Kohler A, Horn SJ, Shapaval V. Metal and Phosphate Ions Show Remarkable Influence on the Biomass Production and Lipid Accumulation in Oleaginous *Mucor circinelloides*. *Journal of Fungi*. 2020;6(4):260.
337. Rao CRK, Trivedi DC. Biphasic synthesis of fatty acids stabilized silver nanoparticles: Role of experimental conditions on particle size. *Materials Chemistry and Physics*. 2006;99(2):354-60.
338. Kumar A, Joshi H, Pasricha R, Mandale AB, Sastry M. Phase transfer of silver nanoparticles from aqueous to organic solutions using fatty amine molecules. *Journal of Colloid and Interface Science*. 2003;264(2):396-401.
339. Sathishkumar Y, Devarayan K, Ki C, Rajagopal K, Lee YS. Shape-controlled extracellular synthesis of silver nanocubes by *Mucor circinelloides*. *Materials Letters*. 2015;159:481-3.
340. Hameed A, Hussain SA, Yang J, Ijaz MU, Liu Q, Suleria HAR, et al. Antioxidants potential of the filamentous fungi (*Mucor circinelloides*). *Nutrients*. 2017;9(10):1101.
341. Husanu E, Chiappe C, Bernardini A, Cappello V, Gemmi M. Synthesis of colloidal Ag nanoparticles with citrate based ionic liquids as reducing and capping agents. *Colloids and Surfaces A: Physicochemical and Engineering Aspects*. 2018;538:506-12.
342. Smitha SL, Nissamudeen KM, Philip D, Gopchandran KG. Studies on surface plasmon resonance and photoluminescence of silver nanoparticles. *Spectrochimica Acta Part A: Molecular and Biomolecular Spectroscopy*. 2008;71(1):186-90.
343. Bekhit M, Abu el-naga MN, Sokary R, Fahim RA, El-Sawy NM. Radiation-induced synthesis of tween 80 stabilized silver nanoparticles for antibacterial applications. *Journal of Environmental Science and Health, Part A*. 2020;55(10):1210-7.
344. Mahmood M, Abid M, Nazar MF, Zafar MN, Raza MA, Ashfaq M, et al. The wet chemical synthesis of surfactant-capped quasi-spherical silver nanoparticles with enhanced antibacterial activity. *Materials Advances*. 2020;1(7):2332-8.
345. Salomoni R, Léo P, Montemor AF, Rinaldi BG, Rodrigues M. Antibacterial effect of silver nanoparticles in *Pseudomonas aeruginosa*. *Nanotechnol Sci Appl*. 2017;10:115-21.

# Publication

One research article was published from dissertation:

Zainab S, Hamid S, Sahar S, Ali N. Fluconazole and biogenic silver nanoparticles-based nano-fungicidal system for highly efficient elimination of multi-drug resistant *Candida* biofilms. *Materials Chemistry and Physics*. 2022 ; 276: 125451.

DOI: <https://doi.org/10.1016/j.matchemphys.2021.125451>



## Fluconazole and biogenic silver nanoparticles-based nano-fungicidal system for highly efficient elimination of multi-drug resistant *Candida* biofilms

Shama Zainab<sup>a</sup>, Sabahat Hamid<sup>a</sup>, Shafaq Sahar<sup>b</sup>, Naeem Ali<sup>a,\*</sup>

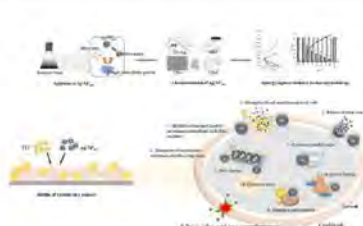
<sup>a</sup> Department of Microbiology, Quid-i-Asam University, Islamabad, Pakistan

<sup>b</sup> Institute of Bioengineering, College of Chemical and Biological Engineering, Zhejiang University, Hangzhou, 310027, China

### HIGHLIGHTS

- Fungus *Aspergillus oryzae* SZ1 was used to synthesize silver nanoparticles (Ag-NP<sub>myc</sub>).
- Ag-NP<sub>myc</sub> in combination with fluconazole showed synergistic effect against virulence of resistant *Candida* sp.
- The combination of drugs promoted significant reduction in secreted aspartyl proteinase of *Candida* sp.
- Mycogenic silver nanoparticles were found to be non-cytotoxic against brine shrimps.

### GRAPHICAL ABSTRACT



### ARTICLE INFO

#### Keywords:

*Candida*  
Mycogenic  
Silver nanoparticle  
Nano-fungicide  
Virulence  
Antibiofilm  
Secreted aspartyl proteinase

### ABSTRACT

**Hypothesis:** Secretion of extracellular hydrolytic enzymes such as secreted aspartyl proteinases (SAP) and biofilm formation are considered as important virulence determinants in resistant strains of *Candida* sp. which facilitate the pathogenicity towards host cells. The resistance in fungal pathogens results in use of high dosage of antifungal drug, therefore in order to study the effect of reduced amount of antifungal, combination therapy was utilized. Currently, no data related to combined effect of mycogenic silver nanoparticles and fluconazole, in SAP inhibition by resistant *Candida* spp. has been described. In this study, synergistic combination along with anti-virulence was used as a way for discovering new antifungal potential of mycogenic silver nanoparticles (Ag-NP<sub>myc</sub>).

**Experiments:** This study utilized Ag-NP<sub>myc</sub>, synthesized using *Aspergillus oryzae* SZ1 and their combined effect with fluconazole on planktonic and 24 h (h) biofilm forms of clinical isolates of six *Candida* species (*C. albicans*, *C. galabrata*, *C. parapsilosis*, *C. krusei*, *C. tropicalis*, *C. albicans* ATCC 24433). The cytotoxic effects of Ag-NP<sub>myc</sub> using brine shrimp lethality assay was also determined. Ag-NP<sub>myc</sub> and fluconazole (FLC) suspensions were used to treat *Candida* sp. biofilms grown on polystyrene surfaces for 24 h (h) and their efficacy was determined by MIC, time-kill growth curve analysis, cell viability analysis (XTT reduction assay), inhibition of virulence factors exopolymers (EPS) and SAP activity. Nanoparticles were characterized using Ultraviolet-Visible (UV-Vis) spectroscopy, X-Ray Diffraction (XRD) and transmission electron microscopy (TEM).

\* Corresponding author.

E-mail address: [naemal2611@gmail.com](mailto:naemal2611@gmail.com) (N. Ali).

<https://doi.org/10.1016/j.matchemphys.2021.125451>

Received 19 August 2021; Received in revised form 10 November 2021; Accepted 15 November 2021  
Available online 18 November 2021

## Other Publications

**Research article:** Inhibition of secreted aspartyl proteinase activity in biofilms of *Candida* species by mycogenic silver nanoparticles, *Artificial cells, nanomedicine, and biotechnology*, 2018, 46(3), pp.551-557.

**Research article:** Deterrence in metabolic and biofilms forming activity of *Candida* species by mycogenic silver nanoparticles. *Journal of Applied Biomedicine*. Journal of Applied Biomedicine 2017, 15(4), 249–255.

**Research article:** Role of catalytic protein and stabilising agents in the transformation of Ag ions to nanoparticles by *Pseudomonas aeruginosa*, *IET nanobiotechnology*, 2016, 10(5), pp.295-300.

**Research article:** Green synthesis of metal nanoparticles by microorganisms; a current prospective. *Journal of nanoanalysis*; 2015, 02 (01): 32-38.

**Research article:** Mycogenesis of silver nanoparticles by different *Aspergillus* species. *Scientia Iranica* 2014, 21(03):1143-1150.

**Abstract published** in 4th ASM Conference on Beneficial Microbes, October 22 – 26, 2012 San Antonio, Texas, Fungi; as noble metal nano-factory and eco-remediator, an emerging green technology approach.

**Abstract published** in 2nd conference on frontiers of nanoscience and nanotechnology September 8-10, 2015 organized by Directorate of science, Institute of nuclear science and technology (PINSTECH) Islamabad, Pakistan

**Poster:** A mechanistic approach in green synthesis of silver nanoparticles at 10th Biennial International Conference of Pakistan Society for Microbiology March 25 – 28, 2015, Department of Microbiology and molecular genetics, University of the Punjab, Lahore.



## Turnitin Originality Report

Biofabrication and applications of metal nanoparticles from Indigenous Fungi  
Shama Zainab

by



From CL QAU (DRSML)

- Processed on 14-Feb-2022 14:07 PKT
- ID: 1762031750
- Word Count: 30698

## Similarity Index

13%

## Similarity by Source

## Internet Sources:

9%

## Publications:

9%

## Student Papers:

3%

Focal Person (Turnitin)  
Quaid-i-Azam University  
Islamabad

## sources:

- 1 < 1% match (Internet from 02-Feb-2022)  
<https://cyberfeninka.org/article/n/1054626>
- 2 < 1% match (Internet from 18-Jan-2022)  
<https://cyberfeninka.org/article/n/1496356>
- 3 < 1% match (Internet from 12-Feb-2022)  
<https://cyberfeninka.org/article/n/1201626>
- 4 < 1% match (student papers from 10-Oct-2012)  
[Submitted to Higher Education Commission Pakistan on 2012-10-10](#)
- 5 < 1% match (student papers from 16-Nov-2017)  
[Submitted to Higher Education Commission Pakistan on 2017-11-16](#)
- 6 < 1% match (student papers from 25-Jan-2018)  
[Submitted to Higher Education Commission Pakistan on 2018-01-25](#)
- 7 < 1% match (student papers from 29-May-2018)  
[Submitted to Higher Education Commission Pakistan on 2018-05-29](#)
- 8 < 1% match (student papers from 21-Jul-2009)  
[Submitted to Higher Education Commission Pakistan on 2009-07-21](#)